Project THEMIS
Technical Report No. 27

THREE-DIMENSIONAL TURBULENT BOUNDARY LAYER FLOW ON ROUGHNESS STRIP OF FINITE WIDTH

by

Walter H. Edling
and
J.E. Cermak

Prepared under

Office of Naval Research

Contract No. N00014-68-A-0493-0001

Project No. NR 062-414/6-6-68 (Code 438)

U.S. Department of Defense

Washington, D.C.

Fluid Dynamics and Diffusion Laboratory
College of Engineering
Colorado State University
Fort Collins, Colorado

April 1974 CER73-74WHE-JEC34

ACKNOWLEDGMENTS

The author wishes to express his sincere gratitude to his advisor, Professor J. E. Cermak, for his assistance and advice during the progress of this study.

Thanks are also extended to the other members of the graduate committee--Professors V. Sandborn, H. Shen, A. Farnell, and R. Meroney--for their comments and review of this dissertation.

Recognition is due to Mr. W. Burt of the Colorado State University Computer Center, Mr. E. Newton of the Lorain County Community College Computer Center, and Mr. G. Gorsline of the Oberlin College Computer Center for their assistance during the processing and plotting of the extensive data involved in the study.

This project was supported by the Office of Naval Research under Contract No. N00014-68-A-0493-0001.

ABSTRACT

THREE-DIMENSIONAL TURBULENT BOUNDARY LAYER FLOW
ON ROUGHNESS STRIP OF FINITE WIDTH

Described are the results of an experimental study of a well developed, turbulent boundary layer on a smooth, flat surface encountering an area of much rougher surface. The roughened area is a strip with its length extending in the direction of the mean flow but of finite width in the surface direction normal to the flow. The resulting three-dimensional flow differs significantly from previously studied cases involving step changes in roughness of infinite extent in the direction normal to the flow.

Extensive experiments were carried out in a wind tunnel having a length of nearly 100 ft (30.5 m) with a boundary layer thickness of the order of 18-20 in. (0.5 m). Pitot tube and hot-wire anemometer measurements were made of mean velocity and Reynolds stress quantities in great detail throughout the flow field. Secondary flow components were measured by a new x-wire technique permitting quick resolution of very small deflections of the mean flow vector. Considerable effort was expended to reduce and examine sources of error. The data obtained is presented both graphically and in tabular form.

Analysis of the three-dimensional, turbulent boundary layer equations is carried out using the experimental results to identify significant terms. Several conclusions are reached regarding the

driving mechanism of the flow, the significant flow parameters, and the effects of the three-dimensionality upon the flow as compared to the analagous two-dimensional case.

TABLE OF CONTENTS

TABLE OF CONTENTS (continued)

LIST OF SYMBOLS

English Symbols	Definition	Dimensions
A,B	Constants in King's law and also in x-wire analysis. In the latter application, $A = \sqrt{2/2}$.	
b,d	Constants in potential solution. (Cylinder radius and height above the floor.)	L
d	Hot-wire diameter.	L
D	Half-width of finite flat plate and also roughness patch.	L
e	Fluctuating, instantaneous voltage. Also voltage perturbation.	V
E	Mean voltage.	V
H	Shape factor.	
k	Karman constant. Also constant in Champagne's work (Reference 51).	
K	Linearizer gain factor.	
K_1, K_2	Constants in logarithmic law.	
l	Hot-wire length.	L
L_e	Characteristic length scale of edge region.	L
L_x, L_y L_z	General characteristic lengths in the x, y, z directions respectively.	L
n	Exponent in power law; also in King's law.	
P	Mean local pressure.	M/LT^2
P_o	Free stream pressure.	M/LT^2
S_c	Electronically linearized calibration constant.	VT/L
S_n	Hot-wire sensitivity to normal velocity component.	VT/L
S_p	Hot-wire sensitivity to parallel velocity component.	VT/L
S_u	Hot-wire sensitivity to u fluctuations.	VT/L

English Symbols	Definition	Dimensions
S_v	Hot-wire sensitivity to v fluctuations.	VT/L
t	Time.	T
u,v,w	Fluctuating velocity components in x, y, z directions respectively.	L/T
U,V,W	Mean velocity components in x, y, z directions respectively.	L/T
u_*	Shear velocity.	L/T
U_I	Apparent velocity indicated by hot-wire.	L/T
U_m	Mean velocity seen by hot-wire.	L/T
U_n	Instantaneous velocity component normal to hot-wire.	L/T
U_p	Instantaneous velocity component parallel to hot-wire.	L/T
x	Coordinate in direction of free stream, parallel to wall.	
y	Coordinate normal to wall.	
y_i	Height of internal boundary layer.	L
y_o	Characteristic roughness height.	L
z	Coordinate orthogonal to x and y .	

Greek Symbols		
α	Hot-wire yaw angle from Champagne's work (Reference 51).	
δ	Boundary layer thickness. Also used to denote a finite increment.	L
δ^*	Displacement thickness.	L
ε	Viscous dissipation.	L^2/T^3
θ	Momentum thickness. Also used to denote an angle.	L

LIST OF SYMBOLS (continued)

Greek Symbols	Definition	Dimensions
ν	Kinematic viscosity	L^2/T
ρ	Density.	M/L^3
τ_o	Wall shear stress.	M/LT^2
Φ	Function defined in equation 3-22.	
χ	Function defined in equation 3-23.	

Subscripts	Definition
i	Subscript with values 1,2,3 identifying components in x,y,z directions respectively.
1,2	Subscripts referring to wires in x-wire array.
I,II, III,IV	Subscripts referring to regions of the flow.
r	Subscript denoting a reference quantity.

Primes

(') Primes are used to denote dummy integration variables; and also dimensionless quantities.

LIST OF TABLES

LIST OF FIGURES

LIST OF FIGURES (continued)

LIST OF FIGURES (continued)

Chapter I

INTRODUCTION

The flow of a fluid over a roughened surface has been studied in various simplified forms. Geometrical simplifications have been used on all types of physical problems and have proved equally useful in the study of turbulent flow over roughness. Furthermore, the analyses resulting from the simplified models have proved to be useful in predicting the behavior of a number of real flows.(1)

Thus, three-dimensional problems have been approximated by two-dimensional models; and in some cases the simplifications can be extended to produce what amounts to a one-dimensional model. In the case of turbulent boundary layer flow, the latter situation would be the similarity-type of solution over a double infinite, uniform surface. Such a solution represents an asymptotic condition which may be approached by a real flow after a suitable period of development or fetch over a roughened region where variation in the lateral direction is negligible. Fully developed pipe flow would be another example. In many situations, however, the flow may clearly depend on all three coordinate directions, or the question may arise as to how significant are the effects of variations in all directions.

The problem investigated in this report is typified by the atmospheric flow over a city, which may involve both a sudden change in surface roughness which extends only a finite distance at right angles to the mean flow direction. Similar conditions would arise in any flow over an area of roughness which varies in the direction lateral to the flow. Examples can be found in flows over forests, croplands, and mountains, wind-tunnel flows over some types of models, patches of roughness on aircraft, ship, or turbomachinery surfaces and open channels.

Attention is focused particularly on the "edge effects" or effects of sudden roughness changes in the lateral direction, and comparison with the equivalent two-dimensional situation is the central theme. Specifically, the behavior of a well-developed, turbulent boundary layer encountering a finite patch of roughness is investigated as a three-dimensional flow of a particular type.

The presence of an "edge" or a sudden change in surface roughness in the direction normal to the mean flow direction creates stress gradients which in turn may be expected to affect the boundary layer development. Earlier work, both theoretical and experimental, has shown qualitatively the existence of weak lateral flow components ("secondary flows") under such conditions. However the details of the driving mechanism have not been clearly established, nor have the effects been measured of the resulting circulation upon the boundary layer. Quantitative data for any such case are completely absent, a fact which is partly due to the great complexity of the problem and the difficulty involved in measuring the required quantities to a sufficient level of accuracy. The work described herein is an attempt to attack and extend the knowledge of this formidable problem.

Terminology

Consideration of terminology is appropriate here since usage and meanings vary in practice. For clarity, the intended meanings are described below and will be followed in subsequent discussion.

As implied above, the term "three-dimensional" implies that dependent variables are functions of three space coordinates and cannot be described without resorting to three independent variables. Furthermore, in this problem all quantities may vary with respect to all three coordinates. Stated differently, the flow does not meet the usual definition of two-dimensionality which requires that the flow must be representable on one typical plane and that the velocity vector is always parallel to that same plane (2,3,4).

Turbulence, of course, is an inherently three-dimensional phenomenon regardless of the geometry of the flow; however the term three-dimensional flow here is in reference to the mean flow quantities, which are understood to be averaged over space scales much larger than the characteristic turbulence macroscale.

The terms vertical flow and cross flow will be used to identify the mean flow components in the vertical and lateral directions. While these components are often referred to as "secondary" flows, this last term will be avoided since it implies quantities which are much smaller, say by an order of magnitude, than the main features of the flow. The term implies that these quantities are of "secondary" importance of perhaps negligible in the analysis, a connotation which may not be correct.

Pertinent Earlier Work

The study of three-dimensional turbulent boundary layers of course involves all of the basic concepts of turbulence as applied in one- or two-dimensional problems. Since these concepts have been extensively discussed by many authors, they will not be repeated here; however the pertinent ideas will be brought forth and discussed at the appropriate point in the analysis (4,5,6,7,8).

Suffice it to say that the basic concepts of turbulence are more or less accepted as the basis for this work. Thus, turbulence is viewed as random fluctuations in the velocity, density, and concentration fields, and it is assumed that mean values of these quantities can be found such that the averages of the fluctuations about the means equal zero. For the purposes of this study, the flow will be assumed to be incompressible and there will be no concentration variations; hence the problem reduces to one containing fluctuating pressure and velocities superimposed on a mean pressure and velocity field.

The ergodic theorem (9) is implicitly accepted in the experimental work since the expectations of quantities are obtained from time averaging rather than ensemble averaging. Since a necessary condition for ergodicity is stationarity (10), this latter concept is also involved in the experiments. Due to the nature of the experimental method and constraints, stationarity was effectively forced upon the system. The experimental outputs were also examined for stationarity. (Actually, since only mean and autocorrelation values were examined, the so-called "weak" stationarity was verified). Apparent nonstationarities were traced to extraneous causes (instrument drift, temperature cycling in the facility, etc), which could be controlled at the source.

Previous efforts to analyze the three-dimensional flow over roughness include the early work by Townsend reported in his book on turbulent shear flow (11). Since this analysis served as one of the starting points for both the experimental and analytical work in this report, it will be reviewed here. Subsequently it will be shown that several of the assumptions are not justified and must be modified for the problem at hand. Nevertheless the insight provided by Townsend's work is very useful and his basic prediction regarding the direction of cross flow is found to be correct.

Townsend began by assuming that the departure from two-dimensional flow is quite small, such as might be expected in the turbulent flow over a flat plate of finite width. (This particular example was later investigated by Elder (12), and his results will also be discussed.) Using the usual turbulent boundary layer equations, Townsend assumed that the cross flow, W, is sufficiently small that its derivatives can be neglected in the z equation, and that the set of equations can be reduced to the approximate forms

$$U\frac{\partial U}{\partial x} + V\frac{\partial U}{\partial y} + W\frac{\partial U}{\partial z} + \frac{\partial \overline{uv}}{\partial y} = \frac{-1}{\rho}\frac{\partial P}{\partial x} + \nu\,\frac{\partial^2 U}{\partial y^2} \tag{1-1}$$

$$\frac{\partial \overline{v^2}}{\partial y} = \frac{-1}{\rho}\frac{\partial P}{\partial y} \tag{1-2}$$

$$\frac{\partial \overline{vw}}{\partial y} + \frac{\partial w^2}{\partial z} = \frac{-1}{\rho}\,\frac{\partial P}{\partial z} \tag{1-3}$$

Proceeding on the basis of the above assumptions, Townsend integrated Eq. (1-2) in the y direction and Eq. (1-3) along a line in the z direction out to the free stream producing the following equations:

$$P + \rho\overline{v^2} = P \tag{1-4}$$

$$\int_z^\infty \frac{\partial \overline{vw}}{\partial y}\,dz - \overline{w^2} = \frac{P - P_o}{\rho} \tag{1-5}$$

These equations are then combined to yield

$$\int_z^\infty \frac{\partial \overline{vw}}{\partial y}\,dz = \overline{w^2} - \overline{v^2} \tag{1-6}$$

Since in general $\overline{w^2}$ is not equal to $\overline{v^2}$, especially close to the wall, Townsend concludes from Eq. (1-6) that $\overline{vw}$ cannot be zero everywhere, and that the existence of this non-zero lateral Reynolds stress implies the presence of cross flow in the boundary layer.

For a plate of finite breadth, 2D, he further estimates the magnitude of the cross flow from the expression

$$\overline{w^2} - \overline{v^2} = 2.2\ \tau_o/\rho \tag{1-7}$$

This approximate expression is based on experimental results quoted from Laufer (13) and agrees with similar values estimated from the data of Klebanoff (14). It is roughly correct only near the wall and varies as the distance from the wall is increased. In addition, the data upon which it is based was taken over relatively smooth walls, and the influence of greatly increased roughness is not known. In any case, the discussion by Townsend is not dependent on the great accuracy of the estimate represented by Eq. (1-7).

From Eqs. (1-6) and (1-7) it can be seen that the integral

$$\int_z^\infty \frac{\partial \overline{vw}}{\partial y}\, dz$$

taken over the half-width of the plate is of the order τ_o/ρ. If the non-zero values of $\partial\overline{vw}/\partial y$ were concentrated at the edge of the plate in a strip of order δ, the layer thickness, then $\partial\overline{vw}/\partial y$ would be of order $\tau_o/\delta\rho$. Townsend discounts this possibility saying that no sign of such large values has been observed. Instead, he assumes arbitrarily that the distribution of $\partial\overline{vw}/\partial y$ varies in a linear fashion from zero at the centerline to a maximum at the edge of the plate according to the relation

$$\frac{\partial \overline{vw}}{\partial y} = \left[\frac{\partial \overline{vw}}{\partial y}\right]_{z = D} \frac{z}{D} \tag{1-8}$$

Equation (1-8) is, of course, the simplest possible form consistent with the requirements of symmetry. This expression is assumed to be at least qualitatively representative of the flow mechanism, and on this assumption Townsend predicted that the stress distribution indicated in Eq. (1-8) would result in a cross flow from the centerline outward. The reasoning leading to this conclusion is not given and seems to be in error. From Eqs. (1-6) and (1-7) it can be seen that $\partial\overline{vw}/\partial y$ is greater than zero on the average. If the assumption in Eq. (1-8) is used, $\partial\overline{vw}/\partial y$ would then have to be greater than zero everywhere in the region $z > 0$. Since $\overline{vw}$ must be zero at the wall, it follows that $\overline{vw}$ must be greater than zero in some neighborhood of the wall; and if a conventional mixing length analysis is assumed, $\partial W/\partial y$ would be less than zero near the wall. With W equal to zero at the wall, this reasoning suggests that W would be less than zero in the region being considered; i.e., the cross flow would be inward not outward. Since several assumptions are involved in the discussion leading to Eqs. (1-6) and (1-8), it is not clear where the apparent inconsistency arises; however the problem is obviously open to review.

The next work reported which relates closely to this problem is that of Elder (12) in 1960. Elder's work was an experimental study of flow past a plate of finite width; and he investigated the laminar, transition, and turbulent regions of the boundary layer as it developed on the plate with particular attention to the edge effects. Therefore the configuration includes the finite plate case discussed by Townsend in his analysis and is similar in some ways to the problem under consideration.

Through study of the mean streamwise velocity distributions and through direct measurements of vorticity by a vane-type vorticity meter, Elder was able to detect "secondary" circulations in the turbulent regions near the plates. It is particularly significant that these cross flows were not detected in the laminar flow regions over the same plates; and Elder concluded that the secondary flow was very likely produced by the anisotropic Reynolds stresses in the turbulent region. The direction of the circulation was such that there was out-flow near the edge of the plate in agreement with Townsend's (stated) prediction.

From rough measurements of the flow vector inclination and from measurements of the rate of rotation of the vorticity meter, Elder was able to describe the general picture of the mean vorticity. He concluded that a large part of the vorticity was contained in circular regions centered slightly beyond the edge of the plate with diameters of the same order of magnitude as the boundary layer thickness. These regions were distributed antisymmetrically above and below the plate; hence could not be confused with lifting or "tip" vortices due to misalignment of the plate in the oncoming stream.

While Elder's measurements are subject to large experimental uncertainties and to the difficulties of interpreting the results of finite-size vane vorticity meters, the general interpretation of the flow behavior is very helpful.

Hinze (15) in 1967 examined the problem of secondary circulations resulting in flows over nonuniform roughness or in conductors of noncircular cross sections. Of the available possible equations, he preferred to examine the energy-balance or turbulent energy equation in the approximate boundary layer form

$$U_2 \frac{\partial}{\partial x_2}\left(\frac{\overline{u_i u_i}}{2}\right) + U_3 \frac{\partial}{\partial x_3}\left(\frac{\overline{u_i u_i}}{2}\right) + \frac{\partial}{\partial x_2} \overline{u_2\left(\frac{u_i u_i}{2} + \frac{p}{\rho}\right)}$$

$$+ \frac{\partial}{\partial x_3}\left[\overline{u_3\left(\frac{u_i u_i}{2} + \frac{p}{\rho}\right)}\right] = - \overline{u_2 u_1} \frac{\partial U_1}{\partial x_2} - \overline{u_3 u_1} \frac{\partial U_1}{\partial x_3}$$

$$+ \frac{\partial}{\partial x_2}\left[\overline{u_i \nu\left(\frac{\partial u_i}{\partial x_2} + \frac{\partial u_2}{\partial x_i}\right)}\right] + \frac{\partial}{\partial x_3}\left[\overline{u_i \nu\left(\frac{\partial u_i}{\partial x_3} + \frac{\partial u_3}{\partial x_i}\right)}\right] - \varepsilon$$

On the basis of experimental evidence, the viscous terms (other than the dissipation) he took to be negligible away from the wall. For similar reasons, the diffusion terms were neglected, and the remaining equation was written as

$$U_2 \frac{\partial}{\partial x_2}\left(\frac{\overline{u_i u_i}}{2}\right) + U_3 \frac{\partial}{\partial x_3}\left(\frac{\overline{u_i u_i}}{2}\right) = - \overline{u_2 u_1} \frac{\partial U_1}{\partial x_2} - \overline{u_3 u_1} \frac{\partial U_1}{\partial x_3} - \varepsilon \qquad (1\text{-}10)$$

This equation simply states that in any small region the advective transport of turbulence energy must be equal to (i.e., account for) any differences between production and dissipation in that region.

To draw further conclusions about the behavior of the secondary flows, Hinze further assumed that U_2 and U_3 may be considered to be of the same order of magnitude, while

$$\left|\frac{\partial}{\partial x_3}\left(\frac{\overline{u_i u_i}}{2}\right)\right| << \left|\frac{\partial}{\partial x_2}\left(\frac{\overline{u_i u_i}}{2}\right)\right| \qquad (1\text{-}11)$$

Therefore the second term in Eq. (1-10) may be neglected, and since

$$\frac{\partial}{\partial x_2}\left(\frac{\overline{u_i u_i}}{2}\right) < 0 \tag{1-12}$$

U_2 will be positive when local production is smaller than local dissipation and negative when production exceeds dissipation.

The implication for atmospheric flow over a city or a boundary layer flow over a patch of roughness is that there would be vertical flow toward the surface since production would exceed dissipation at least near the start of the roughness. This conclusion suggesting a downward flow over the roughness and a corresponding transverse flow from rough areas toward smoother areas agreees well with Townsend's prediction and Elder's findings.

Hinze also points out that the well-known secondary flow toward the corners of a rectangular duct along the corner bisectors may be explained in similar fashion. In this case the production would be expected to exceed dissipation in the corner as a result of the higher turbulence level due the presence of two nearby walls.

The chief limitation of Hinze's result is that only the direction of secondary flow is indicated. Its magnitude cannot be calculated nor even estimated for a given case unless detailed information is available about the dissipation, Reynolds stresses, velocity gradients, and turbulent energy gradients.

The behavior of the flow for large distances downstream from the start of the roughness was not discussed by Hinze, but will be of interest in the present study. Presumably, far downstream the production will decrease since the effective roughness will decrease even though the absolute roughness is constant. At the same time the eddies caused by the leading roughness will eventually cascade down to the dissipation range, and it is possible that the excess of production over dissipation would reverse at some point downstream.

The various efforts described above are the only attempts that have been made to investigate flows which are closely related to the problem at hand. Many other studies have been made of situations in which secondary flows are known to exist. While most of these situations are different enough to preclude direct application of any results, there are some similarities which offer useful clues suggesting possible approaches to the present problem. The lateral flows arising in conductors of noncircular cross section and the more basic problem of the flow along a corner have been considered by various investigators (references 16-21 and many others).

A variety of studies of three-dimensional flows describable in terms of two independent space coordinates were summarized in (22). While these flows cannot be directly related to the problem at hand, certain facets of their behaviors are helpful in interpreting results.

Basic theoretical studies related to edge effects include Howarth's extension (23) of the classical Rayleigh problem. Unfortunately this study is based on viscous, nonturbulent flow, hence the effects of Reynolds stress gradients are not included. Since Elder's work (12) showed that secondary flow was produced at the edge of the plate only after transition occurred, Howarth's analysis is of little help in the turbulent case.

In 1967 Joubert, Perry, and Brown reviewed the state of the affairs regarding three-dimensional turbulent boundary layers (24). At that time they identified two general lines of approach to the problem of yawed turbulent boundary layers.

(1) One approach is to concentrate study on the mean velocity profile and attempt to relate it to fundamental parameters such as shear stress, pressure distribution, fluid properties and boundary layer thickness.

(2) Another approach involves direct attack upon the main-flow and cross-flow velocity components with attempts to represent these components in suitable functional forms which can be related to the other flow parameters.

These categories of techniques are general and represent even today the basic directions of attack upon three-dimensional turbulent boundary layers. The first approach is simply an extension of two-dimensional techniques to problems which are three-dimensional. It is based on the idea that the three-dimensional effects are "secondary," i.e., at least on order of magnitude smaller than the mean flow quantities. Presumably, the cross flow influences will serve to distort the velocity profile in a manner which can be identified and defined with respect to the important engineering parameters.

The chief disadvantage of this approach is that the cross flows are not explicitly involved in the analysis and any information about them can only be inferred from the differences between the three-dimensional case and the equivalent two-dimensional case.

The second approach is in theory more likely to lead to detailed information about the three-dimensional effects although in practice the approach leads to more mathematical complexity and the need for more assumptions which may be difficult to check. Both the work of Townsend (11) and that of Hinze (15) fall into this category since the cross-flow velocity components are retained explicitly.

Within the second category, a technique which has been studied by various people involves the two-dimensional plot of the flow using the flow components W and U as coordinates or independent variables (hodograph plot). Such a representation of flow components was used originally by Gruschwitz (25) in 1935. Later workers such as Johnston (26 27) sought to formulate explicit functional forms for the hodograph; which is to say, functional relationships between W and U . Obviously, simple relationships of this type would be useful if they could be verified since cross flow behavior could then be predicted directly from the mean streamwise velocity profile. Johnston examined various sets of data including his own and proposed that the plots could be reasonably well represented by two straight lines which together with the U axis produced his now well-known triangular form for the hodograph.

Although there is no analytical justification for specific forms of the hodograph, the concept has been studied by a number of workers. Shanebrook and Hatch (28) reviewed a number of polynomial forms which had been proposed earlier and proceeded to develop more generalized forms which could represent flows with complex behaviors such as cross flow reversal. The resulting polynomial forms are used to generate numerical solutions of the momentum integral equations and have produced reasonable agreement with experimental results. Nash and Patel, in their book (4) review several variations of the technique which have been put forth in recent years.

<u>Related Two-Dimensional Works</u>

When considering the flow near the edges of roughness, it may be reasonable in many circumstances to expect that the cross flow and its effects will be comparatively small. If so, it would then follow that the flow field would resemble the analogous two-dimensional flow following an abrupt change in roughness. Analytical and experimental studies of this type have been made both in field and laboratory (29-39), and the problem has been attacked numerically (40-42, 58). While the approaches and techniques utilized by these workers vary widely, certain concepts recur throughout and are generally accepted in one form or another.

Perhaps the most basic of these ideas is the concept of an "internal" boundary layer resulting from abrupt changes in boundary conditions such as surface roughness, which can be traced back to early researchers in fluid mechanics (1). When a fully developed turbulent boundary layer encounters a change in roughness, the entire layer cannot react instantly to the new boundary condition. Instead the effect begins at the surface in the vicinity of the change and propagates outward into the ambient boundary layer. An increase in surface roughness produces an increase in surface shear stress, shear velocity, and velocity gradient near the wall which acts to increase turbulent energy production. The excess energy diffuses outward modifying the velocity and turbulence profiles. The region so influenced by the new wall condition may be viewed as a new boundary layer growing within the original developed layer. At a sufficiently large distance downstream from the discontinuity, the complete layer will approach (asymptotically) a new equilibrium condition.

There is some resemblance between the internal layer and the separation bubble or "canopy" produced at sharp corners of blunt objects in flowing streams and the two phenomena may appear simultaneously and interact. Sharp cornered roughness elements produce local separation bubbles which affect the turbulence production; however the ultimate growth of the internal layer proceeds by a different mechanism than that controlling the behavior of the canopy. Canopy flows would be heavily influenced by the corresponding potential flow and may exhibit phenomena such as reattachment downstream. The internal boundary layer, on the other hand, will never reattach and grows chiefly through turbulent energy transport and diffusion.

Elliot (29) was one of the earlier workers to attempt an analytical solution for the height of the internal boundary layer. Using a momentum integral analysis, he was able to obtain solutions for the layer height, y_i, which could be closely approximated by a very simple power law of the form

$$y_i = ax^n \tag{1-13}$$

with n nearly independent of the roughness conditions and approximately equal to 0.8. Limited experimental data available at that time agreed well with the analytical result.

An interesting feature of Elliot's result was the fact that the wind speed does not appear in Eq. (1-13), while prior experience with laminar and turbulent boundary layers on smooth plates had always shown the usual dependence of layer thickness on stream velocity. To explain this result, Elliot offered a dimensional argument built around the idea that for a rough surface, the viscous sub-layer is sufficiently destroyed to eliminate viscosity on a relevant parameter. Instead, the quantity $u_* y_o$ is taken to be the dominant characteristic of the flow; and the use of this quantity leads to a result very similar to Eq. (1-1).

Panofsky and Townsend (30) modified Elliot's theory somewhat by allowing the shear stress to vary continuously from the value at the wall to the value above the internal layer; while Elliot had assumed a constant value of stress through the internal layer. Results were better than Elliot's in some situations and not so good in others.

An observation made by Panofsky and Townsend during their discussion of experimental results is of interest in the present study. They noted that the growth of internal layers over surface roughness in the atmospheric boundary layer may proceed for a considerable distance downstream before the edge of the internal layer intersects the outer edge of the original boundary layer. On the other hand some reported experimental data involved such thin oncoming boundary layers that intersection occurred almost immediately within the first few data points, and comparative interpretation was difficult. This factor was given major consideration in designing the experiments reported later in this work; and a very thick boundary layer was sought relative to the roughness height.

Blackadar and his co-workers (31) later reported experimental data taken over changing vegetation heights which tend to confirm Panofsky and Townsend's work, particularly in regard to the need for recognizing the variation of shear stress with height above the ground. This approach was an improvement over the earlier assumption that the inner layer which is influenced by the new roughness is a constant stress layer. Introduction of a varying stress eliminated the need for a stress discontinuity to match the outer layer, and the addition of one or more free parameters (in the stress relationship) provided more flexibility in handling different physical situations.

At about the same time, Taylor (32) undertook to apply a mixing-length analysis to the same problem using a mixing length which was a function of a parameter incorporating information about the roughness height, the Coriolis parameter, and the geostrophic wind speed. While there was some question as to the correctness of the length used, numerical solutions of the resulting equations were interesting in that they showed that a very long fetch is required before a new equilibrium flow is established after a roughness change. Stated differently, the effect of a roughness change and the vestigial influence of the previous roughness persist for a considerable distance downstream. Nickerson (38) arrived at a similar result numerically finding that a fetch of 100 times the height was required for adjustment of the velocity profiles.

The same general conclusion was also reached at about the same time by Blom and Wartena (33), who used a modified form of Townsend's theory of self-preservation (38,39). (Self-preservation as defined by Townsend implies that any dependence on distance in the streamwise direction can be completely contained in suitably defined velocity and length scales, which are functions of the streamwise coordinate.)

Blom and Wartena also show the importance of determining the height of the "adapted" layer distinct from the internal boundary layer itself. The internal boundary layer is that region in which the effects of roughness change are noticeable. The adapted layer, on the other hand, is that region within the internal layer which has "adjusted" completely to the new roughness; so that the velocity profile within the adapted layer may be described by a logarithmic form. In particular, they conclude that correct evaluation of the height of the adapted layer is of importance if measured velocity profiles are to be used to determine surface shear stress or the effective roughness height, y_0 .

Yeh (35) obtained a series of measurements over a change of roughness on the floor of a wind tunnel which agreed in general terms with those mentioned above. Yeh noted that the internal layer grew downstream with a slope of 1:13 but that the changes in turbulent intensities and Reynolds stresses were confined below a "critical" surface growing with a slope of 1:25. The latter observation resembles the concept of an adjusted layer described in (33); however the interpretations of the phenomenon differed between the two works. While Blom and Wartena viewed the adjusted layer as a region which had achieved new equilibrium as evidenced by the velocity satisfying the simple logarithmic form, Yeh concluded that the differing rates of growth of the internal layer versus the "critical surface" demonstrated that the flow is not necessarily in equilibrium even after a new logarithmic profile has been achieved. The seeming inconsistency between the two viewpoints is due to the differing definitions of the regions being considered. Blom and Wartona's adapted layer is not the same as the region bounded by the critical surface in Yeh's discussion. Yeh's measurements extended only a short distance downstream from the roughness change and any true adapted region would be close to the wall and difficult to identify clearly. Distinguishing accurately between portions of experimental velocity profiles which are "logarithmic" and portions which are "almost logarithmic" is very difficult.

Yeh's work focused considerable attention on the local region near the roughness change, a region which he calls the "transitory" region and which is characterized by large accelerations of the flow and considerable distortion of the streamlines. This region is extremely complex from an analytical standpoint, and the experimental results contribute toward an understanding of that region of the flow. In particular, these results show that the transitory region extends downstream a distance of the same order as the oncoming boundary layer thickness. Beyond that distance the development of the internal layer proceeds in a more orderly fashion.

Recently, Antonia and Luxton (36, 37) have reported in detail results of extensive experiments on the subject of step changes in surface roughness. The results and conclusions presented are in many ways very similar to those of earlier workers as described above; however there are some significant differences also. The existence of an internal layer which contains the effects of the new roughness is strongly reinforced, and the fact that the external flow is unaffected except for some streamline deflection is again verified.

On the other hand, Antonia and Luxton state that readjustment of the flow to the new surface occurs rapidly within about twenty boundary layer thicknesses and that turbulence profiles become essentially self-preserving in the same distance. Since the layer thickness used in these studies was about 1.9 in. (4.83 cm) they are suggesting that readjustment is complete within about 4 ft (1.22 m) downstream, a distance much less than which would be expected from the predictions of Nickerson or Blom and Wartena. It appears that this difference is due to the relatively small boundary layer thickness used by Antonia and Luxton compared to the 1/8 in. (0.32 cm) slats comprising the roughness. If the rate of growth of the internal layer is similar to that described by Yeh or Blom and Wartena, it would reach the outer edge of the exterior boundary layer in the distance mentioned; however it does not seem likely that complete adjustment would be completed in the same distance. Intuitively, it seems that a parameter relating the exterior boundary layer thickness to the scale of the roughness change should be involved in any relationship defining the internal layer growth and that this parameter might serve to collapse the differences between the results cited. In the various analyses described, such information is incorporated only implicitly through the use of assumed logarithmic profiles of the form

$$u = u_* k^{-1} \ln (y/y_o)$$

in which the characteristic roughness length, y_o, is used to scale the profile. This relationship is actually valid only near the wall and cannot be expected to define the ratio between total layer thickness and roughness height.

The work of Antonia and Luxton is extensive and exposes many details of the flow. Their observations include the following:

1. Turbulence production and energy levels are high near the roughness.
2. Turbulence gradients are large in the internal layer.
3. Mixing and dissipation and integral lengths are much reduced in the internal layer compared to the smooth wall layer.
4. Turbulent energy diffusion is the dominant mechanism controlling internal layer growth.
5. Reynolds shear stress is not constant over the roughness, but decreases near the wall.
6. Turbulence structure in the inner layer is dominated by the roughness geometry.
7. Mean velocity profiles when plotted in the form U vs. $y^{1/2}$ exhibit two straight line portions of different slopes intersecting in the vicinity of the edge of the internal layer.

Most of these observations are not unexpected and several agree generally with earlier findings. Number 7, however, is unique with these authors and serves as a convenient way to define the edge of the internal layer. The applicability of several of these observations to the present three-dimensional problem will be examined in detail later.

Objectives of the Present Study

In light of the extensive works cited in relation to two-dimensional roughness flows, the question of three-dimensional effects follows naturally. The intent of this study is to examine the effects of having a limit or edge of the roughness in the direction lateral to the free stream.

Since complete analysis of the three-dimensional equations is impossible, and since analyses such as those of Townsend (11) and Hinze (15) are of little quantitative help, the primary thrust of this study was experimental and directed at the basic continuity and momentum equations as applied to the problem. After examining the early data, it became evident that previous analyses could be improved by utilizing the experimental results to suggest more realistic assumptions. The early results also pointed out a need for improved techniques and modifications in the data collection methods; changes which were subsequently incorporated.

Chapter II

DESCRIPTION OF EXPERIMENTS

In order to gain more insight into the effects of lateral variations in surface roughness, a wind tunnel experiment was undertaken. Availability of facilities was one factor in the design of the experiment; however several other conditions were sought deliberately to maximize the likelihood of producing useful data even though direct simulation of real atmospheric conditions had to be compromised.

Wind Tunnel

Experiments were performed at the Engineering Research Center of Colorado State University using a meteorological wind tunnel with a test section 6 ft (1.83 m) square and approximately 88 ft (26.8 m) long (see Fig. 1). The tunnel is described in reference (21) and in great detail in reference (43); however certain features are pertinent to this discussion. Perhaps the most important is the fact that a very thick boundary layer can be produced in the test section with stream speeds up to 100 fps (30.5 m/s). Boundary layers 2 ft (60 cm) thick or more are produced by tripping the flow with gravel roughness and a sawtooth strip and allowing it to develop along the test section.

A thick boundary layer is useful in studies of roughness flows. Not only is it physically more convenient to work with thick layers in terms of sensor resolution, but also there is better simulation of the atmospheric condition in which layer thickness exceeds by at least an order of magnitude the usual surface roughness heights. Thick layers also provide more room to observe the development of internal boundary layers before they diffuse to the free stream. For the purposes of this study, it was felt that a thick layer simulating the atmosphere would be essential since lateral and vertical flows were anticipated near the edges of the roughness. If such flow components are present, it is then reasonable to expect that the layer thickness relative to the roughness height will be a significant parameter. Simulation of the atmosphere in a wind tunnel is in general a complex problem and the necessary criteria have been studied extensively (44, 45).

The experiments in this study were performed with the roughness models located 50 ft (15.2 m) from the tripping strips at the entrance. At this point the boundary layer thickness was approximately in in. (46 cm) at the Reynolds numbers used while the roughness elements were 1/4 in. (0.64 cm) high. Therefore, the layer thickness was two orders of magnitude greater than the mean roughness height, and blockage effects due to the roughness were assumed to be negligible. The pressure gradient resulting from increased boundary layer growth over the roughness was eliminated by adjusting the movable ceiling in the tunnel.

Of particular importance to this study is the need to know as much as possible about the oncoming boundary layer before it encounters the roughness patch. Any unusual characteristics of the layer could be expected to produce effects in the test region which would confuse the results. The tunnel chosen had been studied extensively by Zoric (46), who determined that the boundary layer after about 25 ft (7.6 m) approached closely a condition of local similarity. Specifically, he was able to show that the layer in the tunnel could be piecewise represented by a law of the wall close to the wall and a defect law away from the wall which agreed well with experimental measurements along the test section beyond 25 ft (7.6 m). This information is very helpful since wind tunnels cannot provide the extremely long fetch needed to guarantee full development of the boundary layer, and the closeness to similarity provides one measure of the development of the layer at the test section.

While the large size of the tunnel provides certain advantages, a price is paid in that some undesirable characteristics are also magnified. Of these, the "secondary" flows or vertical and cross flow components which develop in boundary layers in noncircular conduits is the most troublesome characteristic of a tunnel of this type. Such flow components, although smaller, are similar to those resulting from the roughness model itself and represent a source of distortion in the results. True simulation of the atmospheric boundary layer would best be achieved by eliminating such components; however that condition cannot be achieved without giving up other desirable characteristics of the thick, well-developed, two-dimensional layer. Any modifications made upstream to tailor the lateral flows immediately introduce other distortions.

The alternative approach is to accept the presence of some cross flow, measure it, and attempt to correct the results and interpretations of data accordingly. In the case of this tunnel, Veenhuizen and Meroney (21) recently examined the secondary flows in detail, and their results provided a starting point for this process. Direct measurements of cross and vertical flows were also taken upstream as part of the present experiments, and the results agreed well with those of Veenhuizen and Meroney. It is felt that the condition of the oncoming boundary layer is well defined. Details of the upstream profiles will be discussed with the other results.

Another problem, one which is common to most wind tunnels, is that of skewness or lack of true two-dimensionality in the oncoming stream and boundary layer. To minimize this effect, the inlet screens were cleaned carefully and the tunnel was checked throughout for leaks. In a tunnel of this size with a variety of access doors and hatches, leaks are a major problem; yet they must all be found and eliminated, especially for studies of this type. It was discovered in preliminary checks that even small leaks upstream produced momentum jets which noticeably modified the velocity distribution and secondary flow pattern in the test section.

After all detectable leaks were corrected, the profiles of velocity and turbulence quantities in the developed boundary layer were symmetrical about the tunnel centerline to within the experimental accuracy (see Figs. 27, 35, 43, 51, 59 and 67). As can be seen, however, the profiles are not completely two-dimensional. The remaining distortion is due to the secondary circulation which transports fluid downward toward the corners along the corner bisectors and upward at the tunnel centerline. The effect is particularly noticeable in the velocity profiles (Fig. 27) where the low momentum fluid being brought up from the floor region depresses the velocity profile at the centerline. The maximums occur correspondingly near the 45° corner bisectors. The effect of the secondary circulations causes in this case a distortion of approximately seven percent in the horizontal velocity profiles.

Although the tunnel has provision for heating and/or cooling both the airstream and the floor of the test section, the tests were performed under neutral conditions. That is, the airstream was cooled to 60° F (15.5°C) to maintain constant temperature during all tests, and no temperature gradients were imposed. Cooling was accomplished by an automatically controlled refrigeration system which is capable of maintaining the mean temperature within a tolerance of ±1/2°F (% 0.3°C). There were irregular fluctuations in local temperature of about 2-5°F (1.1-2.8°C) as a result of cycling in the temperature control system and resulting surging of refrigerant through the coils. These fluctuations had periods of several seconds to about one minute and had little discernible effect on measurements except for hot-wire anemometer outputs. The variations due to temperature sensitivity of hot wires will be considered in detail in the discussion of hot-wire errors.

Tunnel air speed was monitored continuously and maintained within ±1/2 percent.

Roughness Model

The roughness used for the tests reported herein consisted of 1/4 in. (0.63 cm) high by 1 in. (2.54 cm) square blocks arranged in a checkerboard pattern (see Figs. 2, 3, and 4). The blocks rested directly on the smooth floor of the tunnel beginning at a point 50 ft (15.2 m) downstream from the tripping region. The roughness pattern was "closed" in the sense that adjacent blocks were in contact and free flow channels between individual blocks did not exist. It was felt that continuous channels among the elements might permit circulation of the fluid in a way which would confuse the results.

The roughness region was 17 in. (43 cm) wide and was centered on the tunnel floor by reference to a taut wire stretched from the mid-points of the entrance and exit regions of the overall test section.

This method of establishing the centerline was necessary since careful measurements of the flow vector direction indicated that the flow followed the mean centerline as defined above rather than the local centerline measured from the walls of the tunnel at the test region. Small deviations in the local contour of the sidewalls apparently did not affect the flow direction.

The width of the roughness model was selected after some experimentation to provide a workable size without approaching too close to the wall boundary layers. These layers were smaller than the floor layer since tripping was not used on the sidewalls. As a result the lateral space between the edge of the roughness and the wall layers was about 15 in. (38 cm) or twice the half-width of the roughness. Examination of the preliminary results showed that the influence of the roughness extended only about one half-width distance beyond the roughness at a point 15 ft (4.6 m) downstream from the leading edge. Direct interaction between the internal layer due to the roughness and the wall boundary layers was thus avoided.

Using this width, the roughness was extended downstream approximately 18 ft (5.5 m) and measurements were taken to 15 ft (4.6 m) to provide data for aspect ratios up to 10.5:1.

Instrumentation and Preliminary Calibrations

The instrumentation and the calibration procedures employed in the course of the experiments can best be described by referring to separate subsystems even though the various systems might be used together as well as singly.

Voltage Integration Technique

Early attempts at measurements of various quantities in a highly turbulent boundary lead to the realization that a reliable averaging technique would be essential if useful data were to be obtained. Fluctuations of mean values within the boundary layer were of sufficiently large magnitude and time scale that precise and repeatable measurements were difficult to obtain even with maximum damping and filtering applied to the signals. To overcome this problem a Hewlett-Packard Integrating Digital Voltmeter was used in conjunction with an electronic digital timer. A double-pole switch was used to simultaneously apply the test signal to the IDVM and a trigger signal to the timer (see Fig. 5). Returning the switch to the opposite position removed the signal input and turned off the timer. The integrated voltage could then be read together with the integration time to the nearest 0.01 seconds. Use of this system permitted averaging of signals over periods ranging from seconds to several minutes with virtually no timing error. Examination of switching transients with an oscilloscope revealed virtually no switch contact bounce and timing delay between the double switch poles of less than one millisecond.

This system was used for all measurements of mean values of fluctuating voltages. While considerable time is required to carry out repeated integrations of outputs, the results were much more satisfactory. Meaningful values were obtained in several situations where conventional measurements produced useless scatter.

Pressure Measurements

Static, total, and differential pressures were sensed by static and total head tubes and applied to a temperature-controlled capacitance transducer of an MKS Baratron pressure meter (see Fig. 6). The meter on its most sensitive range had a full scale sensitivity of 10^{-2} millimeters of mercury and a least count of 10^{-4} millimeters of mercury. DC and AC outputs were available in addition to the visual output.

Prior to use the Baratron was aligned and checked to manufacturer's specifications by the calibration shop at Colorado State University. Before and after the actual experiments, the unit was calibrated against a Dwyer "Microtector" micromanometer, which is a hook-gage type manometer with electric-contact sensing. The Dwyer values are readily repeatable to within $\pm 5 \times 10^{-4}$ in. (±0.13 mm) of water column and were corrected for temperature and gravity effects. Figures 7 and 8 show the calibration curves for the Baratron on the ranges used during the experiments. The mean error of its outputs in within the uncertainty range of the calibration process; therefore the experimental values taken from the Baratron were used without corrections.

For measurement of free-stream velocity, a 1/8 in. (3.2 mm) diameter United Sensor pitot-static tube was used. The validity of Bernoulli's equation with respect to this particular tube was verified using a whirling-arm calibrator built by Professor Virgil Sandborn at Colorado State University, and the results of the calibration are displayed in Fig. 9. Above 6 fps (1.83 m/s) the errors resulting from the use of Bernoulli's equation are within the uncertainty of the calibration, and it was assumed that the correction factor for this tube was 1.00. (The high readings obtained at speeds below 6 fps (1.83 m/s) are characteristic of total head tubes; although the reason for the error is not understood. The present experiments did not use the tube at those low speeds.)

The combination of the calibrated pitot-static tube and the Baratron instrument were used as the reference for calibration of the hot-wire anemometers and to monitor the free stream velocity continuously during the experiments. Under the test conditions, a variation of ±1 percent in free stream velocity produced a full-scale deflection of the Baratron output; hence it was a simple matter to maintain the tunnel speed within ±1/2 percent, which was the tolerance limit governed by the resolution of the speed controller.

The free stream pressure gradient was adjusted to zero by using the Baratron meter as a null instrument to measure the differential between two static tube outputs, one fixed ahead of the roughness and one movable over the roughness area. Since the outputs of the static tubes fluctuated, the DC output of the Baratron was integrated for a period of 100 seconds, a procedure which made it possible to measure and establish a zero nominal pressure gradient to within ±0.001 millimeters of mercury, which is less than ±0.2 percent of the free stream dynamic pressure at the speeds used in the tests.

Local barometric pressure was measured before and after each test run using a precision mercury barometer with integral temperature and gravity correction adjustments. The perfect-gas law assumptions were used to compute corrected air density; and before each run the dynamic pressures corresponding to the test velocities were computed. In this way the desired Reynolds number of the free stream could be established before each test.

Hot-Wire Anemometer Systems

To measure information about mean and fluctuating velocity components, hot-wire sensors were used in single-wire, yawed-wire, and x-wire configurations. The sensors used were manufactured by Thermo-Systems, Inc. utilizing 0.00015 in. (0.0038 mm) diameter tungsten wire copper plated and solder mounted. The sensing wire length was approximately 0.050 in. (1.25 mm) with a nominal resistance of 6-7 ohms. The sensors were mounted in standard TSI 1/4 in. (0.63 cm) diameter probe holders 19 in. (46 cm) long with integral BNC-type connectors for the 5-meter long probe cables.

Figure 10 shows the arrangement of the anemometer systems and signal processing units used for the experiments. The anemometers were standard DISA, type 55D01, solid-state, constant-temperature units with adjustment provisions for cable compensation, overheat ratio and bridge response characteristics. For all tests in this project, an overheat ratio of 1.45 was used.

From the anemometers the signals were lead to DISA, type 55D10 electronic linearizers and then to DISA, type 55D25 signal processing units, which were used to supply 20 kilohertz low-pass filtering to remove high frequency noise. These last units also contained separate square-wave generators which were used to supply calibration signals for adjustment of the anemometer bridge-response characteristics. Connections were provided between each unit to permit examination of the signals at each stage.

The linearizers contain analogue circuits which operate on the anemometer outputs to produce a voltage which is a linear function of the velocity. Sandborn (47) describes the theory of linearizer operation and points out the need for correct calibration of the unit if results are to reliable.

Essentially, the DISA linearizers are based upon the fact that the hot-wire anemometer output may be quite well represented by an equation of the form

$$E^2 = A + BU^n \tag{2-1}$$

in which n may be equal to 1/2 (then Eq. (2-1) is referred to as King's law) but may also vary from about 0.4 to 0.55. The linearizer operates on the anemometer signal in accordance with Eq. (2-1) to produce a linear voltage-velocity relationship of the form $E = KU$. Adjustments are available to vary the exponent, n, the intercept of the linear relationship (usually adjust to zero), and the overall gain of the system, K. Details of the adjustment procedure will be given in the section on calibration.

Correlator System

The signals after being linearized and filtered were processed through special operational amplifer units which could be used to form the instantaneous sum or difference of the voltages produced by the two anemometer systems (see Fig. 11). Originally designed by Dr. Gilbert Stegen and built in the CSU electronics shop, these units utilize high-gain operational amplifiers to perform the summing or differencing functions and provide DC blocking if desired as well as signal amplification ratios of 1, 2 or 5 (nominally). The sum-difference units were used in conjunction with the x-wire probes to study the x and y (or z) velocity components since the instantaneous voltage sum may be related to the x component of velocity and the difference to the component normal to the x direction in the plane of the cross-wire array. In each case the mean value of the signal is related to the mean value of the velocity component, while the fluctuating portion is related to the fluctuating part of the velocity component.

The mean values were measured using the integrating voltmeter technique. DISA True RMS meters were used to indicate the RMS value of the fluctuating signal, which can be related to the autocorrelations ($\overline{u^2}$, $\overline{v^2}$, or $\overline{w^2}$) of the fluctuations of the velocity components.

To obtain information about the cross-correlations between fluctuating velocity components such as $\overline{uv}$ it is possible to use RMS values of the outputs from each wire together with either the sum of the difference signal (5, 47). Alternatively, it is possible to digitize the sum and difference voltages; multiply the digitized values together point-by-point and average the results over a large number of points. Each of the techniques has advantages and disadvantages which will be discussed in the sections on calibration and error analysis; however for the purposes of this study, a variation of the latter technique was employed through the use of a Princeton Applied Research correlation function computer of "correlator." This device essentially performs the operations of digitizing, multiplication, and averaging in real time and produces results in analogue form (see reference 47 for a discussion of the correlator operation). The results may be recovered using an oscilloscope, x-y recorder, or voltmeter.

One advantage of the correlator is that it not only forms the product of the two signals but is also able to shift one signal through 100 time delay steps and form the product with the other signal for each time shift. That is, the correlator forms, in 100 discrete steps, of the function

$$c(\tau) = \lim_{t \to \infty} \frac{1}{t} \int_0^t [E_1(t')][E_2(t' - \tau)]\, dt' \qquad 0 \le \tau \le T \tag{2-2}$$

which is the cross-correlation function between the two signals, E_1 and E_2, with one signal delayed for an increment of time. Through the use of Taylor's hypothesis this function can be converted into a space correlation in the direction of the flow.

Instrument Carriage

The tunnel used is equipped with an instrument carriage riding on rails centered vertically between the floor and roof (see Fig. 3). Within the carriage are traversing motors to provide remote probe positioning control in the three coordinate directions; although only two were used in the experiments, vertical and lateral. The x-direction travel was accomplished manually since the carriage rails are not absolutely parallel to the vertical and lateral centerlines, and probe realignment was necessary after any repositioning in the x direction.

Vertical and lateral position readout is accomplished through the use of a regulated DC voltage applied to linear, ten-turn potentiometers which are geared via a rack-and-pinion arrangement to the moving parts of the carriage. The output (wiper) voltage is thus proportional to position, although the linear coefficients must be established each time the carriage is relocated by calibration at two points each in the lateral and vertical directions.

Tape Recorder

During the course of the experiments, the desired outputs were read and recorded manually; however representative data samples were also recorded on magnetic tape to provide permanent reference values for checking, verifying, and analyzing of errors. Signals recorded were the sum and difference outputs (see Fig. 11), the AC portions of the individual anemometer outputs (see Fig. 10), and an adjustable DC voltage used as a tape marker. Figure 12 shows the tape recorder and associated input circuits.

Recording was done on 1/2-inch wide tape traveling at 30 inches per second through a Sanborn model 2000 recorder. Since the recorder was limited to a one volt DC or one volt RMS AC input, it was necessary to amplify and/or attenuate the signals to within these limits while still maintaining a maximum signal-to-noise ratio. For the sum and difference signals, only attenuation was needed since the sum-difference units contained sufficient amplification capacity. In the case of the anemometer signals, it was necessary to block the DC output and then amplify the AC signal to a level suitable for recording. This procedure was necessary since the typical peak-to-peak value of the voltage fluctuation produced by the anemometer in response to turbulence is nearly an order of magnitude smaller than the DC output. Attenuating the total output sufficiently for recording reduces the fluctuating signal to a level comparable to the recording noise level.

Blocking of the DC signal was accomplished by a 1000 μF series-connected capacitor which together with the resistive load of the attenuator served as a high-pass RC filter with a rolloff frequency (3 db) of approximately 0.01 hertz.

The attenuators used were purely resistive, 10-step voltage dividers with input impedances of approximately 10,000 ohms (see Fig. 13). Amplification of the anemometer AC signals was accomplished with two Tektronix type RM 122 preamplifiers with a nominal gain factor of 100.

Impedance matching of the inputs to the tape recorder was a problem since the input impedance of the recorder is relatively low (approximately 10,000 ohms). The Tektronix amplifiers were found to be capable of driving this impedance without regulation or distortion; however the direct inputs from the attenuators in the sum-difference circuits were affected by the low recorder impedance, which appears in parallel with the selected portion of the voltage divider (Fig. 13). All attenuators were therefore calibrated in place with normal circuit loadings over a range of frequencies. The attenuation factors were found to agree well with those predicted by calculation of the circuit impedances and were found to be independent of frequency over the range from 10 hertz to 10 khz.

In addition to the preliminary calibrations and outline adjustments of the various pieces of equipment, a variety of ongoing calibration procedures were necessary during the experimentation. In many cases the nature of the calibrations relate to the accuracy limits and errors which may be expected from using the equipment; therefore these factors will be discussed together in the next section.

Chapter III

CALIBRATION PROCEDURES AND ERROR ANALYSES

In the previous chapter the basic instrumentation and sensing devices were described together with some of the preliminary calibration adjustments performed before using the systems. Although these steps establish certain conditions for the operation of the equipment, the actual errors resulting from the use of the equipment will depend on the circumstances surrounding the actual use of the devices and on the calibrations performed in the place and at the time of the experiments. The nature and magnitude of errors must directly influence the interpretation of the resulting data; hence consideration of these errors is essential even though it is recognized that it may not be possible to determine or even identify all errors precisely.

Integrating Digital Voltmeter

Errors in the voltage integration system (Fig. 5) arise from two basic sources: timing errors and errors in the calibration of the voltmeter itself including errors in the integration mode. The timing error results from operator reaction time when manually establishing the integration period and is essentially a random error. These effects were reduced to negligible levels through the use of the switching technique and electronic timer described in Chapter II and Fig. 5. The counter-timer itself was aligned and checked against Bureau of Standards time signals (WWV) in the CSU calibration shop and was checked daily against a stopwatch to detect for any gross changes or drift.

Any errors in voltmeter adjustment and calibration would introduce systematic errors while variables such as drift might introduce both systematic errors while variables such as drift might introduce both systematic and random errors. To establish reliable output, internally derived calibration voltages are provided within the instrument. These were adjusted against a secondary voltage standard in the calibration shop and were then used to zero and calibrate the instrument several times daily.

Possible errors in the integration circuitry were investigated using both constant and fluctuating inputs. For the constant input the voltage of a mercury cell was measured by integrating it for various time periods up to five minutes and comparing results to the instantaneous value obtained from a separate calibrated voltmeter. Errors in the integrated values were virtually undetectable, showing a discrepancy of less than 0.1 percent after five minutes of integration; i.e., less than one millivolt error for a 1.353 volt input.

While this result is encouraging, it does not ensure the integration accuracy when measuring a fluctuating input, a quantity which is more difficult to calibrate. To estimate the accuracy of the IDVM for fluctuating inputs, a biased sine wave was fed simultaneously into the integrating instrument, an averaging (as opposed to true RMS) voltmeter, and a digital voltmeter. A series of values was read from the last instrument and averaged to arrive at a quantity which should represent the mean value of the fluctuating signal. The outputs of all three instruments were compared for a series of runs until it was evident that the mean value of the input was in fact stationary; then the three instruments were compared. The results indicated that the accuracy of the IDVM was well within 0.5 percent, and was nearly independent of frequency up to at least 100 kilohertz.

While calibration against a sine wave input does not in general guarantee accuracy for nonsinusoidal inputs, it was felt that for storage integration circuitry such a technique should be reliable. Discrepancies should only be expected if the fluctuating inputs were to contain fourier components of much higher frequencies and/or amplitudes than those used in the calibration, i.e., signals having spikes with very short rise times. Since no such signals were anticipated, the technique was used with confidence.

As a final point it should be noted that all transducer-mean voltage calibrations were carried out on a black-box basis; which is to say that voltage outputs were recorded corresponding to known values of the measured variable. Any systematic errors remaining in voltage values would thus be consistent from calibration runs to data runs. These calibrations were repeated with sufficient frequency to detect and avoid significant errors due to drift in any part of the system.

Pressure Transducer and Baratron

The overall accuracy of the MKS Baratron pressure measurement system was established by calibration before and after the experiments as described in Chapter II. Daily checks on the system were limited to frequent checks of the zero point (bias) and full-scale adjustments provided within the instrument. The bias in the instrument is very sensitive to the operating temperature of the transducer element, which is provided with an internal heater to maintain constant temperature. However, the equilibrium temperature attained by the heating system is somewhat a function of ambient conditions, and the system was therefore subject to some drift as ambient temperatures in the laboratory fluctuated. In addition, the transducer heater is a step-input device which cycles on and off as needed resulting in a cyclic deviation of the zero point or bias of the instrument. As a result of this fluctuation, pressure measurements made at random times were subject to a random error whose maximum value could be determined by observing the zero-point excursion during the heating cycle. The amount of this maximum excursion was 0.0005 millimeters of mercury and its effect was constant over all ranges since the instrument could be used as a null device anywhere over its operating range. Thus, for pressures much above 0.05 mm.Hg., the effects were negligible but became progressively more significant below that point. For the velocity head measurements, this error was of the order of ±0.1 percent; however for the static pressure gradient measurements, this error becomes the factor establishing the limit to which the gradient can be measured and adjusted. Integration of the Baratron voltage output was necessary to achieve the desired tolerance in static pressure gradient (±0.001 mm.Hg.) since the fluctuation at that level amounts to ±50 percent of the mean value.

Anemometer System

Errors in the anemometer system may also be classed as systematic or random, but in addition may be classified as being due either to the system electronics or to the inherent characteristics of the sensor. Even though constant-temperature operation eliminates the effects of heat storage in the wire sensor and thereby causes the intrinsic time constant of the wire to be effectively zero (47), the frequency response of the system is still limited by the ability of the anemometer bridge to respond quickly enough to maintain true constant temperature. The hot-wire sensor itself is a complex transducer responding to undesirable as well as desirable physical phenomena, and the meaning of the resulting data must be considered carefully.

The DISA anemometers used have provisions for tailoring the electronic response to specific operating conditions. These provisions include direct compensation for cable reactance effects plus adjustments for bridge reactances, wire overheat ratio, and bridge response characteristics as measured by the response to an electronic pulse (square-wave) input which artifically simulates a high-frequency input from the transducer. The square-wave test does not check the total system response and more importantly provides a means of matching the bridge response characteristics of two anemometers used for x-wire measurements. By using matched cables and sensors together with the matched anemometer units, the liklihood of significant errors due to response and phase-shift problems is much reduced.

For the purposes of these tests, an overheat ratio of 1.45 was used and the anemometer responses were each adjusted to 200 khz as defined by the square-wave test procedure outlined in the DISA instructions. Once the anemometers were adjusted, the probes were left in place and the systems were left in operation continuously for the duration of the tests, day and night. Cold resistances were checked daily by turning off the anemometers briefly. By allowing the systems to operate continuously, instrument drift and variations in wire cold-resistance (at the constant tunnel temperature of 60°F) were minimized. In one case a sensor was operated for nearly two weeks, and the total change in sensor resistance was less than 1 percent. Instrument drift was minimized to the point that recalibration of the hot wires was necessary only at intervals of one and one-half to two hours.

Adjustments of the linearizer units was accomplished by trial-and-error using the wind tunnel to produce controlled air velocities. With the tunnel operating at 40 fps, a gain value was selected to produce a desired output voltage, such as 2.00 volts. The air speed was then reduced to 20 fps and the output voltage was again checked. Any deviation from linearity (1.00 volt in this case) was corrected by adjusting the exponent control and then iterating through the same steps. Once the linearity by this process was within the tolerance of the speed control on the tunnel, a series of outputs of the total system were measured for various air speeds over the range of operation anticipated. These values were plotted to detect any systematic deviation from linearity as evidenced by curvature in the voltage-velocity relationship. As the output of each wire approached linearity, an additional checking process was used involving the difference output of the sum-difference unit. At the higher velocity the gains of the linearizers were adjusted until the difference output was exactly zero; then as the velocity was decreased this same output was checked at all points. Any non-zero difference output at lower velocities was a direct measure of mismatch between the calibration curves and was used to assist in achieving close match between curves. Since a deviation from zero of ±0.001 millivolts could be detected, the sensibility of this technique was of the order of 0.1 percent.

After a satisfactory linearization of output was achieved, the calibration data was then computer-fitted to a straight line by the least-squares method using a polynomial fitting routine, no. BMDOSR, originally developed at UCLA; and the resulting line parameters (intercept and slope) were used in the reduction of the data. The computer program also provided various computed statistical parameters for the calibration data and the least-squares regression line. These computed values (listed in Table I) include the standard error of the regression coefficient (slope), the correlation coefficient between the data and the regression line, the variance due to the regression, the variance about the regression, and a computation of the F statistic (50). For this situation the F statistic is of little value since it is useful only to reject the hypothesis that the line slope is zero--a trivial step here since the data was forced to fit a sloping straight line in the linearizing procedure. The remaining parameters are useful since they provide a statistical measure of the uncertainty in the calibration results. Of particular interest is the standard error of the regression coefficient (slope) since it is that value which together with the intercept is used to reduce the data. As can be seen from Table I, the largest standard error in the data runs ultimately retained in the study was approximately three percent of the regression coefficient.

Since the DISA filter units were included in the foregoing "black box" calibration, any discrepancies from unit gain on DC signals passing through the filters were automatically accounted for in the calibration. However the effects of the filters upon AC signals needed to be verified and matched in regard to attenuation of frequencies (roll-off points) and phase shift effects particularly since cross-correlations would eventually be performed on the two outputs.

Two procedures were used to check the matching between the two filter units. First, sine waves of various frequencies were fed into each unit and the rms values of input and output were compared to determine the roll-off (3db attenuation) point for the 20 khz low-pass settings. Within the limited accuracy of this technique, the measured roll-off points agreed with the nominal setting of the filter.

As a second and more accurate check, the correlation function computer was used to examine the relative outputs of each filter channel with a common positively-biased sinusoidal signal applied to the inputs of the linearizers. By cross-correlating the output and the input and comparing the resulting cross-correlation function to the autocorrelation function of the input, the phase shift of each channel could be determined by examining the phase relationship between the correlation functions. Similarly the two outputs were cross-correlated and compared to the autocorrelations of each output to detect any differential phase shift between the two channels. A representative sample of the correlation outputs is displayed in Fig. 14. It must be remembered when examining these functions that the output wave form has been distorted by the linearization operation; hence the sine wave form has been peaked more sharply at the higher voltage peaks and has been flattened at the lower voltage valleys. (The input sine wave was biased with a positive DC voltage so that the total signal was always positive since the linearizer does not function with a negative voltage input). However, the location of the peaks is still valid for determining the overall effect on phase relationships; and as can be seen from Fig. 14, there was no detectable differential phase shift between channel 1 and channel 2. The resolution of this technique is well within $\pm 1°$.

At this point it must be recognized that the phase shift through the linearizer-filter network is also a function of the impedances of the adjacent units; i.e., the output impedance of the anemometers and the input impedance of the sum-difference units. Checking the phase-difference characteristics of the linearizer filter networks does not guarantee phase-matching for the entire system unless the adjacent impedances are identical between channel 1 and channel 2. Repetition of the above procedures with the total circuit connected and with the sinusoidal inputs applied to the anemometer bridge-input connection revealed that the phase relationship between outputs was still matched to within ±1°.

Hot-Wire Sensor Errors

The hot-wire anemometer system is subject to additional errors or distortions besides those due to the electronic system. The hot-wire sensor itself responds to various phenomena and inputs related to its nature and geometry as well as the conditions in the fluid stream being investigated. Complete understanding of all effects has not yet been achieved and some may never be fully resolved; however much progress has been made and the behavior of the sensor must be considered in the light of best available technology.

In the present work the following effects may be expected to be significant:

Fluid temperature effects
Systematic errors due to wire geometry
Errors due to improperly aligned wires
Velocity gradient effects

The influence of each of these will now be considered.

Fluid Temperature Effects

A hot-wire sensor responds both to fluid velocity and temperature (5,47) and the interrelationship of these effects has been extensively studied. In the present experiments the fluid temperature was held constant throughout calibration and data-taking to eliminate the effects of temperature fluctuations; however the cycling of the temperature control system gave rise to short term fluctuations in temperature of the order of ±4-5°F(±2.2.8°C). These variations in turn caused errors in the instantaneous velocity output of approximately ±3 percent; but all velocity values were integrated for periods of 30 seconds or longer and repeated trials indicated that the final fluctuations in integrated outputs due to temperature fluctuations were within ±1½ percent. As a result all hot-wire data reported in this study is subject to an essentially random error of ±1½ percent due to temperature fluctuation in the air stream. Errors due to long-term temperature drift are assumed to be negligible since the mean temperature was maintained within ±1°F.

Analysis of X-Wire Outputs

The fundamental analysis of a hot-wire sensor is based upon the fact that the physical mechanism involved is that of heat loss from the wire to its surroundings (5, 47). The heat loss in turn can be related to certain of the fluid properties (particularly density and temperature), to the fluid velocity, and to the wire geometry and structure. For the present case the density variations are assumed to be negligible (incompressibility assumption) and the temperature is held constant within the limitations discussed above. A given sensor, then, should respond in some way to the velocity of the air passing over it, and the problem becomes one of interpreting the relationship between the output of the sensor-anemometer system and the velocity field giving rise to that output.

The linearization and calibration process described in the preceding section serves as the starting point for this interpretation, since the process established a (linear) relationship between the velocity of the air at the sensor and the output voltage produced by the total anemometer-linearizer system. However, this relationship is valid only for the conditions existing at the point of calibration; i.e., a steady, uniform air stream encountering the sensor at a particular position and orientation. When the wire is placed in a region containing turbulence, the instantaneous velocity vector will vary widely in direction and magnitude, and all three velocity components will affect the wire output in varying amounts. It is thus necessary to relate the wire output under these conditions to the velocity components in terms of the calibration results in such a way that information about each component can be recovered. At least as many independent measurements must be taken as there are variables to be identified. The usual methods used to obtain these measurements are to operate the same sensor in a variety of orientations in the flow (yawed wires) or to operate more than one sensor simultaneously as close together as possible but at different orientations (wire arrays).

Each of the techniques mentioned has advantages and disadvantages. A single yawed wire requires only one sensor and electronic system and as a result is much easier to maintain and operate in terms of calibration, drift, matching, etc. The chief disadvantage of the technique is that repeated measurements must be taken at the same point but at different orientations to discriminate between the flow variables. Such measurements necessarily occur with some time delay between them and conditions must be closely controlled to avoid errors due to unwanted fluctuations in the system between measurement. In spite of careful control, each separate measurement introduces its own random error to influence the subsequent solution of the simultaneous equations. Small errors introduced this way into the set of (usually three) equations may give rise to much magnified errors in final results depending on the nature of the solution matrix.

The most common arrays used are the two-wire types ("x"-wires) although three-wire probes have been constructed. The advantage of an x-wire probe lies in its ability to provide simultaneous information from two sensor positions to eliminate the need for repeated measurements at one position. Its disadvantages arise from the fact that two complete electronic systems must be operated and must be matched and calibrated carefully to avoid errors due to differing characteristics. In addition the processing of the outputs gives rise to output information which is difficult to interpret.

Both techniques were used in the present tests; the x-wire to measure much of the repetitive data and the single yawed wire to provide a cross check on the x-wire results. To estimate the errors possible in the results it is necessary to examine the physical and mathematical relationships for both techniques with particular attention to the assumptions and approximations involved. Details of this analysis are given in the Appendix. Correction factors resulting from the analysis were applied to the data where appropriate.

Output System Calibrations

The devices used for data output consisted of the DISA rms meters, the Princeton correlator, and an x-y recorder to plot the output of the correlator in addition to the tape recorder. Each of these units were adjusted and calibrated in the calibration shop before usage and were then checked twice daily or more against their internal calibration sources to maintain zero point settings and full scale gain adjustments.

The x-y recorder was checked at least once daily against battery supply measured with the Hewlett-Packard integrating digital voltmeter.

At the start of each day and at the beginning of each new tape reel, the tape recording system was fed a shorted input and then a measured DC signal on each channel to provide a reference check for each tape reel. Prior to the tests, reproduction levels and roll-off points of the recorder were calibrated by recording a series of signals ranging from DC to 10 Khz on each channel and comparing the output rms values to the input values. The Tektronix preamplifier characteristics were mapped in the same way as were the CSU sum-difference units. These experimental gain factors differed significantly from the nominal values and were used in the data reduction. Each of these procedures was also repeated after the experiments were completed to ascertain that no significant change had occurred.

Carriage Effects

As stated earlier, the instrument carriage was equipped with linear, ten-turn potentiometers for position indication. Initial checks revealed that linearity of the voltage output was sufficient to guarantee positional accuracy within about three mm or about 1/64 in. For work very close to the wall in thin boundary layers, this tolerance would be too large; however it was deemed acceptable for most of the measurements performed in the present tests. The voltage outputs of the potentiometers were measured with a digital voltmeter and were calibrated daily by measuring the position of the probe centerline and the corresponding voltages at two points each in the vertical and horizontal directions. The values were checked at least twice daily although the voltage output was remarkably constant and rarely required correction.

Recalibration was necessary each time the carriage was moved in the x-direction (along the carriage rails) since the tracks were not absolutely parallel to the floor.

Since secondary flow measurements were eventually attempted, the blockage effects and flow distortion due to the carriage structure were expected to be significant. The main portion of the carriage consists of a structure about four inches (10 cm) thick spanning the tunnel at the level midway between the roof and the floor. (See Fig. 22.) The leading edge of this structure consists of a semi-cylinder with a diameter of 4.25 in. (108 cm). Probes were normally mounted on a slender boom about 3 ft (0.9 m) ahead of this main structure. The boom in turn is carried on 1.25 in. (32 mm) rods extending vertically downward from the main carriage.

The oncoming air flow can be expected to deflect downward below the structure and upward over the structure causing a vertical component of the velocity in regions above and below the carriage, which would confuse secondary flow results. To estimate this effect, a potential flow solution was constructed and free stream pressure measurements were taken to verify the solution.

The initial solution was obtained by assuming that the carriage behaves as a simple cylinder since the leading edge can be expected to dominate the effect. To account for the fixed boundaries (floor and ceiling) an infinite row of cylinders must be solved. The added or "image" cylinders are placed above and the boundaries, equally spaced and located so that the first image cylinder is the original cylinder reflected in the boundary. Such an arrangement guarantees that the vertical velocity components will vanish at the boundary and the streamline midway between the cylinders functions as the boundary.

The potential solution to this problem is available from potential flow theory (2) and is given by an infinite series corresponding to the infinite row of cylinders.

An approximation using the first three terms (i.e., three cylinders) was attempted and proved to be sufficiently accurate as determined by the residual vertical component at the wall. (The vertical velocity became equal to zero within one in. (25 mm) of the boundary.) This solution as given in (2) as

$$u = U_\infty \left\{ 1 + \frac{b^2[(y-2d)^2 - x^2]}{[x^2 + (y-2d)^2]^2} + \frac{b^2(y^2 - x^2)}{(x^2 + y^2)^2} + \frac{b^2[y+2d)^2 - x^2}{[x^2 + (y+2d]^2} \right\} \quad (3\text{-}1)$$

$$v = -2b^2 x U_\infty \left\{ \frac{y - 2d}{[x^2 + (y-2d)^2]^2} + \frac{y}{(x^2 + y^2)^2} + \frac{y + 2d}{[x^2 + (y+2d)^2]^2} \right\} \quad (3\text{-}2)$$

where b is the cylinder radius and d is the cylinder height above the floor.

Pressure distributions measured with the carriage in place were compared with the distributions predicted by the solutions and it was found that the measured values were slightly higher although the shape of the distributions agreed very well. This effect was presumed to be due to the presence of the floor and ceiling boundary layer displacement thicknesses which cause the blockage effect to be greater than in the purely potential flow case. It was found that the measured pressure distribution could be matched very closely by assuming that the effective cylinder diameter was one and one-half times larger than the actual carriage leading edge. Evidently this adjustment accounts for the increased blockage resulting from the presence of boundary layers as well as stray effects due to the smaller carriage components. Figure 23 shows the computed pressure distribution compared to the measured values. (Note in Fig. 23 that the pressure values measured <u>in the boundary layer</u> are subject to large turbulence effects, the interpretation of which is not reliable.)

This potential solution was used to predict vertical flow components resulting from the carriage effect so that secondary flow measurements in the boundary layer could be interpreted more reliably. Also, the effects upon the mean velocities were estimated from this same solution, and all values are tabulated in Table IV.

Attempted Measurements of $\overline{vw}$

The use of either a single yawed wire or an x-wire probe permits the measurement of all components of the Reynolds stress tensor except the $\overline{vw}$ term. Hinze (5) suggests that in principle it should be possible to obtain measurements of $\overline{vw}$ by using a modified x-wire probe having one wire in the x-y plane and one wire in the x-z plane, both wires being yawed to the oncoming flow within their respective planes. This probe will be referred to as a "crossplane" probe.

Such a probe was constructed on special order by Thermo-Systems, Incorporated, and a series of measurements were attempted with it.

Analysis of the output of such a probe may be carried out in the same fashion as for the x-wire probe, with appropriate adjustments for the new geometry. Calling the wire in the x-y plane number 1 and the wire in the x-z plane number 3 and using Eq. (A-14), it may be seen that

$$E_1 = S_n\left\{[(U_m + u)\cos\theta_1 + v\sin\theta_1]^2 + w^2\right\}^{1/2} + S_p(U_m + u)\sin\theta_1$$

$$- S_p\, v\cos\theta_1 \tag{3-3}$$

The wire in the x-z plane was yawed clockwise to the oncoming flow when viewed from above, hence its output may be written as

$$E_3 = S_n\left\{[(U_m + u)\cos\theta_3 + (-w)\sin\theta_3]^2 + v^2\right\}^{1/2} + S_p(U_m + u)\sin\theta_3$$

$$- S_p\,(-w)\cos\theta_3 \tag{3-4}$$

Expanding as before for the x-wire probe and retaining terms to the same order of magnitude results in the following equation for the fluctuating protion of the difference voltage:

$$e_1 - e_3 = S_n[u(\cos\theta_1 - \cos\theta_3) + v\sin\theta_1 + w\sin\theta_3]$$

$$+ S_p\, u(\sin\theta_1 - \sin\theta_3) - S_p(v\cos\theta_1 + w\cos\theta_3) \tag{3-5}$$

Assuming that the influence of the u component may be neglected if the two wire angles are nearly equal and again using the experimentally determined calibration values from the probe, it is possible to rewrite Eq. (3-5) as

$$e_i - e_3 = 0.0695\ v + 0.0516\ w \tag{3-6}$$

which, when squared, produces Eq. (3-7).

$$\overline{(e_i - e_3)^2} = (0.0695)^2\overline{v^2} + 2(0.0695)(0.0516)\overline{vw} + (0.0516)^2\overline{w^2} \tag{3-7}$$

Thus it is evident that even to the level of approximation assumed, this probe responds to a mixture of $\overline{v^2}$, $\overline{w^2}$, and $\overline{vw}$. Solving for $\overline{vw}$ produces Eq. (3-8).

$$\overline{vw} = 139.4\ \overline{(e_1 - e_3)^2} - 0.673\ \overline{v^2} - 0.371\ \overline{w^2} \tag{3-8}$$

Equation (3-8) was used to reduce the data taken with this cross plane probe; however it may be noted immediately that the level of uncertainty in values of $\overline{vw}$ will be very high. The term $\overline{vw}$ may be expected to be relatively small and must be obtained from the differences among three separate measurements of quantities which are all larger than $\overline{vw}$. In addition, the smaller magnitude of $\overline{vw}$ means that the various terms neglected in the expansions leading to Eq. (3-5) will assume greater importance and will result in much larger relative errors. Thus, while in theory it is possible to measure $\overline{vw}$ with such a probe, the results obtained were completely inconclusive.

Measurements of Vertical and Lateral Mean Flow Components

One of the features of interest in a three dimensional flow of this type is the existence of lateral and vertical mean flow components. Attempts to detect such components visually with tufts, smoke tracers, and liquid films on the floor were completely fruitless. The high turbulence level in the boundary layer near the roughness produced turbulent mixing which obliterated any visual transport effects that may have been present.

The fact that turbulent mixing effectively hides the visual effects of lateral and vertical transport by the mean flow is of course significant in itself. The implication is that the influence of the y and z components of the mean flow are much smaller than the influence of the turbulent mixing. Nevertheless, quantitative measurements would be more satisfying and were pursued.

Veenhuizen (21) had demonstrated earlier that secondary flow components in the boundary layer of this same tunnel could be measured using a yawed wire technique involving careful (and tedious) positioning and calibration of a single yawed wire. The success of his efforts suggested that it might be possible to extract similar results from an x-wire probe which is sensitive not only to the fluctuating component perpendicular to its axis as discussed earlier, but also to the mean flow component in that same direction. Just as the rms value of the fluctuating difference voltage can be related to the v or w fluctuations, so can the DC level of the difference voltage be related to mean flow components, V or W. The difficulty with this procedure lies with the fact that measuring the DC level of the difference requires processing of the complete signal from each wire (DC plus AC). The DC level of each wire is also related to the mean flow component in the x direction, which may be one or more orders of magnitude greater than the largest cross flow components. Measurement of the cross flow thus entails measuring the very small difference between two large signals. (Resolution on the order of 10 mv was required to obtain this difference. Typical individual wire voltages might be 4000 mv and 3990 mv.) While forming the difference reliably is within the capability of the operational amplifiers used, the problems of drift and proper calibration are much more imposing. However, a technique was developed which permitted measurement of the cross flows within a usable uncertainty level.

If the x-wire probe is installed in the horizontal plane, perfectly aligned with the mean flow centerline, and perfectly calibrated, then the DC difference voltage could be adjusted to be exactly zero when the cross flow W is zero. Imperfections or errors can thus arise from four sources, each of which may produce a voltage contribution to the total DC difference voltage output. Specifically, these may be identified as

E_y, difference output due to probe yaw, or misalignments, relative to the flow centerline. Yaw produces an apparent lateral flow component.

E_b, difference output due to probe bias or calibration mismatch between individual wires resulting in a non-zero difference when no cross flow is present.

E_e, difference output due to systematic errors caused by turbulence effects on the wires.

E_w, difference output actually due to the cross flow component.

The total probe DC difference output is the algebraic sum of the four voltages, and since the unwanted quantities may actually be larger than the desired quantity E_w, they must be accounted for.

The yaw output E_y may be eliminated by careful alignment of the probe to the physical mean flow centerline. This step was accomplished first each time after the carriage was moved to a new location. For a probe oriented in the horizontal plane, alignment was made relative to a taut wire stretched the length of the tunnel centerline. For the vertical plane orientation, a precision bubble level was used.

The probe bias output E_b is the most troublesome quantity since it is influenced by very slight calibration errors and by differential drift between the two anemometer systems. Effects of these factors may be better understood by referring to hypothetical calibration curves for the individual wires (see Fig. 24). While the slopes and linearity of each calibration curve can be established to within two to three percent of the mean velocity, these errors become much more significant when small DC differences are examined for cross flows. It is a simple matter of gain adjustment to shift the calibration curve of either wire to effect a match at a given mean velocity; however a change in mean velocity causes a change in the difference output due to slight curvature or non-parallelism of the wire calibration curves. In addition, adjustment to eliminate E_b must necessarily be done where E_e and E_w are both zero. Although E_e is effectively zero in the free stream, E_w, due to secondary circulations and carriage effects, is not. Thus there is no location where the probe can be adjusted to eliminate E_b, and this fact together with the unknown effects of E_e result in a voltage difference containing three unknowns.

To resolve the dilemna, it was noted that both E_b and E_e should be realatively independent of 180° rotations of the probe. E_b is entirely an electrical bias due to differences in gain adjustments for a given mean velocity and is therefore independent of any probe rotations. E_e is the effect of mean square voltages due to turbulent fluctuations at a point which adds to the DC output of each wire. Since the effect is due to a squared fluctuation, it can be assumed that the effect is largely unchanged by a 180° rotation of the probe. The cross flow voltage E_w is however reversed in sign by a 180° rotation; hence the outputs for two probe orientations differing by 180° of rotation in a plane perpendicular to the mean flow centerline may be written as

$$\begin{aligned} E &= (E_b + E_e) + E_w \\ E &= (E_b + E_e) - E_w \end{aligned} \tag{3-9}$$

Therefore the cross flow may be recovered by measuring the DC difference outputs at two orientations and taking one-half the difference between them. With this technique it is not necessary that the wires be perfectly matched; i.e., that E_b be exactly zero. Drift effects are minimized since the two measurements may be taken within a few minutes and the error will be the amount of differential drift (change in E_b) occurring between the first and second measurement. This drift effect is not insignificant since a very reasonable drift of 0.1 percent in the mean velocity calibration curves produces variations of one percent in the largest cross flow values. Since the cross flows may pass through zero at some points, relative errors become very large. (Fortunately the <u>sensitivities</u>, S_u and S_v, of the wires are related to the slopes of the calibration curves which remain relatively constant during the drifting process.)

Although E_b and E_e vary greatly from point to point in the boundary layer, the quantity $E_b + E_e$ is automatically redetermined at each point of measurement. As can be seen, the sum of the two measured outputs is equal to twice the sum of $E_b + E_e$; hence this quantity can be monitored. Repeated pairs of measurements at a given point give an indication of drift since E_e is presumably constant at a point. Fluctuations in the various quantities including the cross flow itself were accounted for by integrating the outputs over periods of one minute or more. Measurements of vertical flow components were obtained in a similar fashion, using the probe in a vertical plane. The effect of the carriage in deflecting the flow downward was readily noticeable; therefore the carriage potential solution was used to correct the vertical component results. Of course the procedure of linearly superimposing the potential solution and the measured boundary layer results is questionable; however it was felt that this procedure should give at least a reasonable estimate of the vertical flow components.

Chapter IV

EXPERIMENTAL RESULTS AND OBSERVATIONS

Early results in some ways followed trends which might be expected intuitively; however there were certain characteristics which were unexpected. Figure 68, for example, shows the lateral profile of $\overline{uw}$ in the region over the roughness two feet downstream from the leading edge. Over the roughness the profile is nearly two-dimensional, i.e., independent of z. The transition from this two-dimensional region over the roughness to the two-dimensional region outside the roughness is accomplished abruptly in a relatively narrow strip which is essentially a vertically-oriented shear plane. Within this shear plane, turbulence quantities rise to values which are significantly greater than those in the region over the roughness. Peak values of quantities in the shear layer were deliberately sought out by ovserving rms outputs during traversing.

Greater retardation of the flow and higher turbulence levels are expected over the roughness. The abrupt changes in the z direction, however, are interesting in that the abruptness persists downstream, and similar patterns are found 15 feet (4.6 m) from the leading edge (see Figs. 70 and 72). Recent work (57) examining flows over multiple strips of roughness have reported a periodic but less abrupt variation of flow quantities in the z direction. Townsend (11) in his work assumed a linear variation of $\overline{vw}$ in the z direction from the center-line of the roughness--a logical but now questionable assumption in the light of these results.

Variations in vertical planes parallel to the flow were much as expected and the existence of an internal boundary layer was readily observed from vertical profiles of velocity and turbulence quantities. A picture of the flow thus emerged consisting of a nearly two-dimensional region over the roughness bounded by vertical shear layers in the region of the edges of the roughness (see Figs. 25 and 26). As the flow progresses downstream, the internal layer diffuses upward into the exterior boundary layer while the edge shear layers diffuse laterally into the internal and surrounding exterior boundary layer.

The model suggested here and depicted in Fig. 26 is approximate since the regions and boundaries between them are not so sharply defined and other influences such as lateral and vertical velocity components are not represented; however it is helpful to visualize this model when examining the detailed results.

Experimental Results

Figure 25 shows the coordinate system used for all measurements and discussion in this report. The x-, y- and x- coordinates were measured from the leading edge, floor, and roughness centerline, respectively. Since most data was taken over the half of the roughness nearest the tunnel windows (see Fig. 3), the z- coordinate is negative for most values.

Table III contains a listing of final velocity and turbulence data measured at distances of 2, 4, 7, 9, 11, 13, and 15 feet (0.6, 1.2, 2.1, 2.7, 3.4, 4.0, and 4.6 m) from the leading edge of the roughness as well as upstream a distance of three feet (0.9 m) from the leading edge. The data in Table III was measured with an x-wire probe calibrated and corrected according to the discussion in Chapter III.

Since the x-wire array can measure only $\overline{u^2}$, $\overline{v^2}$ and $\overline{uv}$ in the vertical position, each traverse was repeated with the wire in the horizontal position to obtain values of $\overline{w^2}$ and $\overline{uw}$ as well as duplicate values of $\overline{u^2}$ to be compared with those obtained from vertical measurements. In addition, mean velocity measurements can be taken with the wires in either position, and a number of velocity values were measured both ways at a given location. These repeated data values provide one measure of repeatability as well as an indication of errors due to turbulence and velocity gradient effect. Those values which were corrected according to Eq. (A-51) were compared to the uncorrected values and it was found that the use of Eq. (A-51) reduced the systematic errors due to turbulence. Since the velocity values also contain random errors, comparison of these repeated data points had to be done statistically. Among the data in Table III, there are 82 repeated points; hence the sample size is adequate to be significant. Presumably, if there are no systematic differences between velocity values obtained from vertically versus horizontally oriented probes, then the algebraic differences

$$\text{difference} = (\text{velocity})_{\substack{\text{measured}\\ \text{vertically}}} - (\text{velocity})_{\substack{\text{measured}\\ \text{horizontally}}}$$

should have an average value of zero. An average greater than zero would indicate that the vertical probe reports a higher velocity than the horizontal probe while the reverse would be true for an average less than zero. A summary of computations for the differences so defined is as follows:

	Mean value of differences	Standard deviation of differences
Uncorrected data	+ 0.195 fps	0.550 fps
Corrected data	+ 0.091 fps	0.545 fps

From these results it is evident that a vertical probe tends to report a higher velocity than a horizontal probe. This result is reasonable since, according to Eq. (A-51), a vertical probe is influenced primarily by $\overline{w^2}$ while a horizontal probe is influenced by $\overline{v^2}$, which is smaller than $\overline{w^2}$ in most regions. Correction of the data by Eq. (A-51) is seen to reduce the systematic discrepancy between values. (This comparison, of course, does not guarantee the accuracy of either value.)

The standard deviation of the differences, which can be interpreted as a measure of the scatter or uncertainty in the velocity data, is nearly unchanged by the correction process, as might be expected. The value of 0.545 fps is about 1.3 percent of the free stream velocity and about three percent of the measured velocities near the roughness. Since 95 percent of the differences should fall within two standard deviations, the uncertainty is about ±2.6 percent in the outer levels of the boundary layer and about ±6 percent near the wall for all but a few data values. These values compare well with the discussion in Chapter III where it was pointed out that a scatter of ±1½ percent in measured free stream velocities occurred due to temperature fluctuations. If the additional calibration uncertainty is added, the value of ±2.6 percent seen here is consistent with those earlier results.

Another factor to be considered when examining the mean velocity data would be the influence of the carriage. However, a computation of the velocity perturbations using the potential solution described in Chapter III (see Table IV) revealed that the maximum effect is approximately 0.14 percent of the free stream velocity and may be neglected. It can be noted however that the effect of the carriage in the potential solution is to increase the mean velocity below y = 16 in. (41 cm) and to decrease it above that point.

The possibility of systematic errors due to turbulence but not accounted for in the foregoing discussions still remains since turbulence could affect the heat transfer in both positions. Some cross checks were performed using the pitot tube directly with good results; and since the pitot tube is influenced by turbulence in a different way, such agreement suggests that the undetermined effects are minimal.

Interpretation of the data is facilitated by reducing it to graphical form; therefore plots of the velocity and turbulence results from Table III are presented in Figs. 27 through 74. Examination of these graphs underscores the difficulty involved in adequately mapping a complex, three-dimensional flow field. In spite of the very large number of data points obtained, there can still be found regions where more dense data fields would be very helpful.

The data is plotted in groupings according to the following order: velocities, $\overline{u^2}$, $\overline{v^2}$, $\overline{w^2}$, $\overline{uv}$, and $\overline{uw}$. Within each grouping are horizontal profiles (in the z direction), vertical profiles taken along the flow centerline (z = 0), and vertical profiles taken near the edge of the roughness (z = -8.5 in. or -21.6 cm). All points plotted in Figs. 27 through 74 are data points; i.e., there are no interpolated points shown.

As can be seen from these graphs and Table III, most of the data were obtained by taking horizontal traverses of the flow field at several heights above the surface until a level was reached where the influence of the roughness was not readily noticeable. The two vertical profiles at each x station were taken to aid in interpolation and to provide accurate vertical reference profiles.

Figure 27 depicts two horizontal velocity profiles taken three ft (0.9 m) upstream from the beginning of the roughness, and these profiles show clearly the influence of the secondary flows in the oncoming boundary layer discussed earlier in Chapter III. Depression of the profiles at the center of the tunnel results from low momentum fluid being transported upward by the secondary circulation.

The effects felt by the boundary layer upon encountering the roughness are sharply noticeable in the horizontal velocity profiles given in Figs. 28 through 32. Of particular interest is the edge region in which the transition occurs from the region affected by the roughness to the undisturbed flow. As x = 2 ft (0.6 m) this transition region extends about 1 in. (25 mm) over the roughness field and a similar distance into the region over the smooth floor. Farther downstream the influence of the roughness has penetrated farther upward into the boundary layer; however the abruptness of the edge region is preserved even at x = 15 ft (4.6 m)(Fig. 32). In fact, the sharp "corner" in the velocity profiles at z = -7.50 in. (19 cm) occurs at almost exactly the same point at 2 ft (0.6 m) and at 15 ft (4.6 m). To the left of the roughness edge, however, the influence of the roughness does propagate to the left into the undisturbed layer, and a retardation of the velocity near the wall at x = 15 ft (4.6 m) can be discerned beyond a = -15 in. (-38 cm) versus -11 in. (-28 cm) at x - 2 ft (0.6 m).

In total, then, the edge effect seems to propagate outward at a noticeable rate, but it does not appear to propagate into the region above the roughness. As a result, the horizontal velocity profiles above the roughness have much the same general form at all distances downstream. In this region the chief effect of moving downstream is that the retardation of the flow progresses upward into the boundary layer. In a broad sense it can be said that the existence of an edge itself does not significantly alter the velocity profiles over the roughness except in the immediate vicinity of that edge regardless of the distance downstream.

Figures 33 and 34 contain the vertical velocity profiles at the centerline of the flow ($z = 0$) and near the edge of the roughness. Since the profiles are plotted with offset origins for clarity, the upward propagation of the internal boundary layer is not directly obvious; however by superimposing the undisturbed profile ($x = -3$ ft) upon succeeding profiles the development of the internal layer may be readily traced. The dotted line shows the approximate development of this layer; however its location is subject to considerable uncertainty due to scatter in the data and the difficulty involved in detecting the point where the profiles diverge.

In similar fashion the horizontal profiles of $\sqrt{\overline{u^2}}$ are shown in Figs. 35 through 40 and vertical profiles are presented in Figs. 41 and 42 for centerline and edge regions respectively. It should be noted that the profiles closest to the wall in Figs. 36 and 37 have been offset for clarity, for these are the profiles which show the greatest differences between a horizontally and a vertically-oriented probe as discussed in Chapter III.

Of interest in Figs. 36 through 40 are the edge regions with peak values of $\sqrt{\overline{u^2}}$ near $z = -7.50$ in. (19 cm) or about 1 in. (25 mm) inside the edge of the roughness. Comparing the locations of these peaks to the velocity profiles it may be seen that the level of this turbulent component is greatest at the point where the slope of the horizontal velocity profile is the greatest. This fact suggests that turbulent production results from the shearing action in the edge region, as might be expected and this production adds to that resulting from the roughness itself.

Unlike the behavior of the velocity profiles, the larger levels of turbulence in the edge region do not appear to affect the regions away from the edge. Even at 15 ft (4.6 m) the shape of the turbulence profile closest to the wall does not show any lateral diffusion of turbulent energy away from the edge region. In fact the profiles closest to the wall at 2 ft (0.6 m) and 15 ft (4.6 m) are virtually identical when allowance is made for the slight difference in vertical height.

Vertical propagation of the internal boundary layer is again noticeable if the curves in Figs. 41 and 42 are superimposed; although the uncertainty is even greater than when using the velocity profiles.

In the next series of figures, numbered 43 through 50, the vertical turbulence component $\sqrt{\overline{v^2}}$ is presented. The general pattern of this component is similar to $\sqrt{\overline{u^2}}$ with a peaking about one in. inside the edge of the roughness which persists downstream but does not appear to diffuse laterally. Again the distribution of this quantity is remarkably independent of z except in the immediate neighborhood of the edge.

The vertical distributions in Figs. 49 and 50 also provide an indication of internal layer growth if the upstream profile is superimposed on succeeding profiles; although the accuracy is no better than with the velocity or $\sqrt{\overline{u^2}}$ profiles.

Very similar observations may be made in regard to the profiles of $\overline{w^2}$ in Figs. 51 through 58. It may be noted, however, that the lateral fluctuations, w, are everywhere larger than the corresponding vertical fluctuations, v, as might be expected in a nonisotropic turbulence field near a wall. The Reynolds stress quantity, $\overline{uv}$, is plotted in Figs. 59 through 66. The horizontal profiles have much the same form as the other quantities, and again there seems to be very little spreading of the edge effect. On the other hand, the vertical profiles, which have been plotted with offsets in Figs. 65 and 66, display abrupt changes in slope at heights above the wall which increase with x. These points, which might be taken as the upper limit of the internal layer, are quite distinct up to x = 7 ft (2.1 m); and the point at 15 ft (4.6 m) is also distinguishable although not so clearly.

The $\overline{uw}$ profiles in Figs. 67 through 74 are particularly interesting since $\overline{uw}$ will normally be zero in a flow which is independent of z but may be expected to be non-zero in the present case wherever $\frac{\partial \overline{u}}{\partial z} \neq 0$. It may be noted, for example in Fig. 68, that $\overline{uw}$ is nearly zero over the roughness and away from the roughness wherever $\frac{\partial \overline{u}}{\partial z} \simeq 0$. In the edge or shear layer region $\overline{uw}$ attains values which are comparable in magnitude to $\overline{uv}$; and furthermore the values of $\overline{uw}$ are positive where $\frac{\partial \overline{u}}{\partial z} < 0$ a fact which would be in agreement with conventional eddy-viscosity postulates.

Measurements of the lateral mean flow component, W, are listed in Table V, while values of the vertical component, V, are given in Table VI. The values are very small relative to other quantities and the uncertainties are large; hence detailed surveys of all regions were not attempted. Representative values were obtained at x = -3, 7, and 15 ft (-0.9, 2.1, and 4.6 m).

In Tables V and VI, four quantities are listed for comparison with and in relation to the discussion of cross flow measurement techniques in Chapter III. The "corrected velocity" values represent the final values obtained using the probe yaw-calibration factors. The "velocity" values are the raw reduced values using the mean flow calibration factors and assuming that $S_v/S_u = 1.000$. The terms "mean" and "bias" voltages are arbitrary designations and refer to the values obtained by taking one-half of the difference and one-half of the sum of the probe outputs in two positions 180° apart. (See Eqs. 3-9 and the discussion following.)

The mean voltage is the value from which the cross flow velocity, is derived. The bias voltage is a measure of the quantity $(E_b + E_e)$ from Eq. (3-9) and it is listed since changes in this value from point to point give an indication of the rate of instrument drift coupled with turbulence effects. It will be noted that successive values do not change greatly. The occasional large step changes were the result of deliberate readjustments of the zero points on the linearizers in an effort to keep the bias voltage near zero.

Figures 75, 76, and 77 are maps of the cross flow data at x = -3,7, and 15 ft (-0.9, 2.1, and 4.6 m), respectively. Several comments may be made in reference to this data.

Upstream from the roughness at x = -3 ft or -0.9 m (Fig. 75), the crossflow near the floor tends to be inward toward the centerline. It can also be seen that the pattern is not symmetrical but is skewed to the right near the floor. Higher in the boundary layer, which is about 15 in. (38 cm) thick at this point, the flow is outward and skewed to the left.

The maximum value of W is about 0.7 - 0.8 percent of the mean flow velocity, a value which is remarkably similar to the values reported by Veenhuizen (21) for the same tunnel. Although Veenhuizen also found asymmetry in the secondary flow and generally similar patterns of inflow near the floor with outflow in the corner bisector region, the details of his patterns differ somewhat from the present results. Much of the difference may be due to the fact that Veenhuizen used tripping roughness on all four walls of the entrance region to achieve quadrilateral symmetry. In the present tests, only the entrance floor was roughened--the walls were left smooth to minimize the wall boundary layers and keep them away from the test surface.

It must be recognized from these results that the oncoming boundary layer already contains cross flow and vertical flow components as well as asymmetries of the form and amounts depicted in Fig. 75.

Moving to the limited data at x = 7 ft or 2.1 m (Fig. 76), it can be seen that the cross flow is beginning to reverse near the floor, so that the inflow is changing to outflow. At x = 15 ft or 4.6 m (Fig. 77) an outflow has developed with a maximum magnitude of about 1.5 percent of the free stream velocity.

It is interesting to note that there is a vestigial region of inflow noticeable about 4 in. (10 cm) above the floor. Also, the skewness to the right introduced by the oncoming flow persists even at 15 ft (4.6 m) along the roughness as evidenced by the vanishing of the cross flow off-center near z = +4 in. (10 cm).

In view of these results, the diagram of model of the flow depicted in Fig. 26 may be modified slightly by including an outward flow pattern near the floor. The data of Fig. 77 suggests that this cross flow decreases rapidly away from the floor and there is no obvious inflow farther from the floor within the range of the data.

The outflow over the roughness requires that mass be supplied to the region over the roughness to satisfy continuity. In a two-dimensional problem, the outflow would imply a corresponding downflow within the internal boundary layer; however in a three-dimensional flow a second possibility exists. Mass may also be supplied by convection if, over an increment of length in the x direction, the amount of mass arriving from upstream exceeds the amount leaving downstream.

Some measurements of V, the mean flow component in the vertical direction, were taken by the same technique used for W, and the results are listed in Table VI. Data was obtained for the upstream boundary layer at x = -3 ft (-0.9 m) and over the roughness at x = 15 ft (4.6 m); and these sets of values are plotted in Figs. 78 and 79, respectively. For all values of V in Table VI, the corrected velocity includes a correction for the carriage effect obtained by using the potential solution described in Chapter III. Although the vertical component is rather minuscule throughout much of the flow field, some noticeable effects may be detected. The region near z = 4 in. (10 cm) is of particular interest, because it is a region of slight upflow ahead of the roughness (Fig. 78), while in the same region over the roughness at x = 15 ft (Fig. 79) there is a noticeable downflow. Referring again to Fig 77, it can be seen that this region corresponds to the locus of zero cross flow. To the left and to the right of this region in Fig. 79

can be detected regions of slight upflow (near z = -8 in. (-20 cm) and z = + 20 in. (51 cm)), and the skewness to the right is again evident. The values of vertical velocity nearest the floor at x = 15 ft (4.6 m) are uniformly downward in the region corresponding to that of strongest outflow. Allowing for the displacement of the flow pattern to the right, it can be seen that the total downflow region is approximately the same width as the roughness pattern.

These results are most interesting since they agree with the qualitative predictions of Townsend (11) and Hinze (15) discussed in Chapter I. The data values herein provide a reasonable estimate of the magnitudes and distributions of these flow components, and it may immediately be seen that the effect upon the mean flow vector is indeed small. As an example, the largest cross flow, which is measured at y = 0.56 in. (1.4 cm) or about 0.3 in. (0.8cm) above the tops of the roughness elements, is about 0.5 fps (0.15 m/s). The mean velocity at that point is about 15-16 fps (4.6-4.9 m/s); hence the flow vector is deflected less than two degrees.

Examinations of the gradients of W provide one possible reason why attempts to measure $\overline{vw}$ were fruitless. The largest value of $\partial W/\partial y$ is of the order of 8 fps/ft (8 m/s/m), which is at least an order of magnitude smaller than typical values of $\partial U/\partial y$. If it is assumed that an eddy-viscosity model is even crudely appropriate to describe the relationship between $\overline{vw}$ and $\partial W/\partial y$, and if it is further assumed that such eddy viscosity would be the same quantity used to analyze $\overline{uv}$ in terms of $\partial \overline{U}/\partial y$, then the maximum value of $\overline{vw}$ would be at least an order of magnitude smaller than the larger values of $\overline{uv}$.

It should be noted that the value of W must become zero at the wall (actually at the surface of the roughness elements), and there must be a larger gradient of W below the last data points. However, that region falls within one roughness height from the tops of the roughness elements, and the flow in that region can be expected to be dominated by local effects of individual elements.

Chapter V

ANALYSIS OF RESULTS

It has been observed (see Fig. 26) that the flow field may be regarded as having several distinguishable regions within which the conditions may be consistent; yet there are significant differences when comparing one region to another. Therefore it is necessary to examine each region individually if justifiable simplifications of the equations are to be made. The conventional three-dimensional boundary layer approximations do not apply uniformly and must be modified according to the conditions prevailing in each region--conditions which may be inferred from the experimental results.

In Fig. 26 four regions have been delineated and numbered for reference taking into account the symmetry about the vertical center plane of the flow. Region I consists of the turbulent boundary layer sufficiently far from the roughness edge that roughness effects are of second order or smaller. To the first order of approximation, this region consists of the undisturbed boundary layer, and for large values of $|z|$, the influence of the roughness strip will approach zero. The upper and lower boundaries of Region I are the free stream and the smooth wall respectively. As the roughness edge is approached, Region I must at some point match Region IV up to the height of the inner boundary layer and Region II from that point up to the free stream.

Region II consists of that portion of the boundary layer over the roughness and above the inner layer; i.e., above Regions III and IV. To the first order of approximation, Region II consists of that part of the original boundary layer which has not yet been affected by the growth of the internal layer even though it is above the roughness.

The lower boundary of Region II is the upper limit of penetration of the inner layer, and Region II extends to the free stream. The lateral boundaries of this region blend smoothly with Region I; in fact, if it were not for secondary effects such as cross and vertical flows and displacements due to growth of the inner layer, there would be no distinguishable changes at the interface between Regions I and II.

Regions III and IV constitute the inner layer and contain the effects of the roughness which are significant even to first order analysis. Region III is marked by flow quantities which are relatively independent of z; while Region IV contains gradients in the z direction which are of the same order of magnitude as the y gradients. Except for second-order effects, Region III behaves much like a flow over a two-dimensional step change in roughness, with the lower boundary being the roughened surface and the upper boundary being the top of the internal boundary layer, which increases in height with increasing x.

Region IV is quite narrow in the z direction, extending only a short distance each side of the edge. It serves as the region of adjustment between III and I. The lower boundary of Region IV is complex since it contains a large step change in surface roughness in the z direction as well as a small step change in mean surface elevation due to the roughness elements. Region IV is three-dimensional in the broadest sense with significant dependence on all three coordinate directions.

In passing it should be noted that the leading edge section of the roughness $(x = 0)$ is avoided in this analysis since it contains even more complex features. Sections of the flow near the leading edge corners will contain gradients of the same order of magnitude in all three coordinate directions; hence only the complete set of equations with all terms retained would be valid.

With the four regions identified, the momentum equations can be examined for each, with subscripts used to identify the regions. The general form of the equations assuming incompressibility and steady flow would be

Continuity:

$$\frac{\partial U}{\partial x} + \frac{\partial V}{\partial y} + \frac{\partial W}{\partial z} = 0 \tag{5-1}$$

Momentum:

$$\begin{aligned} U \frac{\partial U}{\partial x} + V \frac{\partial U}{\partial y} + W \frac{\partial U}{\partial z} + \frac{\partial \overline{u^2}}{\partial x} + \frac{\partial \overline{uv}}{\partial y} + \frac{\partial \overline{uw}}{\partial z} \\ = - \frac{1}{\rho} \frac{\partial P}{\partial x} + \nu \left(\frac{\partial^2 U}{\partial x^2} + \frac{\partial^2 U}{\partial y^2} + \frac{\partial^2 U}{\partial z^2} \right) \end{aligned} \tag{5-2}$$

$$\begin{aligned} U \frac{\partial V}{\partial x} + V \frac{\partial V}{\partial y} + W \frac{\partial V}{\partial z} + \frac{\partial \overline{uv}}{\partial x} + \frac{\partial \overline{v^2}}{\partial y} + \frac{\partial \overline{vw}}{\partial z} \\ = - \frac{1}{\rho} \frac{\partial P}{\partial y} + \nu \left(\frac{\partial^2 V}{\partial x^2} + \frac{\partial^2 V}{\partial y^2} + \frac{\partial^2 V}{\partial z^2} \right) \end{aligned} \tag{5-3}$$

$$\begin{aligned} U \frac{\partial W}{\partial x} + V \frac{\partial W}{\partial y} + W \frac{\partial W}{\partial z} + \frac{\partial \overline{uw}}{\partial x} + \frac{\partial \overline{vw}}{\partial y} + \frac{\partial \overline{w^2}}{\partial z} \\ = - \frac{1}{\rho} \frac{\partial P}{\partial z} + \nu \left(\frac{\partial^2 W}{\partial x^2} + \frac{\partial^2 W}{\partial y^2} + \frac{\partial^2 W}{\partial z^2} \right) \end{aligned} \tag{5-4}$$

Simplification of these equations must now be done by referring to the known properties of the flow and the experimental values. Attention will be focused upon the flow field away from the leading edge of the roughness recognizing that the assumptions proposed may not be valid there. A key factor in the following analysis is the conclusions to be drawn about the flow components V and W. Referring to the velocity maps in Figs. 75 through 79 and making due allowances for the oncoming secondary flows and the flow skewness in the tunnel discussed in Chapter IV, it may be concluded that the influence of the roughness upon V and W is twofold. First, an outflow (W) is produced near the roughened surface. Second, a corresponding downflow (V) exists over the roughness in contrast to the usual upward flow which exists in two-dimensional boundary layers.

Region I

In Region I several terms may be neglected on the basis of the above discussion and the data. The curvature (viscous) terms are neglected except for the y term in the x equation. Comparison of Figs. 36 and 40 reveals very little change of $\overline{u^2}$ in the x direction, and on this basis the term $\frac{\partial \overline{u^2}}{\partial x}$ is neglected. Since there is a discernable z gradient of U, in the data, and W is non-zero near the boundary of Regions I and IV, the convective terms involving these quantities are retained at this time. The $\overline{uw}$ term is neglected even though $\frac{\partial \overline{uw}}{\partial z} \neq 0$ near the wall (see Figs. 69, 70, 72) since its magnitude is at least an order less than the other terms. With the pressure term retained, the x equation becomes

$$\left[U \frac{\partial U}{\partial x} + V \frac{\partial U}{\partial y} + W \frac{\partial U}{\partial z} + \frac{\partial \overline{uv}}{\partial y} = -\frac{1}{\rho}\frac{\partial P}{\partial x} + \nu \frac{\partial^2 U}{\partial y^2}\right]_I \tag{5-5}$$

When considering the y equation, the data must be used to estimate the order of magnitude of the terms. On that basis it is possible to neglect the convective terms and the $\overline{uv}$ term. Although $\overline{vw}$ measurements were quantitatively inconclusive, they do suggest an upper bound for this quantity which would make it negligible compared to the $\overline{v^2}$ term. (In addition the other terms in the Reynolds stress tensor exhibit no large z gradients; and this fact together with the fact that W is relatively small would suggest, from eddy viscosity arguments, that $\overline{vw}$ is negligible. In any case, varies only slowly with z; hence $\frac{\partial \overline{vw}}{\partial z}$ will also be small.) With viscous terms neglected, the y equation then becomes

$$\left[\frac{\partial \overline{v^2}}{\partial y} = -\frac{1}{\rho}\frac{\partial P}{\partial y}\right]_I \tag{5-6}$$

This equation may be integrated to form

$$[P(x,y,z) + \rho\overline{v^2}(x,y,z)]_I = P_o \tag{5-7}$$

where P_o is the uniform pressure outside the boundary layer.

The behavior of the terms in the z equation is more difficult to analyze since all of the terms are small; however the data can again be used to establish estimates of the largest likely values of the terms. When this step is done, the results show that the convective and Reynolds stress terms (except $\frac{\partial \overline{vw}}{\partial y}$) are remarkably similar in magnitude. Thus the z equation in total is one order of magnitude smaller than the z equation and if retained at all must be in the form

$$\left[U\frac{\partial W}{\partial x} + V\frac{\partial W}{\partial y} + W\frac{\partial W}{\partial z} + \frac{\partial \overline{uw}}{\partial x} + \frac{\partial \overline{w^2}}{\partial z} = -\frac{1}{\rho}\frac{\partial P}{\partial z}\right]_I \tag{5-8}$$

The continuity equation must be retained in total, and Region I is thus represented by Eqs. (5-1),(5-5),(5-7), and (5-8). The momentum transport in the lateral (z) direction away from the roughness is seen to be a complex process described by Eq. (5-8), which is of higher order than the x or y equations. Physically this result is apparent from the fact that the influence of the roughness upon Region I is relatively small even at 15 ft (4.6 m) downstream.

Region II

Region II would be identical with the corresponding portion of the upstream boundary layer except that the vertical mean motion has been perturbed by the roughness. Instead of an upward motion normally seen in a growing boundary layer, there is now a downward motion. The momentum and mass conservation equations in this region may be approximated by the forms

$$[U \frac{\partial U}{\partial x} + V \frac{\partial U}{\partial y} + \frac{\partial \overline{uv}}{\partial y}]_{II} = 0 \tag{5-9}$$

$$[P(x,y) + \rho\overline{v^2}(x,y)]_{II} = P_o \tag{5-10}$$

$$[\frac{\partial U}{\partial x} + \frac{\partial V}{\partial y}]_{II} = 0 \tag{5-11}$$

Since $\overline{v^2}$ is small throughout Region II and varies little in the x direction, the pressure throughout this region is nearly constant; therefore the impressed pressure on Regions III and IV is nearly constant.

Region III

Perhaps the most surprising aspect of Region III is the lack of dependence upon z, a fact which makes it possible to neglect the z derivatives in the x momentum equation. The data also indicates that the $\overline{u^2}$ term may also be neglected leaving

$$[U \frac{\partial U}{\partial x} + V \frac{\partial U}{\partial y} + \frac{\partial \overline{uv}}{\partial y} = - \frac{1}{\rho} \frac{\partial P}{\partial x} + \nu \frac{\partial^2 U}{\partial y^2}]_{III} \tag{5-12}$$

The result is equivalent to assuming that Region III is two-dimensional insofar as the mean flow is concerned.

The terms in the y and z equations are clearly smaller than those in the x equation with the exception of the vertical gradient of $\overline{v^2}$. These equations become

$$\left[\frac{\partial \overline{v^2}}{\partial y} = -\frac{1}{\rho}\frac{\partial P}{\partial y}\right]_{III} \tag{5-13}$$

or $$[P(x,y,z) + \rho\overline{v^2}(x,y,z)]_{III} = P_o \tag{5-14}$$

and in the z direction

$$\left[U\frac{\partial W}{\partial x} + V\frac{\partial W}{\partial y} + W\frac{\partial W}{\partial z} + \frac{\partial \overline{uw}}{\partial x} + \frac{\partial \overline{vw}}{\partial y} + \frac{\partial \overline{w^2}}{\partial z} = -\frac{1}{\rho}\frac{\partial P}{\partial z}\right]_{III} \tag{5-15}$$

In consideration of Eq. (5-13) and the fact that $\left[\frac{\partial \overline{v^2}}{\partial y}\right]_{III}$ varies slowly with x, the pressure term in Eq. (5-12) may be neglected, leaving

$$\left[U\frac{\partial U}{\partial x} + V\frac{\partial U}{\partial y} + \frac{\partial \overline{uv}}{\partial y} = \nu\frac{\partial^2 V}{\partial y^2}\right]_{III} \tag{5-16}$$

(A similar comment may be made in regard to Eq. (5-5.)

Region IV

Region IV is unique since it is highly three-dimensional with large gradients in the z direction. It is also unique because it is relatively narrow in the z direction and furthermore because the vertical velocity, V, is very small in this region. Not only does the data indicate that V is small, but also it may be observed that V must pass through zero as $|z|$ increases in the vicinity of the edge of the roughness since $V < 0$ over the roughness but $V > 0$ in the undisturbed boundary layer away from the roughness. The data indicates that the $\overline{v^2}$ term dominates the y equation and the U convective and $\overline{w^2}$ terms dominate the z equation. If the $\overline{vw}$ terms are again neglected, the momentum and continuity equations for Region IV can be written as

$$\left[U \frac{\partial U}{\partial x} + W \frac{\partial U}{\partial z} + \frac{\partial \overline{uv}}{\partial y} + \frac{\partial \overline{uw}}{\partial z} = \nu \left(\frac{\partial^2 U}{\partial y^2} + \frac{\partial^2 U}{\partial z^2}\right)\right]_{IV} \tag{5-17}$$

$$\left[\frac{\partial \overline{v^2}}{\partial y} = - \frac{1}{\rho} \frac{\partial P}{\partial y}\right]_{IV} \tag{5-18}$$

which can be written as

$$[P(x,y,z) + \rho\overline{v^2}(x,y,z)]_{IV} \doteq P_o \tag{5-19}$$

$$\left[U \frac{\partial W}{\partial x} + \frac{\partial \overline{w^2}}{\partial z} = - \frac{1}{\rho} \frac{\partial P}{\partial z}\right]_{IV} \tag{5-20}$$

$$\left[\frac{\partial U}{\partial x} + \frac{\partial W}{\partial z}\right]_{IV} = 0 \tag{5-21}$$

Analysis

Equations (5-17) through (5-21) representing Region IV provide the keys to understanding the mechanism which drives the vorticity seen in the present data, that of Elder (12), and the predictions of Townsend (11) and Hinze (15). If Eq. (5-19) is substituted into Eq. (5-20), the result is

$$\left[U \frac{\partial W}{\partial x} + \frac{\partial \overline{w^2}}{\partial z} = \frac{\partial \overline{v^2}}{\partial z}\right]_{IV} \tag{5-22}$$

or

$$\left[U \frac{\partial W}{\partial x} = \frac{\partial}{\partial z} (\overline{v^2} - \overline{w^2})\right]_{IV} \tag{5-23}$$

These equations may be compared to those proposed by Townsend (see Eqs. (1-1) through (1-7), and several differences will be noted; however it is interesting that Townsend with no data correctly predicted that the secondary-flow driving force would be related to the difference $(\overline{w^2} - \overline{v^2})_{IV}$. The chief difference between the present results and Townsend's reasoning is his assumption that $\overline{vw}$ would be the dominant driving term--an assumption which does not appear to be correct. He also felt that the driving mechanism would be distributed widely away from the edge while the present results show that it is concentrated in Region IV. In addition, the U convective term in the z equation is significant but was neglected in his analysis.

If it is assumed that viscous effects are minor away from the wall, it is possible to check the balance represented by Eq. (5-17) at five locations in Region IV at the section x = 15 ft (4.6 m). The measurements at that location are sufficiently complete and five horizontal profiles are available together with a vertical profile at z = 7.81 in. (19.8 cm). Graphical evaluation of derivatives from the experimental data is subject to considerable uncertainty; therefore the results of such an evaluation must be viewed with reservation. The value of $[\frac{\partial U}{\partial x}]_{IV}$ is particularly unreliable because of the spacing between data values in the x direction. Nevertheless, the process serves as a rough check on the validity of Eq. (5-17) as well as revealing the relative impact of the individual terms.

Table VII lists the results of this evaluation at z = 7.81 in. and x - 15 ft. The same process may be carried out for other values of z with similar results; however it is necessary to interpolate data and then differentiate the interpolated values, hence the uncertainty is much greater and the results are less conclusive.

It may be seen from the values in Table VII that Eq. (5-17) is reasonably satisfied within the uncertainty levels of the process. The x pressure gradient is assumed to be zero since it may be estimated by differentiating Eq. (5-19) with respect to x and evaluating from the data. The results show that the pressure gradient term is at least an order of magnitude smaller than the other terms in the x equation.

Equation (5-17) is basically a two-dimensional, boundary-layer type of equation in x and z except for the $\overline{uv}$ and y curvature terms. This equation together with the continuity equation, (5-21), represent a two-dimensional shear layer modified by the presence of these two terms, which incorporate the influence of the variation in the third (y) direction. The z equation, (5-20), also represents such a shear layer with the modifying influence of the developing cross flow carried in the convective term.

Recognizing that Region IV behaves like a modified shear layer provides a clue for further analysis of the data since it may be expected that the parameters applicable in shear layers should be significant in this situation.

If Eqs. (5-17) and (5-23) were to be non-dimensionalized, scaling factors would be required for the mean velocities, the turbulent velocities, and for each of the coordinate directions. With the non-dimensionalized quantities denoted by primes, the velocity and turbulence reference quantities by the subscript, r, and the reference lengths by L_x, L_y, and L_z, the following relations may be defined:

$$U' = \frac{U}{U_r}\ ,\ W' = \frac{W}{U_r}\ ,\ u' = \frac{u}{u_r}\ ,\ v' = \frac{v}{u_r}\ ,\ w' = \frac{w}{u_r}\ ,\ x' = \frac{x}{L_x}\ ,$$

$$y' = \frac{y}{L_y}\ ,\ z' = \frac{z}{L_z} \tag{5-24}$$

From the physical dimensions of the data, it is reasonable to take $L_y \approx L_z$. Using these definitions it is possible to rewrite Eqs. (5-17) and (5-23) as

$$\frac{\partial U'}{\partial x'} + \frac{L_x}{L_y}\left[\frac{W'}{U'}\frac{\partial U'}{\partial z'}\right] + \frac{L_x}{L_y}\frac{u_r^2}{U_r^2}\left[\frac{1}{U'}\frac{\partial \overline{u'v'}}{\partial y'}\right] + \frac{L_x}{L_y}\frac{u_r^2}{U_r^2}\left[\frac{1}{U'}\frac{\partial \overline{u'w'}}{\partial z'}\right]$$

$$= \frac{L_x}{L_y}\frac{\nu}{U_r L_y}\left[\frac{\partial^2 U'}{\partial y'^2} + \frac{\partial^2 U'}{\partial z'^2}\right] \tag{5-25}$$

$$\frac{\partial W'}{\partial x'} = \frac{L_x}{L_y}\frac{u_r^2}{U_r^2}\left[\frac{1}{U'}\frac{\partial}{\partial z'}\left(\overline{v'^2} - \overline{w'^2}\right)\right] \tag{5-26}$$

Thus it may be seen that the significant dimensionless ratios are u_r^2/U_r^2, L_x/L_y, and the Reynolds number, $\nu/u_r L_y$.

Furthermore these are the only ratios which may be formed from the reference quantities, a fact which is readily obvious but may be proved (54) by forming the matrix

	U_r	u_r	L_x	L_y	ν
M	0	0	0	0	0
L	1	1	1	1	2
T	-1	-1	0	0	-1

(5-27)

There are five variables and the rank of this matrix is two, therefore only three independent dimensionless ratios may be formed.

Proper selection of the reference quantities will reduce the differential terms to a common order of magnitude and cause the scaling information to be contained with the dimensionless ratios. Several different length and velocity reference are available and the choice must be guided by consideration of the nature of the flow.

A closely related question is in regard to the two-dimensionality of the flow in Region III over the roughness. The similarity behavior of the oncoming boundary layer in the tunnel used has been well established by the work of Zoric (46), from which the appropriate length and velocity scaling parameters may be appied to that layer.

If analagous information can be established, even approximately, for Region III, then Region IV should be governed by the relationships between Region I and Region III since it is these relationships which establish the variation in the z direction in the vicinity of the edge.

The well established boundary layer parameters are examined first. These parameters include the boundary layer thickness, δ, the displacement and momentum thicknesses defined by

$$\delta^* = \int_0^\infty \frac{U_\infty - U}{U_\infty}\, dy \tag{5-28}$$

$$\theta = \int_0^\infty \frac{U}{U_\infty}\left[\frac{U_\infty - U}{U_\infty}\right] dy \tag{5-29}$$

plus the shape factor, $H = \frac{\delta^*}{\theta}$, and the shear velocity, $u_* = (\tau_w/\rho)^{1/2}$. In principle, δ^*, θ and H could be defined for either the total boundary layer or for the inner layer only (i.e., Region III); however the outer edge of the inner layer is not defined by a constant free stream condition and interpretation of parameters so defined would be difficult. It is readily possible to define an internal layer height, y_i, although evaluation of this quantity from the data is subject to some uncertainty.

The quantities δ^*, θ and H were evaluated directly from the vertical velocity profile data at the centerline and near the edge of the roughness (Figs. 33 and 34), and the results are shown on Fig. 80 and Table VIII. To evaluate these parameters, no attempt was made to fit particular functional forms to the data; but rather the data was evaluated graphically exactly as it stands. This was necessary due to the irregularity of the profiles, especially near the leading edge, which cannot be expected to fit regular boundary layer laws.

The boundary layer thickness δ was estimated from the data plots and is very uncertain due to sparsity of data in the outer region.

To obtain the inner layer thickness, y_i, profiles of velocity and turbulence quantities over the roughness were superimposed on the corresponding upstream profiles, and the value of y was noted at which the profile slopes deviated from the upstream value. By this method estimates of y_i for each x station were obtained from the velocity, $\sqrt{\overline{u^2}}$, $\sqrt{\overline{v^2}}$, $\sqrt{\overline{w^2}}$, and $\overline{uv}$ data and are listed in Table VIII. The average of these estimates was taken to be the value of y_i.

It may be seen from the values in Table VIII that the estimates of y_i vary considerably and that no one quantity is a completely consistent predictor of the average. However the estimates based on $\sqrt{\overline{v^2}}$ are the most consistent, and the $\sqrt{\overline{v^2}}$ data is easiest to use for this purpose since it shows the most distinct change of slope.

An effort was made to use the technique suggested by Antonia and Luxton (36,37) involving a plot of U vs. $y^{1/2}$ to distinguish the edge of the internal layer (see Chapter 1). Near the leading edge of the roughness these plots do in fact show a distinct change in slope; however the effect diminishes rapidly with increasing x and (beyond $x = 7$ ft) is no better than the techniques used. It is interesting to note in passing that the values of y_i suggested by this latter technique tend to be slightly smaller than those listed in Table VIII, a discrepancy also noted by Antonia and Luxton in their paper (36).

The upstream values of δ, δ^*, θ and H may be roughly compared to values extrapolated from Zoric's data replotted against Reynolds number. One of Zoric's values seems to be somewhat inconsistent with his others; however if that one is discounted, the extrapolation based on the remaining values agrees well with the present data for δ^* and θ. Zoric's values for δ are larger than the apparent value in the present tests; however it is very difficult to define δ without a certain amount of arbitrariness. Also shown in Table VIII are values of shear velocity, u_*, obtained from plots of $\frac{yU_\infty}{\nu}$ vs. $\frac{U}{U_\infty}$ after the method described by Pierce (55), which is essentially a graphical solution for u_* of the logarithmic law

$$\frac{U}{U_*} = K_1 \log \frac{yu_*}{\nu} + K_2 \tag{5-30}$$

Semi-logarithmic plots of the vertical velocity profiles do in fact exhibit a well-defined straight line region extending through the inner layer; hence Eq. (5-30) can be used to represent these profiles. However the values of u_* as obtained by this method will not necessarily give the wall shear stress except as a first approximation. The well-known Ludwieg-Tillmann relationship (56) for wall shear stress in terms of [redacted] and θ is not readily valid for a flow involving an inner layer; and its application here produces values of u_* of the order of one foot per second over the roughness, which is unrealistically low.

Values of u_* obtained from $\overline{uv}$ measurements extrapolated to the wall are also tabulated in Table VIII, and it may be noted that the value at x = 3 ft agrees well with that obtained from Eq. (5-30). This agreement should not be given too much emphasis since the uncertainty of either method is at least ±10 percent above and beyond inherent uncertainties in the data. It may be noted that downstream after the roughness change there is a very large discrepancy between the two sets of values, a fact which underscores the limited value of extrapolating to the wall data taken away from the wall. In regard to this last point, it may be observed that measurements closer to the roughness are of no help since local effects of each roughness element dominate. Since Stanton tube techniques are useless among the roughness elements, it would seem that if precise wall shear values are ever to be obtained, it will be by improved direct measurements even though such attempts were unsuccessful at the time of this study.

The upstream values of u_* agree quite well with extrapolations of Zoric's data; hence it is felt that the values reported are not entirely useless but may be examined for trends together with the values of the other boundary layer parameters.

Figure 80 contains the plots against x of δ^*, θ, H, and u_*. It may be seen that over the first few feet of the roughness these various parameters are sharply distorted much as has been reported by workers studying the two-dimensional case. After some distance, in this case about 9 ft (2.7 m), the parameters appear to stabilize and exhibit distinguishable trends which may be compared to conventional two-dimensional boundary layers and in particular to Zoric's study.

Zoric reviewed the requirements for a boundary layer approaching similarity stating that it should display displacement and momentum thicknesses which are linear functions of x and a shape factor which approaches a constant value of 1.286. It may be seen from Fig. 80 that δ^* and θ do exhibit a nearly linear dependence on x beyond 8 ft (2.4 m); however the shape factor is greater than 1.286 and shows a distinct growth toward even larger values.

The implications of these results may be related to the earlier observations about the flow in Region III. It is evident that the flow is nearly two-dimensional and shows a tendency to approach similarity, yet the secondary velocity effects are definitely noticeable in the anomalous behavior of the shape factor. The downward flow over the roughness (opposite to that in a two-dimensional boundary layer approaching similarity) convects high-momentum fluid toward the surface causing a decrease in the rates of growth of both δ^* and θ. The effect upon θ is greater due to the change in both velocity and velocity defect; and therefore H increases. This sensitivity of shape factor to secondary flow is, of course, well-known.

When reviewing and considering the behavior of the parameters δ^*, θ, and H, it must be remembered that they have been calculated using the total velocity profile containing both the inner layer (Region III) and the remainder of the outer layer (Region II). The total boundary layer thickness over the roughness cannot be determined with any certainty from the data but is of the order of 18 in. (46 cm); therefore at $x = 7$ ft (2.1 m) the inner layer occupies roughly a third of the total thickness and at 15 ft (4.6 m) somewhat more than half of the total thickness. As a result, the parameters are dominated by the inner layer and if an approach to similarity is suggested by the behavior of these parameters, it would be for the inner layer rather than the total layer. Final total development of similarity in the layer could only be expected far downstream after the inner layer grows to the top of the outer layer and at that point vertical flow effects would still have to be reckoned with.

If there is a trend toward similarity in the inner layer, it should be possible to collapse the vertical velocity profiles to some form of universal profile with the proper choice of coordinates. For normal two-dimensional boundary layers the choice would be

y/δ vs. U/U_∞, and by analogy for the inner layer the values of y_i and U_i might be tried, where U_i is the velocity at y_i. For large values of x, y_i, and U_i will approach δ and U_∞ respectively.

Figure 81 shows the centerline (z = 0) velocity profiles plotted on y/y_i, U/U_i coordinates beginning at x = 7 ft (2.1 m). The data collapses well to a universal profile; but it may be noted that the data at 7 ft does not fit quite as well as that at 9, 11, 13, and 15 ft (2.7, 3.4, 4.0, and 4.6 m). The data for 2 ft and 4 ft (0.6 and 1.2 m) are not plotted but they deviate much more from this profile as might be expected from the discussion surrounding Fig. 80. Also included in Fig. 81 is the velocity profile at x = 15 ft (4.6 m) for U_∞ = 30 ft per second (9.1 m/s), and it may be seen that this data fits the universal profile very well.

The foregoing discussion leads to several conclusions which are of significance in the study of three-dimensional flows over a strip of roughness. The first conclusion is that the three-dimensional effects over much of the roughness away from the edges is sufficiently small that the inner boundary layer behaves very much like a two-dimensional layer even to the extent of tending to develop a condition very close to similarity even before the inner layer has grown to the top of the original boundary layer.

The second conclusion, which is a consequence of the first, is that the flow over the roughness should be characterized by those parameters which are related to the logarithmic laws of two-dimensional boundary layers--in particular the layer thickness, the outer bounding velocity, the shear velocity, and some characteristic measure of the roughness such as y_o.

The three-dimensional characteristics of the flow must necessarily be governed by the differences between the shear velocity and the characteristic roughness height over the smooth and rough areas. If these differences are equal to zero, there is no edge effect. As these differences increase, the driving forces in Eqs. (5-22) and (5-23) also increase although not necessarily in a linear fashion.

A word of caution is in order here to restrain over-generalization of these conclusions. The situation explored here is typical of atmospheric flows since the boundary layer was very thick relative to the roughness height and the inner layer was able to grow for a considerable distance without reaching the outer edge of the total boundary layer. Often in laboratory studies this condition is not in existence, the inner layer penetrates the total layer within a short distance, and furthermore the length in the flow direction is not sufficient to permit development of similarity--before or after penetration of the outer layer.

Flow situations in which the length after roughness changes is limited could not be expected to display a region of near-similarity; however the present tests suggest that they could be regarded as two-dimensional except very near the edges. Since three-dimensional effects are limited at great distances downstream, they could be expected to be even less shortly after the roughness change.

The effect of changing Reynolds number in the free stream is partly indicated by the limited data taken at 30 ft per second (9.1 m/s). Table VIII shows the inner layer thicknesses and shear velocities at x = 15 ft (4.6 m) for both cases, U_∞ = 40 fps (12.2 m/s) and U_∞ = 30 fps (9.1 m/s). If the inner layer thickness were behaving strictly according to $Re^{-1/2}$ (Re based on length along roughness) the ratio should be 0.866. The measured ratio is about 0.81. Interestingly, the measured ratio of shear velocities is also about 0.82. Table V shows a limited number of cross flow measurements taken at x = 15 ft (4.6 m) near the edge of the roughness for U_∞ = 30 fps (9.1 m/s). These values are an order of magnitude smaller than the analagous values at 40 fps (12.2 m/s), a fact which suggests that the cross flows decrease very rapidly with Reynolds number. This decrease in the secondary circulation tends to explain the fact that the inner layer thickness increased more than expected with the change in Reynolds number. The reduction in vertical downflow permits the inner layer to grow faster.

The rate of growth of the inner layer as well as the rate of growth of the shear region over the edge are of interest in this problem, particularly if significant differences from two-dimensional cases occur. The values of y_i are plotted in Fig. 82 against the distance downstream. For comparison purposes the same figure contains plots of growth rates predicted and/or measured by several workers for two-dimensional roughness changes. Panofsky and Townsend (30), in work cited in Chapter I, predicted an internal layer with a growth rate of the order of 1:10 and cited some rough measurements to support the prediction. Yeh's experimental measurements of two-dimensional flow over a changing roughness (35) led him to suggest a growth rate of 1:13 with a virtual origin some distance upstream. However, Yeh's measurements were concentrated in the first few feet after the change and are of limited value here.

Antonia and Luxton (36) returned to the approach originally used by Elliott (29) involving the use of power laws in x to describe the internal layer growth. That a power law might be appropriate to describe the present data is evident from a logarithmic plot of y_i versus x (Fig. 83). The data fits a straight line on these coordinates suggesting an exponent of 0.75. This value may be compared with the value 0.8 predicted by Elliott and observed experimentally by Antonia and Luxton as well as by Huang and Nickerson in numerical work (58). A plot of a 0.5 power law often used to represent bluff body wakes in two dimensions is also shown since the effects of the leading edge of the upstanding roughness should not be overlooked.

It is evident from Fig. 82 that the internal layer grows much faster than the two-dimensional wake. The fact that the growth is slightly less than the 0.8 power law is an indication of the secondary downflow over the roughness; and this effect is one of the more significant results of the otherwise small cross and vertical flow components. Nevertheless, it should be noted that this apparent depression or downward displacement of y_i, it can be said that the effect is just barely noticeable even in this case of a substantial difference in absolute roughness between the smooth and rough surfaces.

The question of growth of the vertical shear layer over the roughness edge is considered next. The lateral spreading of this shear layer is of considerable interest since it determines how much of the total flow region will be significantly affected by the direct influence of the edge, apart from the effects of secondary circulations. Examination of the horizontal velocity profiles (Figs. 28 through 32) suggests that three points may be discerned which could possibly be significant. Two of these points would be the boundaries of the region containing the steepest z gradients (i.e., Region III)--a region which is confined to a narrow band along the edge. The third point is the furthest point away from the edge in Region IV where the influence of the edge can still be discerned. All of these points are subject to considerable uncertainty, especially the third one; however reasonable estimates may be made, and the resulting values have been plotted in Fig. 84 for two different heights above the floor.

From Fig. 84 several points may be noted. First, the region of steep gradients is roughly constant in width both for increasing x and increasing y after an initial growth period. Closer examination reveals that this width attains a maximum value of about 4 in. (10 cm) as x increases and then begins to decrease slowly, with the maximum value occurring near x = 7 ft (2.1 m). A second observation is that the strip closest to the wall is displaced outward (toward the smooth surface) relative to the strip which is higher above the floor. Also this displacement shows a tendency to increase with increasing x, an indication of the outward flow discussed earlier.

It is evident that this region of steep z gradients does not behave as a conventional shear layer, which would spread in proportion to $x^{1/2}$. Here the z gradients are apparently maintained artificially by the conditions bordering the edge--principally the gradients and flux of momentum in the y direction. The decrease in the width of this region with increasing x is due to the fact that the vertical velocity profiles over the roughness are changing more rapidly than the well developed profiles over the smooth wall. At great distances downstream, the continued decrease in effective roughness will tend to reduce (and ultimately eliminate) the difference between smooth and rough profiles, and the region of steep z gradients would tend to vanish.

The outer curves in Fig. 84 on the other hand represent the extent to which the influence of the shear region has diffused into the undisturbed boundary layer. The locus of these growths is a curve roughly proportional to $x^{1/2}$, much as would be expected for a wake or a conventional shear layer.

Significant Parameters

From the preceding discussion it is possible to predict those parameters which are the most likely to be significant in determining the character of the flow for situations similar to the one examined. In particular, the flow studied developed from a thick, well-developed turbulent boundary layer encountering a strip of roughness of finite extent in the direction normal to the flow. Away from the roughness (Region I) the velocity field will be influenced by several parameters including the free stream velocity, U_∞, the boundary layer thickness, δ, the distance from the wall, y, the effective displacement of the wall due to the roughness, $(y_o)_I$ (which may be effectively zero if the wall is smooth), and the shear velocity. Stated functionally, the velocity is given by

$$(U)_I = f_1[U_\infty, \delta, y, (y_o)_I, (u_*)_I] \tag{5-31}$$

Over the roughness the flow (to first approximation) tends toward a similarity form within a short distance downstream. Some distance away from the leading edge it is then possible to represent the functional dependence of the mean velocity in Region III by

$$(U)_{III} = f_2[U_\infty, x, y, (y_o)_{III}, \delta, (u_*)_{III}] \tag{5-32}$$

This equation is predicted on the assumption that the outer portion of the boundary layer (Region II) is undisturbed by the inner layer except for a slight streamline displacement, and that the oncoming layer, of which Region II is a part, is fully developed.

If the flows over the two surfaces were independent and did not interact in the edge region, Eqs. (5-31) and (5-32) would be adequate to describe the problem. However there is interaction which gives rise to W and V velocity components which must be related to the velocity distributions in Regions I and III. Dependence upon the physical dimensions of the problem including the half-width, D, of the roughness field could also be expected. Stated functionally, $(W)_{IV}$, becomes

$$(W)_{IV} = f_3[(U)_I, (U)_{III}, x, y, z, D] \tag{5-33}$$

Considering (5-31) and (5-32), Eq. (5-33) becomes

$$(W)_{IV} = f_3[U_\infty, x, y, z, D, \delta, (y_o)_I, (y_o)_{III}, (u_*)_I, (u_*)_{III}] \tag{5-34}$$

The characteristic parameters, U_∞, D, δ, $(y_o)_I$, $(y_o)_{III}$, $(u_*)_I$, $(u_*)_{III}$ may be formed into nine dimensionless ratios--three velocity ratios and six length ratios. Recalling that Eq. (5-23) implied the existence of one length ratio and one velocity ratio of significance, it can be seen that extensive study of a variety of combinations of conditions would still be needed to identify the most significant parameters and to establish the proper functional dependences.

On the other hand, it is possible to identify the most likely ratios by taking a clue from the pseudo-shear layer behavior of the edge region. This behavior would suggest that Eq. (5-34) might be modified by the assumption that the <u>differences</u> between Region I and Region III are significant. The nearly straight-line velocity gradient across Region IV and the diffusive behavior of this layer lend credence to such an assumption. Equation (5-34) would then become

$$(W)_{IV} = f_4 \left[U_\infty, x, y, z, \delta, [(y_o)_{III} - (y_o)_I], [(u_*)_{III} - (u_*)_I] \right] \quad (5\text{-}35)$$

The characteristic dimensions of the problem would then provide the possible ratios

$$\frac{\delta}{D}, \frac{(y_o)_{III} - (y_o)_I}{D}, \frac{(u_*)_{III} - (u_*)_I}{U_\infty} \quad (5\text{-}36)$$

If one velocity and one length ratio are admissable, then one of the ratios in (5-36) will be dependent on the others. From physical considerations this dependence seems reasonable since prescribing δ and y_o values should establish the u_* values for developed flow.

The ratios in (5-36) involving y_o or u_* would not be known a priori for a given roughness until actual data had been taken. However the value of these ratios would be in guiding detailed study of a variety of cases to determine specific functional relationships for Eq. (5-35). It would then be possible to obtain experimental values for y_o or u_* for a two-dimensional case and use these values to predict the three-dimensional effects for a given strip of the same roughness.

The dimensionless ratios given in Eq. (5-36) do not explicitly depend upon y_i--a fact which may appear unreasonable. However, it must be recalled that the discussion leading to these ratios is predicated upon the assumption that the flow over the roughness is reasonably well developed so that conditions in the inner layer are simple functions of the outer layer parameters and the x distance from the leading edge of the roughness. For the present tests these assumptions are approximately valid for $x > 7$ ft (2.1 m), which is a distance roughly equal to five boundary layer thicknesses. In the region ahead of this point to the beginning of the roughness, it must be expected that the flow in the inner layer may depend upon local conditions including y_i, the roughness leading edge configuration, and turbulence levels in both the inner and outer layers. The distance in the streamwise direction required to produce approximate similarity will also depend on these local conditions. Of course, complete similarity and complete and exclusive dependence upon the ratios in Eq. (5-36) will occur only after an infinite fetch, that is as an asymptotic limit.

Some general observations may be made in respect to the behavior predicted by the quantities in Eq. (5-36). For the present tests the ratio δ/D is of the order of two, which is to say that the approaching layer thickness is approximately the same as the roughness field width (twice the half-width). For atmospheric flows over cities and similar topographic features, this ratio would normally be of unit order but might be as large as ten for strip crops or other narrow terrain features.

Values of the parameter much less than unity are typical of terrain features spread over a wide area. For these situations it is likely that most of the flow will be two-dimensional for all practical purposes with perturbations near the edges in the form of outflows determined by the third ratio $[(u_*)_{III} - (u_*)_I]/U_\infty$.

Small values of the ratio δ/D may also occur when δ is very small. Such situations occur frequently in aerodynamics and wind tunnel studies and some studies of flow over roughness have been carried out under such conditions. The discussion leading to the ratios in Eq. (5-36) would not be valid in such cases--in particular where the condition $(y_o)_{III}/\delta << 1$ does not hold.

One limit on large values of δ/D must be imposed when $D \approx L_e/2$, where L_e is the length scale characterizing the width of Region III; that is when the roughness width is reduced until the edge shear layers begin to interact. Under that condition similarity of the flow over the roughness could no longer be expected and local conditions of roughness and turbulence may again dominate the flow. In the present tests, the edge shear regions extend about 1.5 in. (3.8 cm) over the roughness; hence the situations may be expected to change significantly as the roughness strip width is decreased to the order of 3-4 in. (8-10 cm). As a point of comparison it may be noted that Wang's (57) measurements were taken over a series of alternate smooth and rough strips which were 6 in. (15.2 cm) wide. He reported a regular periodic variation in the flow quantities in the lateral direction, much as would be expected if the present edge regions were juxtaposed by reducing the roughness width and if the pattern were repeated periodically in the z direction.

Conclusions

The objective of this study was to attempt to penetrate the complexities of a common type of three-dimensional, turbulent boundary-layer flow. Following is a summary of the pertinent observations and conclusions resulting from this study:

1. The three-dimensional effects resulting from having an edge or line parallel to the mean flow separating regions of differing roughness are confined largely to the immediate neighborhood of that edge.

2. More specifically, that neighborhood may be thought of as a shear plane extending upward from the edge to the outer limit of the inner boundary layer.

3. The flow in the region away from the roughness is nearly two-dimensional and for first-order analyses may be regarded as two-dimensional.

4. The flow in the region over the roughness but away from the edge is also two-dimensional to first order analysis. Furthermore, this flow shows a definite trend toward similarity after an initial adjustment region following the roughness change.

5. The flow in the shear plane over the edge is highly three-dimensional even to first order analysis. However these strong three-dimensional effects are confined to the narrow shear plane, the width of which does not increase beyond a certain point.

6. Within the shear plane are generated turbulence levels and Reynolds stresses which are significantly larger than those seen anywhere else over the roughness.

7. The effects of the shear plane diffuse into the flow in proportion to the square root of the distance downstream. This diffusive effect is much more noticeable over the smooth surface where turbulence is of lower intensity than it is over the rougher surface where turbulence levels are higher.

8. In the cases examined, the penetration of the edge effect into the region above the roughness was limited to a distance nearly an order of magnitude smaller than the inner layer thickness. This penetration shows no sign of increasing with increasing x.

9. There is additional production of turbulent energy in the edge region in excess of that produced by the roughness itself.

10. The edge shear region gives rise to non-zero values of the $\overline{uw}$ Reynolds stress, which is zero in two-dimensional flow. The quantity $\overline{uw}$ attains values which are comparable in magnitude to local values of $\overline{uv}$.

11. No significant effects of the $\overline{vw}$ stress term were detected in this study; however the difficulties associated with attempting to measure this quantity preclude ruling it out entirely.

12. Values of $\overline{vw}$ inferred from cross flow velocity components assuming an eddy-viscosity model suggest that $\overline{vw}$ is a negligible quantity.

13. The edge region contains lateral (z direction) gradients which are of the same order of magnitude as the vertical (y direction) gradients. The lateral gradients of $\overline{uv}$, $\overline{uw}$, $\overline{u^2}$, $\overline{v^2}$, and $\overline{w^2}$ exhibit this characteristic.

14. The terms $\partial\overline{uw}/\partial z$, $\partial\overline{v^2}/\partial z$, and $\partial\overline{w^2}/\partial z$, which are not significant in two-dimensional flow, arise through the balance in the edge regions.

15. Viscous effects in the edge region arise from curvature of the velocity profiles in the z direction as well as in the y direction. Locally, these curvatures may be of comparable magnitude.

16. The lateral gradients in the edge region give rise to a cross flow component which in turn leads to an eventual downflow in the boundary layer over the roughness.

17. Analysis of the equations of motion leads to the conclusion that the primary driving force for the cross flow is the lateral gradient of the quantity $(\overline{w^2} - \overline{v^2})$ in the edge region.

18. It appears that the presence of an edge has little direct effect upon the velocity and turbulence profiles over the roughness. Instead, the detectable effects appear to be a direct result of the downflow over the roughness.

19. Cross flow velocity components were seen over the roughness with a maximum magnitude of about 1.5 percent of the free stream velocity.

20. The vertical downward flow over the roughness is opposite in direction to the usual upward component seen in two-dimensional boundary layers.

21. The maximum vertical flow component seen is less than one percent of the free stream velocity.

22. The maximum deflection of the flow vector due to these secondary flow components is less than two degrees.

23. The limited data available suggest that the cross flows decrease very rapidly with decreasing Reynolds number. (A 25 percent reduction in Reynolds number produced an order of magnitude decrease in the cross flow component.)

24. The secondary flow components influence the flow over the roughness by transporting high-momentum fluid downward in the boundary layer. The effect is of second order, however it is most noticeable in its effect upon the shape factor, which grows with increasing distance downstream.

25. The parameters which characterize the cross flow and therefore its influence on the remainder of the flow field cannot be verified from the present tests. However the most likely parameters are predicted to be those identified in the dimensionless ratios given in Eq. (5-36).

26. The rate of growth of the internal layer in the x direction is decreased slightly by the vertical downflow. The effect is just noticeable, with an observed decrease of about 15 percent in the exponent of the power law describing the growth of the internal layer.

27. Determination of the inner layer thickness is subject to variations depending on which velocity or turbulence quantity is examined for this purpose. The most distinct and consistent indication is obtained from the $\sqrt{\overline{v^2}}$ data profiles.

28. The technique suggested by Antonia and Luxton (36,37) using half-power plots in y does not define the inner layer clearly at large distances downstream.

28. The ratio δ/D may be conveniently used to categorize flows over various sizes of roughness areas. Values of this ratio of unit order or smaller will characterize a flow which is essentially two-dimensional with local perturbations near the edges of the roughness area.

REFERENCES

1. Schlichting, H., "Boundary Layer Theory," 4th ed., McGraw-Hill, 1960.

2. Robertson, J. M., "Hydrodynamics in Theory and Application," Prentice-Hall, 1965.

3. Batchelor, G. K., "An Introduction to Fluid Dynamics," Cambridge Press, 1967.

4. Nash, J. F., and Patel, V. C., "Three-Dimensional Turbulent Boundary Layers," SBC Technical Books, Atlanta, Ga., 1972.

5. Hinze, J. O., "Turbulence," McGraw-Hill, 1959.

6. Lumley, J. L., and Panofsky, H. A., "The Structure of Atmospheric Turbulence," Interscience, 1964.

7. Lin, C. C., "Turbulent Flows and Heat Transfer," Princeton, 1959.

8. Lin, C. C., "Statistical Theories of Turbulence," Princeton, 1961.

9. Lumley, J. L., "Stochastic Tools in Turbulence," Academic Press, 1970.

10. Bendat, J. S., and Piersol, A. G., "Measurement and Analysis of Random Data," Wiley, 1966.

11. Townsend, A. A., "The Structure of Turbulent Shear Flow," Cambridge Press, 1956.

12. Elder, J. W., "The Flow Past a Flat Plate of Finite Width," J. Fluid Mech., 9, 133-153, 1960.

13. Laufer, J., "The Structure of Turbulence in Fully Developed Pipe Flow," NACA TR 1174, 1955.

14. Klebanoff, P. S., "Characteristics of Turbulence in a Boundary Layer With Zero Pressure Gradient," NACA TN 3178, 1954.

15. Hinze, J. O., "Secondary Currents in Wall Turbulence," Physics of Fluids Supplement, S122-5, 1967.

16. Bragg, G. M., "The Turbulent Boundary Layer in a Corner," J. Fluid Mech., 36, part 3, 485-503, 1969.

17. Brundett, E., "The Production and Diffusion of Vorticity in Channel Flow," University of Toronto, Mech. Engrg. Dept., TP 6302, April, 1963.

18. Leutheusser, H.J., "The Effect of Cross-Section Geometry upon the Resistance to Flow in Conduits," Ph.D. Thesis, University of Toronto, Oct., 1961.

19. Leutheusser, H. J., "Turbulent Flow in Rectangular Ducts," J. Hyd. Div., ASCE, 89, 1963.

20. Toan, N. K., "Application of Integral Methods to the Turbulent Corner Flow Problem," ASME Rep. No. 71-WA/FE-36, Nov., 1971.

21. Veenhuizen, S. D., and Meroney, R. N., "Secondary Flow in a Boundary Layer," Proj. THEMIS TR No. 3, Engrg. Res. Ctr., Colorado State University, June, 1969.

22. Wheeler, A. J., and Johnston, J. P., "Three-Dimensional Turbulent Boundary Layers--Data Sets for Two-Space Coordinate Flows," Rep. No. MD-32, Thermosciences Div., Dept. of Mech. Engrg., Stanford U., Aug., 1972.

23. Howarth, L., "Rayleight's Problem for a Semi-Infinite Plate," Proc. of the Cambridge Philosophical Society, V. 46, 127-140, 1950.

24. Joubert, P. N., Perry, A. E., and Brown, K. C., "Critical Review and Current Developments in Three-Dimensional Turbulent Boundary Layers," Proc. of the Symposium on the Fluid Mechanics of Internal Flows, G.M. Res. Labs., 1965, (Elsevier Publishing Co., 1967).

25. Gruschwitz, E., "Turbulent Reibungsschichten mit Sekundärströmung," Ingenieur-Archiv, VI, 355-365, 1935.

26. Johnston, J. P., "On the Three-Dimensional Turbulent Boundary Layer Generated by Secondary Flow," J. Basic Engrg., Trans. ASME, ser. D, 82, 3, 233-246, Sept., 1960.

27. Johnston, J.P., "Turbulent Boundary Layer at a Plane of Symmetry in a Three-Dimensional Flow," J. Basic Engrg., Trans. ASME, ser. D, 82, 3, 622-628, Sept. 1960.

28. Shanebrook, J. R., and Hatch, D. E., "A Family of Hydograph Models for the Cross Flow Velocity Component of Three-Dimensional Turbulent Boundary Layers," ASME Fluids Engineering Conf., Pittsburgh, Pa., May, 1971.

29. Elliot, W. P., "The Growth of the Atmospheric Internal Boundary Layer," Trans. Am. Geophysical Union, 39, 6, Dec., 1958.

30. Panofsky, H. A., and Townsend, A. A., "Change of Terrain Roughness and the Wind Profile," Quart. J. Roy. Meteor. Soc., 90, 147-155, 1964.

31. Blackadar, A. K., Panofsky, H. A., Glass, P. E., and Boogaard, J. F., "Determination of the Effect of Roughness Change on the Wind Profile," Physics of Fluids Supplement, S209-11, 1967.

32. Taylor, P. A., "The Planetary Boundary Layer above a Change in Surface Roughness," J. Atm. Sci., 26, 432-440, May, 1969.

33. Blom, J., and Wartena, L., "The Influence of Changes in Surface Roughness on the Development of the Turbulent Boundary Layer in the Lower Layers of the Atmosphere," J. Atm. Sci., 26, 255-265, March, 1969.

34. Peterson, E. W., "On the Relation between the Shear Stress and the Velocity Profile after a Change in Surface Roughness," J. Atm. Sci., 26, 773-774, 1969.

35. Yeh, F. F., "Air Flow over Roughness Discontinuity," Ph.D. Dissertation, Colorado State University, 1970.

36. Antonia, R. A., and Luxton, R. E., "The Response of a Turbulent Boundary Layer to a Step Change in Surface Roughness," J. Fluid Mech., 48, part 4, 721-761, 1971.

37. Antonia, R. A., and Luxton, R. E., "The Response of a Turbulent Boundary Layer to an Upstanding Step Change in Surface Roughness," J. Basic Engrg., 22-34, March 1971.

38. Townsend, A. A., "Self-Preserving Flow Inside a Turbulent Boundary Layer," J. Fluid Mech., 22, 773-797, 1965.

39. Townsend, A. A., "The Response of a Turbulent Boundary Layer to Abrupt Changes in Surface Conditions," J. Fluid Mech., 22, 799-822, 1965.

40. Nickerson, E. C., "Boundary Layer Adjustment as an Initial-Value Problem," J. Atm. Sci., 25, 207-213, 1968.

41. Onishi, G., and Estoque, M. A., "Numerical Study on Atmospheric Boundary Layer Flow over Inhomogeneous Terrain," J. Meteor. Soc., Japan, 46, 280-286, 1968.

42. Taylor, P. A., "On Wind and Shear Stress Profiles above a Change in Surface Roughness," Quart. J. Roy. Meteor. Soc., 95, 1969.

43. Plate, E. J. and Cermak, J. E., "Micro-Meteorological Wind Tunnel Facility," Final Report, Fluid Dynamics and Diffusion Laboratory, Colorado State University, No. CER63EJP-JEC9, Feb., 1963.

44. Cermak, J. E., et al., "Simulation of Atmospheric Motion by Wind-Tunnel Flows," Fluid Dynamics and Diffusion Laboratory, Colorado State University, No. CER66JEC-VAS-EJP-GJB-HC-RNM-SI17, May, 1966.

45. Cermak, J. E., "Laboratory Simulation of the Atmospheric Boundary Layer," AIAA Journal, v. 9, n. 9, Sept. 1971, pp. 1746-1754.

46. Zoric, D. L., "Approach of Turbulent Boundary Layer to Similarity," Ph.D. Dissertation, Colorado State University, Dec., 1968.

47. Sandborn, V. A., "Resistance Temperature Transducers," Metrology Press, Fort Collins, Colo., 1972.

48. Tieleman, H. W., "Viscous Region of Turbulent Boundary Layer," Report No. CER67-68HWT21, Engineering Research Center, Colorado State University, Dec. 1967.

49. Gessner, F. B., and Moller, G. L., "Response Behavior of Hot Wires in Shear Flow," JFM, V. 47, p. 3, pp. 449-468, 1971.

50. Draper, N. R., and Smith, H., "Applied Regression Analysis," Wiley, 1966.

51. Champagne, F. H., Sleicher, C. A., and Wehrmann, O. H., "Heat Transfer Experiments with Inclined Hot-Wire."

52. Friehe, C. A., and Schwarz, W. H., "Deviations from the Cosine Law for Yawed Cylindrical Anemometer Sensors," ASME Applied Mech. Div., No. 68-WA/APM-16.

53. Webster, C. A. G., "A Note on the Sensitivity to Yaw of a Hot-Wire Anemometer," JFM, V. 12, pp. 307-312, 1962.

54. Langhaar, H. L., "Dimensional Analysis and Theory of Models," Wiley, 1951.

55. Pierce, F. L., "Three-Dimensional Turbulent Boundary Layers," Proc. Fluidics and Internal Flow, Part II, Internal Flows, Pennsylvania State University, Dept. of Mech. Engrg., Oct. 1968.

56. Ludwieg, H., and Tillmann, W., "Investigations of the Wall-Shearing Stress in Turbulent Boundary Layers," NACA TM 1285, 1950.

57. Wang, H., and Nickerson, E. C., "Response of a Turbulent Boundary Layer to Lateral Roughness Discontinuities," Project THEMIS, Tech. Rep. No. 18, Colorado State University, Engineering Research Center Report CER71-72HW-ECN51, July 1972.

58. Huang, Chin-hua, and Nickerson, E. C., "Numerical Simulation of Wind, Temperature, Shear Stress and Turbulent Energy over Nonhomogeneous Terrain," Project THEMIS, Tech. Rep. No. 12, Colorado State University, Engineering Research Center Report CER71-72CHECN23, March, 1972.

APPENDIX A

Analysis of X-Wire Errors

Yawed wire behavior has been studied extensively by many workers. An extensive treatment together with a considerable number of bibliographic references are given in reference (47); and this source will be used as the starting point for this analysis.

The most commonly used relationships for a yawed wire exposed to three turbulent velocity components may be obtained from Fig. 15. If a wire is operated at various angles to a uniform, non-turbulent flow, the voltage output is found to vary with the mean velocity and with the yaw angle, ψ. Furthermore, to a first order approximation the wire is found to respond only to turbulent velocity components in the plane defined by the wire and the mean velocity vector (47). Stated as a total differential, the rate of change of voltage, E, may be written as

$$dE = \frac{\partial E}{\partial U} dU + \frac{\partial E}{\partial \psi} d\psi \qquad \text{(A-1)}$$

If the differentials are replaced by the perturbations e, u, and $\varepsilon\psi$, and if, by referring to Fig. 15, $\varepsilon\psi$ is expressed as

$$\varepsilon\psi = \tan^{-1} \frac{v}{U_m + u} \approx \frac{v}{U_m + u} \approx \frac{v}{U_m} \qquad \text{(A-2)}$$

then Eq. (A-1) becomes

$$e = \frac{\partial E}{\partial U} u + \frac{\partial E}{\partial \psi} \frac{v}{U_m} \qquad \text{(A-3)}$$

The differentials may be obtained from experimental calibration curves and may be thought of as coefficients of sensitivity, S_u and S_v, to u and v fluctuations respectively. That is

$$e = S_u u + S_v v \qquad \text{(A-4)}$$

where $S_u = \frac{\partial E}{\partial U}$, and $S_v = \frac{1}{U} \frac{\partial E}{\partial \Psi}$.

If rms or mean square voltages are measured, the turbulence correlations may be identified by squaring Eq. (A-4) to obtain

$$\overline{e^2} = S_u{}^2\ \overline{u^2} + S_u S_v \overline{uv} + S_v{}^2\ \overline{v^2} \tag{A-5}$$

Measurements of the voltage for three wire positions (i.e., three values of the angle, ψ) will provide three equations in the form of (A-5) which may be solved simultaneously for $\overline{u^2}$, $\overline{v^2}$, and $\overline{uv}$. If the wire plane is rotated 90°, similar results may be obtained for $\overline{u^2}$, $\overline{w^2}$, and $\overline{uw}$; therefore all components of the Reynolds stress tensor can be measured except $\overline{vw}$. For a given wire plane, angle and velocity calibrations are needed in each of the wire positions used to establish the appropriate values of S_u and S_v.

Systematic errors arise in this technique due to the assumption in passing from Eq. (A-1) to Eq. (A-2); i.e., that the differentials can be replaced by finite perturbations. For low turbulence levels, say below 10 percent, this assumption should not cause undue error; however the error will increase with increasing turbulence level. At levels of 20 percent to 30 percent turbulence, which are commonly encountered, the errors must be expected to be significant.

Turning attention to x-wire operation, Sandborn (47) gives the basic relations for two wires in the xy plane yawed at angles $+\psi$ and $-\psi$ as

$$\left.\begin{aligned} e_1 &= S_{u1}u + S_{v1}v \\ e_2 &= S_{u2}u + S_{v2}v \end{aligned}\right\} \tag{A-6}$$

Here the subscript 1 refers to a wire yawed at an angle $+\psi$ and the subscript 2 refers to the wire yawed at an angle $-\psi$ to the flow. If the wires and the associated anemometers are adjusted so that $Su_1 = Su_2$ and $Sv_2 = -Sv_1$, then the mean squares of the instantaneous sum and difference voltages produce

$$\overline{(e_i + e_2)^2} = 4S_u^2\overline{u^2}$$

$$\overline{(e_1 - e_2)^2} = 4S_v^2\overline{v^2} \tag{A-7}$$

Also

$$\overline{e_1^2} - \overline{e_2^2} = 4S_uS_v\,\overline{uv} \tag{A-8}$$

Since the instantaneous sum and difference voltages can be formed readily with operational amplifiers, the x-wire technique provides a convenient way to measure the correlation quantities without the need for multiple calibrations, repeated data readings, and solutions of simultaneous equations. Unfortunately, the results produced by x-wires have differed noticeably from yawed single-wire results at the same location and have displayed more scatter (36, 37, 47). It is therefore necessary to examine the x-wire operation more carefully.

Referring again to Fig. 15, it is apparent that all three velocity components affect the wire output; however it is well known that the component perpendicular to the wire is much more influential than the component parallel to the wire (5, 47, 51, 52, 53). In fact in many applications of the hot-wire, it is assumed that the effect of the component parallel to the wire is neglibible. To examine the relative influence of these components we will assume that the instantaneous total voltage output of the wire can be represented by the relationship

$$E - S_nU_n + S_pU_p \tag{A-9}$$

where U_n and U_p are the velocity components normal and parallel to the wire and S_n and S_p are the sensitivities of the wire output to the normal and parallel velocity components. Equation (A-9) itself involves no approximations since the voltage may be arbitrarily decomposed in this fashion; however experimental evaluation of S_n and S_p over the necessary ranges of U_n and U_p may present difficulties later.

From Fig. 15 it follows that

$$U_n = \left\{ \left[(U_m + u) \cos\theta + v \sin\theta \right]^2 + w^2 \right\}^{1/2} \tag{A-10}$$

$$U_p = (U_m + u) \sin\theta - v \cos\theta \tag{A-11}$$

At this point it can be seen that if $+\psi$ is changed to $-\psi$, Eqs. (A-10) and (A-11) become

$$U_n = \left\{ \left[(U_m + u) \cos\theta - v \sin\theta \right]^2 + w^2 \right\}^{1/2} \tag{A-12}$$

$$U_p = (U_m + u) \sin\theta + v \cos\theta \tag{A-13}$$

Considering the $+\psi$ case, (A-11) and (A-10) may be substituted in (A-9) to produce

$$E_1 = S_{n1} \left\{ \left[(U_m + u) \cos\theta + v \sin\theta \right]^2 + w^2 \right\}^{1/2} + S_{p1}(U_m + u) \sin\theta - S_{p1}\, v \cos\theta \tag{A-14}$$

For the second wire, the angle of inclination is $-\psi$, and its voltage, E_2, becomes

$$E_2 = S_{n2} \left\{ \left[(U_m + u) \cos\theta - v \sin\theta \right]^2 + w^2 \right\}^{1/2} + S_{p2}(U_m + u) \sin\theta + S_{p2}\, v \cos\theta \tag{A-15}$$

These relations can be examined for any value of θ; however $\theta = \pm 45°$ are the usual values used for x-wires. Thus, $\sin\theta = \cos\theta = \sqrt{2}/2$, and these equations become (with $A = \sqrt{2}/2$)

$$E_1 = AS_{n1}\left\{\left[(U_m + u + v\right]^2 + 2w^2\right\}^{\frac{1}{2}} + AS_{p1}(U_m + u - v) \qquad \text{(A-16)}$$

$$E_2 = AS_{n2}\left[(U_m + u - v)^2 + 2w^2\right]^{\frac{1}{2}} + AS_{p2}(U_m + u + v) \qquad \text{(A-17)}$$

In practice, θ may not be exactly $\pm 45°$, hence a possible source of error is introduced to be examined later. It would also be convenient if $S_{n1} = S_{n2}$ and $S_{p1} = S_{p2}$. The degree to which such wire matching can be achieved must also be considered. If it is assumed for now that the wires can be so matched, then the sum and difference voltages of the two wires will be

$$E_1 + E_2 = AS_n\left\{\left[(U_m + u + v)^2 + 2w^2\right]^{\frac{1}{2}} + \left[(U_m + u - v)^2 + 2w^2\right]^{\frac{1}{2}}\right\} + 2AS_p(U_m + u) \qquad \text{(A-18)}$$

$$E_1 - E_2 = AS_n\left\{\left[(U_m + u + v)^2 + 2w^2\right]^{\frac{1}{2}} - \left[(U_m + u - v)^2 + 2w^2\right]^{\frac{1}{2}}\right\} - 2AS_p v \qquad \text{(A-19)}$$

These equations may be written for convenience as

$$E_1 + E_2 = AS_n(\Phi^{\frac{1}{2}} + \chi^{\frac{1}{2}}) + 2AS_p(U_m + u) \qquad \text{(A-20)}$$

$$E_1 - E_2 = AS_n(\Phi^{\frac{1}{2}} - \chi^{\frac{1}{2}}) - 2AS_p v \qquad \text{(A-21)}$$

where

$$\Phi^{\frac{1}{2}} = (U_m{}^2 + 2U_m u + u^2 + 2U_m v + 2uv + v^2 + 2w^2{}^{\frac{1}{2}} \qquad \text{(A-22)}$$

$$\chi^{\frac{1}{2}} = (U_m{}^2 + 2U_m u + u^2 - 2U_m v - 2uv + v^2 + 2w^2{}^{\frac{1}{2}} \qquad \text{(A-23)}$$

At this point it is evident that the sum and difference voltage outputs of the x-wires are complex functions of all three turbulence components. Further mathematical analysis is possible only if the expressions (A-22) and (A-23) can be expanded in infinite series, a step which is permissable only if the relative magnitudes of the various terms within the brackets can be identified. Since it would be useful to extract the mean velocity, expansion would be desirable under the conditions that

$$U_m^2 > 2U_m u + u^2 + 2U_m v + 2uv + v^2 + 2w^2 \qquad \text{(A-24)}$$

and

$$U_m^2 > 2U_m u + u^2 - 2U_m v - 2uv + v^2 + 2w^2 \qquad \text{(A-25)}$$

recalling that u, v, and w still represent instantaneous values.

For low levels of turbulence, the inequalities may be expected to hold nearly all of the time; however it must be recognized that since u, v, w are random vaiables, there is always a finite probability that the various instantaneous terms on the right hand sides will add up to more than U_m^2 at certain instants of time. (Physically, reversals of this inequality will be related to flow reversal caused by isolated large fluctuations. The hot-wire senses only the movement of the fluid; hence reverse flow is rectified in the voltage output.) The probability of reversal of inequalities (A-24) and (A-25) will increase with increasing turbulence levels. In principle it should be possible to compute the probability of these inequalities not holding after the statistical distributions of u, v, w are measured. Such a computation would serve as a check on the goodness of the assumption.

Expanding (A-22) in a binomial series on the basis of (A-24) results in the following expression

$$\phi^{1/2} = U_m + \frac{1}{2U_m}(2U_m u + u^2 + 2U_m v + 2uv + v^2 + 2w^2)$$
$$+ \frac{(\frac{1}{2})(-\frac{1}{2})}{2U_m^3}(2U_m u + u^2 + 2U_m v + 2uv + v^2 + 2w^2)^2$$
$$+ \frac{(\frac{1}{2})(-\frac{1}{2})(-3/2)}{6U_m^5}(2U_m u + 2U_m v + ---)^3 + --- \tag{A-26}$$

which becomes

$$\phi^{1/2} = U_m + u + \frac{u^2}{2U_m} + v + \frac{uv}{U_m} + \frac{v^2}{2U_m} + \frac{w^2}{U_m}$$
$$- \frac{1}{8U_m^3}\left[4U_m^2u^2 + 4U_m^2v^2 + 8U_m^2uv + O(u^3)\right] + O(u^3) \tag{A-27}$$

or finally

$$\phi^{1/2} = U_m + u + v + \frac{w^2}{U_m} + --- O(u^3) \tag{A-28}$$

Similarly, (A-23) becomes

$$\chi^{1/2} = U_m + \frac{1}{2U_m}(2U_m u + u^2 - 2U_m v - 2uv + v^2 + 2w^2$$
$$- \frac{1}{8U_m^3}(2U_m u + u^2 - 2U_m v - 2uv + v^2 + 2w^2)^2 + --- O(u^3) \tag{A-29}$$

or

$$\chi^{1/2} = U_m + u + \frac{u^2}{2U_m} - v - \frac{uv}{U_m} + \frac{v^2}{2U_m} + \frac{w^2}{U_m} - \frac{u^2}{2U_m} - \frac{v^2}{2U_m} + \frac{uv}{U_m} + --- O(u^3) \tag{A-30}$$

Finally

$$\chi^{1/2} = U_m + u - v + \frac{w^2}{U_m} + --- O(u^3) \tag{A-31}$$

Expansion (A-31) and (A-28) may be used in (A-20) and (A-21) to produce

$$E_1 + E_2 = AS_n(2U_m + \frac{2w^2}{U_m}) + 2AS_p(U_m + u) + --- + O(u^3) \tag{A-32}$$

$$E_1 - E_2 = AS_n(2v) - 2AS_p v + --- + O(u^3) \tag{A-33}$$

From this point the analysis will depend on how the signals are processed electronically. In the present tests the DC portions were separated from the AC portions by a high pass filter with a roll-off frequency below 1 hz. The effect, then, is to split the voltages in (A-32) and (A-33) into mean and fluctuating parts. The mean values are

$$\overline{E_1 + E_2} = AS_n(2U_m + 2\,\frac{\overline{w^2}}{U_m}) + 2AS_p U_m + --- + O(\overline{u^3}) \tag{A-34}$$

$$\overline{E_1 - E_2} = O(\overline{u^3}) \tag{A-35}$$

and the fluctuating parts are

$$(e_1 + e_2) = AS_n(2u + \frac{2w^2}{U_m}) + 2AS_p u + --- + O(u^3) \tag{A-36}$$

$$(e_1 - e_2) = AS_n(2v) - 2AS_p v + --- + O(u^3) \tag{A-37}$$

It should be noted in regard to the terms $\overline{O(u^3)}$ that higher-order correlations may not necessarily be smaller than lower-order correlations. Subsequent neglect of these terms involves such an assumption; although it is a reasonable one in light of experimental results in turbulent flow.

At this point it is possible to relate S_n and S_p to the calibration process, which is carried out in the free stream where the turbulence is negligible. The mean sum voltage during calibration may be obtained from (A-34) as

$$\overline{E_1 + E_2} = 2A(S_n + S_p)U_m \tag{A-38}$$

Hence the linearized calibration constant S_c is equal to

$$S_c = 2A(S_n + S_p) \tag{A-39}$$

To obtain an approximate relationship between S_n and S_p, the results presented by Champagne (51) are used. Champagne obtained a relationship between the velocity indicated by a wire yawed at an angle, α, and the velocity indicated by the wire normal to the flow in the form

$$U^2(\alpha) = U^2(0)[\cos^2\alpha + k^2\sin^2\alpha] \tag{A-40}$$

or

$$U(\alpha) = U(0)[\cos^2\alpha + k^2\sin^2\alpha]^{\frac{1}{2}} \tag{A-41}$$

Expanding (A-41) in a binomial series, since

$$U(\alpha) = U(0)[\cos\alpha + \frac{1}{2\cos} k^2\sin^2\alpha + ---] \tag{A-42}$$

$$U(\alpha) = U(0)[\cos\alpha + \frac{1}{2}(\frac{\sin\alpha}{\cos\alpha}) k^2\sin^2\alpha +---] \tag{A-43}$$

$$U(\alpha) = U_n + \frac{k^2}{2} (\tan \alpha)U_p + --- \tag{A-44}$$

Now the inclined wire is calibrated in operating position to produce a voltage, $E(\alpha)$

$$E(\alpha) = S_I U(\alpha) \tag{A-45}$$

$$E(\alpha) = S_I U_n + \frac{k^2}{2}(\tan \alpha)S_I U_p + --- \tag{A-46}$$

Recalling (A-9)

$$E = S_n U_n + S_p U_p \tag{A-9}$$

It follows that

$$\frac{S_p}{S_n} \cong \frac{k^2}{2} \tan \alpha \tag{A-47}$$

For the wires used in the present tests, the length: diameter ratio is 333, for which Champagne gives the value of $k = 0.15$. Hence, since $\alpha = 45°$

$$\frac{S_p}{S_n} = 0.112 \tag{A-48}$$

Using (A-48) and (A-39), values for S_n and S_p may be obtained in terms of the calibration constant, S_c, as

$$S_n = \frac{S_c}{2.0224A} \qquad S_p = \frac{0.0112}{2.0224A} S_c \tag{A-49}$$

Several comments should be noted at this point. First, the ratio between S_p and S_n given by Eq. (A-47) varies with angle in a nonlinear fashion so that for large levels of turbulence where the direction of the flow vector varies widely, this ratio will be in error due to nonlinear averaging. Nevertheless, for the wires used, S_p is obviously much smaller than S_n, and this error can be reasonably neglected. (In fact, it would not be unreasonable to neglect S_p entirely. For other wire configurations where $1/d$ is smaller, the entire analysis given above would have to be reconsidered including the original proposition represented by Eq. (A-9).

Another point to note in regard to Eq. (A-34) is that the rms value of the w fluctuation affects the mean (DC) output of the wires and therefore the mean velocity measurements. Examination of Fig. 15 reveals that this result is physically realistic since both $+w$ and $-w$ fluctuations add to the voltage output whereas + and - fluctuations of u and v add and subtract alternately and therefore cancel. The w effect does not appear in the difference output, Eq. (A-35), since both wires are affected equally.

A correction for the error due to $\overline{w^2}$ may be obtained by solving (A-34), which is quadratic in U_m, using (A-49) to relate the calibration coefficient, S_c. After some algebra, the result is

$$U_m = \frac{\frac{\overline{E_1 + E_2}}{S_c} + \sqrt{\left(\frac{\overline{E_1 + E_2}}{S_c}\right)^2 - \frac{4\overline{w^2}}{1.0112}}}{2} \tag{A-50}$$

Here, it can be noted that $\frac{\overline{E_1 + E_2}}{S_c}$ is just the apparent velocity, U_I, indicated by the x-wire and U_m is the correct velocity. Therefore

$$U_m = \frac{1}{2}\left[U_I + \sqrt{U_I^2 - \frac{4\overline{w^2}}{1.0112}}\right] \tag{A-51}$$

Equation (A-51) was used to correct all mean velocity measurements taken with x-wires. (When the wires are turned to the horizontal plane, $\overline{w^2}$ is replaced by $\overline{v^2}$.) As can be seen from (A-51), the indicated velocity is too high as a result of the influence of the w fluctuations.

Turning next to the u fluctuations, it can be seen from Eq. (A-36) that the w fluctuations also affect the fluctuating portion of the sum voltage. In these tests (and in common practice) the rms value of $e_1 + e_2$ is measured. Mathematically, if Eq. (A-36) squared and terms of order u^3 are neglected, the result becomes

$$\overline{(e_1 + e_2)^2} = \overline{\left[2A(S_n + S_p)\, u + 2AS_n \frac{w^2}{U_m}\right]^2} \tag{A-52}$$

It is evident that the influence of w^2 is of order $\overline{uw^2}/U_m$, which should be small relative to $\overline{u^2}$. (The value of $\overline{uw^2}$ may be either positive or negative and therefore could cause the rms voltage to be either too high or too low depending on local conditions.) Neglecting this term and using Eq. (A-39) leads to

$$\overline{(e_1 + e_2)^2} = S_c^{\,2}\, \overline{u^2} \tag{A-53}$$

which is identical to Eq/ (A-7) and restates the usual assumption that the sum rms voltage is directly a function of $\overline{u^2}$. Equation (A-53) was used for initial reduction of $\overline{u^2}$ data and the results were compared to sample yawed wire data.

Analysis of $\overline{v^2}$ follows from Eq. (A-37). Neglecting terms of order u^3v, the rms output of the difference voltage becomes, using (A-49)

$$\overline{(e_1 - e_2)^2} = 0.951\ S_c{}^2\ \overline{v^2} \tag{A-54}$$

The Reynolds stress $\overline{uv}$ (or $\overline{uw}$) was determined by feeding the fluctuating portions of the sum and difference voltages into the Princeton correlator, which forms the instantaneous product of these inputs and time-averages the result. Mathematically, this operation is equivalent to multiplying together Eqs. (A-36) and (A-37) and forming the mean value of the product.

$$\overline{(e_1 + e_2)(e_1 - e_2)} = 4A^2(S_n{}^2 - S_p{}^2)\ \overline{uv} + 4A^2(S_n{}^2 - S_nS_p)\ \frac{\overline{vw^2}}{U_m} \tag{A-55}$$

Neglecting the $\overline{vw^2}$ term and using (A-49), the result is

$$\overline{(e_1 + e_2)(e_1 - e_2)} = 0.978\ S_c{}^2\ \overline{uv} \tag{A-56}$$

At this point it may be noted that Eq. (A-56) is very similar to Eq. (A-8) differing only in the definition of the sensitivity coefficient, S_c, versus S_u and S_v. If the assumptions leading to Eqs. (A-53), (A-54), and (A-56) were all reasonably correct, it could be expected that the experimentally determined quantity, $S_v = \frac{I}{U}\frac{\partial E}{\partial \psi}$, would be equal to 0.978 S_c and $S_u = S_c$. Measurements of the value of $\frac{\bar{I}}{\bar{U}}\frac{\partial E}{\partial \psi}$ were obtained over a range of ±10° using a vernier angle fixture on a thermo-systems calibrator. The resulting data was linearized by computer-fitting straight lines to each set by the least-squares procedure. (See Fig. 16, which is an example of the data and resulting least-squares lines for each wire.)

The resulting values of S_V differed greatly from the predicted value of 0.978 S_c--the discrepancy being as great as 16 percent. Even though the best value obtained among the probes used in the tests differed by only one percent from the ideal value, the reason for the discrepancies in the other probes was sought in more detail.

Microscopic examination revealed that the wire angles were not exactly 45° as required by the assumption leading to Eqs. (A-16) and (A-17). Ultimately, the wires were microphotographed on a Bausch and Lomb metallurgical microscope (metallograph) equipped with a traversing stage. During this procedure, the probes were clamped against a straight edge and the pictures were double-exposed--once with the wire in focus and once with the straight edge in focus. Then the wire angle was measured directly from the photographs using a precision vernier protractor. The results revealed wide variations in wire angles as well as wire curvature which meant that the wire tangent varied along the length of the wire. Two example photographs are included in Fig. 17; and since photo duplicated copies of these pictures may not be too clear, tracings of the wire shapes are included in Fig. 18.

The discrepancies in wire slope appeared to correlate with the variations in S_V determined experimentally. To establish a more firm relationship, the angle dependencies in Eqs. (A-14) and (A-15) were retained and carried through the derivation to the same level of approximation. The steps are straightforward, although tedious, and the results are

$$S_n = \frac{S_c}{\cos\theta_1 + \cos\theta_2 + \frac{1}{2}k^2\tan\alpha(\sin\theta_1 + \sin\theta_2)} \tag{A-57}$$

$$S_p = S_n(\frac{1}{2}k^2\tan\alpha) \tag{A-58}$$

$$e_1 + e_2 = S_n\left[u(\cos\theta_1 + \cos\theta_2) + v(\sin\theta_1 - \sin\theta_2)\right]$$

$$+ S_p u(\sin\theta_1 + \sin\theta_2) + S_p v(\cos\theta_2 - \cos\theta_1) \tag{A-59}$$

$$e_1 - e_2 = S_n\left[u(\cos\theta_1 - \cos\theta_2) + v(\sin\theta_1 + \sin\theta_2)\right]$$

$$+ S_p u(\sin\theta_1 - \sin\theta_2) - S_p v(\cos\theta_2 + \cos\theta_1) \tag{A-60}$$

where

$$\theta_1 = 90° - \psi_1$$
$$\theta_2 = 90° - \psi_2$$

and α is taken as the average of ψ_1 and ψ_2.

As can be seen from Eqs. (A-59) and (A-60), there now appears an influence of v upon the sum voltage and u upon the difference voltage depending on how much the wire angles deviate from ±45°. Computation of these terms revealed that for the worst case the cross influence of u and v was two or more orders of magnitude smaller than the other terms; hence these effects were neglected.

Using the measured angles from the microphotographs, the values of S_v/S_u were evaluated from Eqs. (A-57) through (A-60). These results were then compared to the experimental values of S_v/S_u obtained by yaw calibration (see Table II). Comparing the predicted values to the experimental values, it can be seen that the results agree reasonably well for two probes (#5236 and #5237). In the case of the other probe, one wire was broken during the photographic efforts and the calculated value is based on the apparent angle, which may well have been altered when the wire was broken.

Examination of the computed values of S_V from Eqs. (A-57) to (A-60) reveals that a cumulative discrepancy of $1\frac{1}{2}°$ in the wire angles causes a change in S_V of roughly four percent. This extreme sensitivity to variations in the probes used underscores the importance of careful calibration for S_V. These points also suggest a likely source for some of the reported variations in x-wire data.

For data reduction the calibrated values of S_V were used. As a further check on the x-wire results, representative data measurements were repeated using the single yawed-wire technique. Figures 19, 20, and 21 show the comparative values obtained. It will be noted that there is considerable scatter in the yawed wire results. In subsequent review of procedures used it was determined that the probable cause for this scatter lies in the somewhat unorthodox technique used to obtain the three values needed at each data location (Eq. (A-5)). Rather than rotating the wire at each data point, the wire was traversed through all points at one angle setting; then it was rotated to the second angle position and traversed again. While this technique minimized errors due to calibration drift and angle position errors (the wire was very carefully calibrated before each traverse), small variations due to traversing position errors led to larger variations in the simultaneous solutions of Eq. (A-5). In retrospect, it would have been better to rotate the wire to three angular positions without moving the traversing mechanism.

In any case, examination of the comparison in Figs. 19, 20, and 21 reveal several facts. First, the values of $\sqrt{\overline{u^2}}$ and of $\overline{uv}$ are slightly higher from the x-wire than from the yawed wire while the values of $\sqrt{\overline{v^2}}$ from both methods agree very well. In addition, comparison of values obtained from different x-wire probes agree with one another if the correction factors are taken into account; hence the probes used seem to produce values of $\overline{uv}$ and $\sqrt{\overline{u^2}}$ which are consistently high by comparison with yawed wire results. The larger errors in outputs involving the sum voltage as opposed to that involving the difference voltage is not unexpected. Equation (A-52) for the sum voltage contains triple correlation terms which are neglected in the data reduction while the lowest order term neglected in the difference rms voltage (Eq. (A-37) would be of order $(\overline{u^3 v})$, a fourth-order correlation term.

Figure 19 also reveals the effect on $\sqrt{\overline{u^2}}$ values of having the wires arranged in a horizontal plane rather than a vertical plane. Within two inches of the wall, higher values of $\sqrt{\overline{u^2}}$ are indicated by both the x-wire and single wire probes when in the horizontal plane. This effect has been discussed at length by Sandborn (47), who ascribes the cause to the steep turbulence gradients near the wall which causes a vertical wire to see considerable variation in $\sqrt{\overline{u^2}}$ along its length.

Considering these various effects, it is evident that the horizontal wire measurements of $\sqrt{\overline{u^2}}$ should be given more credence than the vertical measurements. (Since $\sqrt{\overline{w^2}}$ and $\overline{uw}$ measurements were obtained, as well as $\sqrt{\overline{v^2}}$ and $\overline{uv}$, both horizontal and vertical measurements of $\sqrt{\overline{u^2}}$ were taken throughout the data field.) To examine the discrepancy between x-wire and yawed wire values of

$\sqrt{\overline{u^2}}$, $\sqrt{\overline{v^2}}$, and $\sqrt{\overline{w^2}}$, the differences were tabulated in detail, and it was found that the spread was relatively constant and equal to about four percent. The effect on $\overline{uv}$ values in Fig. 21 is also present; although it is not so clear due to the data scatter. (The average difference for $\overline{uv}$ values in Fig. 21 is closer to six percent, but with a high level of uncertainty.)

The comparisons described here were consistent among three x-wire probes used throughout the study; hence it was decided that correction factors would be applied to the $\sqrt{\overline{v^2}}$, $\sqrt{\overline{w^2}}$, $\overline{uv}$, and $\overline{uw}$ measurements based on the experimental values of S_V for the probe used. No correction was applied for the four percent errors in u values since this error might vary somewhat throughout the field. Values of $\sqrt{\overline{u^2}}$, $\overline{uv}$, and $\overline{uw}$ are therefore slightly high; however the results should be internally consistent.

Velocity Gradient Effects

It was observed in the preceding section that horizontally oriented wires tended to produce higher values of $\sqrt{\overline{u^2}}$ than vertical wires and that this effect has been ascribed to turbulence gradient effects. As an additional note, the recent work of Gessner and Moller (49) may be considered since it pertains to the effects of mean velocity gradients upon the wire outputs. It has been recognized by various workers that hot wires exposed to velocity gradients along their lengths will be subject to errors due to skewed cooling effects (46, 47, 48, 49). Gessner and Moller derived corrections for effects of velocity gradients upon hot-wire outputs in terms of a shear parameter, S, defined by

$$S = \frac{\Delta U/U}{l/d} \tag{A-61}$$

where U is the velocity at the center of the wire, ΔU is the variation in velocity along the wire, and l/d is the length-to-diameter ratio for the wire. Evaluating this parameter for the worst case observed in the present tests reveals that $S = 0.21 \times 10^{-3}$ ($\Delta U/U = 0.08$, $l/d = 333$). For this value of S, the corrections listed by Gessner and Moller are negligible; hence no corrections for this effect are included in the data reduction.

TABLES

Table I

Summary of hot-wire calibration data and regression line analysis

Date	Calibration run	Sample size	Intercept	Slope	Standard Error of slope	Correlation Coeff.	Variances: Due to regression	Variances: About regression	F value
			Regression line analysis						
6-22	1	6	.078	.197	.0037	.9993	13.8915	.0050	2794.
	2	5	.124	.200	.0022	.9998	13.4070	.0016	8422.
	3	5	.180	.198	.0029	.9997	10.4751	.0022	4769.
	4	6	.261	.191	.0036	.9993	13.1105	.0046	2865.
6-23	1	6	.243	.194	.0045	.9989	14.5892	.0078	1868.
	2	5	.396	.192	.0047	.9991	11.5422	.0069	1684.
6-24	1	6	.161	.200	.0042	.9991	14.1609	.0064	2231.
	2	6	.134	.200	.0032	.9995	18.3065	.0047	3895.
6-25	1	8	.229	.198	.0039	.9988	22.8174	.0089	2577.
	2	5	.345	.193	.0049	.9991	16.0637	.0102	1582.
6-26	1	6	.330	.199	.0048	.9988	18.7683	.0110	1713.
	2	6	.335	.195	.0035	.9994	17.9994	.0059	3053.
6-28	1	6	.263	.196	.0032	.9995	17.6153	.0046	3822.
6-29	1	6	.210	.197	.0040	.9992	16.6464	.0069	2425.
	2	4	.245	.195	.0018	.9999	10.2267	.0008	11931.
	3	4	.486	.187	.0065	.9988	7.6444	.0093	820
	4	6	.223	.195	.0034	.9994	16.0067	.0050	3212.
6-30	1	6	.053	.203	.0023	.9998	18.8320	.0024	7960.
	2	6	.317	.191	.0041	.9991	16.3041	.0074	2207.
	3	6	.306	.194	.0029	.9996	16.1582	.0036	4398.
	4	6	.321	.193	.0047	.9988	16.9025	.0100	1648.
7-1	1	6	.173	.198	.0061	.9981	17.3858	.0166	1048.
	2	6	.055	.202	.0043	.9991	17.6148	.0080	2192.
	3	6	.103	.210	.0033	.9995	19.0141	.0052	3649.
7-2	1	6	.007	.202	.0027	.9997	18.5600	.0032	5826.
	2	6	.042	.200	.0029	.9996	18.3819	.0039	4723.
	3	6	.165	.198	.0029	.9996	17.8320	.0039	4530.
	4	6	-.032	.202	.0015	.9999	19.5815	.0011	17721.
7-3	1	6	.109	.201	.0047	.9989	18.7845	.0101	1854.
	2	6	-.029	.205	.0012	.9999	20.2252	.0007	31345.
	3	6	.118	.203	.0047	.9990	18.6508	.0098	1896.
	4	6	.024	.206	.0012	.9999	19.9161	.0007	29273.
7-5	1	6	.100	.201	.0032	.9995	19.0750	.0049	3927.
	2	6	.075	.197	.0014	.9999	19.0488	.0009	20419.
7-6	1	6	-.078	.196	.0041	.9992	18.9099	.0081	2347.
	2	6	.064	.198	.0047	.9989	19.4164	.0109	1783.
7-6	3	6	.133	.198	.0031	.9995	17.8797	.0044	4058.
	4	6	.016	.204	.0026	.9997	18.6060	.0029	6322.
	5	6	.001	.201	.0044	.9991	19.0979	.0090	2123.
7-7	1	6	-.086	.202	.0015	.9999	18.6757	.0011	17817.
	2	6	.103	.201	.0044	.9990	17.8202	.0087	2057.
	3	6	-.065	.204	.0033	.9995	19.0216	.0051	3726.
7-8	1	6	.006	.202	.0036	.9994	16.7856	.0054	3086.
	2	6	-.045	.207	.0024	.9997	19.8008	.0026	7745.

Table II

x-wire Characteristics

Probe Number	Wire Number	Wire Angle (tip-to-tip)	Range of local Wire Angle (min.)	(max)	Average Angle (avg. of 10 pts.)	S_v/S_u Computed	S_v/S_u from angle calibration
5239	1	46°50'	see note			0.916	1.035
	2	47°15'	41°0'	53°30'	46°49'		
5237	1	46°10'	39°15'	51°35'	44°56'	0.956	0.971
	2	47°35'	47°5'	48°0'	46°20'		
5236	1	49°30'	48°0'	52°0'	49°32'	0.830	0.815
	2	50°10'	48°45'	50°15'	49°37'		

Note: Wire #1 on probe #5239 was broken during the photographic process. The wire angle listed is the apparent angle measured across the wire supports and is questionable.

Table III Corrected data listing

NUMBER	TEST NUMBER	X FEET	Y INCHES	Z INCHES	VELOCITY FPS	U RMS FPS	V RMS FPS	W RMS FPS	UV (FPS)X(FPS)	UW (FPS)X(FPS)
1	1	-3.000	0.852	18.714	26.881	3.491	1.487		-1.815	
2	2	-3.000	0.852	16.111	27.114	3.437	1.487		-1.913	
3	3	-3.000	0.852	13.509	27.086	3.356	1.434		-1.794	
4	4	-3.000	0.852	10.906	27.663	3.383	1.445		-1.794	
5	5	-3.000	0.852	8.303	27.118	3.248	1.424		-1.794	
6	6	-3.000	0.852	5.700	25.743	3.329	1.424		-1.794	
7	7	-3.000	0.852	3.097	26.487	3.329	1.424		-1.794	
8	8	-3.000	0.852	0.0	25.637	3.410	1.413		-1.794	
9	9	-3.000	0.852	-2.108	26.192	3.383	1.413		-1.642	
10	10	-3.000	0.852	-4.711	26.438	3.383	1.445		-1.805	
11	11	-3.000	0.852	-7.314	27.363	3.383	1.434		-1.794	
12	12	-3.000	0.852	-9.917	27.887	3.410	1.434		-1.827	
13	13	-3.000	0.852	-12.520	27.908	3.383	1.466		-1.761	
14	14	-3.000	0.852	-15.122	27.784	3.491	1.497		-1.979	
15	15	-3.000	0.852	-17.725	27.592	3.491	1.528			
16	16	-3.000	0.852	18.714		3.383		1.967		-0.082
17	17	-3.000	0.852	16.111		3.383		1.967		0.027
18	18	-3.000	0.852	13.509		3.410		1.967		0.136
19	19	-3.000	0.852	10.906		3.383		1.935		0.055
20	20	-3.000	0.852	8.303		3.302		1.920		-0.462
21	21	-3.000	0.852	5.700		3.329		1.935		-0.217
22	22	-3.000	0.852	3.097		3.275		1.888		-0.082
23	23	-3.000	0.852	0.0	26.150	3.329		1.888		-0.055
24	24	-3.000	0.852	-2.108		3.329		1.904		0.082
25	25	-3.000	0.852	-4.711		3.329		1.904		0.055
26	26	-3.000	0.852	-7.314		3.356		1.935		0.299
27	27	-3.000	0.852	-9.917		3.383		1.951		0.244
28	28	-3.000	0.852	-12.520		3.410		1.983		0.055
29	29	-3.000	0.852	-15.122		3.464		1.983		-0.109
30	30	-3.000	0.852	-17.725	26.915	3.518		2.062		-0.299
31	31	-3.000	5.052	18.714	33.727	2.207	1.298		-1.287	
32	32	-3.000	5.052	13.509	34.391	2.171	1.246		-1.160	
33	33	-3.000	5.052	8.303	33.415	2.207	1.308		-1.213	
34	34	-3.000	5.052	3.097	32.437	2.224	1.308		-1.371	
35	35	-3.000	5.052	0.0	33.116	2.224	1.308		-1.298	
36	36	-3.000	5.052	-2.108	33.343	2.171	1.267		-1.076	
37	37	-3.000	5.052	-7.314	33.565	2.154	1.277		-1.086	
38	38	-3.000	5.052	-12.520	35.173	2.119	1.225		-1.002	
39	39	-3.000	5.052	-17.725	34.647	2.137	1.267		-1.107	
40	40	-3.000	5.052	18.714		2.196		1.516		-0.053
41	41	-3.000	5.052	13.509		2.061		1.475		0.042
42	42	-3.000	5.052	8.303		2.255		1.557		-0.401
43	43	-3.000	5.052	3.097		2.255		1.610		-0.211
44	44	-3.000	5.052	0.0	32.909	2.196		1.568		0.074
45	45	-3.000	5.052	-2.108		2.121		1.547		0.021
46	46	-3.000	5.052	-7.314		2.107		1.495		0.138
47	47	-3.000	5.052	-12.520		2.077		1.475		0.116
48	48	-3.000	5.052	-17.725		2.107		1.475		-0.053
49	49	-3.000	0.572	0.0	24.876	3.366	1.374		-1.755	
50	50	-3.000	0.852	0.0	26.113	3.232	1.385		-1.797	

Table III (Continued)

NUMBER	TEST NUMBER	X FEET	Y INCHES	Z INCHES	VELOCITY FPS	U RMS FPS	V RMS FPS	W RMS FPS	UV (FPS)X(FPS)	UW (FPS)X(FPS)
51	51	-3.000	1.552	0.0	28.428	3.097	1.437		-1.786	
52	52	-3.000	2.252	0.0	29.791	2.854	1.395		-1.625	
53	53	-3.000	3.652	0.0	31.733	2.612	1.374		-1.529	
54	54	-3.000	5.052	0.0	33.313	2.263	1.353		-1.410	
55	55	-3.000	7.852	0.0	36.355	1.946	1.206		-1.076	
56	56	-3.000	10.652	0.0	37.695	1.614	1.018		-0.654	
57	57	-3.000	13.452	0.0	39.092	1.057	0.777		-0.306	
58	58	-3.000	16.252	0.0	39.783	0.503	0.451		-0.069	
59	59	-3.000	19.052	0.0	40.064	0.206	0.209		-0.001	
60	60	-3.000	0.712	0.0	25.588	3.366	1.374		-1.884	
61	61	-3.000	1.132	0.0	27.143	3.205	1.416		-1.905	
62	62	-3.000	0.572	-15.122	26.543	3.796	1.511		-1.886	
63	63	-3.000	0.712	-15.122	27.881	3.685	1.533		-1.909	
64	64	-3.000	0.852	-15.122	28.056	3.517	1.511		-1.851	
65	65	-3.000	1.132	-15.122	29.838	3.489	1.544		-1.920	
66	66	-3.000	1.552	-15.122	30.994	3.207	1.490		-1.793	
67	67	-3.000	2.252	-15.122	32.760	2.941	1.479		-1.793	
68	68	-3.000	5.052	-15.122	36.074	2.255	1.316		-1.214	
69	69	-3.000	7.852	-15.122	38.593	1.489	1.055		-0.593	
70	70	-3.000	10.652	-15.122	39.354	0.830	0.685		-0.181	
71	71	-3.000	13.452	-15.122	40.275	0.436	0.413		0.002	
72	72	-3.000	16.252	-15.122	40.033	0.256	0.217		0.017	
73	73	-3.000	19.052	-15.122	40.471	0.191	0.153		-0.017	
74	74	-3.000	0.572	-15.122	26.163	3.713		2.175		-0.405
75	75	-3.000	0.712	-15.122		3.545		2.127		-0.376
76	76	-3.000	0.852	-15.122		3.601		2.110		-0.261
77	77	-3.000	1.132	-15.122		3.517		2.045		-0.231
78	78	-3.000	1.552	-15.122	31.139	3.251		1.746		-0.231
79	79	-3.000	2.252	-15.122		2.875		1.530		-0.144
80	80	-3.000	5.052	-15.122		2.411		1.168		-0.002
81	81	2.000	0.852	0.0	17.369	4.535		2.829		0.028
82	82	2.000	0.852	-2.108	17.653	4.591		2.867		-0.561
83	83	2.000	0.852	-4.711	18.227	4.563		2.848		0.365
84	84	2.000	0.852	-6.273	17.600	4.783		3.021		-0.308
85	85	2.000	0.852	-6.793	17.620	4.623		2.961		-0.168
86	86	2.000	0.852	-7.314	17.218	4.868		3.098		1.037
87	87	2.000	0.852	-7.574	18.290	4.938		3.007		3.167
88	88	2.000	0.852	-7.834	20.487	4.623		2.870		2.887
89	89	2.000	0.852	-8.095	21.504	4.413		2.665		2.326
90	90	2.000	0.852	-8.355	23.052	4.133		2.486		1.962
91	91	2.000	0.852	-8.876	24.232	3.888		2.237		1.177
92	92	2.000	0.852	-9.917	25.796	3.572		2.065		0.392
93	93	2.000	0.852	-12.520	27.149	3.484		2.075		0.224
94	94	2.000	0.852	-15.122	27.196	3.418		2.062		-0.113
95	95	2.000	0.852	-17.725	27.195	3.352		2.102		0.028
96	96	2.000	0.852	-7.626	19.371	4.868		2.983		3.504
97	97	2.000	0.852	-7.704	19.754	4.728		2.963		3.587
98	98	2.000	0.852	0.0	17.996	4.238	2.115		-3.643	
99	99	2.000	0.852	-2.108		4.342	2.129		-3.784	
100	100	2.000	0.852	-4.711		4.342	2.075		-3.756	

Table III (Continued)

NUMBER	TEST NUMBER	X FEET	Y INCHES	Z INCHES	VELOCITY FPS	U RMS FPS	V RMS FPS	W RMS FPS	UV (FPS)X(FPS)	UW (FPS)X(FPS)
101	101	2.000	0.852	-6.273		4.413	2.260		-4.344	
102	102	2.000	0.852	-6.793		4.518	2.273		-4.260	
103	103	2.000	0.852	-7.314		4.728	2.432		-4.652	
104	104	2.000	0.852	-7.574	19.022	4.693	2.269		-3.839	
105	105	2.000	0.852	-7.626		4.553	2.173		-3.476	
106	106	2.000	0.852	-7.704	19.057	4.553	2.173		-3.476	
107	107	2.000	0.852	-7.834		4.342	2.014		-2.859	
108	108	2.000	0.852	-8.095		4.238	1.933		-2.550	
109	109	2.000	0.852	-8.355	21.649	3.930	1.785		-2.046	
110	110	2.000	0.852	-8.876		3.655	1.586		-1.906	
111	111	2.000	0.852	-9.917		3.325	1.415		-1.878	
112	112	2.000	0.852	-12.520		3.160	1.362		-1.872	
113	113	2.000	0.852	-15.122		3.160	1.362		-1.872	
114	114	2.000	0.852	-17.725		3.188	1.388		-1.906	
115	115	2.000	1.132	0.0	21.342	4.211		2.588		-0.143
116	116	2.000	1.132	-2.108	21.330	4.317		2.627		0.029
117	117	2.000	1.132	-4.711	21.606	4.317		2.647		-0.002
118	118	2.000	1.132	-6.793	21.095	4.424		2.802		0.229
119	119	2.000	1.132	-7.314	21.738	4.636		2.897		1.631
120	120	2.000	1.132	-7.574	22.331	4.600		2.802		2.775
121	121	2.000	1.132	-7.678	23.056	4.459		2.647		2.948
122	122	2.000	1.132	-7.834	23.901	4.317		2.627		2.975
123	123	2.000	1.132	-8.095	24.691	4.247		2.550		2.575
124	124	2.000	1.132	-8.355	25.566	3.963		2.338		2.089
125	125	2.000	1.132	-9.917	28.212	3.433		2.048		0.343
126	126	2.000	1.132	-12.520	28.311	3.256		2.009		0.114
127	127	2.000	1.132	-15.122	28.908	3.256		2.009		-0.002
128	128	2.000	1.132	-17.725	28.742	3.326		2.048		-0.057
129	129	2.000	1.132	-8.876	26.777	3.751		2.163		1.001
130	130	2.000	1.132	-7.054	20.943	4.565		2.839		0.687
131	131	2.000	1.132	0.0	21.312	4.282	2.084		-3.949	
132	132	2.000	1.132	-2.108		4.282	2.084		-3.891	
133	133	2.000	1.132	-4.711		4.317	2.084		-3.862	
134	134	2.000	1.132	-6.793		4.388	2.190		-4.349	
135	135	2.000	1.132	-7.054		4.530	2.257		-4.521	
136	136	2.000	1.132	-7.314		4.530	2.257		-4.149	
137	137	2.000	1.132	-7.574		4.565	2.230		-3.891	
138	138	2.000	1.132	-7.678	23.288	4.565	2.190		-3.520	
139	139	2.000	1.132	-7.834		4.317	2.030		-3.204	
140	140	2.000	1.132	-8.095		4.247	1.950		-2.804	
141	141	2.000	1.132	-8.355		4.035	1.829		-2.432	
142	142	2.000	1.132	-9.917		3.539	1.536		-2.146	
143	143	2.000	1.132	-12.520		3.256	1.562		-2.146	
144	144	2.000	1.132	-15.122		3.326	1.562		-2.232	
145	145	2.000	1.132	-17.725		3.326	1.536		-2.175	
146	146	2.000	1.692	0.0	26.415	3.813		2.185		-0.527
147	147	2.000	1.692	-2.108	26.404	3.893		2.216		-0.448
148	148	2.000	1.692	-4.711	25.671	3.893		2.247		-0.002
149	149	2.000	1.692	-6.273	26.000	3.919		2.263		-0.474
150	150	2.000	1.692	-6.793	26.632	3.919		2.341		-0.026

Table III (Continued)

NUMBER	TEST NUMBER	X FEET	Y INCHES	Z INCHES	VELOCITY FPS	U RMS FPS	V RMS FPS	W RMS FPS	UV (FPS)X(FPS)	UW (FPS)X(FPS)
151	151	2.000	1.692	-7.054	26.779	3.973		2.341		0.474
152	152	2.000	1.692	-7.314	27.627	3.919		2.310		0.739
153	153	2.000	1.692	-7.574	27.197	3.893		2.278		0.923
154	154	2.000	1.692	-7.678	27.389	3.786		2.201		1.187
155	155	2.000	1.692	-7.834	27.829	3.786		2.185		1.107
156	156	2.000	1.692	-8.095	27.723	3.599		2.124		1.213
157	157	2.000	1.692	-8.355	27.876	3.412		2.031		1.002
158	158	2.000	1.692	-8.876	28.650	3.359		1.969		0.554
159	159	2.000	1.692	-9.917	29.326	3.066		1.829		0.185
160	160	2.000	1.692	-12.520	29.756	3.093		1.844		-0.185
161	161	2.000	1.692	-15.122	29.930	3.013		1.829		-0.079
162	162	2.000	1.692	-17.725	29.997	3.093		1.860		-0.026
163	163	2.000	1.692	0.0	26.517	3.866	1.705		-2.637	
164	164	2.000	1.692	-2.108		3.839	1.705		-2.637	
165	165	2.000	1.692	-4.711		3.866	1.705		-2.558	
166	166	2.000	1.692	-6.273		3.866	1.744		-2.690	
167	167	2.000	1.692	-6.793		3.919	1.783		-2.769	
168	168	2.000	1.692	-7.314		3.893	1.770		-2.769	
169	169	2.000	1.692	-7.574	26.814	3.866	1.744		-2.373	
170	170	2.000	1.692	-7.834		3.760	1.667		-2.189	
171	171	2.000	1.692	-7.678	27.229	3.760	1.667		-2.347	
172	172	2.000	1.692	-7.054		3.919	1.783		-2.796	
173	173	2.000	1.692	-8.095		3.599	1.615		-2.163	
174	174	2.000	1.692	-8.355		3.466	1.564		-1.899	
175	175	2.000	1.692	-8.876		3.226	1.449		-1.556	
176	176	2.000	1.692	-9.917		3.066	1.411		-1.498	
177	177	2.000	1.692	-12.520		3.040	1.411		-1.656	
178	178	2.000	1.692	-15.122		3.013	1.411		-1.572	
179	179	2.000	1.692	-17.725		3.066	1.423		-1.719	
180	180	2.000	2.252	0.0	28.550	3.226		1.923		-0.527
181	181	2.000	2.252	-2.108	28.544	3.199		1.923		-0.342
182	182	2.000	2.252	-4.711	28.540	3.199		1.936		-0.264
183	183	2.000	2.252	-6.273	29.342	3.226		1.949		-0.185
184	184	2.000	2.252	-6.793	27.901	3.226		1.974		-0.002
185	185	2.000	2.252	-7.054	28.377	3.253		1.974		0.132
186	186	2.000	2.252	-7.314	28.960	3.226		1.974		0.291
187	187	2.000	2.252	-7.834	29.203	3.253		1.949		0.342
188	188	2.000	2.252	-8.876	29.379	2.960		1.808		0.474
189	189	2.000	2.252	-9.917	29.546	2.906		1.770		0.106
190	190	2.000	2.252	-12.520	29.939	2.826		1.744		-0.002
191	191	2.000	2.252	-15.122	30.441	2.880		1.783		-0.238
192	192	2.000	2.252	-17.725	30.660	2.906		1.833		-0.079
193	193	2.000	2.252	0.0	28.765	3.231	1.465		-1.740	
194	194	2.000	2.252	-2.108		3.210	1.454		-1.730	
195	195	2.000	2.252	-4.711		3.189	1.444		-1.698	
196	196	2.000	2.252	-6.273		3.231	1.495		-1.687	
197	197	2.000	2.252	-6.793		3.316	1.505		-1.740	
198	198	2.000	2.252	-7.054		3.316	1.516		-1.825	
199	199	2.000	2.252	-7.314		3.231	1.495		-1.582	
200	200	2.000	2.252	-7.834		3.083	1.454		-1.487	

Table III (Continued)

NUMBER	TEST NUMBER	X FEET	Y INCHES	Z INCHES	VELOCITY FPS	U RMS FPS	V RMS FPS	W RMS FPS	UV (FPS)X(FPS)	UW (FPS)X(FPS)
201	201	2.000	2.252	-8.876		3.019	1.413		-1.424	
202	202	2.000	2.252	-9.917		2.914	1.402		-1.403	
203	203	2.000	2.252	-12.520		2.829	1.402		-1.540	
204	204	2.000	2.252	-15.122		2.788	1.444		-1.551	
205	205	2.000	2.252	-17.725		2.851	1.444		-1.604	
206	206	4.000	0.852	0.0	18.538	4.355		2.754		-1.065
207	207	4.000	0.852	-2.108	18.541	4.388		2.754		-1.358
208	208	4.000	0.852	-4.711	18.320	4.453		2.754		-0.479
209	209	4.000	0.852	-6.273	18.793	4.453		2.754		-0.693
210	210	4.000	0.852	-6.793	19.213	4.421		2.810		-0.533
211	211	4.000	0.852	-7.314	19.460	4.550		2.885		-0.080
212	212	4.000	0.852	-7.834	20.418	4.616		2.754		1.491
213	213	4.000	0.852	-8.095	21.686	4.290		2.641		1.252
214	214	4.000	0.852	-7.574	19.829	4.680		2.828		1.012
215	215	4.000	0.852	-7.939	21.439	4.485		2.735		1.518
216	216	4.000	0.852	-8.355	21.641	4.160		2.566		1.145
217	217	4.000	0.852	-8.876	24.118	3.932		2.266		0.825
218	218	4.000	0.852	-9.917	25.060	3.445		2.023		0.160
219	219	4.000	0.852	-12.520	26.505	3.283		1.948		-0.133
220	220	4.000	0.852	-15.122	27.330	3.185		1.948		-0.346
221	221	4.000	0.852	-17.725	27.061	3.217		1.929		-0.399
222	222	4.000	0.852	0.0	18.608	4.401	2.137		-3.278	
223	223	4.000	0.852	-2.108	18.500	4.535	2.137		-3.503	
224	224	4.000	0.852	-4.711	18.415	4.535	2.137		-3.784	
225	225	4.000	0.852	-6.273	18.192	4.535	2.184		-3.867	
226	226	4.000	0.852	-6.793	18.370	4.535	2.200		-3.923	
227	227	4.000	0.852	-7.314	18.484	4.868	2.345		-4.260	
228	228	4.000	0.852	-7.574	19.557	4.901	2.297		-4.063	
229	229	4.000	0.852	-7.834	19.696	4.768	2.184		-3.139	
230	230	4.000	0.852	-7.939	20.145	4.601	2.105		-3.195	
231	231	4.000	0.852	-8.095	21.168	4.568	2.105		-3.082	
232	232	4.000	0.852	-8.355	22.292	4.401	2.024		-2.802	
233	233	4.000	0.852	-8.876	23.870	4.101	1.831		-2.017	
234	234	4.000	0.852	-9.917	25.733	3.568	1.622		-1.737	
235	235	4.000	0.852	-12.520	26.671	3.334	1.478		-1.626	
236	236	4.000	0.852	-15.122	27.572	3.267	1.446		-1.569	
237	237	4.000	0.852	-17.725	27.732	3.301	1.446		-1.636	
238	238	4.000	1.412	0.0	23.450	4.190		2.553		-0.369
239	239	4.000	1.412	-2.108	23.106	4.190		2.516		-0.342
240	240	4.000	1.412	-4.711	23.450	4.219		2.553		0.290
241	241	4.000	1.412	-6.273	23.790	4.248		2.553		0.421
242	242	4.000	1.412	-6.793	23.705	4.276		2.572		0.712
243	243	4.000	1.412	-7.314	24.824	4.276		2.479		1.318
244	244	4.000	1.412	-7.574	25.399	4.190		2.442		1.713
245	245	4.000	1.412	-7.834	25.351	4.162		2.423		1.871
246	246	4.000	1.412	-7.939	24.790	4.162		2.386		1.556
247	247	4.000	1.412	-8.095	25.188	4.047		2.349		1.424
248	248	4.000	1.412	-8.355	26.160	3.932		2.218		1.318
249	249	4.000	1.412	-8.876	26.955	3.760		2.144		0.923
250	250	4.000	1.412	-9.917	28.146	3.444		1.994		0.527

Table III (Continued)

NUMBER	TEST NUMBER	X FEET	Y INCHES	Z INCHES	VELOCITY FPS	U RMS FPS	V RMS FPS	W RMS FPS	UV (FPS)X(FPS)	UW (FPS)X(FPS)
251	251	4.000	1.412	-12.520	28.156	3.185		1.920		0.158
252	252	4.000	1.412	-15.122	28.904	3.157		1.901		-0.002
253	253	4.000	1.412	-17.725	29.367	3.157		1.938		-0.002
254	254	4.000	1.412	-13.561	28.467	3.157	1.920			
255	255	4.000	1.412	0.0	22.567	4.363	2.023		-3.690	
256	256	4.000	1.412	-2.108		4.248	2.023		-3.690	
257	257	4.000	1.412	-4.711		4.219	2.010		-3.584	
258	258	4.000	1.412	-6.273		4.190	1.984		-3.110	
259	259	4.000	1.412	-6.793		4.162	2.010		-3.427	
260	260	4.000	1.412	-7.314	24.241	4.276	1.997		-3.427	
261	261	4.000	1.412	-7.574		4.133	1.933		-3.057	
262	262	4.000	1.412	-7.834		4.133	1.920		-2.847	
263	263	4.000	1.412	-7.939	25.684	4.133	1.881		-2.847	
264	264	4.000	1.412	-8.095		3.903	1.792		-2.636	
265	265	4.000	1.412	-8.355	26.450	3.874	1.727		-2.451	
266	266	4.000	1.412	-8.876		3.616	1.649		-2.003	
267	267	4.000	1.412	-9.917		3.358	1.520		-1.977	
268	268	4.000	1.412	-12.520		3.157	1.444		-1.845	
269	269	4.000	1.412	-15.122		3.071	1.431		-1.709	
270	270	4.000	1.412	-17.725		3.100	1.431		-1.687	
271	271	4.000	2.252	0.0	27.380	3.763		2.257		-0.549
272	272	4.000	2.252	-2.108	27.669	3.763		2.257		-0.083
273	273	4.000	2.252	-4.711	27.779	3.711		2.225		0.138
274	274	4.000	2.252	-6.273	27.864	3.557		2.225		0.412
275	275	4.000	2.252	-6.793	27.464	3.505		2.178		0.823
276	276	4.000	2.252	-7.314	27.862	3.480		2.131		0.878
277	277	4.000	2.252	-7.574	28.184	3.428		2.131		0.797
278	278	4.000	2.252	-7.834	28.132	3.480		2.131		0.769
279	279	4.000	2.252	-7.939	28.737	3.428		2.083		0.741
280	280	4.000	2.252	-8.095	29.306	3.377		2.035		0.933
281	281	4.000	2.252	-8.355	29.215	3.273		1.987		0.878
282	282	4.000	2.252	-8.876	29.114	3.196		1.939		0.576
283	283	4.000	2.252	-9.917	29.468	2.990		1.876		0.384
284	284	4.000	2.252	-10.958	29.850	2.912		1.828		0.274
285	285	4.000	2.252	-12.520	30.559	2.861		1.813		0.219
286	286	4.000	2.252	-13.561	30.899	2.835		1.813		0.138
287	287	4.000	2.252	-15.122	30.929	2.835		1.813		0.165
288	288	4.000	2.252	-17.725	31.433	2.809		1.828		0.083
289	289	4.000	2.252	0.0	27.691	3.632	1.736		-2.937	
290	290	4.000	2.252	-2.108		3.749	1.758		-2.937	
291	291	4.000	2.252	-4.711		3.749	1.736		-2.800	
292	292	4.000	2.252	-6.273		3.661	1.736		-2.800	
293	293	4.000	2.252	-6.793		3.661	1.715		-2.746	
294	294	4.000	2.252	-7.314	28.126	3.515	1.704		-2.525	
295	295	4.000	2.252	-7.574		3.398	1.683		-2.470	
296	296	4.000	2.252	-7.834		3.486	1.651		-2.389	
297	297	4.000	2.252	-7.939		3.427	1.619		-2.278	
298	298	4.000	2.252	-8.095		3.398	1.619		-2.306	
299	299	4.000	2.252	-8.355		3.339	1.608		-2.196	
300	300	4.000	2.252	-8.876		3.222	1.566		-1.839	

Table III (Continued)

NUMBER	TEST NUMBER	X FEET	Y INCHES	Z INCHES	VELOCITY FPS	U RMS FPS	V RMS FPS	W RMS FPS	UV (FPS)X(FPS)	UW (FPS)X(FPS)
301	301	4.000	2.252	-9.917		2.959	1.460		-1.811	
302	302	4.000	2.252	-10.958		2.929	1.449		-1.734	
303	303	4.000	2.252	-12.520		2.870	1.470		-1.811	
304	304	4.000	2.252	-13.561		2.870	1.449		-1.811	
305	305	4.000	2.252	-15.122		2.900	1.481		-1.811	
306	306	4.000	2.252	-17.725		2.900	1.481		-1.811	
307	307	4.000	2.952	0.0	29.360	3.129		1.962		-0.326
308	308	4.000	2.952	-2.108	29.113	3.206		1.976		-0.326
309	309	4.000	2.952	-4.711	29.257	3.129		1.962		0.054
310	310	4.000	2.952	-6.273	29.658	3.129		1.989		0.517
311	311	4.000	2.952	-6.793	30.142	3.154		1.989		0.570
312	312	4.000	2.952	-7.314	30.128	3.102		1.897		0.544
313	313	4.000	2.952	-7.574	30.359	3.102		1.897		0.652
314	314	4.000	2.952	-7.834	30.260	3.077		1.910		0.489
315	315	4.000	2.952	-7.939	29.979	2.974		1.897		0.489
316	316	4.000	2.952	-8.095	29.880	3.000		1.857		0.544
317	317	4.000	2.952	-8.355	30.286	2.923		1.844		0.544
318	318	4.000	2.952	-8.876	30.694	2.872		1.844		0.408
319	319	4.000	2.952	-9.917	31.575	2.795		1.753		0.489
320	320	4.000	2.952	-10.958	31.213	2.770		1.753		0.131
321	321	4.000	2.952	-12.520	30.984	2.770		1.740		0.141
322	322	4.000	2.952	-13.561	32.029	2.718		1.753		0.033
323	323	4.000	2.952	-15.122	31.545	2.718		1.753		0.054
324	324	4.000	2.952	-17.725	31.994	2.667		1.767		-0.163
325	325	4.000	2.952	0.0	29.699	3.154	1.536		-2.228	
326	326	4.000	2.952	-2.108		3.154	1.536		-2.119	
327	327	4.000	2.952	-4.711		3.154	1.557		-2.310	
328	328	4.000	2.952	-6.273		3.257	1.568		-2.174	
329	329	4.000	2.952	-6.793		3.206	1.547		-2.174	
330	330	4.000	2.952	-7.314	30.144	3.051	1.515		-2.146	
331	331	4.000	2.952	-7.574		3.000	1.495		-2.092	
332	332	4.000	2.952	-7.834		3.000	1.484		-1.875	
333	333	4.000	2.952	-7.939		2.949	1.463		-1.760	
334	334	4.000	2.952	-8.095		2.949	1.452		-1.760	
335	335	4.000	2.952	-8.355		2.923	1.452		-1.663	
336	336	4.000	2.952	-8.876		2.847	1.442		-1.608	
337	337	4.000	2.952	-9.917		2.795	1.420		-1.532	
338	338	4.000	2.952	-10.958		2.692	1.399		-1.631	
339	339	4.000	2.952	-12.520		2.615	1.399		-1.619	
340	340	4.000	2.952	-13.561		2.641	1.410		-1.555	
341	341	4.000	2.952	-15.122		2.667	1.431		-1.631	
342	342	4.000	2.952	-17.725		2.692	1.442		-1.739	
343	343	7.000	0.852	0.0	19.068	4.312		2.749		-0.457
344	344	7.000	0.852	-2.108	19.336	4.410		2.749		-0.753
345	345	7.000	0.852	-4.711	19.643	4.476		2.768		-0.215
346	346	7.000	0.852	-7.314	20.182	4.639		2.825		0.457
347	347	7.000	0.852	-7.834	20.876	4.606		2.768		2.071
348	348	7.000	0.852	-8.876	23.716	4.116		2.391		1.453
349	349	7.000	0.852	-9.917	25.334	3.658		2.165		0.538
350	350	7.000	0.852	-12.520	26.931	3.430		2.015		0.269

Table III (Continued)

NUMBER	TEST NUMBER	X FEET	Y INCHES	Z INCHES	VELOCITY FPS	U RMS FPS	V RMS FPS	W RMS FPS	UV (FPS)X(FPS)	UW (FPS)X(FPS)
351	351	7.000	0.852	-15.122	27.993	3.299		1.977		-0.215
352	352	7.000	0.852	-17.725	27.679	3.332		1.977		-0.323
353	353	7.000	0.852	-0.807	19.666					
354	354	7.000	0.852	-3.410	19.614					
355	355	7.000	0.852	-6.273	19.665					
356	356	7.000	0.852	-6.793	19.849					
357	357	7.000	0.852	-7.574	20.904	4.639		2.806		1.372
358	358	7.000	0.852	-7.939	21.372	4.639		2.825		2.179
359	359	7.000	0.852	-8.355	22.141	4.280		2.560		1.937
360	360	7.000	0.852	-13.561	27.330					
361	361	7.000	0.852	-7.887	21.419	4.573		2.806		2.017
362	362	7.000	0.852	-7.991	22.467	4.476		2.655		1.937
363	363	7.000	0.852	0.0	19.586	4.410	2.030		-3.254	
364	364	7.000	0.852	-2.108		4.443	2.062		-3.443	
365	365	7.000	0.852	-4.711		4.410	2.062		-3.335	
366	366	7.000	0.852	-7.314		4.639	2.141		-3.684	
367	367	7.000	0.852	-7.574		4.737	2.141		-3.497	
368	368	7.000	0.852	-7.834	21.375	4.672	2.093		-3.012	
369	369	7.000	0.852	-7.939	21.693	4.639	2.062		-2.905	
370	370	7.000	0.852	-8.355		4.410	1.967		-2.474	
371	371	7.000	0.852	-8.875		4.083	1.826		-1.963	
372	372	7.000	0.852	-9.917		3.724	1.652		-1.694	
373	373	7.000	0.852	-12.520		3.430	1.495		-1.910	
374	374	7.000	0.852	-15.122		3.398	1.464		-1.748	
375	375	7.000	0.852	-17.725		3.299	1.448		-1.748	
376	376	7.000	0.852	-18.688		3.201	1.432		-1.641	
377	377	7.000	1.634	0.052	23.740	4.218		2.548		-0.274
378	378	7.000	1.634	-0.754	24.057					
379	379	7.000	1.634	-2.054	24.108	4.188		2.510		-0.412
380	380	7.000	1.634	-3.355	24.012					
381	381	7.000	1.634	-4.655	24.570	4.159		2.510		0.549
382	382	7.000	1.634	-6.215	25.683					
383	383	7.000	1.634	-6.735	24.968	4.100		2.510		0.631
384	384	7.000	1.634	-7.255	25.311	4.071		2.435		0.769
385	385	7.000	1.634	-7.515	25.589	3.984		2.397		1.043
386	386	7.000	1.634	-7.775	25.775	4.012		2.378		1.208
387	387	7.000	1.634	-7.879	26.115	3.984		2.378		1.098
388	388	7.000	1.634	-8.296	27.323	3.866		2.340		1.098
389	389	7.000	1.634	-8.816	27.219	3.749		2.225		0.906
390	390	7.000	1.634	-9.336	27.679					
391	391	7.000	1.634	-9.856	27.772	3.486		2.074		0.549
392	392	7.000	1.634	-11.156	28.336					
393	393	7.000	1.634	-12.456	28.961	3.222		1.959		0.440
394	394	7.000	1.634	-13.757	29.370					
395	395	7.000	1.634	-15.057	29.890	3.134		1.940		0.083
396	396	7.000	1.634	-16.357	30.100					
397	397	7.000	1.634	-17.657	30.098	3.163		1.921		-0.055
398	398	7.000	1.634	-18.177	29.879					
399	399	7.000	1.634	0.052	23.990	4.130	2.052		-3.596	
400	400	7.000	1.634	-2.054		4.159	2.052		-3.458	

Table III (Continued)

NUMBER	TEST NUMBER	X FEET	Y INCHES	Z INCHES	VELOCITY FPS	U RMS FPS	V RMS FPS	W RMS FPS	UV (FPS)X(FPS)	UW (FPS)X(FPS)
401	401	7.000	1.634	-4.655		4.071	1.999		-3.239	
402	402	7.000	1.634	-6.735		4.071	1.972		-2.882	
403	403	7.000	1.634	-7.255	25.425	4.071	1.933		-2.800	
404	404	7.000	1.634	-7.515		4.130	1.920		-2.937	
405	405	7.000	1.634	-7.775		4.042	1.880		-2.498	
406	406	7.000	1.634	-7.879	26.851	3.925	1.854		-2.608	
407	407	7.000	1.634	-8.296		3.866	1.815		-2.470	
408	408	7.000	1.634	-8.816		3.837	1.776		-2.306	
409	409	7.000	1.634	-9.856		3.427	1.604		-2.032	
410	410	7.000	1.634	-12.456		3.368	1.538		-2.087	
411	411	7.000	1.634	-15.057		3.163	1.486		-1.647	
412	412	7.000	1.634	-17.657		3.075	1.460		-1.702	
413	413	7.000	1.634	-18.177		3.017	1.460		-1.730	
414	414	7.000	2.335	0.052	26.221	3.951		2.487		-0.447
415	415	7.000	2.335	-0.754	26.617					
416	416	7.000	2.335	-2.054	26.448	3.898		2.421		-0.239
417	417	7.000	2.335	-3.355	26.627					
418	418	7.000	2.335	-4.655	26.372	3.924		2.421		0.179
419	419	7.000	2.335	-6.215	26.795	3.898		2.371		0.747
420	420	7.000	2.335	-6.735	27.173	3.763		2.387		0.597
421	421	7.000	2.335	0.052	26.390	3.898	1.933		-3.432	
422	422	7.000	2.335	-2.054		3.871	1.933		-3.164	
423	423	7.000	2.335	-4.655		3.844	1.947		-3.045	
424	424	7.000	2.335	-6.215		3.844	1.920		-2.836	
425	425	7.000	2.335	-6.735		3.736	1.865		-2.477	
426	426	7.000	2.335	-7.255	28.546	3.583		2.183		1.152
427	427	7.000	2.335	-7.515	28.051	3.505		2.196		1.263
428	428	7.000	2.335	-7.775	27.886	3.480		2.157		1.016
429	429	7.000	2.335	-7.879	27.871	3.454		2.118		0.988
430	430	7.000	2.335	-8.296	28.030	3.428		2.104		1.098
431	431	7.000	2.335	-8.816	29.424	3.247		2.025		0.961
432	432	7.000	2.335	-9.856	29.937	3.016		1.893		0.961
433	433	7.000	2.335	-11.156	30.031	2.938		1.827		0.604
434	434	7.000	2.335	-12.456	30.128	2.886		1.789		0.302
435	435	7.000	2.335	-13.757	30.216	2.809		1.762		0.329
436	436	7.000	2.335	-15.057	30.195	2.758		1.762		0.219
437	437	7.000	2.335	-16.357	30.986	2.706		1.776		0.138
438	438	7.000	2.335	-17.657	31.378	2.784		1.789		0.083
439	439	7.000	2.335	-18.177	31.113	2.784		1.802		0.138
440	440	7.000	2.335	-7.255		3.593	1.789		-2.800	
441	441	7.000	2.335	-7.515		3.531	1.789		-2.746	
442	442	7.000	2.335	-7.775		3.480	1.723		-2.608	
443	443	7.000	2.335	-8.296		3.403	1.710		-2.470	
444	444	7.000	2.335	-8.816		3.350	1.644		-2.306	
445	445	7.000	2.335	-9.856		3.145	1.578		-2.004	
446	446	7.000	2.335	-11.156		3.042	1.512		-1.713	
447	447	7.000	2.335	-12.456		2.912	1.486		-1.790	
448	448	7.000	2.335	-13.757		2.886	1.486		-1.746	
449	449	7.000	2.335	-15.057		2.835	1.486		-1.757	
450	450	7.000	2.335	-17.657		2.835	1.473		-1.888	

Table III (Continued)

NUMBER	TEST NUMBER	X FEET	Y INCHES	Z INCHES	VELOCITY FPS	U RMS FPS	V RMS FPS	W RMS FPS	UV (FPS)X(FPS)	UW (FPS)X(FPS)
451	451	7.000	2.335	-18.177		2.835	1.473		-1.757	
452	452	7.000	3.036	0.026	28.391	3.421		2.149		-0.171
453	453	7.000	3.036	-0.754	28.317					
454	454	7.000	3.036	-2.054	28.195	3.395		2.161		-0.057
455	455	7.000	3.036	-3.355	28.366	3.421		2.149		0.315
456	456	7.000	3.036	-4.655	28.788	3.368		2.161		0.429
457	457	7.000	3.036	-6.215	29.062	3.290		2.068		0.515
458	458	7.000	3.036	-6.735	29.081	3.211		2.027		0.916
459	459	7.000	3.036	-7.255	28.920	3.211		2.027		0.772
460	460	7.000	3.036	-7.515	29.293	3.194		2.027		0.830
461	461	7.000	3.036	-7.775	30.063	3.131		1.974		0.716
462	462	7.000	3.036	-8.296	29.798	3.105		1.906		0.601
463	463	7.000	3.036	-8.816	29.273	2.947		1.826		0.687
464	464	7.000	3.036	-9.856	30.051	2.895		1.839		0.572
465	465	7.000	3.036	-11.156	31.342	2.711		1.732		0.390
466	466	7.000	3.036	-12.456	30.768	2.659		1.719		0.332
467	467	7.000	3.036	-13.757	31.437	2.578		1.705		0.297
468	468	7.000	3.036	-15.057	31.507	2.552		1.678		0.194
469	469	7.000	3.036	-17.657	31.465	2.552		1.705		0.091
470	468	7.000	3.036	0.026	29.034	3.420	1.724		-2.857	
471	469	7.000	3.036	-2.054		3.472	1.756		-2.635	
472	470	7.000	3.036	-4.655		3.420	1.745		-2.551	
473	471	7.000	3.036	-6.215		3.368	1.702		-2.413	
474	472	7.000	3.036	-6.735		3.239	1.670		-2.385	
475	473	7.000	3.036	-7.255	29.438	3.212	1.670		-2.080	
476	474	7.000	3.036	-7.515		3.212	1.617		-2.108	
477	475	7.000	3.036	-7.775		3.160	1.617		-1.897	
478	476	7.000	3.036	-8.296		3.083	1.552		-1.653	
479	477	7.000	3.036	-8.816		2.979	1.531		-1.719	
480	478	7.000	3.036	-9.856		2.876	1.509		-1.564	
481	479	7.000	3.036	-11.156		2.772	1.446		-1.464	
482	480	7.000	3.036	-12.456		2.668	1.414		-1.476	
483	481	7.000	3.036	-13.757		2.617	1.381		-1.554	
484	482	7.000	3.036	-15.057		2.617	1.403		-1.576	
485	483	7.000	3.036	-17.657		2.617	1.403		-1.531	
486	484	7.000	3.738	0.026	30.418	3.195		1.993		-0.141
487	485	7.000	3.738	-2.054	29.809	3.107		1.993		-0.114
488	486	7.000	3.738	-4.655	30.018	3.129		1.993		0.170
489	487	7.000	3.738	-6.215	30.711	3.064		1.926		0.368
490	498	7.000	3.738	-6.735	31.508	3.042		1.940		0.283
491	489	7.000	3.738	-7.255	31.375	2.955		1.860		0.567
492	490	7.000	3.738	-7.775	31.393	2.955		1.846		0.396
493	491	7.000	3.738	-8.296	31.080	2.867		1.807		0.510
494	492	7.000	3.738	-8.816	31.241	2.823		1.781		0.425
495	493	7.000	3.738	-9.856	31.761	2.736		1.754		0.396
496	494	7.000	3.738	-11.156	32.904	2.648		1.701		0.198
497	495	7.000	3.738	-12.456	32.940	2.560		1.674		0.396
498	496	7.000	3.738	-13.757	32.829	2.582		1.661		0.085
499	497	7.000	3.738	-15.057	32.833	2.582		1.674		0.057
500	498	7.000	3.738	-17.657	32.792	2.626		1.687		0.057

Table III (Continued)

NUMBER	TEST NUMBER	H FEET	Y INCHES	Z INCHES	VELOCITY FPS	U RMS FPS	V RMS FPS	W RMS FPS	UV (FPS)X(FPS)	UW (FPS)X(FPS)
501	499	7.000	3.738	0.026	30.641	3.107	1.571		-2.209	
502	500	7.000	3.738	-2.054		3.086	1.603		-2.152	
503	501	7.000	3.738	-4.655		3.107	1.582		-1.699	
504	502	7.000	3.738	-6.215		3.064	1.593		-1.983	
505	503	7.000	3.738	-6.735		3.042	1.571		-1.785	
506	504	7.000	3.738	-7.255	31.598	2.976	1.549		-1.840	
507	505	7.000	3.738	-7.775		2.867	1.517		-1.671	
508	506	7.000	3.738	-8.296		2.823	1.486		-1.530	
509	507	7.000	3.738	-8.816		2.714	1.453		-1.495	
510	508	7.000	3.738	-9.856		2.736	1.432		-1.461	
511	509	7.000	3.738	-11.156		2.670	1.421		-1.506	
512	510	7.000	3.738	-12.456		2.605	1.399		-1.461	
513	511	7.000	3.738	-13.757		2.539	1.378		-1.428	
514	512	7.000	3.738	-15.057		2.582	1.399		-1.518	
515	513	7.000	3.738	-17.657		2.605	1.432		-1.608	
516	514	7.000	0.652	0.0	16.356	4.324		2.813		0.108
517	515	7.000	0.932	0.0	18.931	4.461		2.813		0.054
518	516	7.000	1.213	0.0	21.337	4.324		2.716		-0.054
519	517	7.000	1.494	0.0	22.825	4.221		2.660		-0.002
520	518	7.000	1.774	0.0	24.234	4.282		2.585		-0.002
521	519	7.000	2.055	0.0	25.030	4.202		2.492		-0.002
522	520	7.000	2.335	0.0	26.882	4.094		2.459		0.162
523	521	7.000	2.896	0.0	28.119	3.824		2.160		-0.081
524	522	7.000	3.457	0.0	29.347	3.474		2.083		-0.108
525	523	7.000	4.018	0.0	30.452	3.232		2.036		-0.002
526	524	7.000	4.579	0.0	32.376	2.963		1.879		-0.054
527	525	7.000	5.140	0.0	33.193	2.635		1.752		0.054
528	526	7.000	6.543	0.0	34.269	2.406		1.657		-0.002
529	527	7.000	7.946	0.0	35.054	2.011		1.427		
530	528	7.000	9.348	0.0	35.892	1.878		1.374		
531	529	7.000	10.751	0.0	37.585	1.734		1.311		
532	530	7.000	13.556	0.0	39.781	1.180		0.787		
533	531	7.000	16.361	0.0	40.041	0.595		0.409		
534	532	7.000	0.652	0.0	16.422	4.238	2.011		-2.999	
535	533	7.000	0.932	0.0	19.462	4.272	2.120		-3.412	
536	534	7.000	1.213	0.0	21.411	4.339	2.133		-3.541	
537	535	7.000	1.494	0.0		4.238	2.120		-3.671	
538	536	7.000	1.774	0.0		4.137	2.120		-3.412	
539	537	7.000	2.055	0.0		4.003	2.044		-3.309	
540	538	7.000	2.335	0.0	27.135	4.092	1.968		-3.231	
541	539	7.000	2.896	0.0		3.590	1.828		-2.922	
542	540	7.000	3.457	0.0		3.432	1.727		-2.456	
543	541	7.000	4.018	0.0		3.220	1.599		-2.275	
544	542	7.000	4.579	0.0		3.062	1.548		-1.861	
545	543	7.000	5.140	0.0	32.544	2.666	1.419		-1.758	
546	544	7.000	6.543	0.0		2.243	1.326		-1.158	
547	545	7.000	7.946	0.0		1.991	1.213		-1.096	
548	546	7.000	9.348	0.0		1.901	1.172		-0.962	
549	547	7.000	10.751	0.0		1.669	1.070		-0.775	
550	548	7.000	13.556	0.0		1.167	0.792		-0.424	

Table III (Continued)

NUMBER	TEST NUMBER	X FEET	Y INCHES	Z INCHES	VELOCITY FPS	U RMS FPS	V RMS FPS	W RMS FPS	UV (FPS)X(FPS)	UW (FPS)X(FPS)
551	549	7.000	16.361	0.0		0.603	0.606		-0.099	
552	550	7.000	0.652	-7.255	16.013	4.530		2.968		-0.314
553	551	7.000	0.932	-7.255	20.461	4.428		2.793		1.228
554	552	7.000	1.213	-7.255	22.388	4.293		2.638		1.201
555	553	7.000	1.494	-7.255	24.484	4.023		2.528		1.436
556	554	7.000	1.774	-7.255	25.924	4.033		2.455		1.149
557	555	7.000	2.055	-7.255	27.400	3.846		2.362		1.175
558	556	7.000	2.335	-7.255	27.628	3.608		2.190		0.914
559	557	7.000	2.896	-7.255	29.222	3.449		2.113		0.757
560	558	7.000	3.457	-7.255	29.951	3.237		2.005		0.679
561	559	7.000	4.018	-7.255	30.777	2.971		1.835		0.626
562	560	7.000	4.579	-7.255	32.016	2.614		1.726		0.600
563	561	7.000	5.140	-7.255	33.320	2.492		1.695		0.387
564	562	7.000	6.543	-7.255	34.228	2.161		1.508		0.292
565	563	7.000	7.946	-7.255	34.589	1.931		1.406		0.198
566	564	7.000	9.348	-7.255	35.921	1.769		1.271		0.167
567	565	7.000	10.751	-7.255	37.001	1.527		1.075		0.146
568	566	7.000	12.154	-7.255	38.108	1.314		0.930		0.084
569	567	7.000	13.556	-7.255	39.028	1.132		0.765		0.046
570	568	7.000	16.361	-7.255	39.005	0.626		0.465		0.029
571	569	7.000	0.652	-7.255	18.183	4.474	2.194		-4.007	
572	570	7.000	0.932	-7.255	20.913	4.440	2.163		-4.033	
573	571	7.000	1.213	-7.255	23.219	4.356	2.057		-3.153	
574	572	7.000	1.494	-7.255		4.224	2.019		-3.128	
575	573	7.000	1.774	-7.255		4.092	1.929		-3.025	
576	574	7.000	2.055	-7.255		3.854	1.828		-2.637	
577	575	7.000	2.335	-7.255	28.840	3.696	1.803		-2.482	
578	576	7.000	2.896	-7.255		3.326	1.688		-2.171	
579	577	7.000	3.457	-7.255		3.156	1.594		-2.145	
580	578	7.000	4.018	-7.255		2.861	1.521		-1.861	
581	579	7.000	4.579	-7.255		2.601	1.430		-1.758	
582	580	7.000	5.140	-7.255	33.313	2.428	1.388		-1.551	
583	581	7.000	6.543	-7.255		2.172	1.275		-1.318	
584	582	7.000	7.946	-7.255		1.971	1.192		-1.096	
585	583	7.000	9.348	-7.255		1.820	1.121		-0.797	
586	584	7.000	10.751	-7.255		1.640	1.028		-0.662	
587	585	7.000	12.154	-7.255		1.308	0.863		-0.459	
588	586	7.000	16.361	-7.255		0.664	0.514			
589	587	4.000	0.530	0.0	14.935	4.292		2.782		0.053
590	588	4.000	0.811	0.0	18.552	4.313		2.745		-0.002
591	589	4.000	1.091	0.0	21.342	4.512		2.671		
592	590	4.000	1.372	0.0	23.257	4.540		2.540		
593	591	4.000	1.653	0.0	24.792	4.255		2.374		
594	592	4.000	1.933	0.0	26.489	3.884		2.281		
595	593	4.000	2.214	0.0	27.717	3.694		2.201		-0.002
596	594	4.000	2.775	0.0	29.493	3.292		2.015		
597	595	4.000	3.336	0.0	30.594	3.141		1.838		
598	596	4.000	3.898	0.0	31.261	2.663		1.735		
599	597	4.000	4.459	0.0	31.756	2.513		1.703		
600	598	4.000	5.020	0.0	32.766	2.412		1.662		-0.021

Table III (Continued)

NUMBER	TEST NUMBER	X FEET	Y INCHES	Z INCHES	VELOCITY FPS	U RMS FPS	V RMS FPS	W RMS FPS	UV (FPS)X(FPS)	UW (FPS)X(FPS)
601	599	4.000	6.423	0.0	33.333	2.237		1.568		
602	600	4.000	7.826	0.0	34.728	2.110		1.486		
603	601	4.000	10.633	0.0	36.758	1.634		1.173		
604	602	4.000	13.439	0.0	38.499	1.206		0.769		
605	603	4.000	16.245	0.0	39.623	0.653		0.447		
606	604	4.000	0.530	0.0		4.211	2.059		-2.729	
607	605	4.000	0.811	0.0		4.356	2.085		-3.395	
608	606	4.000	1.091	0.0		4.471	2.137		-3.755	
609	607	4.000	1.372	0.0		4.356	2.072		-3.488	
610	608	4.000	1.653	0.0		4.125	1.968		-3.195	
611	609	4.000	1.933	0.0		3.894	1.865		-3.142	
612	610	4.000	2.214	0.0		3.655	1.749		-2.743	
613	611	4.000	2.775	0.0		3.300	1.619		-2.290	
614	612	4.000	3.336	0.0		2.944	1.515		-1.726	
615	613	4.000	3.898	0.0		2.640	1.438		-1.416	
616	614	4.000	4.459	0.0		2.513	1.416		-1.353	
617	615	4.000	5.020	0.0		2.360	1.395		-1.353	
618	616	4.000	6.423	0.0		2.234	1.332		-1.203	
619	617	4.000	7.826	0.0		2.030	1.238		-1.161	
620	618	4.000	10.633	0.0		1.625	1.049		-0.767	
621	619	4.000	13.439	0.0		1.117	0.819		-0.384	
622	620	4.000	16.245	0.0		0.533	0.483		-0.117	
623	621	4.000	0.530	-7.532	14.280	4.970		2.956		2.239
624	622	4.000	0.811	-7.532	19.565	4.683		2.827		1.918
625	623	4.000	1.091	-7.532	22.352	4.397		2.607		1.535
626	624	4.000	1.372	-7.532	24.447	4.046		2.406		1.739
627	625	4.000	1.653	-7.532	26.114	3.855		2.258		1.330
628	626	4.000	1.933	-7.532	28.351	3.632		2.112		1.100
629	627	4.000	2.214	-7.532	28.337	3.334		2.146		0.793
630	628	4.000	2.775	-7.532	29.592	3.135		1.830		0.665
631	629	4.000	3.336	-7.532	31.298	2.712		1.759		0.563
632	630	4.000	3.898	-7.532	31.973	2.563		1.697		0.409
633	631	4.000	4.459	-7.532	32.386	2.488		1.655		0.409
634	632	4.000	5.020	-7.532	32.636	2.240		1.594		0.307
635	633	4.000	6.423	-7.532	33.831	2.040		1.450		0.379
636	634	4.000	7.826	-7.532	34.765	1.941		1.326		0.225
637	635	4.000	10.633	-7.532	36.674	1.443		1.039		0.092
638	636	4.000	13.439	-7.532	38.516	0.971		0.679		0.041
639	637	4.000	16.245	-7.532	39.056	0.473		0.350		0.020
640	638	4.000	0.530	-7.532		4.874	2.256		-3.965	
641	639	4.000	0.811	-7.532		4.683	2.179		-3.837	
642	640	4.000	1.091	-7.532		4.397	2.041		-3.709	
643	641	4.000	1.372	-7.532		4.110	1.918		-3.326	
644	642	4.000	1.653	-7.532		3.855	1.796		-2.686	
645	643	4.000	1.933	-7.532		3.632	1.704		-2.558	
646	644	4.000	2.214	-7.532		3.334	1.625		-2.302	
647	645	4.000	2.775	-7.532		3.011	1.501		-1.816	
648	646	4.000	3.336	-7.532		2.688	1.450		-1.714	
649	647	4.000	3.898	-7.532		2.488	1.357		-1.586	
650	648	4.000	4.459	-7.532		2.363	1.357		-1.351	

Table III (Continued)

NUMBER	TEST NUMBER	X FEET	Y INCHES	Z INCHES	VELOCITY FPS	U RMS FPS	V RMS FPS	W RMS FPS	UV (FPS)X(FPS)	UW (FPS)X(FPS)
651	649	4.000	5.020	-7.532		2.314	1.337		-1.279	
652	650	4.000	6.423	-7.532		2.040	1.244		-1.126	
653	651	4.000	7.826	-7.532		1.866	1.152		-0.890	
654	652	4.000	10.633	-7.532		1.518	0.987		-0.645	
655	653	4.000	13.439	-7.532		1.094	0.741		-0.276	
656	654	4.000	16.245	-7.532		0.597	0.494		-0.102	
657	655	2.000	0.500	0.0	14.361	4.233		2.768		-0.002
658	656	2.000	0.780	0.0	18.923	4.376		2.731		0.064
659	657	2.000	1.059	0.0	22.072	4.404		2.639		-0.002
660	658	2.000	1.339	0.0	24.726	4.233		2.436		
661	659	2.000	1.618	0.0	26.025	3.865		2.251		
662	660	2.000	1.898	0.0	27.807	3.580		2.085		
663	661	2.000	2.178	0.0	29.318	3.151		1.965		0.052
664	662	2.000	2.737	0.0	30.254	2.951		1.849		
665	663	2.000	3.296	0.0	30.626	2.775		1.799		
666	664	2.000	3.855	0.0	31.470	2.626		1.748		
667	665	2.000	4.414	0.0	32.275	2.525		1.722		
668	666	2.000	4.974	0.0	33.080	2.376		1.653		-0.103
669	667	2.000	6.372	0.0	34.653	2.225		1.560		
670	668	2.000	7.770	0.0	35.642	1.975		1.437		
671	669	2.000	10.566	0.0	37.422	1.600		1.116		
672	670	2.000	13.362	0.0	38.413	1.075		0.630		
673	671	2.000	16.158	0.0	39.574	1.200		0.341		
674	672	2.000	0.500	0.0	14.656	4.067	2.001		-2.919	
675	673	2.000	0.780	0.0	18.856	4.318	2.050		-3.602	
676	674	2.000	1.059	0.0	22.229	4.123	1.962		-3.478	
677	675	2.000	1.339	0.0		4.067	1.862		-3.291	
678	676	2.000	1.618	0.0		3.817	1.687		-2.671	
679	677	2.000	1.898	0.0		3.427	1.537		-2.236	
680	678	2.000	2.178	0.0	28.555	3.148	1.451		-1.987	
681	679	2.000	2.737	0.0		2.795	1.378		-1.589	
682	680	2.000	3.296	0.0		2.575	1.348		-1.515	
683	681	2.000	3.855	0.0		2.452	1.368		-1.540	
684	682	2.000	4.414	0.0		2.378	1.358		-1.441	
685	683	2.000	4.974	0.0		2.231	1.297		-1.341	
686	684	2.000	6.372	0.0		2.109	1.287		-1.162	
687	685	2.000	7.770	0.0		1.937	1.175		-0.983	
688	686	2.000	10.566	0.0		1.520	0.983		-0.636	
689	687	2.000	13.362	0.0		1.030	0.770		-0.308	
690	688	2.000	16.158	0.0		0.539	0.497		-0.110	
691	689	2.000	0.500	-7.791	16.025	4.882		2.960		2.660
692	690	2.000	0.780	-7.791	20.933	4.692		2.759		3.482
693	691	2.000	1.059	-7.791	23.606	4.534		2.613		3.040
694	692	2.000	1.339	-7.791	25.463	4.184		2.394		2.280
695	693	2.000	1.618	-7.791	27.356	3.740		2.192		1.469
696	694	2.000	1.898	-7.791	27.835	3.424		2.065		0.963
697	695	2.000	2.178	-7.791	29.463	3.144		1.958		0.836
698	696	2.000	2.737	-7.791	30.408	2.748		1.819		0.557
699	697	2.000	3.296	-7.791	31.079	2.649		1.740		0.431
700	698	2.000	3.855	-7.791	31.661	2.550		1.699		0.431

Table III (Continued)

NUMBER	TEST NUMBER	X FEET	Y INCHES	Z INCHES	VELOCITY FPS	U RMS FPS	V RMS FPS	W RMS FPS	UV (FPS)X(FPS)	UW (FPS)X(FPS)
701	699	2.000	4.414	-7.791	33.123	2.476		1.647		0.380
702	700	2.000	4.974	-7.791	33.544	2.302		1.627		0.324
703	701	2.000	6.372	-7.791	35.205	2.179		1.524		0.324
704	702	2.000	7.770	-7.791	36.076	1.956		1.381		0.213
705	703	2.000	10.566	-7.791	37.238	1.461		1.044		0.172
706	704	2.000	13.362	-7.791	38.260	0.916		0.634		0.040
707	705	2.000	16.158	-7.791	39.116	0.544		0.389		0.025
708	706	2.000	0.500	-7.791	16.211	4.655	2.153		-3.506	
709	707	2.000	0.780	-7.791	21.155	4.717	2.092		-3.013	
710	708	2.000	1.059	-7.791	23.507	4.436	1.967		-2.890	
711	709	2.000	1.339	-7.791		3.992	1.818		-2.645	
712	710	2.000	1.618	-7.791		3.659	1.664		-2.337	
713	711	2.000	1.898	-7.791		3.367	1.593		-2.029	
714	712	2.000	2.178	-7.791	29.729	3.049	1.684		-1.784	
715	713	2.000	2.737	-7.791		2.708	1.442		-1.397	
716	714	2.000	3.296	-7.791		2.610	1.331		-1.446	
717	715	2.000	3.855	-7.791		2.489	1.270		-1.299	
718	716	2.000	4.414	-7.791		2.366	1.240		-1.357	
719	717	2.000	4.974	-7.791		2.294	1.169		-1.279	
720	718	2.000	6.372	-7.791		2.147	1.079		-1.082	
721	719	2.000	7.770	-7.791		1.879	0.948		-0.875	
722	720	2.000	10.566	-7.791		1.440	0.645		-0.580	
723	721	2.000	13.362	-7.791		0.927	0.414		-0.226	
724	722	2.000	16.158	-7.791		0.562	0.242		-0.044	
725	723	11.000	2.094	0.0	25.724	3.901		2.514		-0.002
726	724	11.000	2.094	-2.187	25.134	3.826		2.484		-0.002
727	725	11.000	2.094	-4.821	26.181	3.875		2.484		0.569
728	725	11.000	2.094	-3.504	25.138	3.901		2.468		0.543
729	727	11.000	2.094	-2.714	25.615	4.026		2.514		0.414
730	728	11.000	2.094	-6.139	25.716	3.901		2.469		1.059
731	729	11.000	2.094	-6.929	26.049	3.776		2.375		1.007
732	730	11.000	2.094	-7.456	26.569	3.850		2.375		1.447
733	731	11.000	2.094	-7.983	27.033	3.676		2.329		1.188
734	732	11.000	2.094	-8.773	28.595	3.526		2.190		1.369
735	733	11.000	2.094	-10.091	29.348	3.251		2.036		0.826
736	734	11.000	2.094	-11.408	28.918	3.126		1.943		0.595
737	735	11.000	2.094	-12.725	29.134	3.025		1.881		0.465
738	736	11.000	2.094	-14.043	29.914	2.976		1.850		0.414
739	737	11.000	2.094	-15.360	30.239	2.976		1.866		0.414
740	738	11.000	2.094	-16.677	30.344	2.901		1.835		0.414
741	739	11.000	2.094	-17.995	30.063	2.876		1.835		0.388
742	740	11.000	2.094	-18.522	30.534	2.876		1.866		0.233
743	741	11.000	2.094	0.0	25.237	4.006	2.018		-3.497	
744	742	11.000	2.094	-2.187		3.980	2.044		-3.578	
745	743	11.000	2.094	-2.714		4.031	2.031		-3.281	
746	744	11.000	2.094	-3.504		4.006	2.005		-3.578	
747	745	11.000	2.094	-4.821		3.801	1.979		-3.120	
748	746	11.000	2.094	-6.139		3.827	1.965		-3.362	
749	747	11.000	2.094	-6.929		3.801	1.913		-3.228	
750	748	11.000	2.094	-7.456	27.030	3.776	1.926		-2.851	

Table III (Continued)

NUMBER	TEST NUMBER	X FEET	Y INCHES	Z INCHES	VELOCITY FPS	U RMS FPS	V RMS FPS	W RMS FPS	UV (FPS)X(FPS)	UW (FPS)X(FPS)
751	749	11.000	2.094	-7.383		3.649	1.861		-2.932	
752	750	11.000	2.094	-8.773		3.444	1.744		-2.393	
753	751	11.000	2.094	-10.091		3.266	1.640		-2.206	
754	752	11.000	2.094	-11.408		3.163	1.601		-2.001	
755	753	11.000	2.094	-12.725		3.062	1.575		-2.044	
756	754	11.000	2.094	-14.043		2.934	1.509		-1.905	
757	755	11.000	2.094	-15.360		2.960	1.509		-1.926	
758	756	11.000	2.094	-16.677		2.934	1.496		-1.839	
759	757	11.000	2.094	-17.995		2.909	1.484		-1.618	
760	758	11.000	2.094	-18.522		2.883	1.496		-1.743	
761	759	15.000	0.750	0.0	17.383	4.385	2.015		-3.179	
762	760	15.000	1.030	0.0	19.377	4.232	2.080		-3.424	
763	761	15.000	1.310	0.0	22.389	4.257	2.080		-3.424	
764	762	15.000	1.590	0.0	23.422	4.128	2.080		-3.532	
765	763	15.000	1.870	0.0	24.209	4.103	2.080		-3.315	
766	764	15.000	2.150	0.0	25.476	4.000	2.054		-3.532	
767	765	15.000	2.710	0.0	26.897	3.820	2.041		-3.125	
768	766	15.000	3.270	0.0	28.597	3.590	1.936		-2.989	
769	767	15.000	3.830	0.0	29.205	3.461	1.844		-2.798	
770	768	15.000	4.390	0.0	30.314	3.359	1.831		-2.554	
771	769	15.000	4.950	0.0	30.735	3.180	1.780		-2.500	
772	770	15.000	5.650	0.0	31.808	2.974	1.635		-1.984	
773	771	15.000	6.350	0.0	33.136	2.821	1.570		-1.929	
774	772	15.000	7.750	0.0	35.097	2.436	1.413		-1.413	
775	773	15.000	10.545	0.0	37.754	1.770	1.139		-0.837	
776	774	15.000	13.345	0.0	39.053	1.282	0.879		-0.521	
777	775	15.000	16.145	0.0	38.733	0.820	0.646		-0.158	
778	776	15.000	0.750	0.0		4.356		2.903		0.266
779	777	15.000	1.030	0.0	19.209	4.500		2.866		0.066
780	778	15.000	1.310	0.0		4.471		2.792		
781	779	15.000	1.590	0.0		4.413		2.735		
782	780	15.000	1.870	0.0		4.211		2.641		
783	781	15.000	2.150	0.0	25.092	4.010		2.585		-0.002
784	782	15.000	2.710	0.0		3.952		2.492		
785	783	15.000	3.270	0.0		3.865		2.379		
786	784	15.000	3.830	0.0		3.519		2.285		
787	785	15.000	4.390	0.0		3.318		2.210		
788	786	15.000	4.950	0.0		3.231		2.117		
789	787	15.000	5.650	0.0		3.115		2.061		
790	788	15.000	6.350	0.0		2.798		1.929		
791	789	15.000	7.750	0.0		2.423		1.742		
792	790	15.000	10.545	0.0		1.846		1.349		
793	791	15.000	13.345	0.0		1.356		0.936		
794	792	15.000	16.145	0.0		0.866		0.637		
795	773	15.000	0.750	0.0	16.781	4.500		2.903		-0.027
796	774	15.000	0.750	-2.138	16.918	4.500		2.885		-0.002
797	775	15.000	0.750	-3.426	16.938	4.471		2.866		0.319
798	776	15.000	0.750	-4.714	17.066	4.587		2.978		0.693
799	777	15.000	0.750	-6.002	17.078	4.529		2.903		-0.002
800	778	15.000	0.750	-6.775	17.086	4.587		2.978		-0.266

Table III (Continued)

NUMBER	TEST NUMBER	X FEET	Y INCHES	Z INCHES	VELOCITY FPS	U RMS FPS	V RMS FPS	W RMS FPS	UV (FPS)X(FPS)	UW (FPS)X(FPS)
801	779	15.000	0.750	-7.290	17.196	5.019		3.054		0.613
802	780	15.000	0.750	-7.806	18.506	4.730		2.978		2.529
803	781	15.000	0.750	-8.321	20.129	4.413		2.735		2.609
804	782	15.000	0.750	-8.836	22.205	4.125		2.510		2.264
805	783	15.000	0.750	-9.867	23.518	3.663		2.266		1.491
806	784	15.000	0.750	-11.155	24.203	3.519		2.191		0.719
807	785	15.000	0.750	-12.443	24.439	3.490		2.155		0.746
808	786	15.000	0.750	-13.731	24.871	3.490		2.136		0.825
809	787	15.000	0.750	-15.019	25.472	3.404		2.080		0.372
810	788	15.000	0.750	-16.307	25.930	3.375		2.098		0.613
811	789	15.000	0.750	-17.595	26.544	3.404		2.080		0.399
812	790	15.000	0.750	-18.110	26.106	3.433		2.061		0.187
813	791	15.000	0.750	-9.351	22.267	3.750		2.285		1.278
814	792	15.000	0.750	0.0	17.191	4.312	2.011		-3.324	
815	793	15.000	0.750	-2.138		4.535	2.036		-3.637	
816	794	15.000	0.750	-3.426		4.452	2.049		-3.511	
817	795	15.000	0.750	-4.714		4.424	2.049		-3.511	
818	796	15.000	0.750	-6.002		4.284	2.049		-3.700	
819	797	15.000	0.750	-6.775		4.508	2.100		-3.574	
820	798	15.000	0.750	-7.290		4.927	2.250		-4.201	
821	799	15.000	0.750	-7.806	18.652	4.591	2.074		-3.324	
822	800	15.000	0.750	-8.321		4.340	1.999		-2.822	
823	801	15.000	0.750	-8.836		4.004	1.798		-2.383	
824	802	15.000	0.750	-9.351		3.724	1.684		-2.069	
825	803	15.000	0.750	-9.867		3.584	1.621		-1.882	
826	804	15.000	0.750	-11.155		3.444	1.533		-2.032	
827	805	15.000	0.750	-12.443		3.416	1.495		-1.896	
828	806	15.000	0.750	-13.731		3.360	1.433		-1.806	
829	807	15.000	0.750	-15.019		3.303	1.421		-1.756	
830	808	15.000	0.750	-16.307		3.331	1.421		-1.826	
831	809	15.000	0.750	-17.595		3.331	1.421		-1.776	
832	810	15.000	0.750	-18.110		3.331	1.408		-1.756	
833	811	15.000	1.870	0.0	23.901	4.076		2.560		0.103
834	812	15.000	1.870	-2.138	24.461	4.026		2.591		0.078
835	813	15.000	1.870	-3.426	24.421	3.976		2.484		0.078
836	814	15.000	1.870	-4.714	24.112	4.125		2.560		0.595
837	815	15.000	1.870	-6.002	24.419	4.001		2.529		0.723
838	816	15.000	1.870	-6.775	24.757	4.001		2.529		0.852
839	817	15.000	1.870	-7.290	24.870	4.051		2.529		1.085
840	818	15.000	1.870	-7.806	25.796	3.901		2.468		1.266
841	819	15.000	1.870	-8.321	26.867	3.751		2.329		1.240
842	820	15.000	1.870	-8.836	27.370	3.575		2.252		1.344
843	821	15.000	1.870	-9.351	27.758	3.501		2.205		1.318
844	822	15.000	1.870	-9.867	27.581	3.376		2.098		0.956
845	823	15.000	1.870	-11.155	28.101	3.251		2.005		0.620
846	824	15.000	1.870	-12.443	27.791	3.126		1.912		0.723
847	825	15.000	1.870	-13.731	28.600	3.176		1.912		0.543
848	826	15.000	1.870	-15.019	28.836	3.126		1.928		0.569
849	827	15.000	1.870	-17.595	29.953	2.926		1.881		0.129
850	828	15.000	1.870	-18.110	29.852	2.976		1.881		0.207

Table III (Continued)

NUMBER	TEST NUMBER	X FEET	Y INCHES	Z INCHES	VELOCITY FPS	U RMS FPS	V RMS FPS	W RMS FPS	UV (FPS)X(FPS)	UW (FPS)X(FPS)
851	828	15.000	1.870	0.0	23.776	3.961	2.034		-3.293	
852	829	15.000	1.870	-2.138		4.011	2.047		-3.420	
853	830	15.000	1.870	-3.426		3.961	2.021		-3.141	
854	831	15.000	1.870	-4.714		4.085	2.021		-3.496	
855	832	15.000	1.870	-6.002		3.887	1.958		-3.166	
856	833	15.000	1.870	-6.775		4.011	1.983		-3.217	
857	834	15.000	1.870	-7.290		3.986	1.996		-3.166	
858	835	15.000	1.870	-7.806	26.046	3.862	1.933		-2.862	
859	836	15.000	1.870	-8.321		3.714	1.844		-2.736	
860	837	15.000	1.870	-8.836		3.615	1.781		-2.457	
861	838	15.000	1.870	-9.351		3.466	1.731		-2.406	
862	839	15.000	1.870	-9.867		3.318	1.680		-2.153	
863	840	15.000	1.870	-11.155		3.218	1.617		-2.153	
864	841	15.000	1.870	-12.443		3.218	1.604		-2.280	
865	842	15.000	1.870	-13.731		3.169	1.528		-2.204	
866	843	15.000	1.870	-15.019		3.095	1.503		-1.844	
867	844	15.000	1.870	-17.595		3.046	1.491		-1.784	
868	845	15.000	1.870	-18.110		3.046	1.478		-1.824	
869	846	15.000	3.550	0.0	28.766	3.551		2.360		-0.103
870	847	15.000	3.550	-2.138	28.554	3.551		2.360		0.129
871	848	15.000	3.550	-3.426	28.404	3.575		2.375		-0.002
872	849	15.000	3.550	-4.714	28.650	3.476		2.360		0.284
873	850	15.000	3.550	-6.002	29.294	3.501		2.267		0.310
874	851	15.000	3.550	-6.775	30.470	3.376		2.283		0.465
875	852	15.000	3.550	-7.290	30.071	3.350		2.190		0.491
876	853	15.000	3.550	-7.806	30.082	3.350		2.190		0.801
877	854	15.000	3.550	-8.321	30.087	3.325		2.144		0.826
878	855	15.000	3.550	-8.836	30.240	3.201		2.098		0.646
879	856	15.000	3.550	-9.867	30.729	3.025		1.990		0.595
880	857	15.000	3.550	-11.155	30.409	3.025		1.943		0.362
881	858	15.000	3.550	-12.443	31.572	2.951		1.912		0.388
882	859	15.000	3.550	-15.019	32.211	2.826		1.881		0.362
883	860	15.000	3.550	-17.595	32.504	2.750		1.881		0.233
884	861	15.000	3.550	-18.110	32.403	2.750		1.866		0.103
885	862	15.000	3.550	0.0	28.452	3.626	1.965		-2.868	
886	863	15.000	3.550	-2.138		3.575	1.990		-2.972	
887	864	15.000	3.550	-3.426		3.575	1.952		-2.842	
888	865	15.000	3.550	-4.714		3.526	1.875		-2.635	
889	866	15.000	3.550	-6.002		3.476	1.862		-2.429	
890	867	15.000	3.550	-6.775		3.426	1.862		-2.480	
891	868	15.000	3.550	-7.290		3.401	1.825		-2.429	
892	869	15.000	3.550	-7.806		3.275	1.761		-2.299	
893	870	15.000	3.550	-8.321		3.226	1.735		-2.144	
894	871	15.000	3.550	-8.836		3.151	1.710		-2.015	
895	872	15.000	3.550	-9.867		3.075	1.671		-1.886	
896	873	15.000	3.550	-11.155		3.000	1.620		-1.937	
897	874	15.000	3.550	-12.443		2.876	1.569		-1.757	
898	875	15.000	3.550	-15.019		2.876	1.569		-1.911	
899	876	15.000	3.550	-17.595		2.826	1.543		-1.886	
900	877	15.000	3.550	-18.110		2.800	1.543		-1.731	

Table III (Continued)

NUMBER	TEST NUMBER	X FEET	Y INCHES	Z INCHES	VELOCITY FPS	U RMS FPS	V RMS FPS	W RMS FPS	UV (FPS)X(FPS)	UW (FPS)X(FPS)
901	878	15.000	6.350	0.0	32.383	2.686		1.700		-0.040
902	879	15.000	6.350	-2.138	32.867	2.611		1.731		
903	880	15.000	6.350	-4.714	32.634	2.538		1.731		0.131
904	881	15.000	6.350	-6.002	32.433	2.489		1.680		0.201
905	882	15.000	6.350	-7.290	32.290	2.440		1.639		0.251
906	883	15.000	6.350	-8.578	33.318	2.365		1.609		0.231
907	884	15.000	6.350	-9.867	34.075	2.291		1.578		0.431
908	885	15.000	6.350	-12.443	34.052	2.143		1.487		0.150
909	886	15.000	6.350	-15.019	34.718	2.094		1.446		0.090
910	887	15.000	6.350	-17.595	34.156	2.021		1.456		-0.002
911	888	15.000	6.350	0.0		2.661	1.456		-1.405	
912	889	15.000	6.350	-2.138		2.587	1.477		-1.405	
913	890	15.000	6.350	-4.714		2.513	1.416		-1.455	
914	891	15.000	6.350	-6.002		2.464	1.395		-1.405	
915	892	15.000	6.350	-7.290		2.464	1.385		-1.304	
916	893	15.000	6.350	-8.578		2.267	1.344		-1.174	
917	894	15.000	6.350	-9.867		2.218	1.283		-1.164	
918	895	15.000	6.350	-12.443		2.119	1.252		-1.124	
919	896	15.000	6.350	-15.019		2.119	1.252		-1.153	
920	897	15.000	6.350	-17.595		2.119	1.252		-1.174	
921	898	15.000	2.850	0.0	27.150	3.657		2.425		-0.154
922	899	15.000	2.850	-2.138	26.744	3.782		2.456		0.077
923	900	15.000	2.850	-3.426	26.844	3.682		2.410		0.256
924	901	15.000	2.850	-4.714	27.239	3.657		2.394		0.384
925	902	15.000	2.850	-6.002	27.523	3.583		2.394		0.537
926	903	15.000	2.850	-6.775	28.184	3.608		2.364		0.717
927	904	15.000	2.850	-7.290	29.292	3.484		2.287		0.537
928	905	15.000	2.850	-7.806	29.391	3.459		2.240		0.691
929	906	15.000	2.850	-8.321	29.227	3.384		2.210		0.768
930	907	15.000	2.850	-8.836	29.216	3.235		2.103		0.640
931	908	15.000	2.850	-9.351	29.285	3.260		2.103		0.435
932	909	15.000	2.850	-9.867	29.986	3.110		2.057		0.640
933	910	15.000	2.650	-11.155	29.720	3.011		1.995		0.384
934	911	15.000	2.850	-12.443	30.458	2.986		1.934		0.307
935	912	15.000	2.850	-13.731	31.122	3.011		1.903		0.102
936	913	15.000	2.850	-15.019	31.243	2.961		1.903		0.051
937	914	15.000	2.850	-17.595	31.584	2.812		1.887		0.128
938	915	15.000	2.850	-18.110	31.609	2.787		1.857		0.026
939	916	15.000	2.650	0.0	27.267	3.657	1.980		-2.942	
940	917	15.000	2.850	-2.138		3.856	2.057		-3.172	
941	918	15.000	2.850	-3.426		3.832	2.006		-2.763	
942	919	15.000	2.850	-4.714		3.632	1.968		-2.814	
943	920	15.000	2.850	-6.002		3.682	1.929		-2.609	
944	921	15.000	2.850	-6.775		3.608	1.917		-2.481	
945	922	15.000	2.850	-7.290		3.583	1.866		-2.456	
946	923	15.000	2.850	-7.806	28.753	3.484	1.816		-2.328	
947	924	15.000	2.850	-8.321		3.384	1.765		-2.328	
948	925	15.000	2.850	-8.836		3.309	1.778		-2.174	
949	926	15.000	2.850	-9.351		3.135	1.701		-2.123	
950	927	15.000	2.850	-9.867		3.210	1.688		-2.046	

Table III (Continued)

NUMBER	TEST NUMBER	X FEET	Y INCHES	Z INCHES	VELOCITY FPS	U RMS FPS	V RMS FPS	W RMS FPS	UV (FPS)X(FPS)	UW (FPS)X(FPS)
951	928	15.000	2.850	-11.155		3.085	1.612		-1.842	
952	929	15.000	2.850	-12.443		3.036	1.599		-1.790	
953	930	15.000	2.850	-13.731		3.036	1.587		-2.046	
954	931	15.000	2.850	-15.019		2.936	1.536		-1.842	
955	932	15.000	2.850	-17.595		2.836	1.510		-1.714	
956	933	15.000	2.850	-18.110		2.836	1.497		-1.688	
957	934	15.000	0.750	-7.806	18.683	4.580		2.885		2.315
958	935	15.000	1.030	-7.806	21.333	4.498		2.796		2.022
959	936	15.000	1.310	-7.806	23.048	4.387		2.706		1.706
960	937	15.000	1.590	-7.806	24.624	4.084		2.544		1.461
961	938	15.000	2.150	-7.806	25.218	3.725		2.329		1.194
962	939	15.000	2.710	-7.806	27.585	3.448		2.227		0.828
963	940	15.000	3.270	-7.806	28.792	3.326		2.138		0.536
964	941	15.000	3.830	-7.806	30.192	3.132		2.067		0.585
965	942	15.000	4.390	-7.806	31.212	2.937		1.967		0.463
966	943	15.000	4.950	-7.806	32.396	2.841		1.916		0.414
967	944	15.000	6.350	-7.806	33.949	2.598		1.736		0.366
968	945	15.000	7.750	-7.806	34.542	2.185		1.575		0.170
969	946	15.000	10.549	-7.806	36.116	1.749		1.234		0.097
970	947	15.000	13.349	-7.806	37.770	1.311		0.913		0.097
971	948	15.000	16.149	-7.806	38.981	0.825		0.541		0.049
972	949	15.000	0.750	-7.806		4.635	2.112		-3.045	
973	950	15.000	1.030	-7.806		4.415	2.082		-3.045	
974	951	15.000	1.310	-7.806		4.387	2.067		-3.167	
975	952	15.000	1.590	-7.806		4.139	2.007		-2.972	
976	953	15.000	2.150	-7.806		3.725	1.887		-2.728	
977	954	15.000	2.710	-7.806		3.449	1.798		-2.363	
978	955	15.000	3.270	-7.806		3.339	1.737		-2.143	
979	956	15.000	3.830	-7.806		3.173	1.707		-1.949	
980	957	15.000	4.390	-7.806		3.063	1.662		-1.754	
981	958	15.000	4.950	-7.806		2.925	1.602		-1.730	
982	959	15.000	6.350	-7.806		2.594	1.497		-1.583	
983	960	15.000	7.750	-7.806		2.180	1.333		-1.194	
984	961	15.000	10.549	-7.806		1.793	1.154		-0.852	
985	962	15.000	13.349	-7.806		1.297	0.868		-0.512	
986	963	15.000	16.149	-7.806		0.800	0.599		-0.195	

Table III (Continued)

NUMBER	TEST NUMBER	X FEET	Y INCHES	Z INCHES	VELOCITY FPS	U RMS FPS	V RMS FPS	W RMS FPS	UV (FPS)X(FPS)	UW (FPS)X(FPS)
987	987	9.000	.438	0.000	14.161	4.020	2.207	3.034		
988	988	9.000	.716	0.000	17.661	4.121	2.195	2.997		
989	989	9.000	.994	0.000	21.537	4.171	2.220	2.886		
990	990	9.000	1.273	0.000	22.715	3.869	2.183	2.849		
991	991	9.000	1.968	0.000	28.146	3.719	2.109	2.651		
992	992	9.000	2.664	0.000	29.502	3.518	2.047	2.442		
993	993	9.000	4.055	0.000	31.479	3.015	1.739	2.035		
994	994	9.000	5.446	0.000	33.874	2.492	1.517	1.776		
995	995	9.000	6.838	0.000	35.427	2.241	1.393	1.628		
996	996	9.000	8.229	0.000	37.066	1.950	1.282	1.467		
997	997	9.000	9.620	0.000	37.676	1.749	1.159	1.307		
998	998	9.000	11.011	0.000	37.865	1.518	1.085	1.221		
999	999	9.000	12.403	0.000	38.344	1.286	.962	.974		
1000	1000	9.000	13.794	0.000	39.975	1.045	.826	.740		
1001	1001	9.000	15.185	0.000	40.651	.754	.678	.629		
1002	1002	9.000	16.576	0.000	40.512	.492	.506	.419		
1003	1003	9.000	17.968	0.000	40.285	.372	.407	.321		
1004	1004	9.000	20.750	0.000	39.988	.191	.247	.197		
1005	1005	11.000	.625	0.000	16.311	4.271	2.183	3.009		
1006	1006	11.000	.736	0.000	17.332	4.322	2.158	3.034		
1007	1007	11.000	1.014	0.000	19.166	4.070	2.170	2.910		
1008	1008	11.000	1.291	0.000	22.056	4.121	2.220	2.824		
1009	1009	11.000	1.569	0.000	24.176	3.970	2.220	2.688		
1010	1010	11.000	2.263	0.000	26.475	3.618	2.133	2.540		
1011	1011	11.000	2.957	0.000	27.933	3.417	2.010	2.442		
1012	1012	11.000	4.345	0.000	31.186	3.015	1.862	2.047		
1013	1013	11.000	5.733	0.000	32.934	2.563	1.578	1.788		
1014	1014	11.000	7.121	0.000	35.615	2.412	1.430	1.640		
1015	1015	11.000	8.509	0.000	36.538	2.000	1.282	1.480		
1016	1016	11.000	9.896	0.000	36.672	1.749	1.245	1.356		
1017	1017	11.000	11.284	0.000	38.349	1.568	1.098	1.184		
1018	1018	11.000	12.672	0.000	39.483	1.226	.950	.987		
1019	1019	11.000	14.060	0.000	39.409	1.085	.851	.752		
1020	1020	11.000	15.448	0.000	40.087	.804	.715	.617		
1021	1021	11.000	18.224	0.000	39.723	.382	.432	.284		
1022	1022	11.000	21.000	0.000	40.450	.181	.210	.197		
1023	1023	13.000	.555	0.000	15.334	4.020	2.121	3.083		
1024	1024	13.000	.625	0.000	14.967	3.970	2.096	3.009		
1025	1025	13.000	.904	0.000	19.029	4.171	2.195	2.923		
1026	1026	13.000	1.183	0.000	21.481	4.121	2.183	2.836		
1027	1027	13.000	1.462	0.000	22.904	3.920	2.170	2.812		
1028	1028	13.000	2.160	0.000	25.942	3.769	2.109	2.590		
1029	1029	13.000	2.858	0.000	28.346	3.518	2.096	2.429		
1030	1030	13.000	4.253	0.000	31.464	3.116	1.911	2.146		
1031	1031	13.000	5.649	0.000	33.293	2.513	1.603	1.948		
1032	1032	13.000	7.045	0.000	34.408	2.382	1.455	1.702		
1033	1033	13.000	8.440	0.000	35.676	2.070	1.356	1.566		
1034	1034	13.000	9.836	0.000	37.334	1.799	1.184	1.393		
1035	1035	13.000	11.231	0.000	38.180	1.538	1.110	1.159		
1036	1036	13.000	12.627	0.000	38.509	1.407	1.048	.974		

Table III (Continued)

NUMBER	TEST NUMBER	X FEET	Y INCHES	Z INCHES	VELOCITY FPS	U RMS FPS	V RMS FPS	W RMS FPS	UV (FPS)X(FPS)	UW (FPS)X(FPS)
1037	1037	13.000	15.418	0.000	39.182	.804	.728	.617		
1038	1038	13.000	18.209	0.000	40.014	.382	.432	.308		
1039	1039	13.000	21.000	0.000	40.209	.231	.247	.173		

CORRECTED DATA FOR U(MEAN) = 30 FPS

NUMBER	TEST NUMBER	X FEET	Y INCHES	Z INCHES	VELOCITY FPS	U RMS FPS	V RMS FPS	W RMS FPS	UV (FPS)X(FPS)	UW (FPS)X(FPS)
1040	1040	15.000	20.742	0.000	29.998	.158	.206	.145		
1041	1041	15.000	19.657	0.000	29.800	.197	.266	.182		
1042	1042	15.000	18.255	0.000	29.610	.316	.339	.218		
1043	1043	15.000	16.853	0.000	29.359	.385	.412	.327		
1044	1044	15.000	15.451	0.000	28.994	.661	.569	.436		
1045	1045	15.000	14.050	0.000	28.676	.849	.605	.605		
1046	1046	15.000	12.648	0.000	28.801	.997	.690	.739		
1047	1047	15.000	11.246	0.000	28.376	1.125	.860	.932		
1048	1048	15.000	9.844	0.000	27.649	1.283	.957	1.126		
1049	1049	15.000	8.443	0.000	26.439	1.589	1.060	1.247		
1050	1050	15.000	7.041	0.000	25.561	1.747	1.150	1.356		
1051	1051	15.000	5.639	0.000	24.229	2.062	1.308	1.514		
1052	1052	15.000	4.237	0.000	22.153	2.487	1.453	1.719		
1053	1053	15.000	3.536	0.000	21.637	2.615	1.514	1.816		
1054	1054	15.000	2.835	0.000	20.416	2.842	1.586	1.925		
1055	1055	15.000	2.135	0.000	18.391	2.901	1.610	2.071		
1056	1056	15.000	1.434	0.000	16.050	3.138	1.647	2.095		
1057	1057	15.000	1.153	0.000	14.619	3.089	1.623	2.192		
1058	1058	15.000	.873	0.000	12.736	3.079	1.574	2.264		
1059	1059	15.000	.688	0.000	11.622	3.030	1.526	2.252		

Table IV

Summary of results from carriage-effect potential solution

y (inches)	$\overline{U}$ (fps)	$\overline{V}$ (fps)	q^2 (fps)	(p-p)/ $(fps)^2$	Notes
42 000	39.755	0.000	1580.433	9.784	Carriage
40 800	39.756	-0.018	1580.516	9.742	Centerline
39 600	39.759	-0.036	1580.763	9.619	
38 400	39.764	-0.054	1581.168	9.416	
37 200	39.771	-0.071	1581.723	9.139	
36 000	39.779	-0.086	1582.415	8.792	
34 800	39.790	-0.101	1583.232	8.384	
33 600	39.801	-0.114	1584.155	7.922	
32 400	39.814	-0.125	1585.169	7.415	
31 200	39.828	-0.135	1586.255	6.873	
30 000	39.842	-0.143	1587.394	6.303	
28 800	39.857	-0.150	1588.569	5.715	
27 600	39.872	-0.155	1589.764	5.118	
26 400	39.887	-0.158	1590.963	4.519	
25 200	39.901	-0.160	1592.151	3.925	
24 000	39.916	-0.160	1593.316	3.342	
22 800	39.930	-0.159	1594.448	2.776	
21 600	39.944	-0.157	1595.538	2.231	
20 400	39.957	-0.154	1596.579	1.711	
19 200	39.969	-0.149	1597.564	1.218	
18 000	39.981	-0.144	1598.489	0.756	
16 800	39.992	-0.138	1599.351	0.324	
15 600	40.002	-0.131	1600.149	-0.074	
14 400	40.011	-0.123	1600.880	-0.440	
13 200	40.019	-0.115	1601.545	-0.773	
12 000	40.027	-0.107	1602.144	-1.072	
10 800	40.033	-0.098	1602.676	-1.338	
9 600	40.039	-0.088	1603.144	-1.572	
8 400	40.044	-0.079	1603.547	-1.774	
7 200	40.049	-0.069	1603.888	-1.944	
6 000	40.052	-0.059	1604.167	-2.083	
4 800	40.055	-0.049	1604.384	-2.192	
3 600	40.057	-0.039	1604.542	-2.271	
2 400	40.058	-0.029	1605.640	-2.320	
1 200	40.058	-0.019	1604.680	-2.340	
0 000	40.058	-0.009	1604.661	-2.330	Tunnel Floor
-1 200	40.057	0.002	1604.583	-2.291	

Note: The solution is based upon an oncoming mean velocity of 40 fps. Values are computed for the location corresponding to the probe location used in the tests (three feet upstream from the cylinder representing the carriage).

Table V

Cross-flow (W) data

TEST NUMBER	X FEET	Y INCHES	Z INCHES	VELOCITY (FPS)(W)	MEAN VOLTAGE	BIAS VOLTAGE	CORRECTED VELOCITY (FPS) (W)
1	15.000	20.100	0.0	0.055	0.006	0.069	0.053
2	15.000	17.987	0.0	0.020	0.002	0.062	0.019
3	15.000	15.176	0.0	-0.002	0.0	0.063	-0.002
4	15.000	12.366	0.0	0.019	0.002	0.063	0.018
5	15.000	9.556	0.0	0.062	0.006	0.067	0.060
6	15.000	6.746	0.0	0.043	0.004	0.067	0.042
7	15.000	3.935	0.0	-0.068	-0.007	0.066	-0.066
8	15.000	1.125	0.0	-0.249	-0.025	0.050	-0.241
9	15.000	0.563	0.0	-0.573	-0.058	0.045	-0.554
10	15.000	1.125	14.954	0.201	0.020	0.066	0.194
11	15.000	1.125	12.312	0.291	0.029	0.066	0.281
12	15.000	1.125	9.670	0.202	0.020	0.066	0.195
13	15.000	1.125	7.028	0.157	0.016	0.070	0.152
14	15.000	1.125	4.386	-0.021	-0.002	0.062	-0.020
15	15.000	1.125	-0.898	-0.181	-0.018	0.059	-0.175
16	15.000	1.125	-6.182	-0.358	-0.036	0.062	-0.346
17	15.000	1.125	-8.824	-0.162	-0.016	0.066	-0.157
18	15.000	1.125	-11.466	-0.156	-0.016	0.071	-0.151
19	15.000	1.125	-14.108	-0.096	-0.010	0.063	-0.093
20	15.000	1.125	-16.750	0.021	0.002	0.071	0.020
21	15.000	1.125	-19.392	0.073	0.007	0.072	0.071
22	15.000	0.563	-19.392	0.039	0.004	0.065	0.038
23	15.000	0.563	-16.750	-0.036	-0.004	0.065	-0.035
24	15.000	0.563	-14.108	-0.185	-0.019	0.065	-0.179
25	15.000	0.563	-11.466	-0.398	-0.040	0.072	-0.385
26	15.000	0.563	-10.145	-0.445	-0.045	0.061	-0.430
27	15.000	0.563	-8.824	-0.341	-0.034	0.060	-0.329
28	15.000	1.828	20.238	0.020	0.002	0.066	0.019
29	15.000	1.828	17.596	0.061	0.006	0.067	0.059
30	15.000	1.828	12.312	0.115	0.012	0.069	0.111
31	15.000	1.828	7.028	0.089	0.009	0.065	0.086
32	15.000	1.828	1.744	-0.072	-0.007	0.062	-0.070
33	15.000	1.828	-3.540	-0.155	-0.016	0.067	-0.150
34	15.000	1.828	-8.824	-0.041	-0.004	0.070	-0.040
35	15.000	1.828	-14.108	0.003	0.0	0.074	0.003
36	15.000	1.828	-19.392	0.103	0.011	0.070	0.100
37	15.000	3.233	20.238	0.048	0.005	0.071	0.046
38	15.000	3.233	12.312	0.007	0.001	0.073	0.007
39	15.000	3.233	7.028	-0.037	-0.004	0.070	-0.036
40	15.000	3.233	1.744	-0.019	-0.002	0.066	-0.018
41	15.000	3.233	-3.540	-0.039	-0.004	0.064	-0.038
42	15.000	3.233	-8.824	0.039	0.004	0.070	0.038
43	15.000	3.233	-14.108	0.061	0.006	0.077	0.059
44	15.000	3.233	-19.392	0.081	0.008	0.073	0.078
45	15.000	5.340	20.238	0.143	0.014	0.024	0.138
46	15.000	5.340	12.312	0.081	0.008	0.018	0.078
47	15.000	5.340	7.028	-0.014	-0.001	0.025	-0.014
48	15.000	5.340	1.744	0.049	0.005	0.030	0.047
49	15.000	5.340	-3.540	0.017	0.002	0.032	0.016
50	15.000	5.340	-8.824	0.069	0.007	0.037	0.067

Table V (Continued)

TEST NUMBER	X FEET	Y INCHES	Z INCHES	VELOCITY (FPS)(W)	MEAN VOLTAGE	BIAS VOLTAGE	CORRECTED VELOCITY (FPS) (W)
51	15.000	5.340	-14.108	0.030	0.003	0.034	0.029
52	15.000	5.340	-19.392	-0.053	-0.005	0.037	-0.051
53	15.000	5.340	-0.898	-0.004	0.0	0.039	-0.004
54	15.000	9.556	20.238	0.188	0.019	0.042	0.182
55	15.000	9.556	12.312	0.110	0.011	0.045	0.106
56	15.000	9.556	7.028	0.079	0.008	0.042	0.075
57	15.000	9.556	1.744	0.022	0.002	0.041	0.021
58	15.000	9.556	-3.540	0.009	0.001	0.041	0.009
59	15.000	9.556	-8.824	-0.033	-0.003	0.038	-0.032
60	15.000	9.556	-14.108	-0.083	-0.008	0.040	-0.080
61	15.000	9.556	-19.392	-0.138	-0.014	0.037	-0.133
62	15.000	19.392	20.238	0.056	0.006	0.036	0.054
63	15.000	19.392	12.312	0.119	0.012	0.037	0.115
64	15.000	19.392	7.028	0.090	0.009	0.033	0.087
65	15.000	19.392	1.744	0.045	0.005	0.032	0.043
66	15.000	19.392	-3.540	0.043	0.004	0.033	0.042
67	15.000	19.392	-8.824	0.028	0.003	0.034	0.027
68	15.000	19.392	-14.108	-0.052	-0.005	0.033	-0.050
69	15.000	19.392	-19.392	-0.046	-0.005	0.033	-0.044
70	15.000	13.771	20.238	0.218	0.022	0.029	0.211
71	15.000	13.771	12.312	0.170	0.017	0.034	0.164
72	15.000	13.771	7.028	0.080	0.008	0.036	0.077
73	15.000	13.771	1.744	0.053	0.005	0.033	0.051
74	15.000	13.771	-3.540	-0.042	-0.004	0.036	-0.041
75	15.000	13.771	-8.824	-0.063	-0.006	0.033	-0.061
76	15.000	13.771	-14.108	-0.090	-0.009	0.032	-0.087
77	15.000	13.771	-19.392	0.001	0.0	0.035	0.001

Table V (Continued)

TEST NUMBER	X FEET	Y INCHES	Z INCHES	VELOCITY (FPS) (w)	MEAN VOLTAGE	BIAS VOLTAGE	CORRECTED VELOCITY (FPS) (w)
129	7.000	20.375	-2.720	0.088	0.009	0.010	0.108
130	7.000	14.049	-2.720	-0.004	0.0	0.001	-0.005
131	7.000	8.444	-2.720	0.097	0.010	-0.001	0.119
132	7.000	5.641	-2.720	0.047	0.005	-0.002	0.058
133	7.000	2.838	-2.720	-0.038	-0.004	0.002	-0.047
134	7.000	2.207	-2.720	-0.077	-0.008	0.001	-0.094
135	7.000	2.137	-18.625	0.219	0.022	-0.019	0.269
136	7.000	2.137	-14.308	0.206	0.021	-0.021	0.253
137	7.000	2.137	-9.990	0.076	0.008	-0.017	0.093
138	7.000	2.137	-5.673	-0.044	-0.004	-0.014	-0.054
139	7.000	2.137	-1.356	0.010	0.001	-0.017	0.012
140	7.000	2.137	2.962	0.047	0.005	-0.014	0.058
141	7.000	2.137	7.279	0.109	0.011	-0.021	0.134
142	7.000	2.137	13.755	0.125	0.013	-0.021	0.153
143	7.000	1.156	-18.625	0.130	0.013	-0.021	0.160
144	7.000	1.156	-14.308	0.102	0.010	-0.021	0.125
145	7.000	1.156	-9.990	0.073	0.007	-0.021	0.090
146	7.000	1.156	-5.673	0.072	0.007	-0.021	0.088
147	7.000	1.156	-1.356	0.087	0.009	-0.021	0.107
148	7.000	1.156	2.962	0.127	0.013	-0.021	0.156
149	7.000	1.156	7.279	0.112	0.011	-0.021	0.137
150	7.000	1.156	13.755	0.047	0.005	-0.022	0.058
151	7.000	0.876	2.962	0.192	0.019	-0.022	0.236
152	7.000	0.876	-1.356	0.055	0.006	-0.022	0.067
153	7.000	0.876	-5.673	0.039	0.004	-0.022	0.048
154	7.000	0.876	-9.990	0.008	0.001	-0.022	0.010
155	7.000	0.876	-14.308	0.080	0.008	-0.022	0.098
156	7.000	0.876	-18.625	0.130	0.013	-0.022	0.160
157	7.000	0.596	-18.625	0.137	0.014	-0.022	0.168
158	7.000	0.596	-14.308	0.049	0.005	-0.022	0.060
159	7.000	0.596	-9.990	-0.035	-0.004	-0.022	-0.043
160	-3.000	20.625	0.0	0.039	0.004	0.0	0.048
161	-3.000	16.817	0.0	-0.034	-0.003	0.0	-0.042
162	-3.000	14.037	0.0	-0.094	-0.009	0.003	-0.115
163	-3.000	11.257	0.0	-0.056	-0.006	0.003	-0.069
164	-3.000	8.478	0.0	-0.072	-0.007	0.0	-0.088
165	-3.000	5.698	0.0	-0.039	-0.004	0.002	-0.048
166	-3.000	2.918	0.0	-0.010	-0.001	-0.002	-0.012
167	-3.000	1.528	0.0	-0.120	-0.012	-0.006	-0.147
168	-3.000	0.973	0.0	-0.042	-0.004	-0.006	-0.052
169	-3.000	0.417	0.0	-0.081	-0.008	-0.006	-0.099
170	-3.000	1.806	19.000	-0.017	-0.011	-0.004	-0.021
171	-3.000	1.806	13.933	0.046	-0.004	-0.003	0.056
172	-3.000	1.806	8.867	-0.015	-0.010	-0.002	-0.018
173	-3.000	1.806	3.800	0.035	-0.006	-0.004	0.043
174	-3.000	1.806	-1.267	0.019	-0.007	-0.006	0.023
175	-3.000	1.806	-6.333	0.117	0.003	-0.002	0.144
176	-3.000	1.806	-11.400	0.240	0.015	-0.002	0.294
177	-3.000	1.806	-16.467	0.231	0.014	-0.001	0.284
178	-3.000	1.806	-19.000	0.275	0.019	-0.002	0.337

Table V (Continued)

TEST NUMBER	X FEET	Y INCHES	Z INCHES	VELOCITY (FPS)(W)	MEAN VOLTAGE	BIAS VOLTAGE	CORRECTED VELOCITY (FPS) (W)
179	-3.000	0.556	19.000	-0.003	-0.009	-0.002	-0.004
180	-3.000	0.556	13.933	0.051	-0.004	-0.002	0.063
181	-3.000	0.556	8.867	0.029	-0.006	-0.002	0.035
182	-3.000	0.556	3.800	-0.029	-0.012	-0.002	-0.036
183	-3.000	0.556	-1.267	-0.042	-0.013	-0.002	-0.052
184	-3.000	0.556	-6.333	0.031	-0.006	-0.002	0.038
185	-3.000	0.556	-11.400	0.129	0.004	-0.002	0.158
186	-3.000	0.556	-16.467	0.119	0.003	-0.002	0.146
187	-3.000	0.556	-19.000	0.174	0.008	-0.002	0.213
188	-3.000	4.308	19.000	0.015	-0.008	0.0	0.018
189	-3.000	4.308	13.933	0.015	-0.008	0.003	0.018
190	-3.000	4.308	8.867	0.006	-0.008	-0.001	0.007
191	-3.000	4.308	3.800	-0.064	-0.016	0.004	-0.079
192	-3.000	4.308	-1.267	-0.060	-0.015	0.0	-0.074
193	-3.000	4.308	-6.333	-0.011	-0.010	0.004	-0.014
194	-3.000	4.308	-11.400	0.060	-0.003	-0.001	0.074
195	-3.000	4.308	-16.467	0.040	-0.005	0.0	0.049
196	-3.000	4.308	-19.000	0.028	-0.006	0.001	0.034
197	-3.000	11.257	19.000	0.121	0.003	-0.009	0.149
198	-3.000	11.257	13.933	0.068	-0.002	-0.010	0.084
199	-3.000	11.257	8.867	0.102	0.001	-0.010	0.125
200	-3.000	11.257	3.800	-0.086	-0.018	-0.010	-0.105
201	-3.000	11.257	-1.267	-0.162	-0.025	-0.010	-0.199
202	-3.000	11.257	-6.333	-0.238	-0.033	-0.008	-0.292
203	-3.000	11.257	-11.400	-0.231	-0.032	-0.009	-0.284
204	-3.000	11.257	-16.467	-0.264	-0.036	-0.009	-0.324
205	-3.000	11.257	-19.000	-0.289	-0.038	-0.011	-0.354
206	-3.000	19.597	19.000	0.009	-0.008	-0.013	0.011
207	-3.000	19.597	13.933	-0.020	-0.011	-0.011	-0.024
208	-3.000	19.597	8.867	-0.029	-0.012	-0.011	-0.035
209	-3.000	19.597	3.800	-0.057	-0.015	-0.013	-0.070
210	-3.000	19.597	-1.267	-0.110	-0.020	-0.011	-0.135
211	-3.000	19.597	-6.333	-0.112	-0.020	-0.012	-0.138
212	-3.000	19.597	-11.400	-0.161	-0.025	-0.012	-0.197
213	-3.000	19.597	-16.467	-0.180	-0.027	-0.010	-0.221
214	-3.000	19.597	-19.000	-0.153	-0.024	-0.010	-0.188

Table V (Continued)

CROSSFLOW DATA U = 30 FEET PER SECOND

TEST NUMBER	X FEET	Y INCHES	Z INCHES	VELOCITY (FPS)(W)	MEAN VOLTAGE	BIAS VOLTAGE	CORRECTED VELOCITY (FPS) (W)
263	15.000	20.750	-8.500	0.080	0.008	0.0	0.098
264	15.000	16.853	-8.500	-0.011	-0.001	-0.002	-0.013
265	15.000	14.050	-8.500	0.013	0.001	-0.004	0.016
266	15.000	11.246	-8.500	0.028	0.003	-0.005	0.034
267	15.000	8.443	-8.500	0.063	0.006	0.002	0.077
268	15.000	5.639	-8.500	0.159	0.016	0.001	0.195
269	15.000	4.237	-8.500	0.211	0.021	0.003	0.259
270	15.000	3.536	-8.500	0.172	0.017	0.009	0.211
271	15.000	2.835	-8.500	0.103	0.010	0.005	0.126
272	15.000	2.135	-8.500	0.031	0.003	0.002	0.038
273	15.000	1.714	-8.500	-0.004	0.0	0.002	-0.005
274	15.000	1.434	-8.500	-0.004	0.0	0.002	-0.005
275	15.000	1.153	-8.500	-0.014	-0.001	0.002	-0.017
276	15.000	0.873	-8.500	-0.035	-0.004	0.002	-0.043
277	15.000	0.593	-8.500	-0.002	0.0	0.002	-0.002

Table VI

Cross-flow (V) data

TEST NUMBER	X FEET	Y INCHES	Z INCHES	VELOCITY (FPS)	MEAN VOLTAGE	BIAS VOLTAGE	CORRECTED VELOCITY (FPS) (V)
78	15.000	19.392	20.238	-0.306	-0.025	0.035	-0.238
79	15.000	19.392	12.312	-0.405	-0.033	0.029	-0.337
80	15.000	19.392	7.028	-0.366	-0.030	0.028	-0.298
81	15.000	19.392	1.744	-0.360	-0.030	0.036	-0.292
82	15.000	19.392	-3.540	-0.266	-0.022	0.029	-0.199
83	15.000	19.392	-8.824	-0.204	-0.017	0.031	-0.136
84	15.000	19.392	-14.108	-0.207	-0.017	0.029	-0.140
85	15.000	19.392	-19.392	-0.151	-0.012	0.025	-0.083
86	15.000	13.771	20.238	-0.153	-0.013	0.030	-0.094
87	15.000	13.771	12.312	-0.330	-0.027	0.034	-0.270
88	15.000	13.771	7.028	-0.302	-0.025	0.031	-0.242
89	15.000	13.771	1.744	-0.270	-0.022	0.032	-0.210
90	15.000	13.771	-3.540	-0.160	-0.013	0.029	-0.100
91	15.000	13.771	-8.824	-0.118	-0.010	0.030	-0.058
92	15.000	13.771	-14.108	-0.185	-0.015	0.028	-0.126
93	15.000	13.771	-19.392	-0.211	-0.017	0.030	-0.151
94	15.000	9.556	20.238	-0.106	-0.009	0.026	-0.057
95	15.000	9.556	12.312	-0.195	-0.016	0.025	-0.146
96	15.000	9.556	7.028	-0.242	-0.020	0.027	-0.193
97	15.000	9.556	1.744	-0.225	-0.018	0.023	-0.176
98	15.000	9.556	-3.540	-0.107	-0.009	0.026	-0.058
99	15.000	9.556	-8.824	-0.072	-0.006	0.026	-0.024
100	15.000	9.556	-14.108	-0.129	-0.011	0.025	-0.080
101	15.000	9.556	-19.392	-0.172	-0.014	0.026	-0.123
102	15.000	5.340	20.238	-0.004	0.0	0.025	0.031
103	15.000	5.340	12.312	-0.184	-0.015	0.025	-0.149
104	15.000	5.340	7.028	-0.202	-0.017	0.027	-0.168
105	15.000	5.340	1.744	-0.172	-0.014	0.024	-0.137
106	15.000	5.340	-3.540	-0.055	-0.005	0.026	-0.020
107	15.000	5.340	-8.824	-0.023	-0.002	0.025	0.012
108	15.000	5.340	-14.108	-0.002	0.0	0.027	0.032
109	15.000	5.340	-19.392	-0.043	-0.003	0.026	-0.008
110	15.000	3.233	20.238	0.040	0.003	0.024	0.068
111	15.000	3.233	12.312	-0.049	-0.004	0.022	-0.022
112	15.000	3.233	7.028	-0.102	-0.008	0.020	-0.075
113	15.000	3.233	1.744	-0.152	-0.012	0.020	-0.125
114	15.000	3.233	-3.540	-0.016	-0.001	0.020	0.011
115	15.000	3.233	-8.824	-0.015	-0.001	0.020	0.013
116	15.000	3.233	-14.108	0.107	0.009	0.023	0.134
117	15.000	3.233	-19.392	0.038	0.003	0.022	0.065
118	15.000	1.828	20.238	-0.115	-0.009	0.022	-0.093
119	15.000	1.828	12.312	-0.117	-0.010	0.022	-0.094
120	15.000	1.828	7.028	-0.173	-0.014	0.022	-0.151
121	15.000	1.828	1.744	-0.182	-0.015	0.022	-0.159
122	15.000	1.828	-3.540	-0.166	-0.014	0.022	-0.144
123	15.000	1.828	-8.824	-0.175	-0.014	0.022	-0.153
124	15.000	1.828	-14.108	-0.055	-0.005	0.022	-0.033
125	15.000	1.828	-19.392	-0.110	-0.009	0.022	-0.088
126	15.000	1.125	-19.392	-0.134	-0.011	0.022	-0.114
127	15.000	1.125	-14.108	-0.091	-0.008	0.022	-0.071

Table VI (Continued)

TEST NUMBER	X FEET	Y INCHES	Z INCHES	VELOCITY (FPS)	MEAN VOLTAGE	BIAS VOLTAGE	CORRECTED VELOCITY (FPS) (V)
128	15.000	1.125	-8.824	-0.211	-0.017	0.022	-0.192
215	-3.000	10.562	-18.341	-0.320	-0.026	-0.004	-0.269
216	-3.000	10.562	-11.400	-0.258	-0.021	-0.010	-0.206
217	-3.000	10.562	-6.333	-0.188	-0.015	-0.009	-0.136
218	-3.000	10.562	-1.267	-0.123	-0.010	-0.004	-0.071
219	-3.000	10.562	3.800	-0.088	-0.007	-0.007	-0.037
220	-3.000	10.562	8.867	-0.087	-0.007	0.0	-0.035
221	-3.000	10.562	13.933	-0.042	-0.003	-0.006	0.010
222	-3.000	10.562	17.987	0.071	0.006	-0.006	0.123
223	-3.000	14.037	-18.341	-0.115	-0.009	-0.010	-0.055
224	-3.000	14.037	-11.400	-0.144	-0.012	-0.009	-0.083
225	-3.000	14.037	-6.333	-0.093	-0.008	-0.009	-0.038
226	-3.000	14.037	-1.267	-0.050	-0.004	-0.007	0.010
227	-3.000	14.037	3.800	0.036	0.003	-0.008	0.096
228	-3.000	14.037	8.867	0.087	0.007	-0.007	0.147
229	-3.000	14.037	13.933	0.010	0.001	-0.007	0.070
230	-3.000	14.037	17.987	0.042	0.003	-0.007	0.102
231	-3.000	16.817	-18.341	-0.049	-0.004	-0.011	0.016
232	-3.000	16.817	-11.400	-0.137	-0.011	-0.010	-0.072
233	-3.000	16.817	-6.333	-0.117	-0.010	-0.011	-0.051
234	-3.000	16.817	-1.267	-0.082	-0.007	-0.012	-0.017
235	-3.000	16.817	3.800	-0.040	-0.003	-0.006	0.025
236	-3.000	16.817	8.867	-0.054	-0.004	-0.006	0.011
237	-3.000	16.817	13.933	-0.097	-0.008	0.0	-0.032
238	-3.000	16.817	17.987	-0.029	-0.002	0.0	0.036
239	-3.000	20.986	-18.341	-0.267	-0.022	-0.008	-0.199
240	-3.000	20.986	-11.400	-0.307	-0.025	-0.009	-0.238
241	-3.000	20.986	-6.333	-0.283	-0.023	-0.009	-0.215
242	-3.000	20.986	-1.267	-0.263	-0.022	-0.008	-0.194
243	-3.000	20.986	3.800	-0.193	-0.016	-0.006	-0.124
244	-3.000	20.986	8.867	-0.148	-0.012	-0.007	-0.080
245	-3.000	20.986	13.933	-0.080	-0.007	-0.004	-0.011
246	-3.000	20.986	17.987	0.017	0.001	-0.004	0.085
247	-3.000	20.625	3.800	-0.135	-0.011	-0.038	-0.067
248	-3.000	16.817	3.800	-0.123	-0.010	-0.027	-0.057
249	-3.000	14.037	3.800	-0.074	-0.006	-0.022	-0.013
250	-3.000	11.257	3.800	-0.061	-0.005	-0.014	-0.008
251	-3.000	8.478	3.800	-0.061	-0.005	-0.009	-0.016
252	-3.000	5.698	3.800	-0.049	-0.004	-0.010	-0.013
253	-3.000	2.918	3.800	-0.037	-0.003	-0.004	-0.011
254	-3.000	0.695	3.800	-0.037	-0.003	0.004	-0.019
255	-3.000	20.625	8.867	-0.098	-0.008	-0.034	-0.030
256	-3.000	16.817	8.867	-0.086	-0.007	-0.034	-0.021
257	-3.000	14.037	8.867	-0.074	-0.006	-0.033	-0.013
258	-3.000	11.257	8.867	-0.110	-0.009	-0.026	-0.057
259	-3.000	8.478	8.867	-0.086	-0.007	-0.022	-0.041
260	-3.000	5.698	8.867	-0.123	-0.010	-0.015	-0.087
261	-3.000	2.918	8.867	-0.061	-0.005	-0.008	-0.035
262	-3.000	0.695	8.867	-0.061	-0.005	0.0	-0.043

Table VII

Evaluation of Terms in Eq. 5-17

x	y	z	U	$\frac{\partial U}{\partial z}$	$\frac{\partial U}{\partial x}$	W	$\frac{\partial uv}{\partial y}$	$\frac{\partial uw}{\partial z}$	$U\frac{\partial U}{x}$	$W\frac{\partial U}{\partial z}$	Residual (see note)
ft	in	in	fps	$\frac{fps}{ft}$	$\frac{fps}{ft}$	fps	$\frac{(fps)^2}{ft}$	$\frac{(fps)^2}{ft}$	$\frac{(fps)^2}{ft}$	$\frac{(fps)^2}{ft}$	$\frac{(fps)^2}{ft}$
15	0.75	-7.81	19.0	-35.2	-0.25	-0.27	-2.92	-1.62	-4.75	+9.50	+0.21
15	1.87	-7.81	26.0	-22.8	-0.24	-0.09	+5.20	-1.20	-6.24	-2.05	-0.19
15	2.85	-7.81	29.6	- 6.0	-0.14	-0.02	+3.56	-0.16	-4.14	+0.12	-0.62
15	3.55	-7.81	30.6	- 2.8	-0.13	+0.06	+4.00	0.00	-3.98	-0.17	-0.15
15	6.35	-7.81	33.0	- 3.6	-0.12	+0.01	+4.00	0.00	-3.96	-0.04	0.00

Note: The residual may be expected to reflect the effects of the viscous terms as well as uncertainties in the determinations of the various quantities.

Table VIII

Boundary Layer Parameters

x (ft.)	δ^* (in.)	θ (in.)	H	$u_*^{(1)}$ (ft/sec)	$u_*^{(2)}$ (ft/sec)	Estimates of y_i (in.): Based on U data	Based on $\overline{u^2}$ data	Based on $\overline{v^2}$ data	Based on $\overline{uv}$ data	Average	U_I (ft/sec)
I. Centerline Data											
-3	2.25	1.67	1.35	1.39	1.4						
2	2.69	1.79	1.50	3.89	2.1	2.8	3.0	2.7	2.8	2.76	
4	2.87	1.89	1.52	3.57	2.0	4.4	3.9	4.5	4.4	4.18	31.5
7	2.49	1.78	1.40	3.15	2.0	5.0	7.2	7.4	4.8	6.28	34.1
9	2.50	1.57	1.59	3.13		6.1	7.8	8.7		7.55	36.2
11	2.64	1.73	1.53	3.08		7.1	9.5	9.3		8.43	36.5
13	2.77	1.80	1.54	3.07		9.4	10.2	9.7		9.55	37.0
15	2.95	1.90	1.55	3.05	1.8	10.4	10.7	10.0	10.5	10.32	37.5
15 (3)	3.11	1.98	1.57	2.49		12.65	12.3	12.8	12.7 (4)	12.61	28.8
II. Data Near Edge of Roughness											
2	2.49	1.74	1.43	3.87							
4	2.85	1.93	1.48	3.70							
7	2.83	1.82	1.56	3.35							
15	3.12	2.07	1.51	3.12							

Notes: (1) From Semi-logarithmic plots
(2) From $\overline{uv}$ data
(3) Values for $U_\infty = 30$ ft/sec
4) From $\overline{w^2}$ data

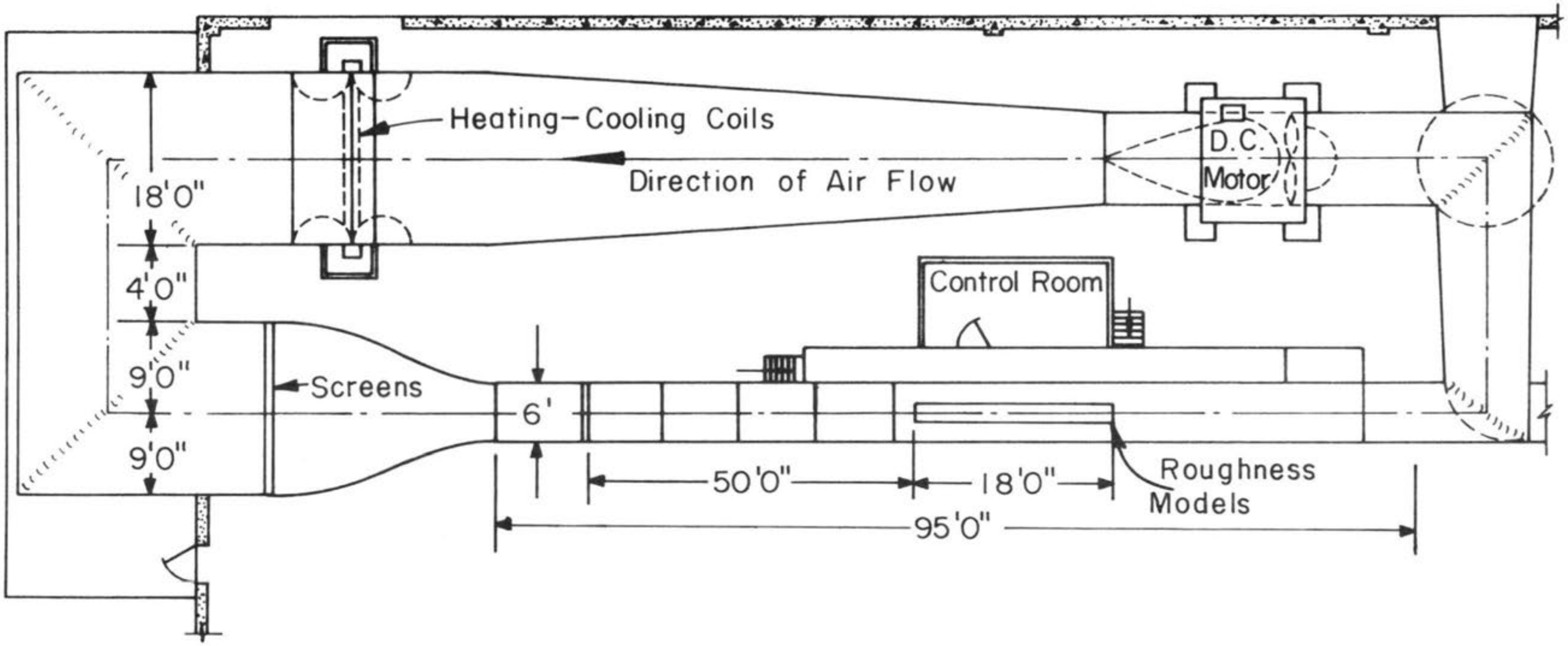

Fig. 1 Plan view of wind tunnel.

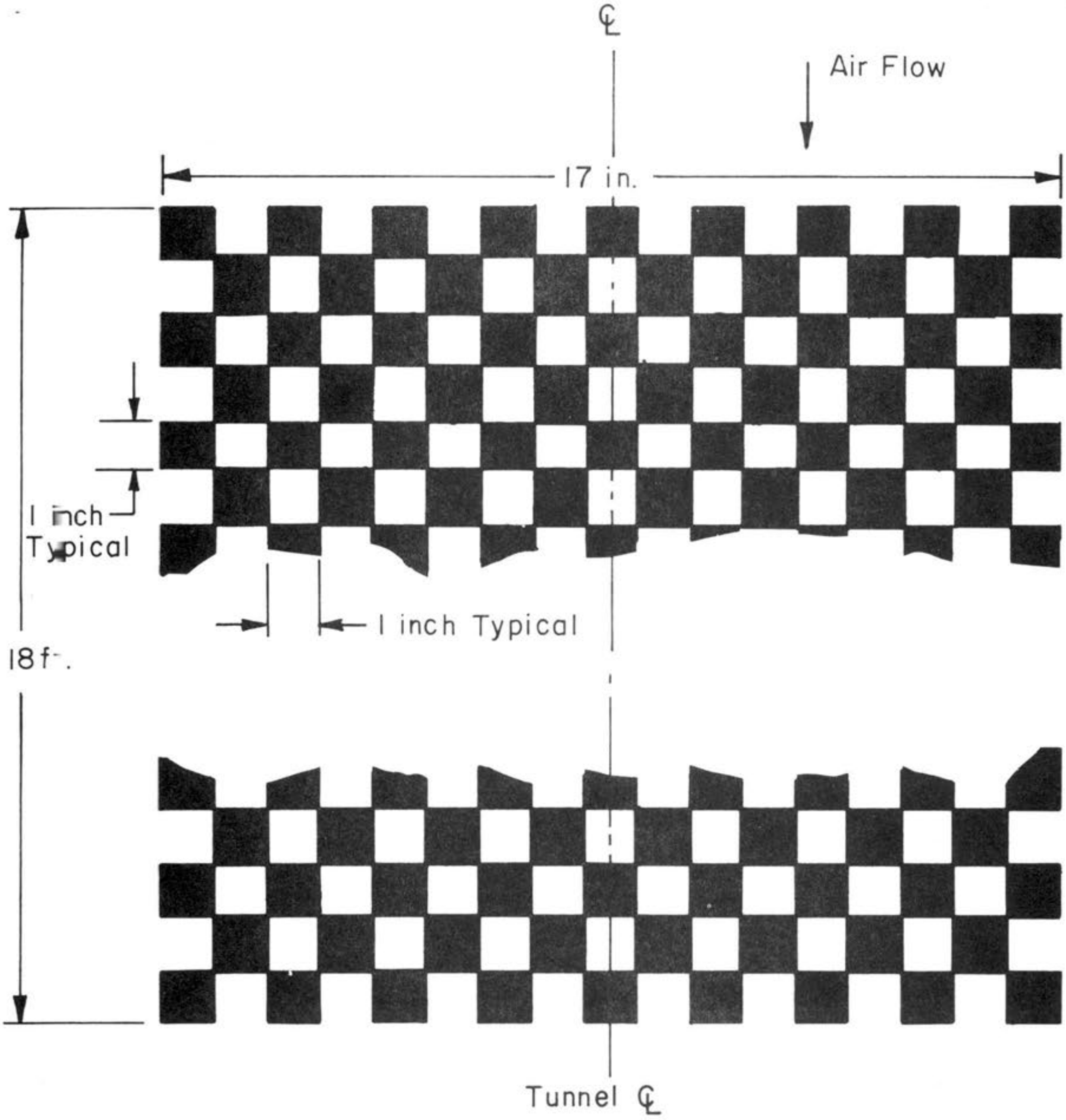

Fig. 2 Roughness pattern.

Fig. 3 Photograph of roughness model.

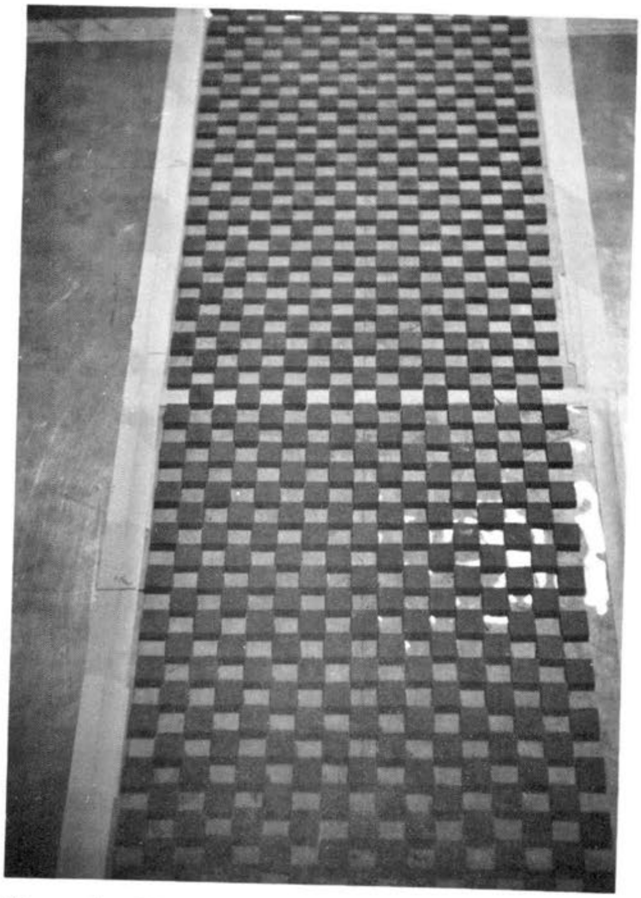

Fig. 4 Close-up photograph of roughness.

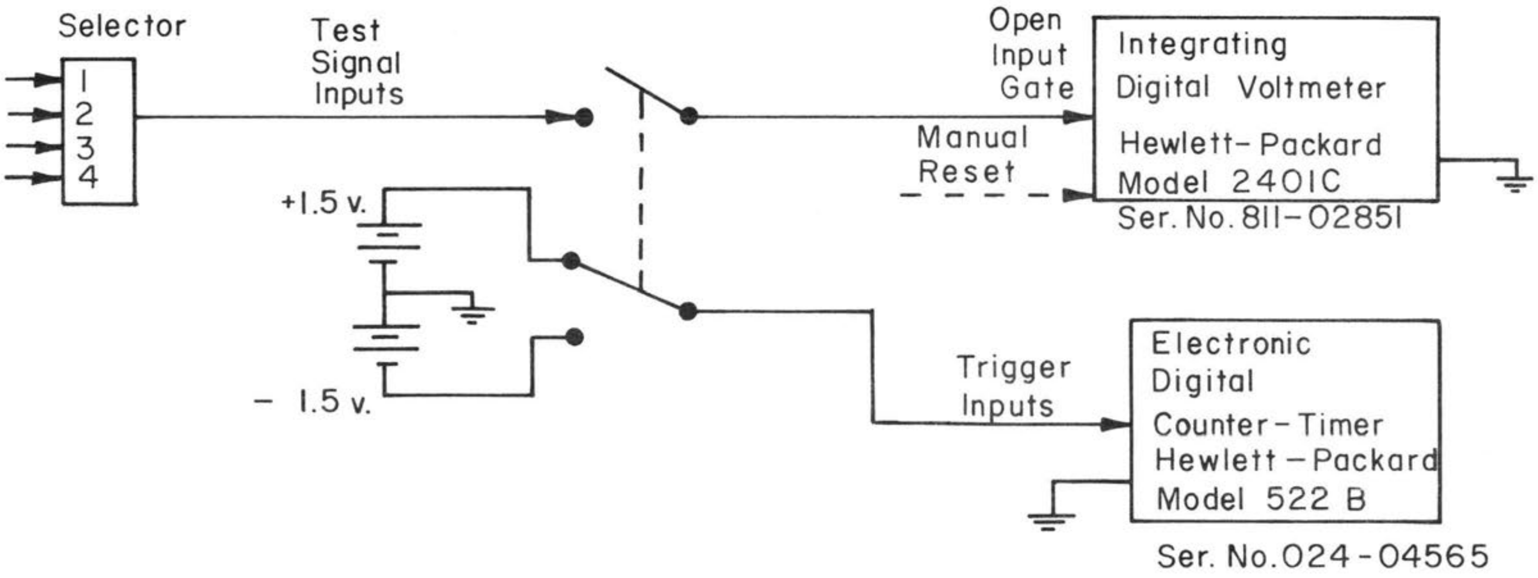

Fig. 5 Block diagram of voltage integration circuit.

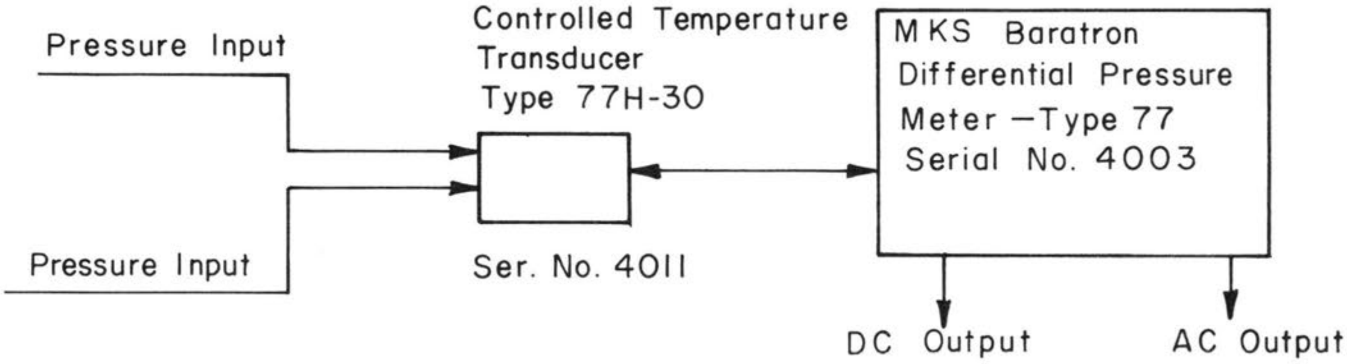

Fig. 6 Block diagram of pressure measurement circuit.

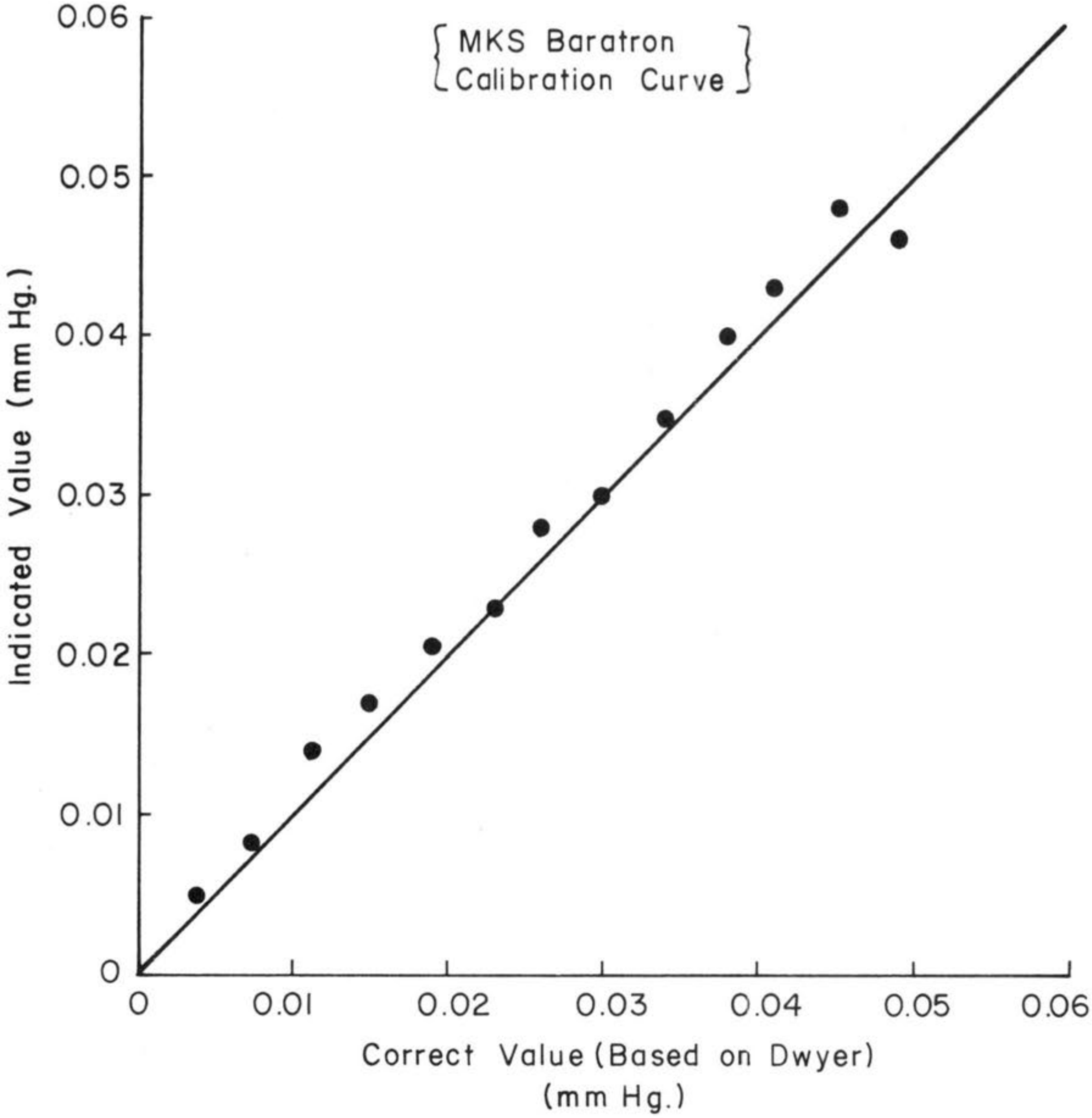

Fig. 7 MKS Baratron calibration curve--low pressures.

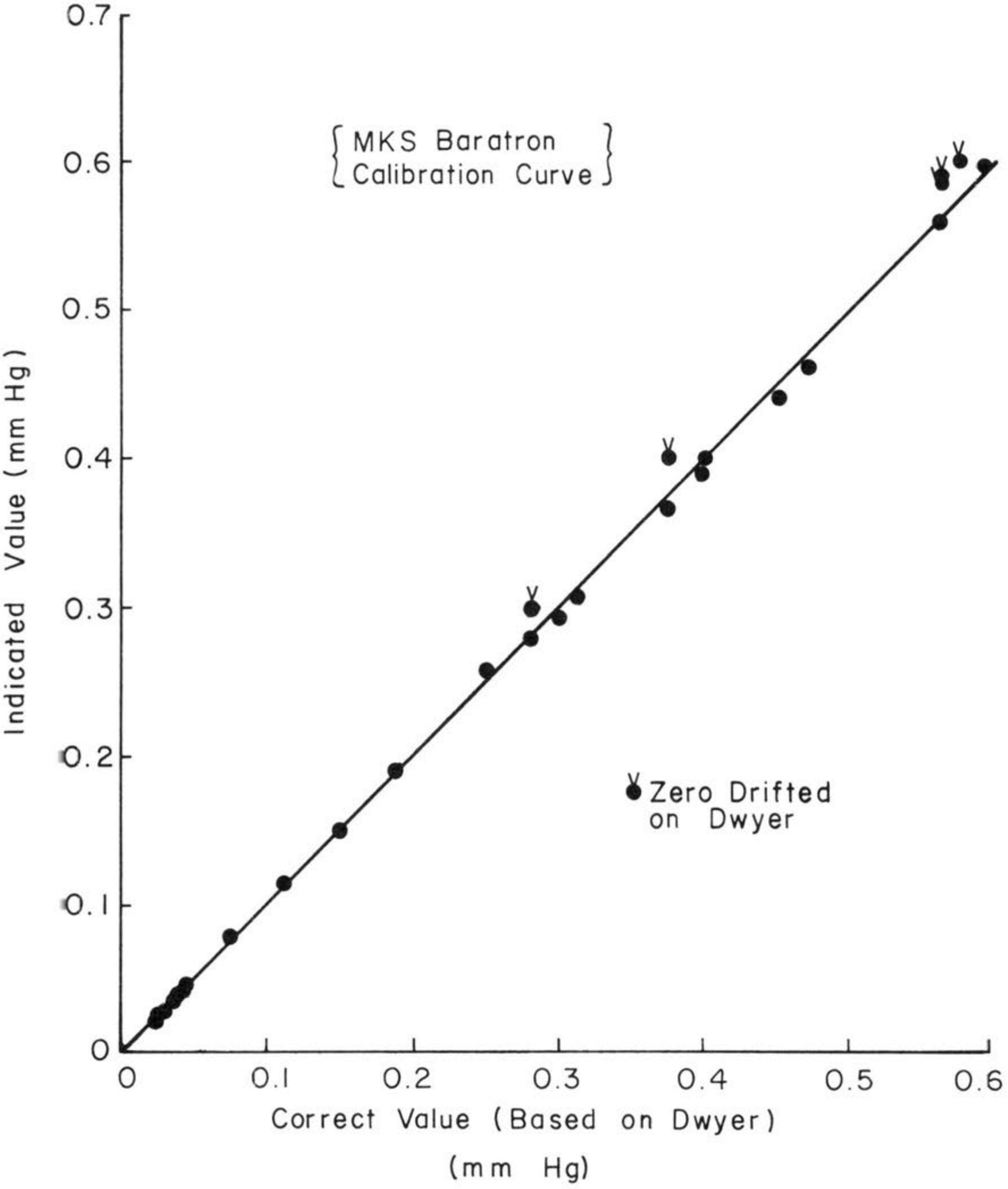

Fig. 8 MKS Baratron calibration curve--intermediate pressures.

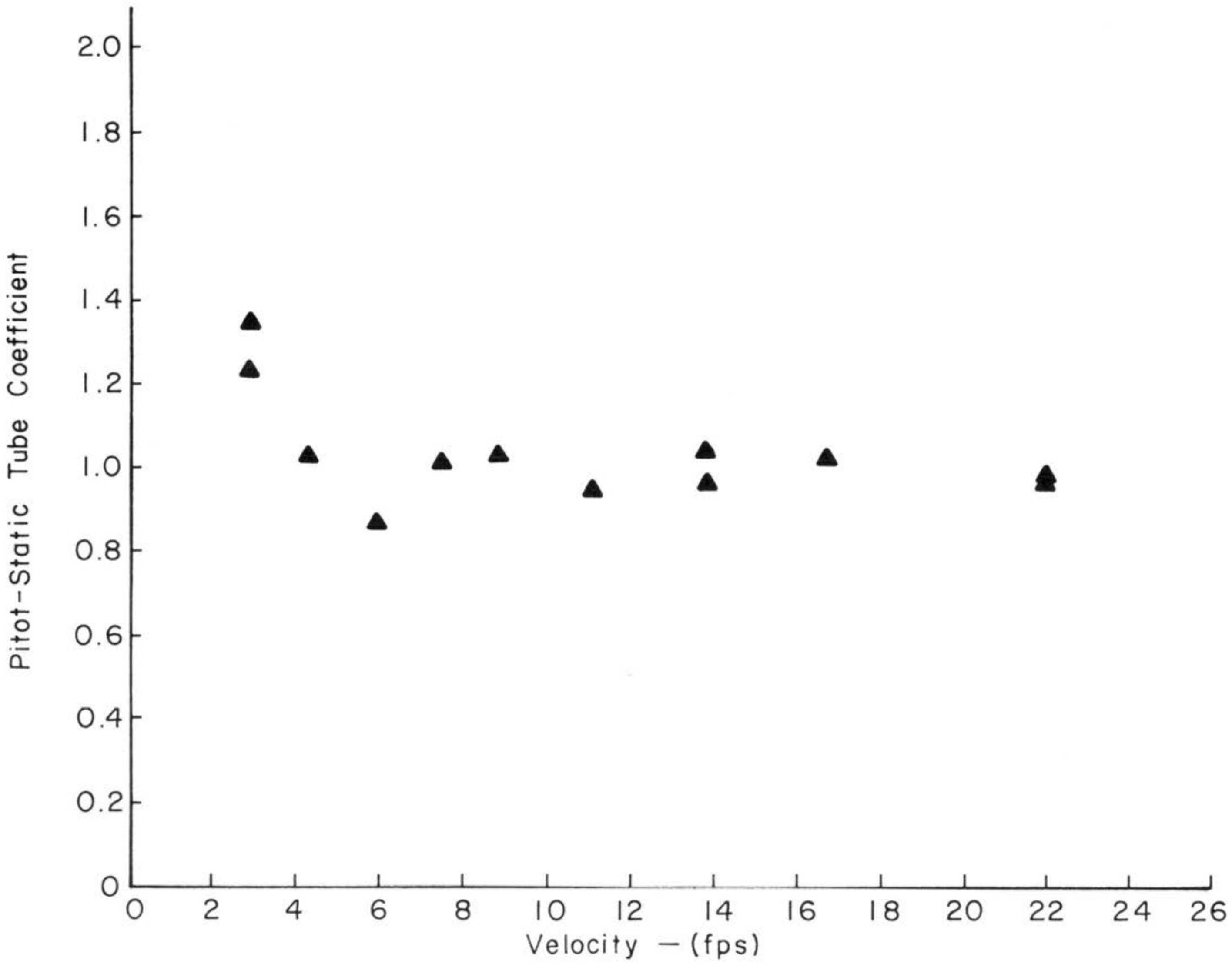

Fig. 9 Pitot-static tube calibration curve.

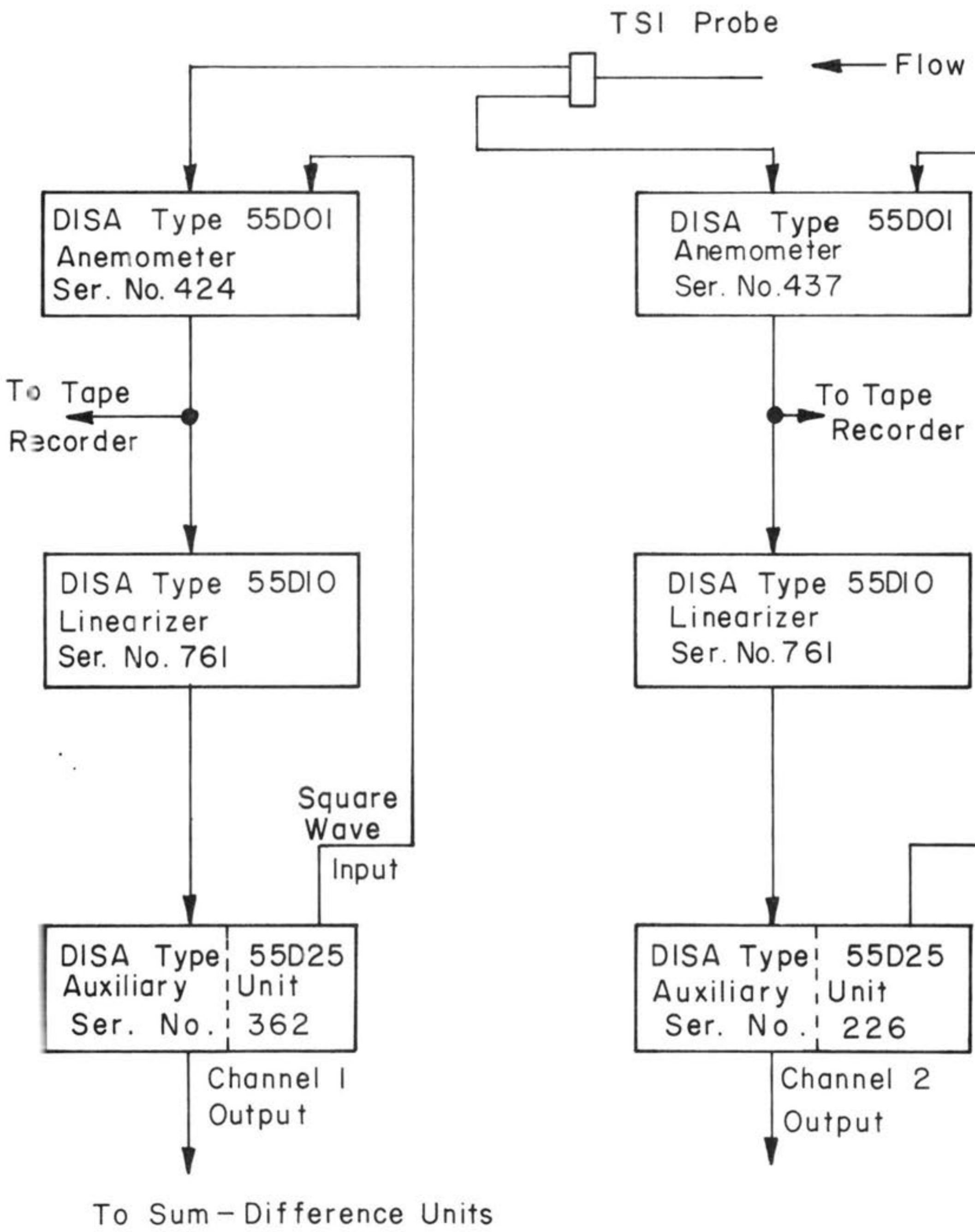

Fig. 10 Block diagram of anemometer systems.

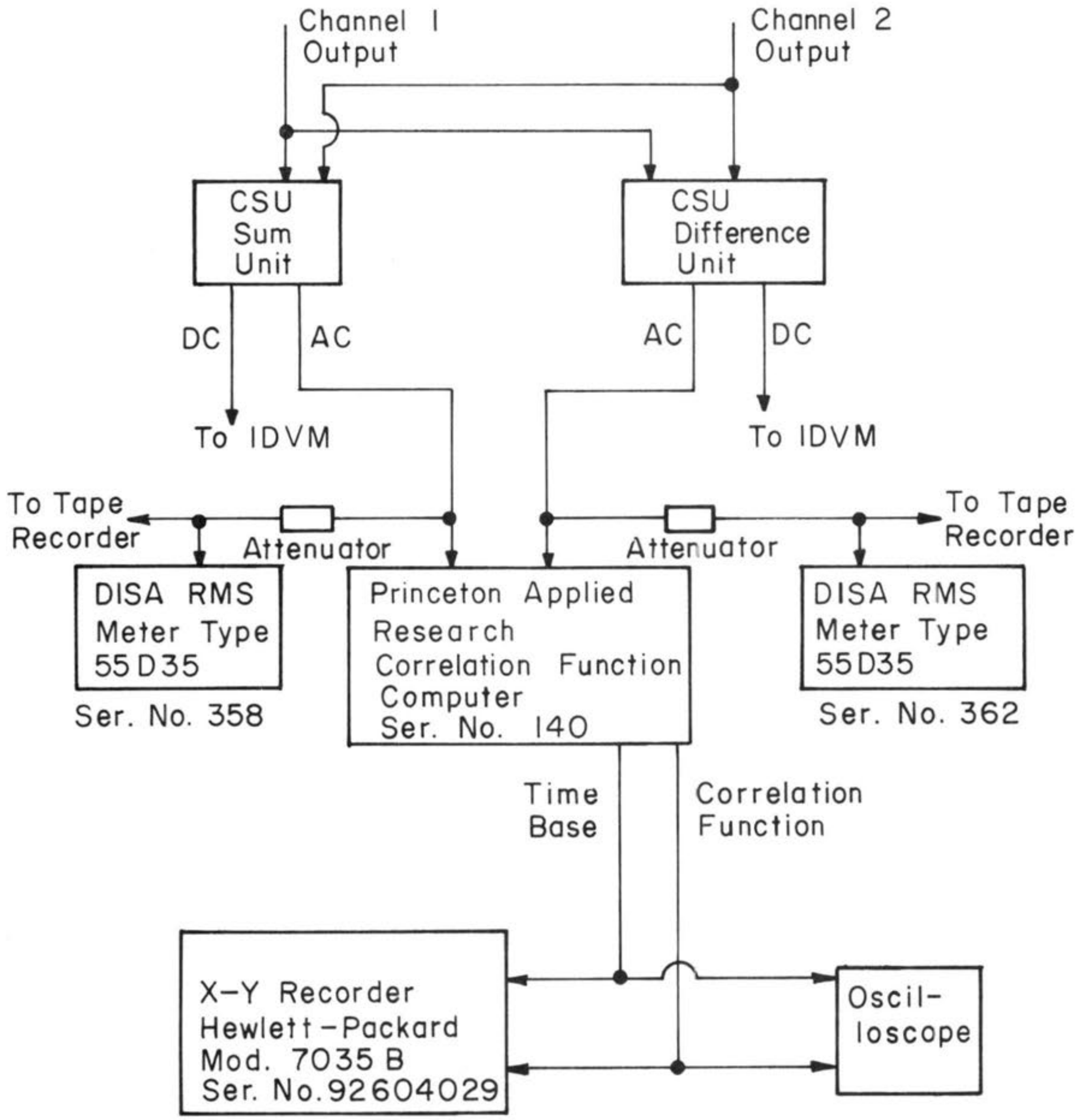

Fig. 11 Block diagram of correlator system.

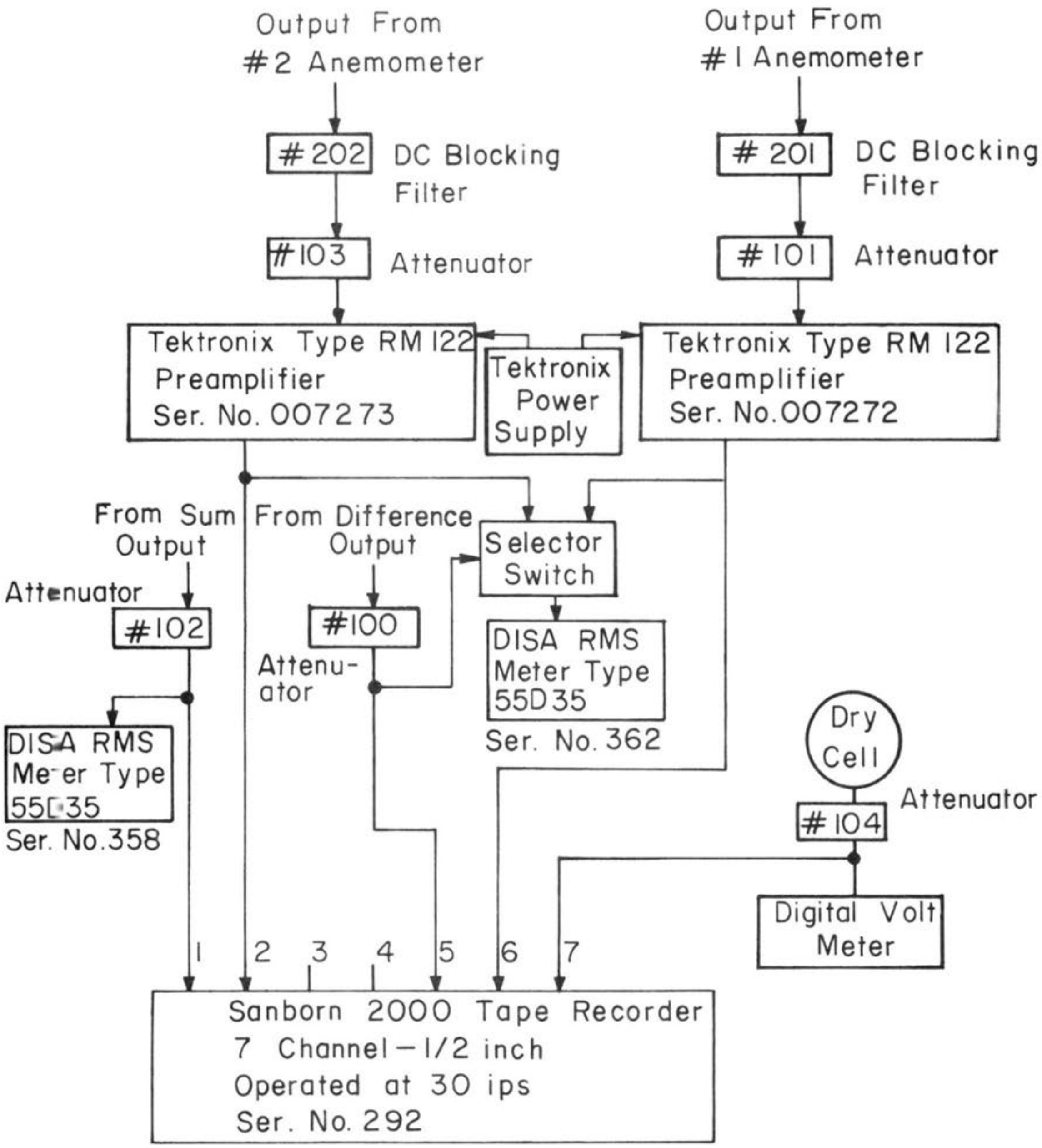

Fig. 12 Block diagram of recorder system.

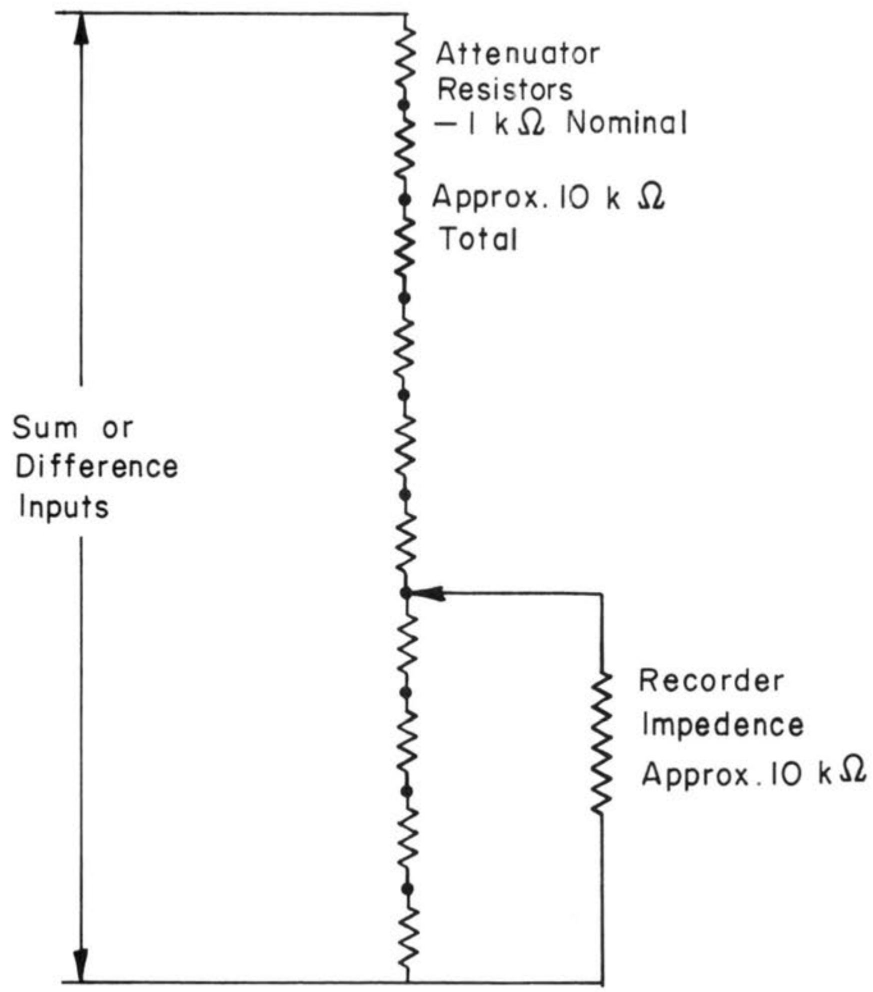

Fig. 13 Schematic of voltage dividers.

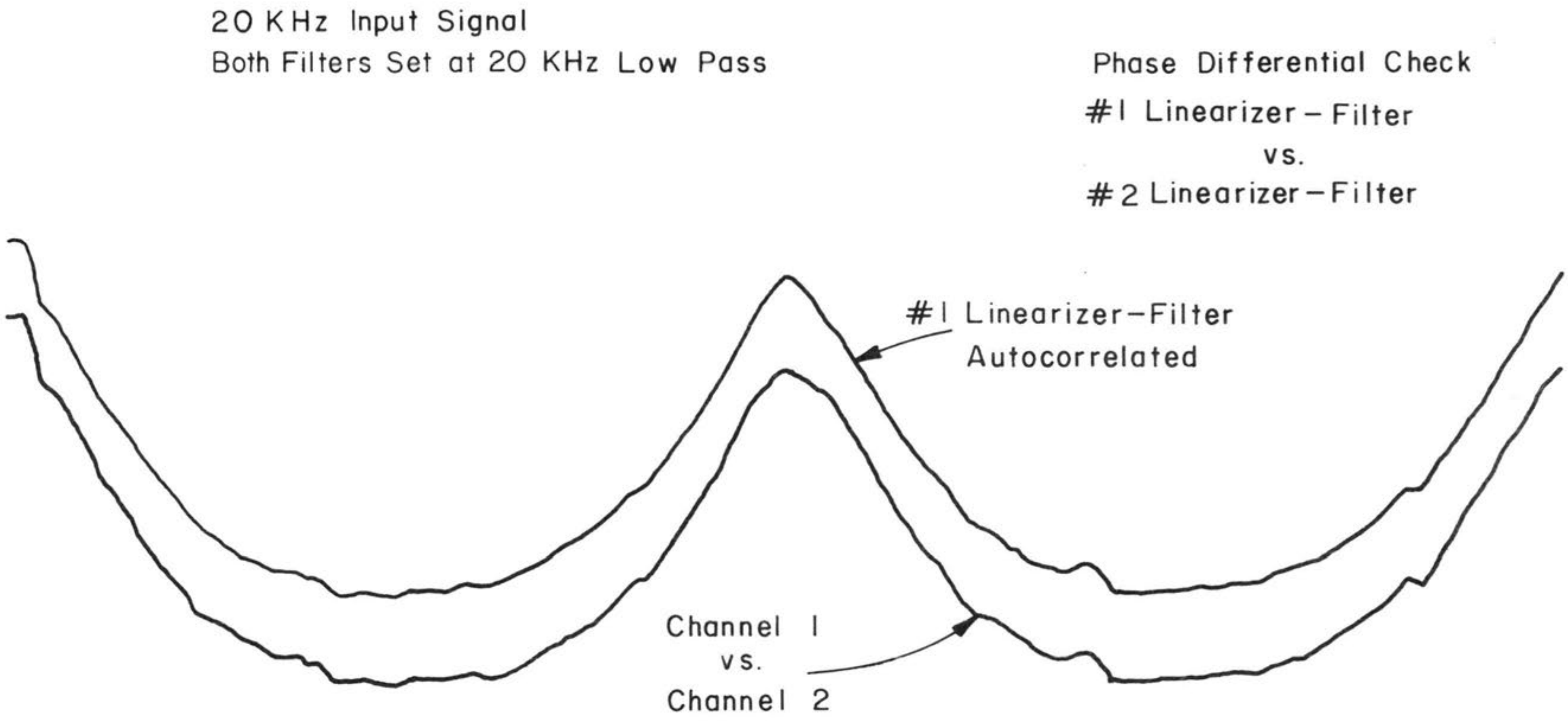

Fig. 14 Typical phase-shift check.

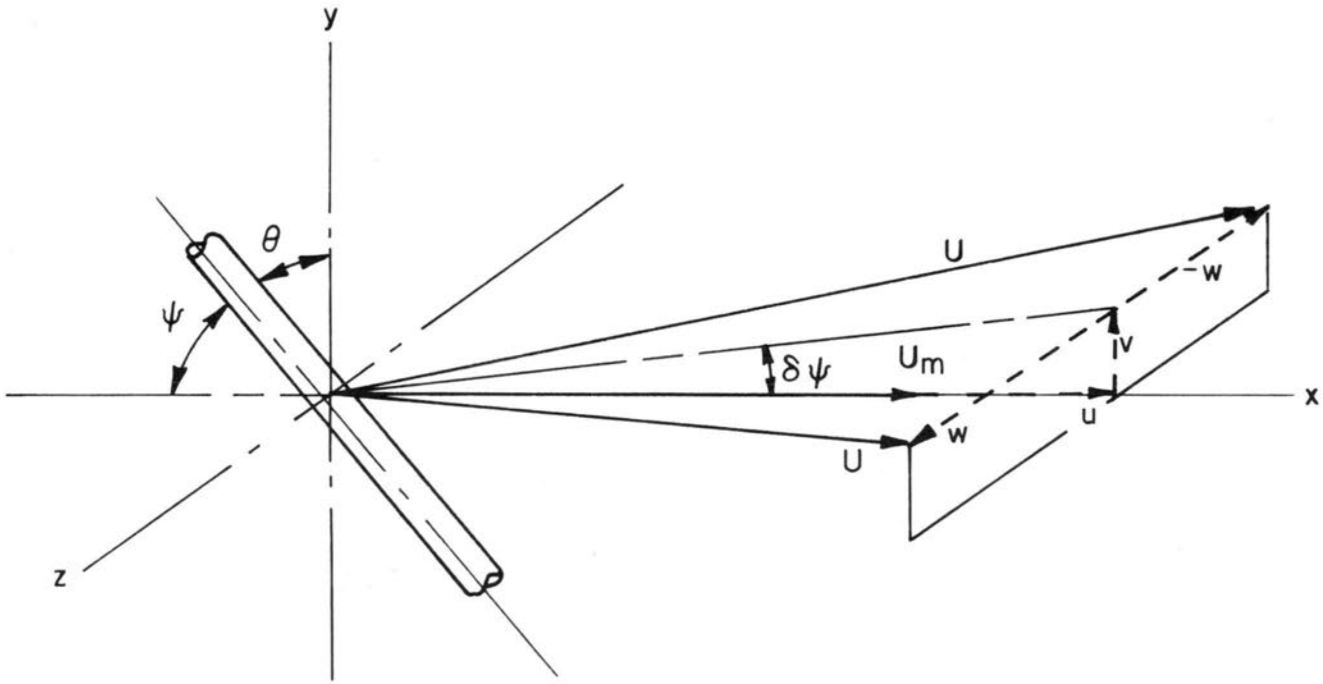

Fig. 15 Hot-wire coordinate system.

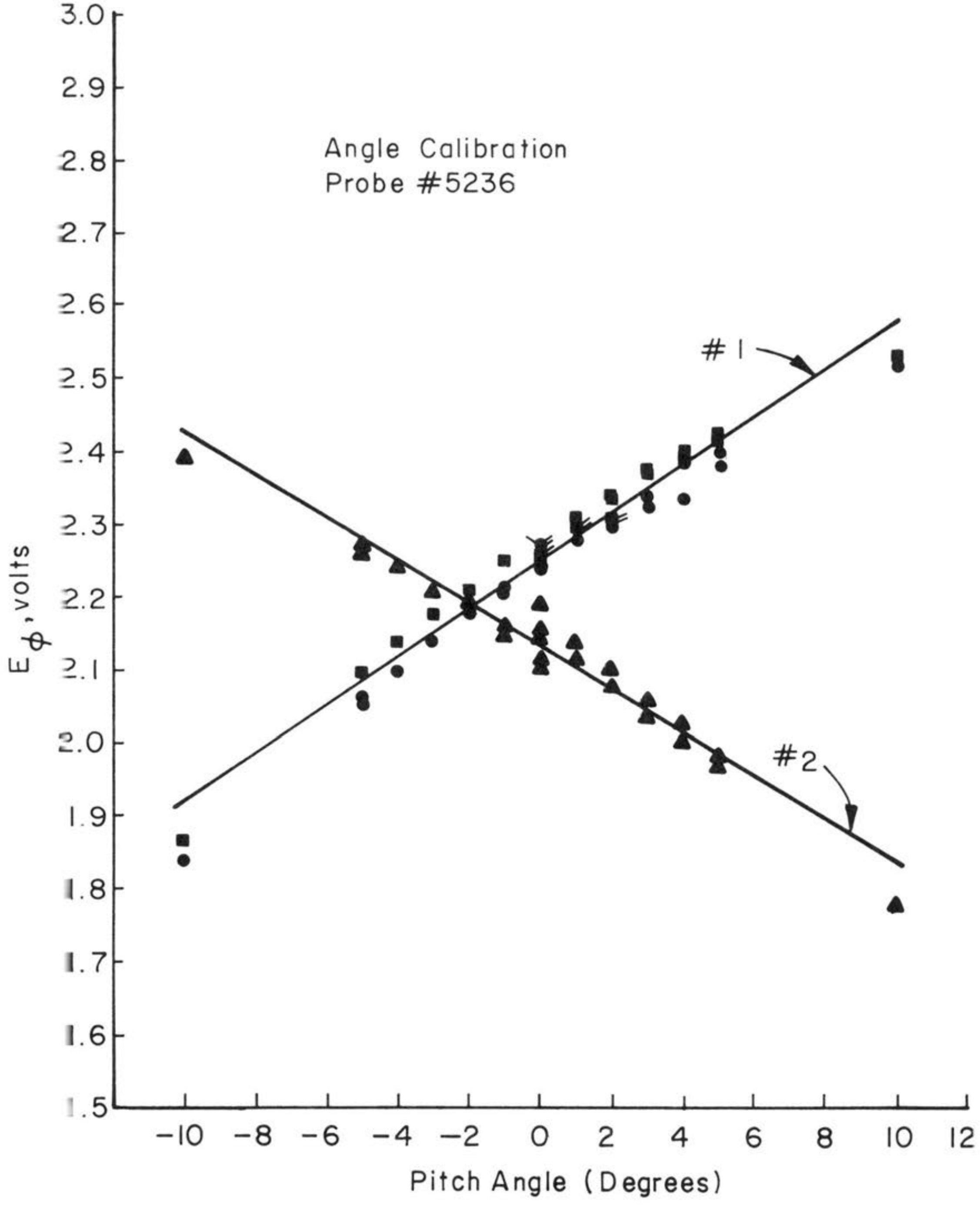

Fig. 16 Sample angle calibration for x-wire probe.

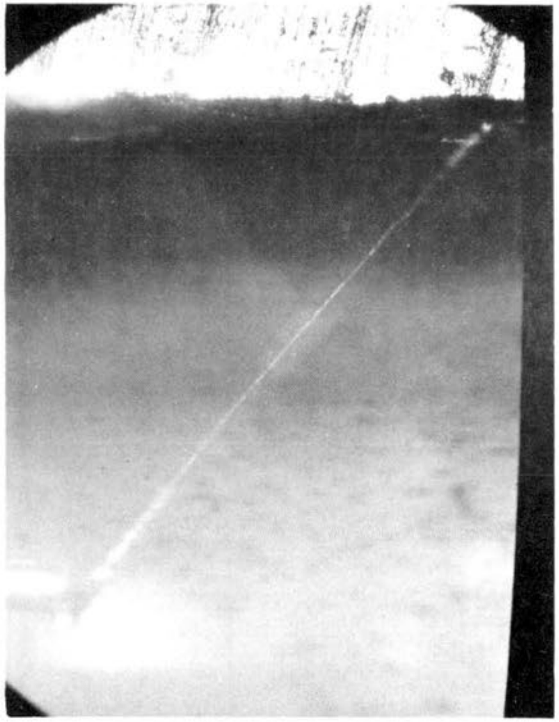

Wire #
Probe No. 5236

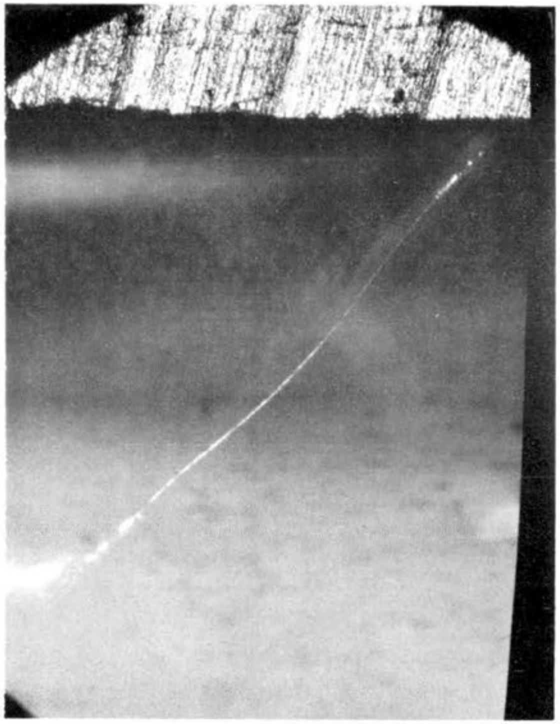

Wire #
Probe No. 5239

Fig. 17 Typical x-wire microphotographs.

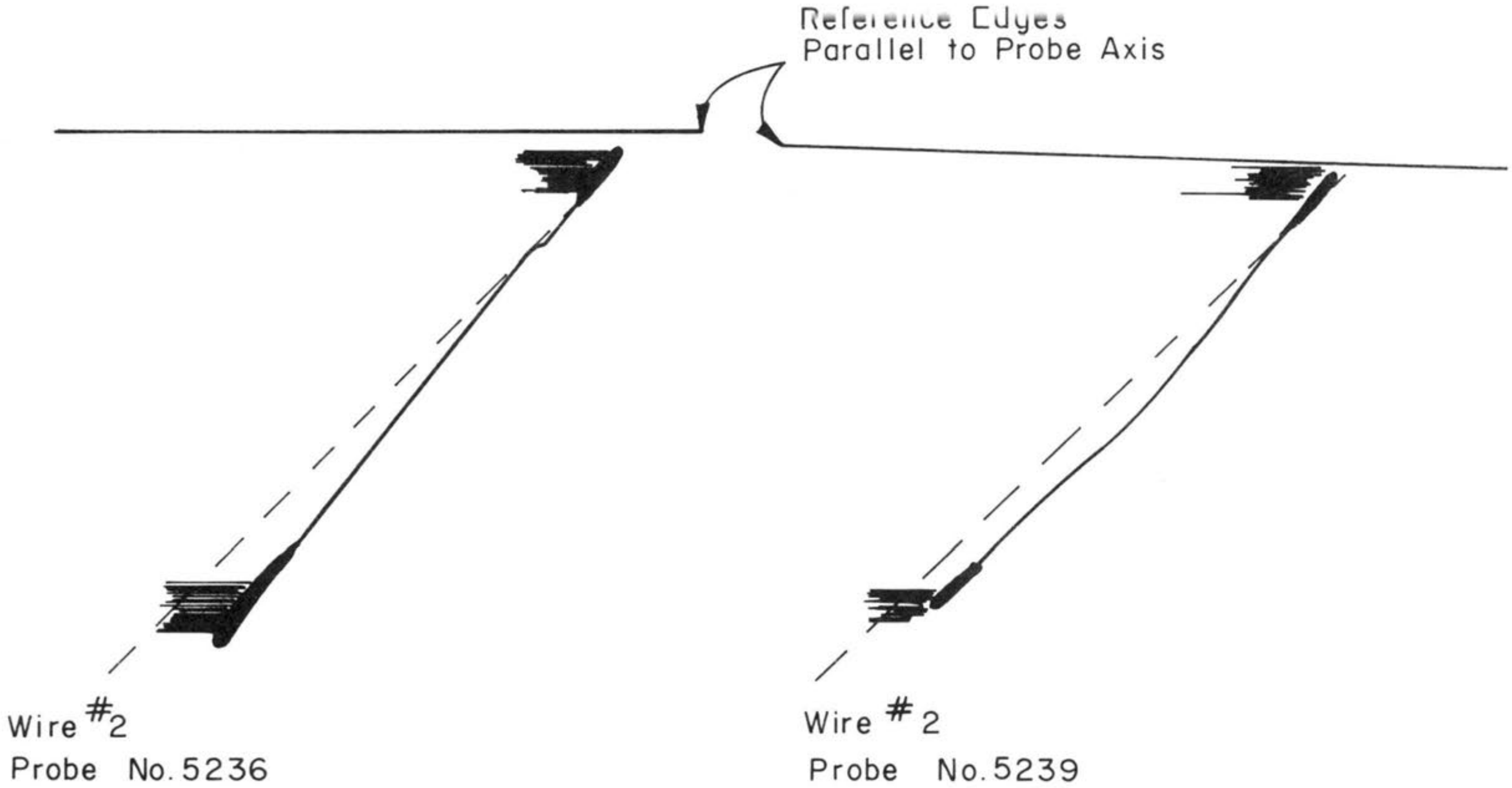

Fig. 18 Tracings of x-wire microphotographs.

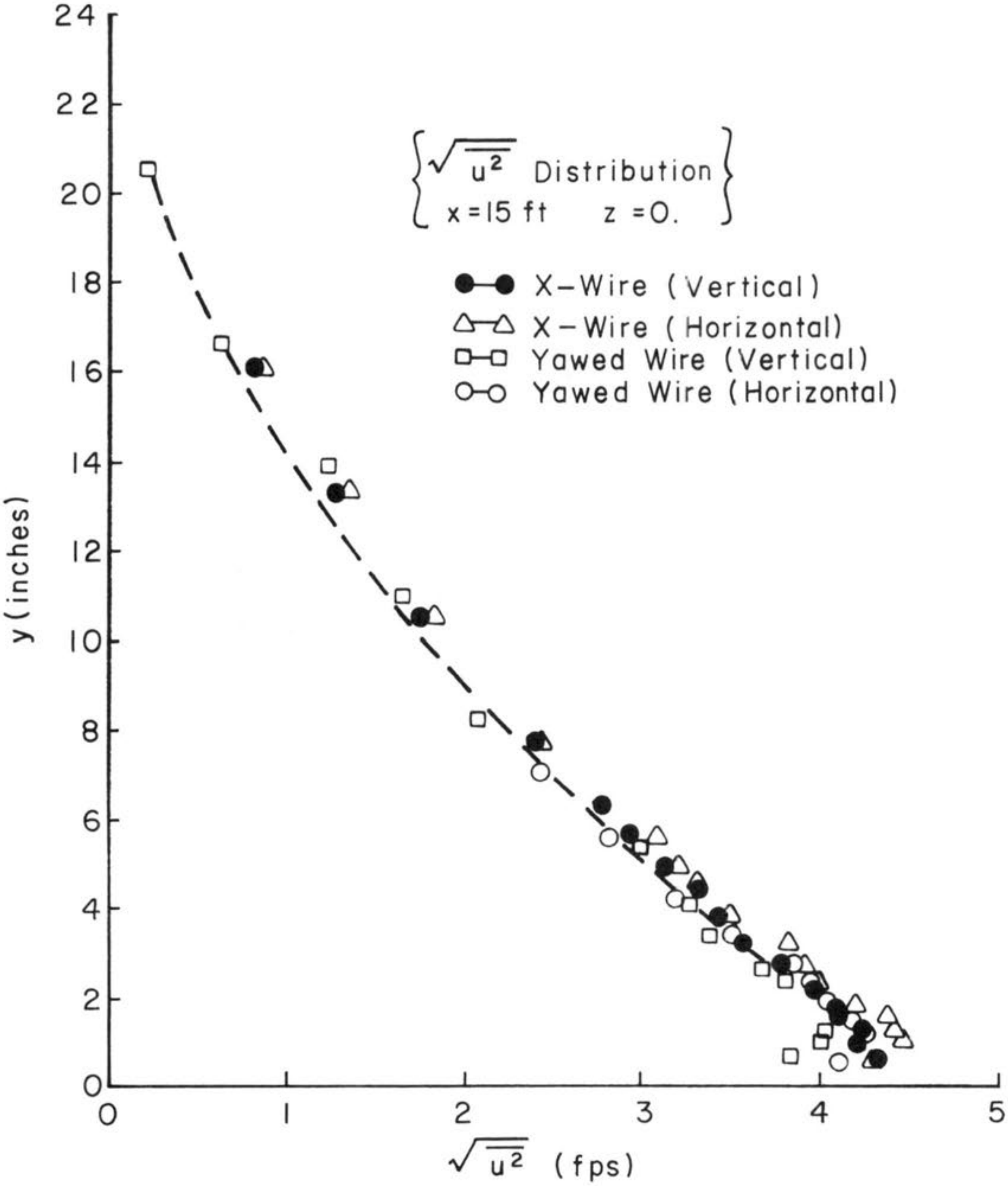

Fig. 19 Comparison of $\sqrt{\overline{u^2}}$ values obtained by different methods.

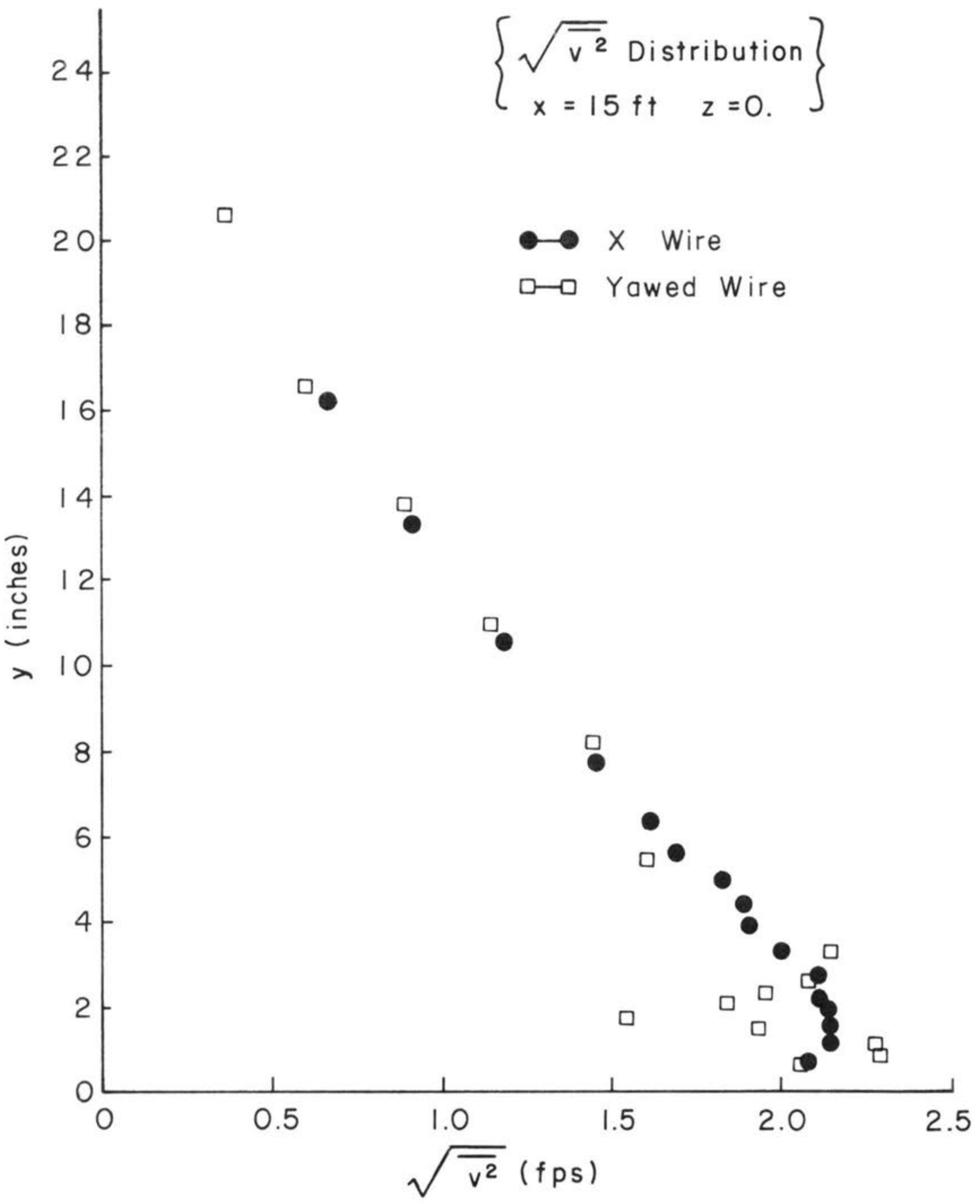

F_g. 20 Comparison of $\sqrt{\overline{v^2}}$ values obtained by different methods.

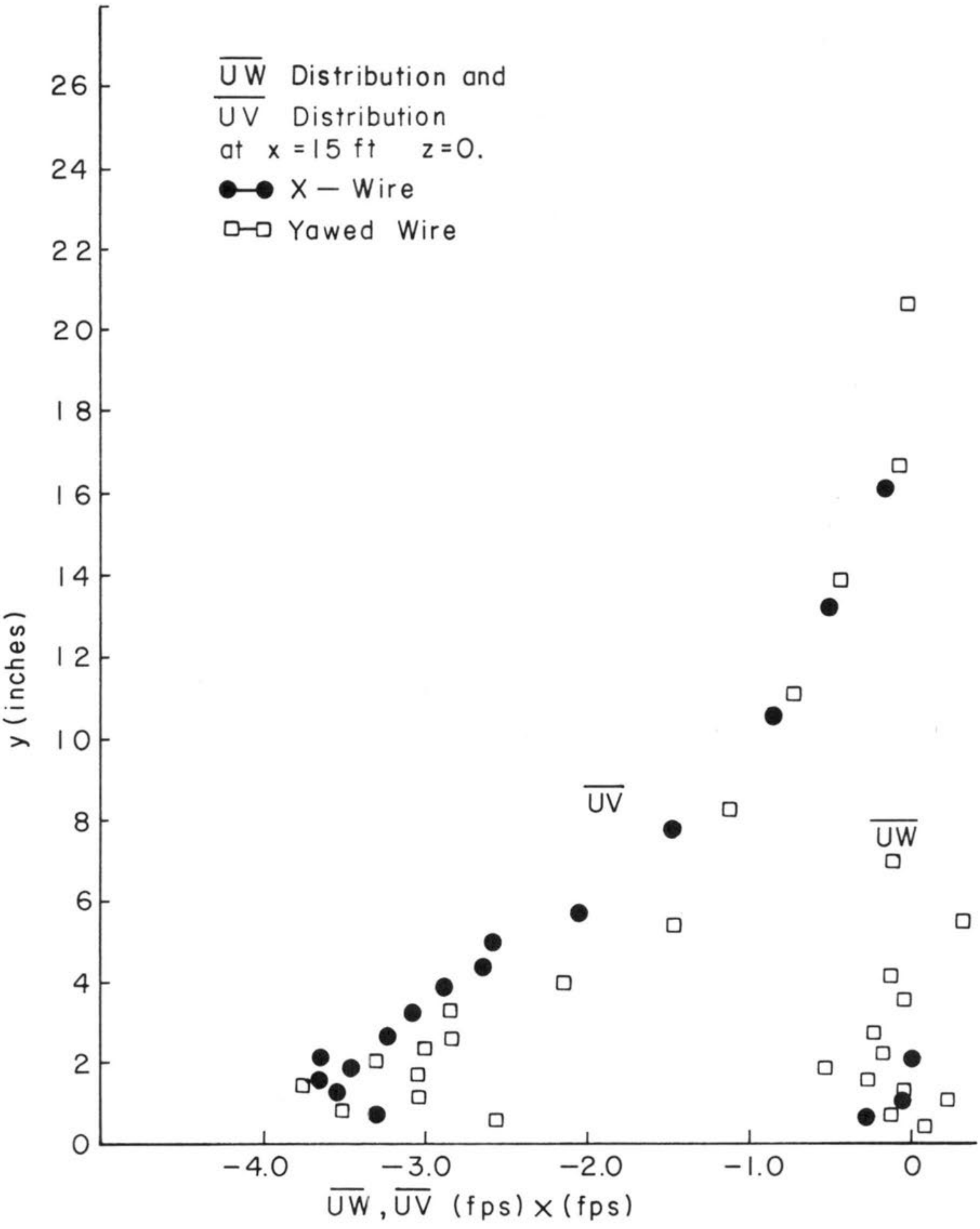

Fig. 21 Comparison of $\overline{uv}$ and $\overline{uw}$ values obtained by different methods.

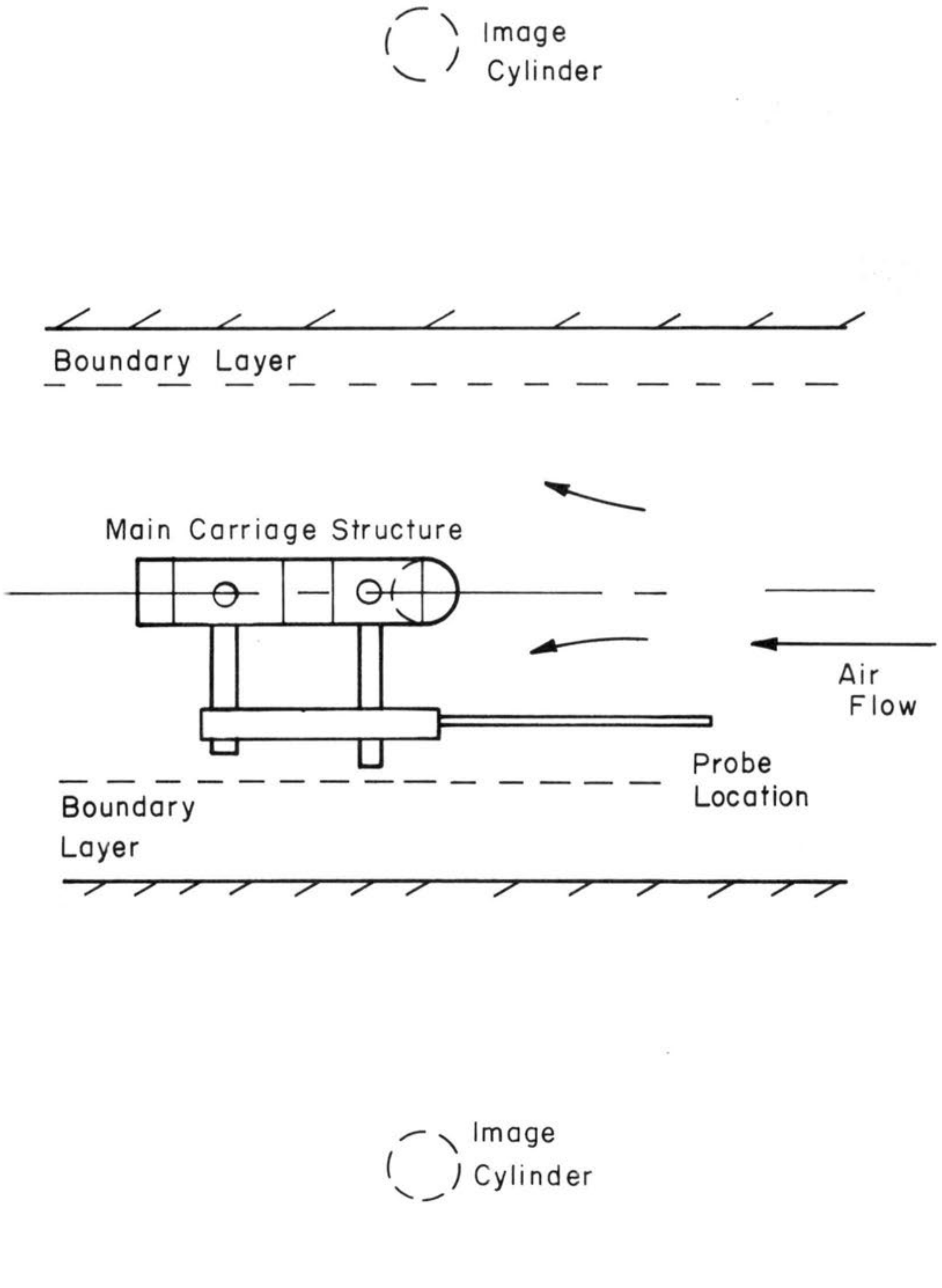

Fig. 22 Diagram of instrument carriage and image cylinders.

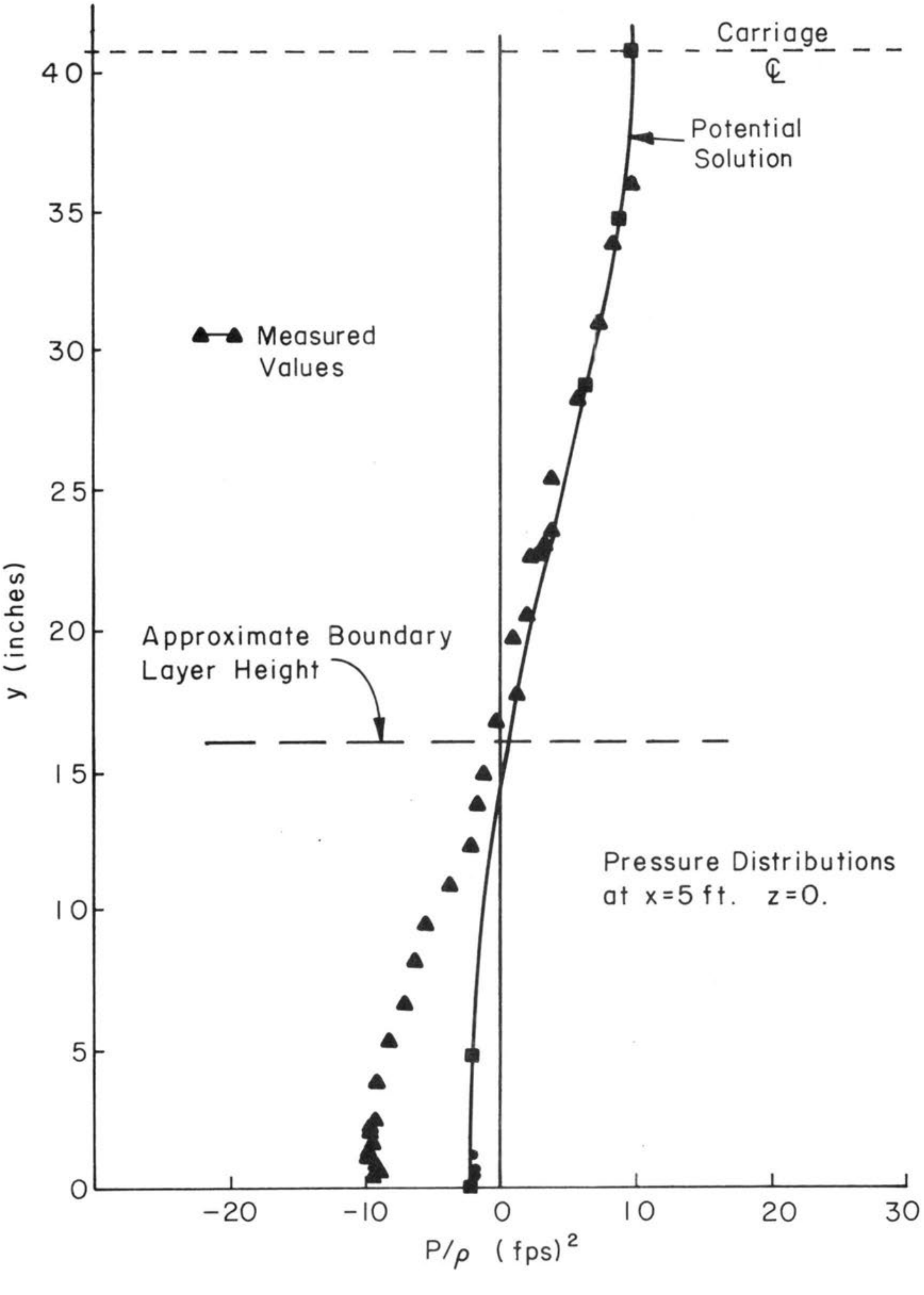

Fig. 23 Measured and calculated pressure distributions ahead of carriage.

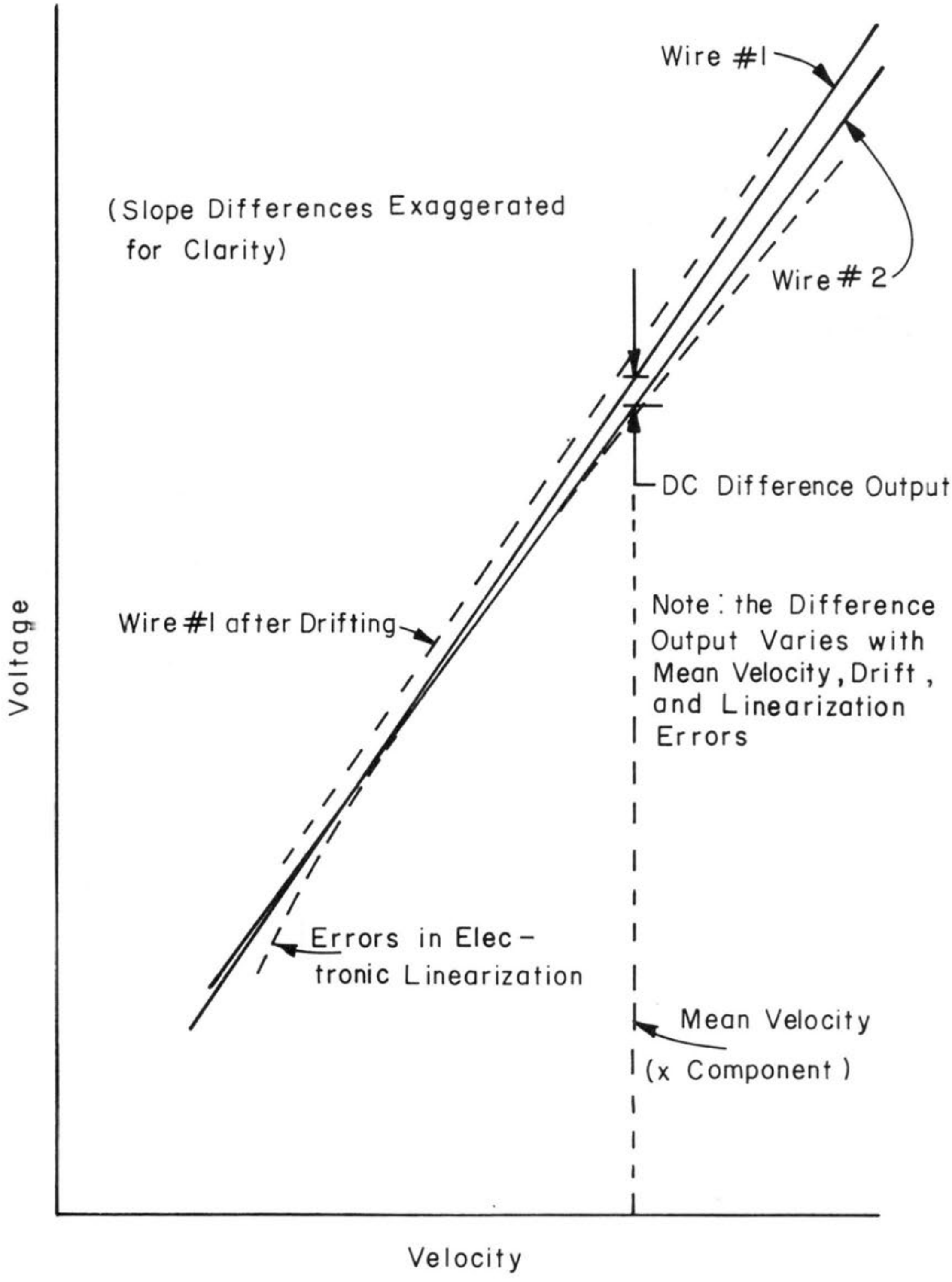

Fig. 24 Effects of small errors in hot-wire calibrations.

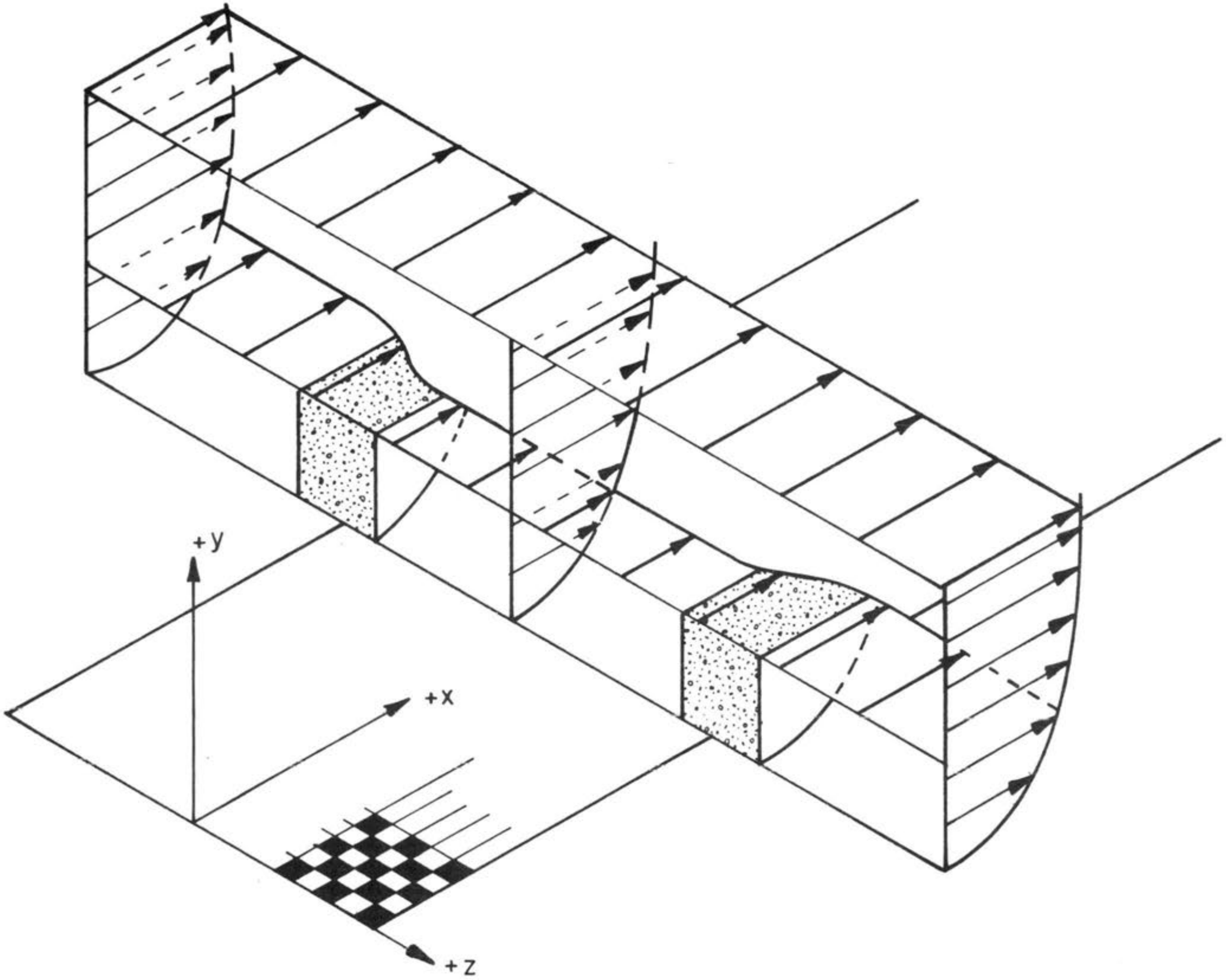

Fig. 25 Coordinate system and general view of flow pattern.

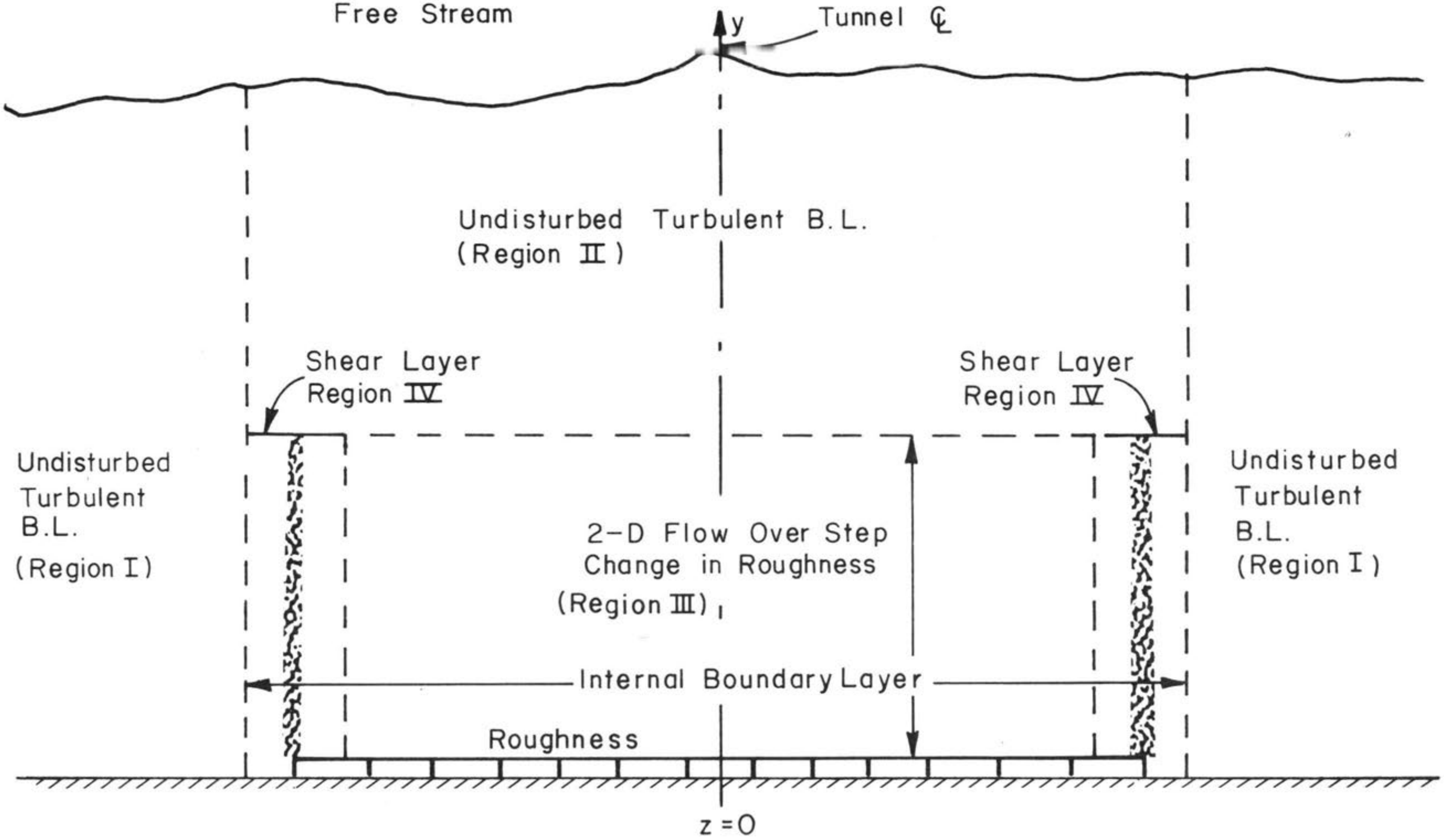

Fig. 26 Cross section of flow looking downstream.

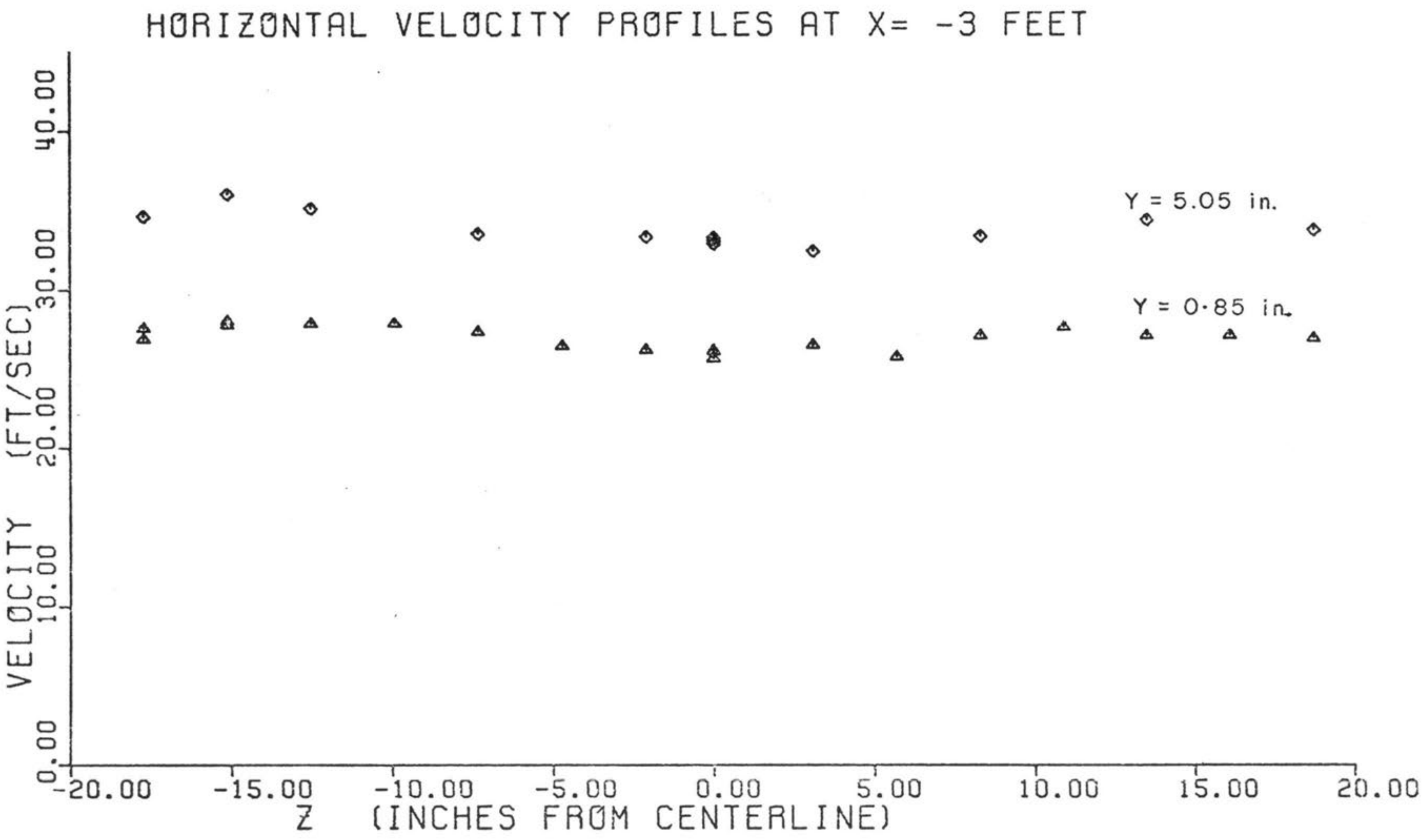

Fig. 27 Horizontal velocity profiles at x = -3 feet.

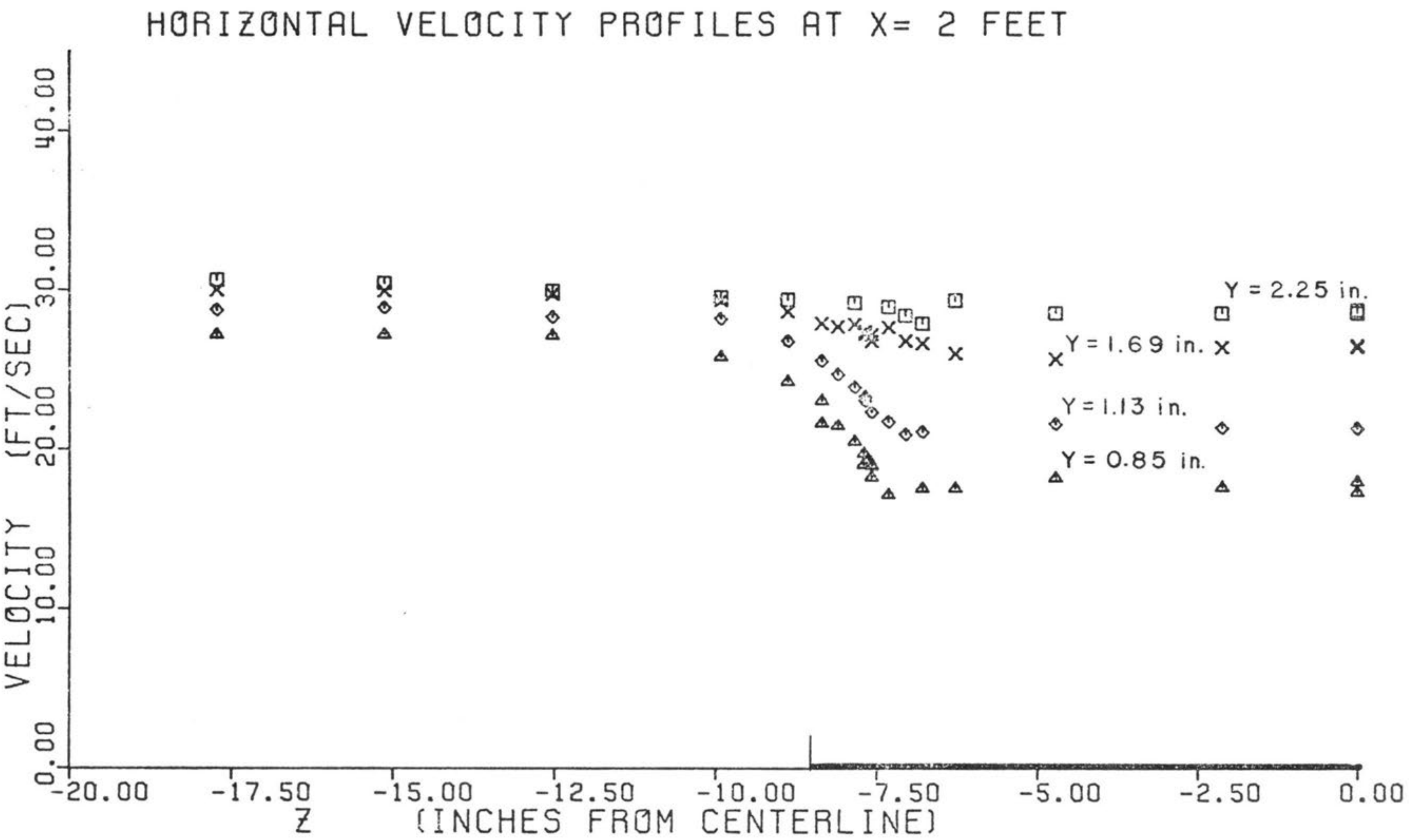

Fig. 28 Horizontal velocity profiles at x = 2 feet.

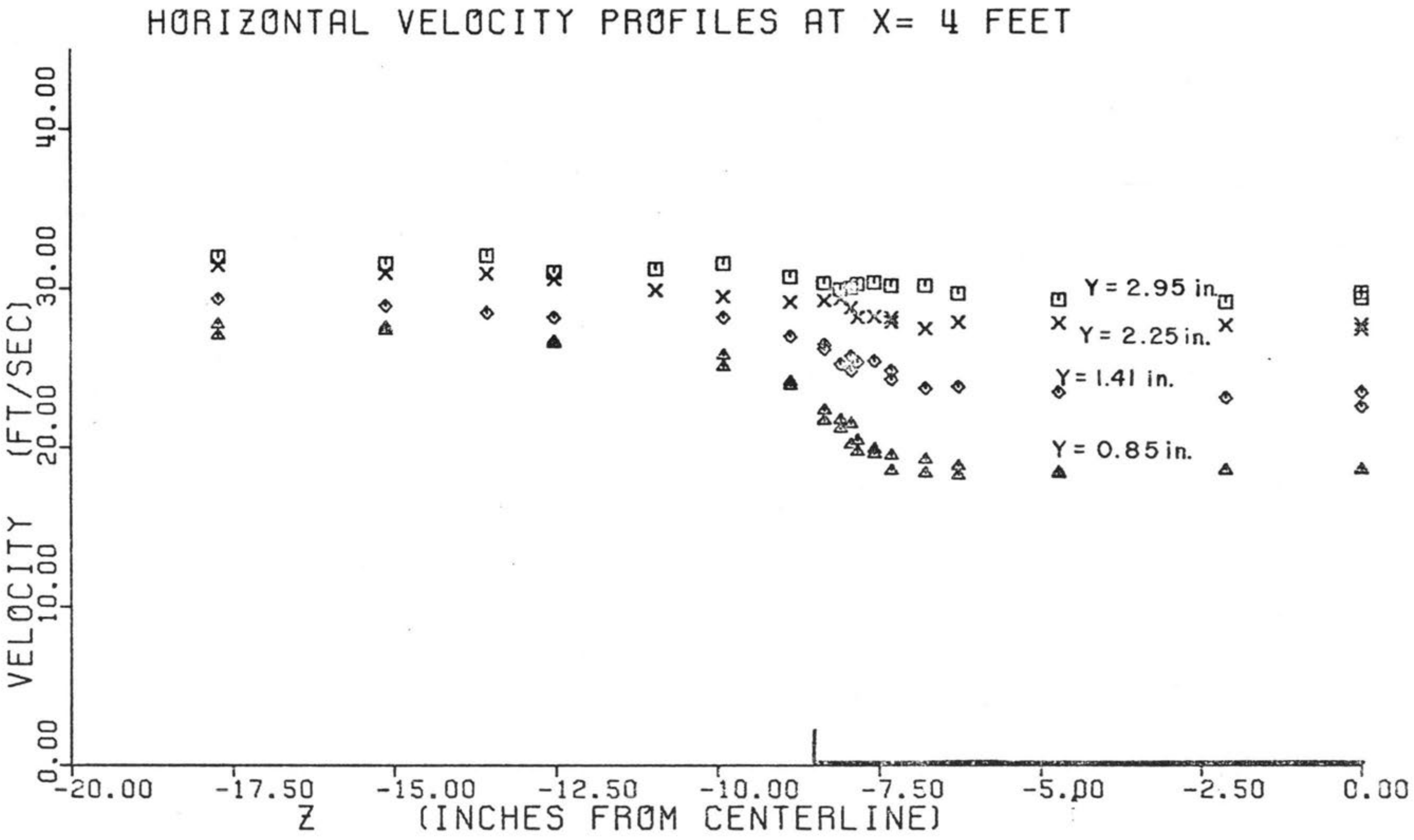

Fig. 29 Horizontal velocity profiles at x = 4 feet.

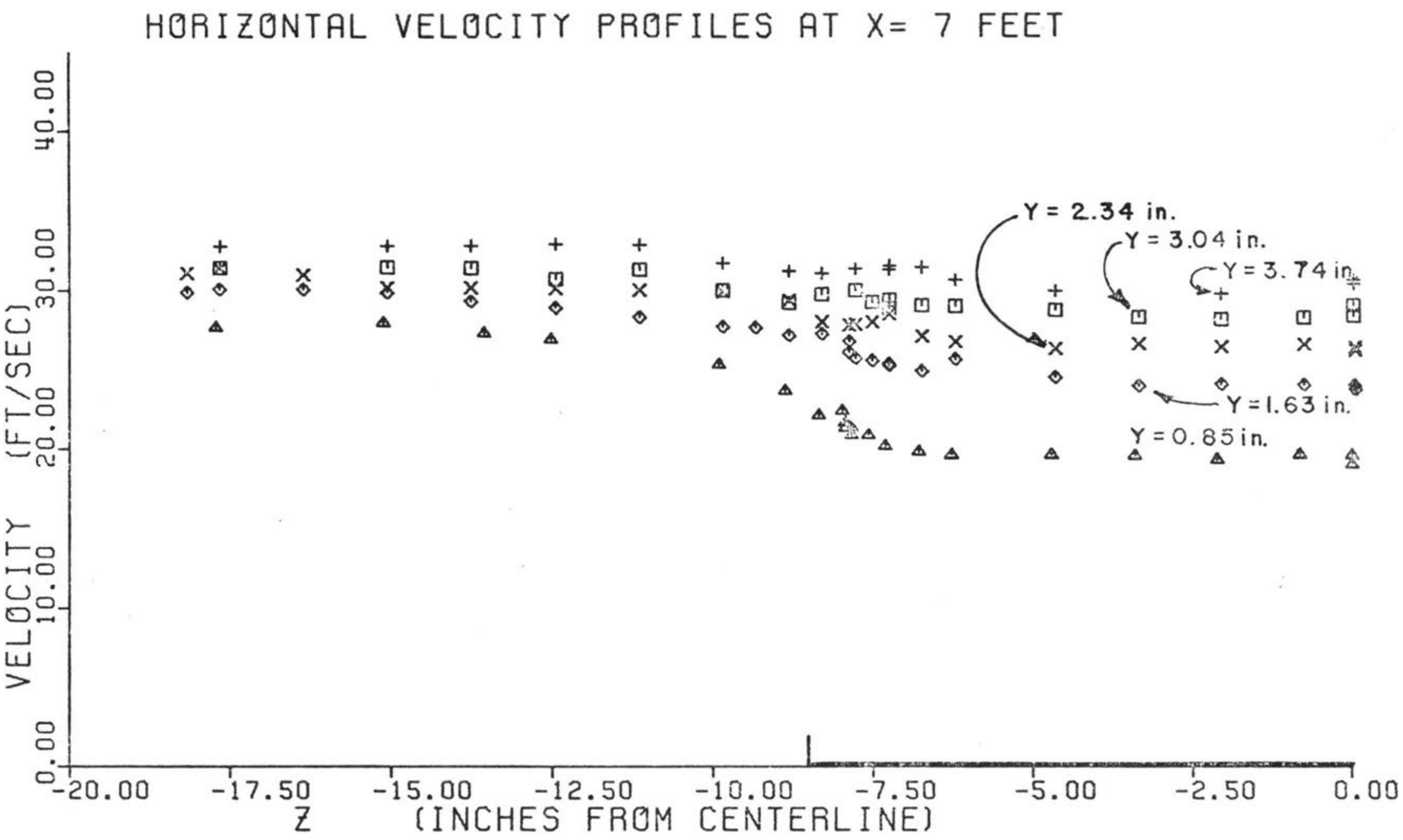

Fig. 30 Horizontal velocity profiles at x = 7 feet.

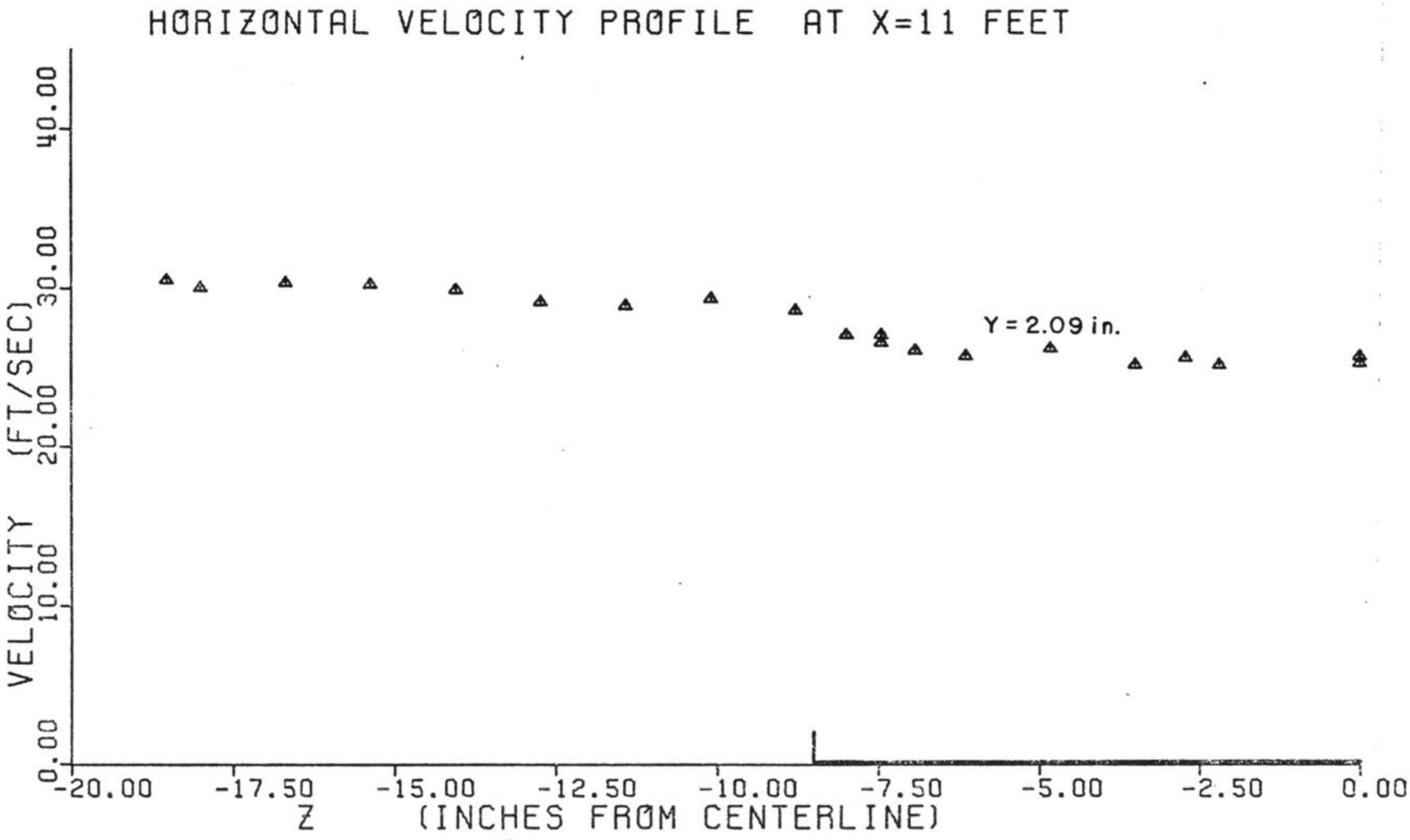

Fig. 31 Horizontal velocity profiles at x = 11 feet.

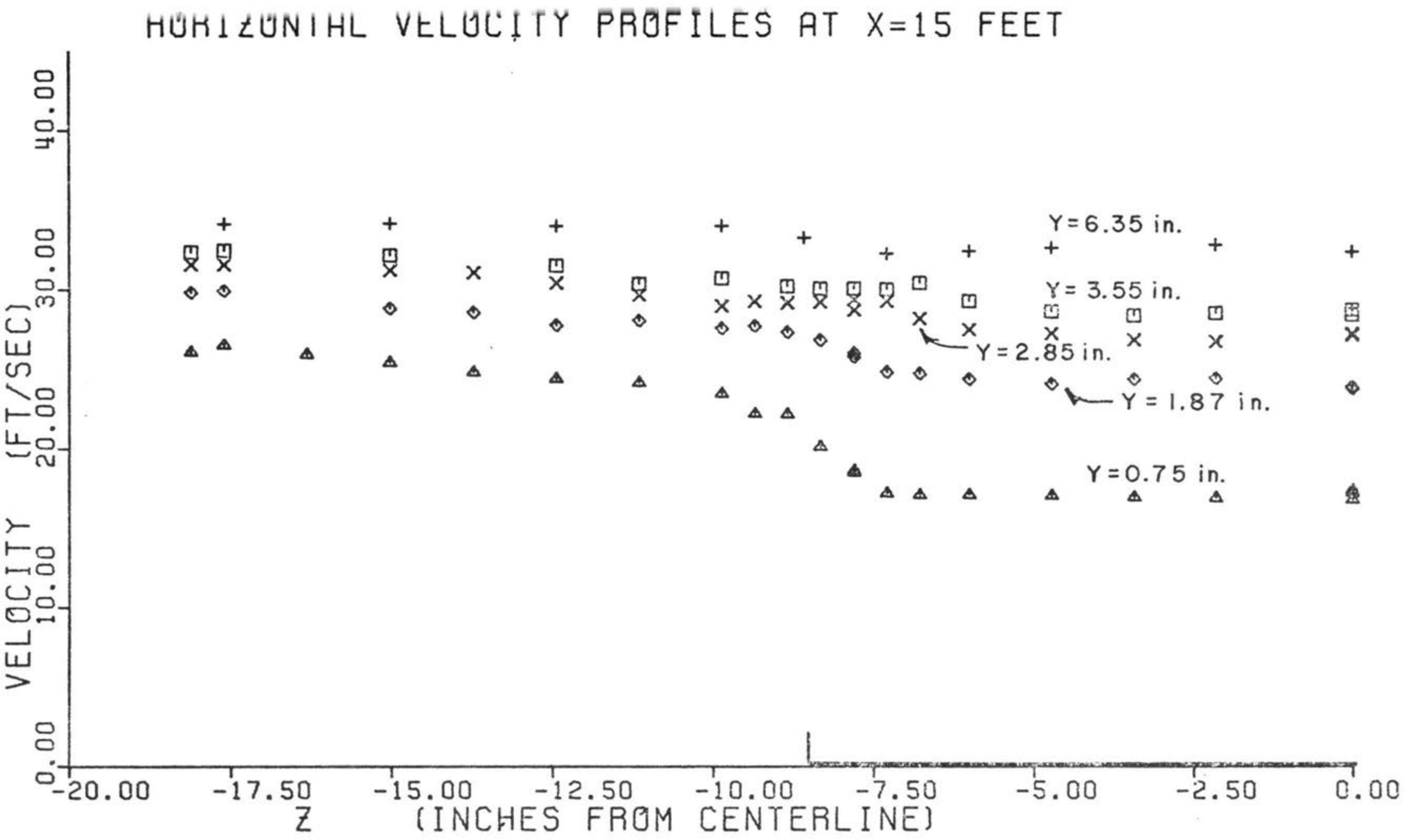

Fig. 32 Horizontal velocity profiles at x = 15 feet.

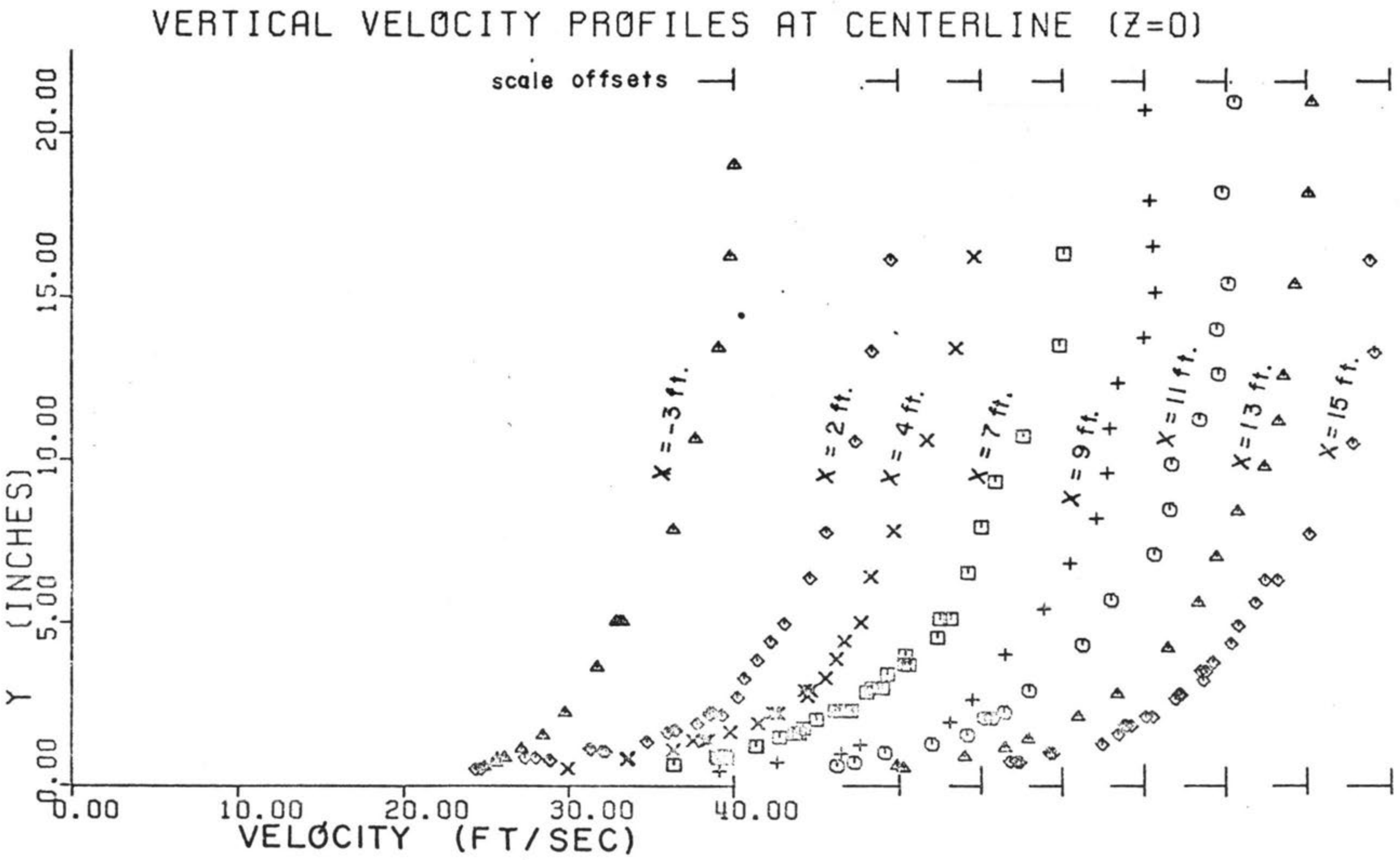

Fig. 33 Vertical velocity profiles at centerline (z = 0).

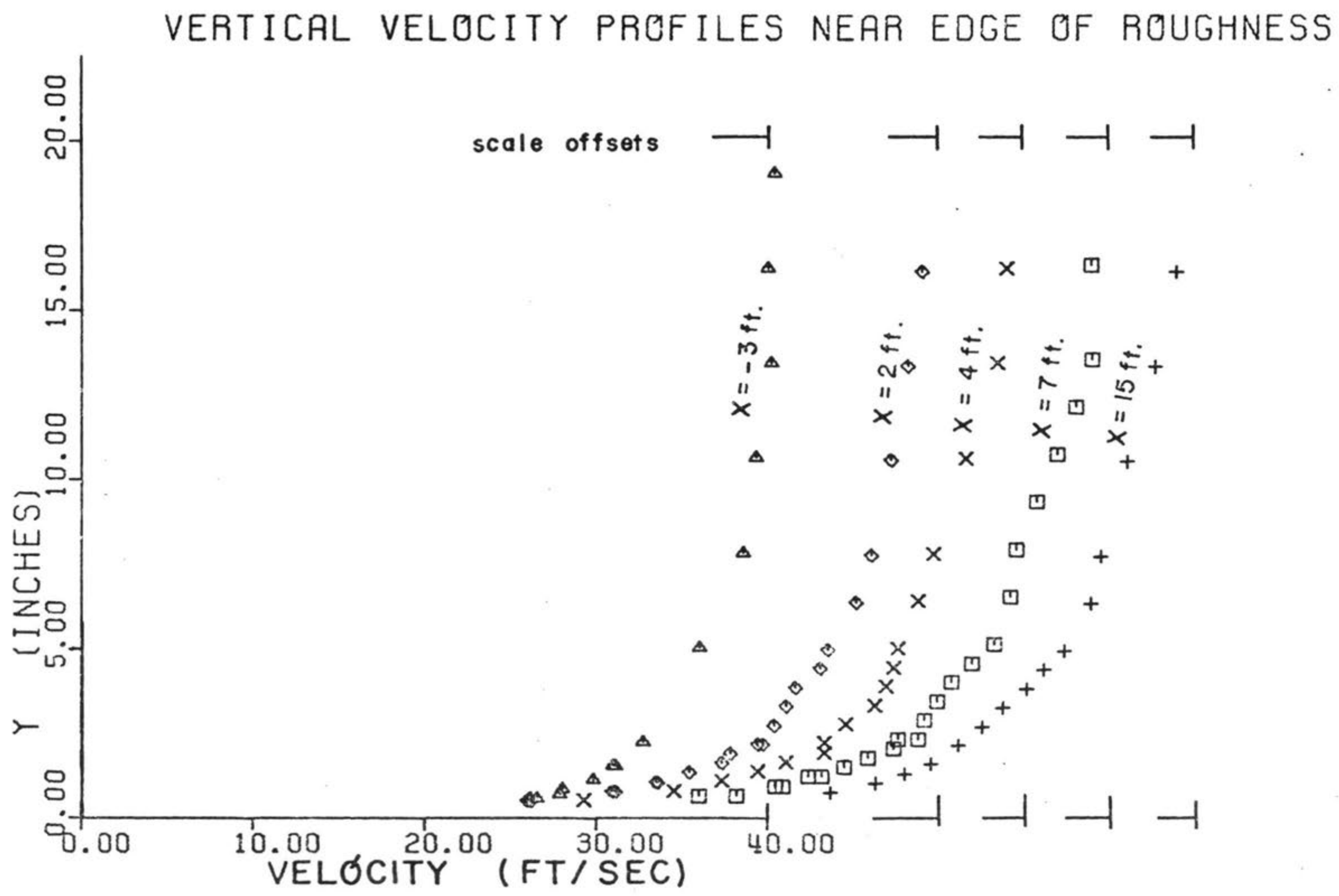

Fig. 34 Vertical velocity profiles near edge of roughness.

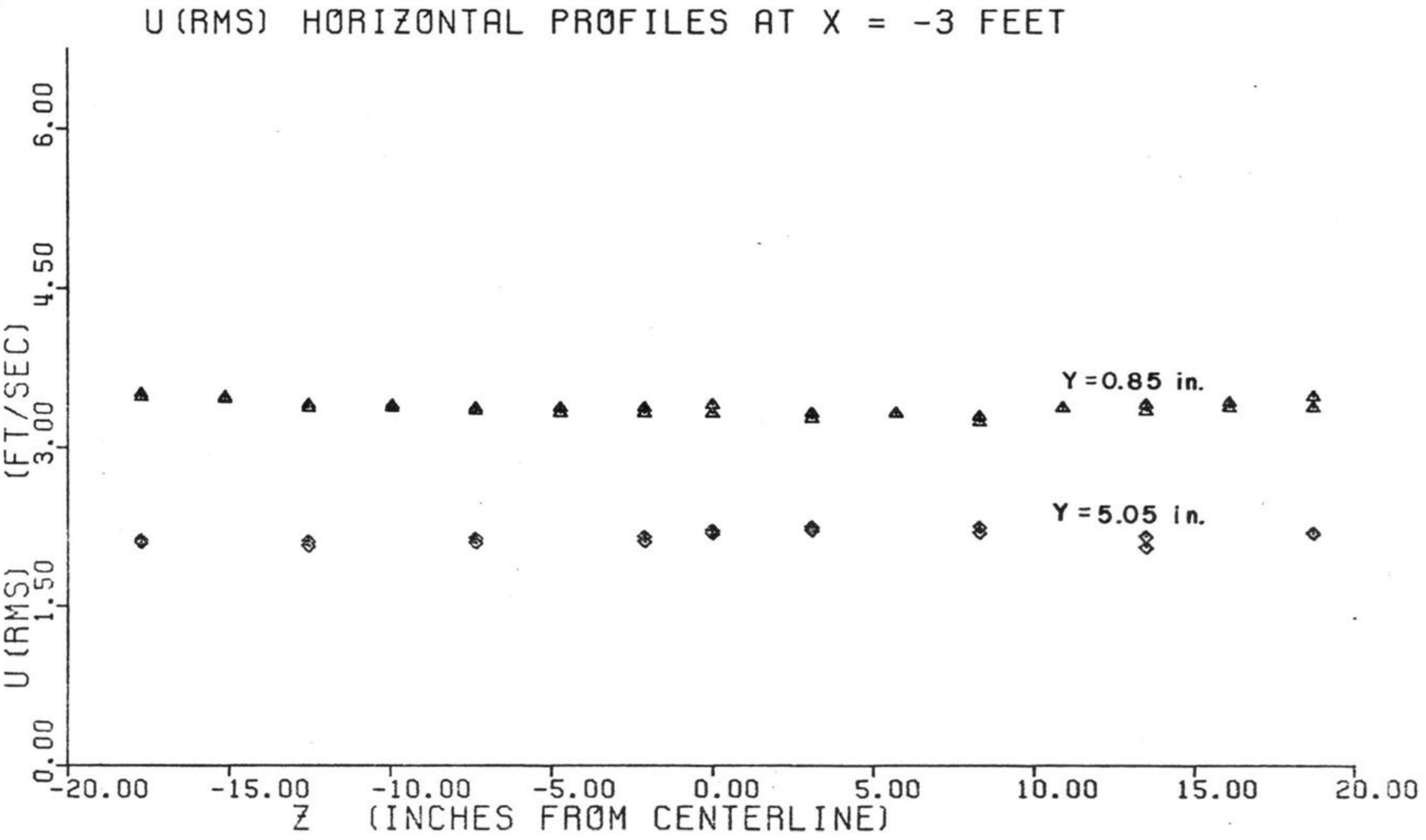

Fig. 35 $\overline{u^2}$ horizontal profiles at x = -3 feet.

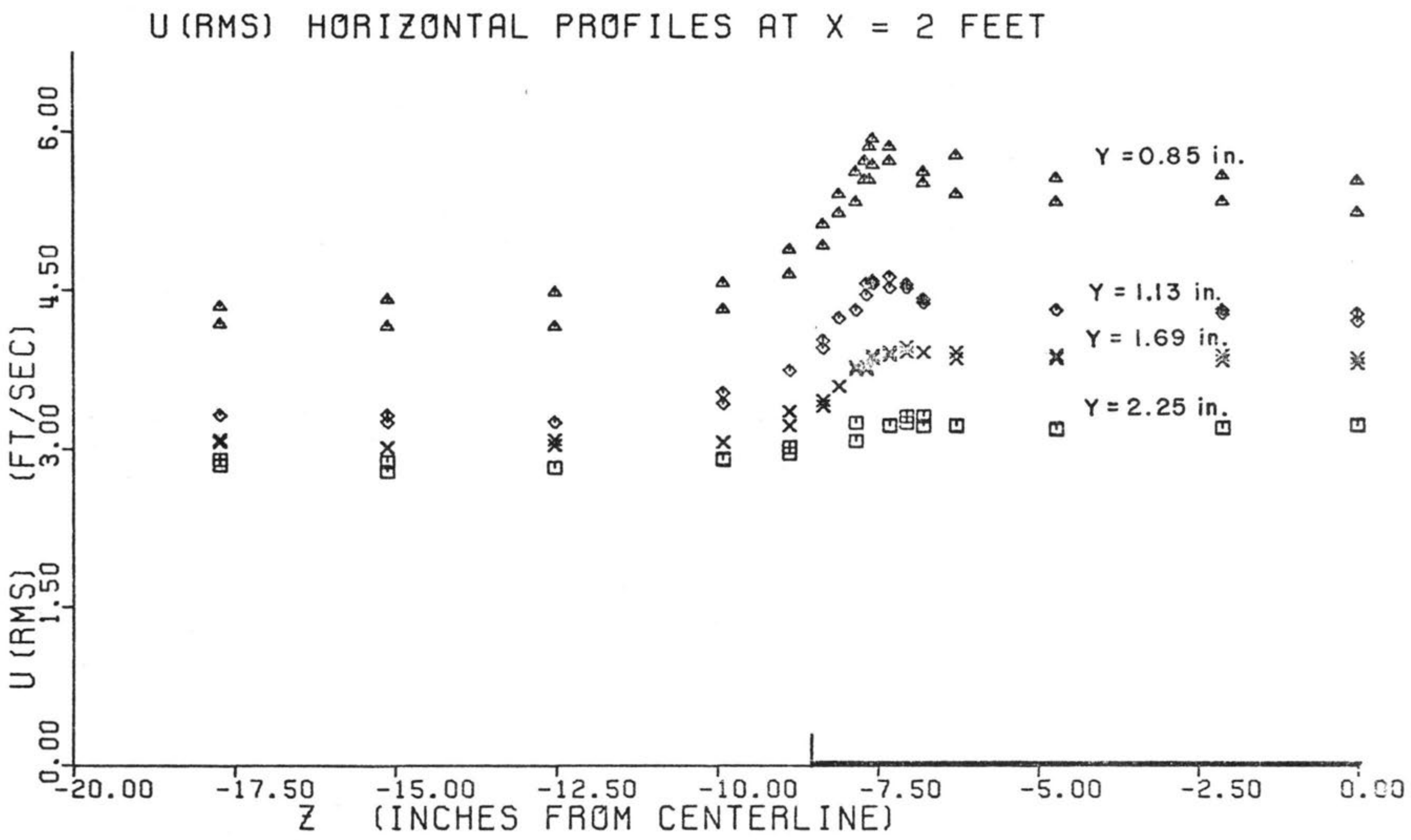

Fig. 36 $\overline{u^2}$ horizontal profiles at x = 2 feet.

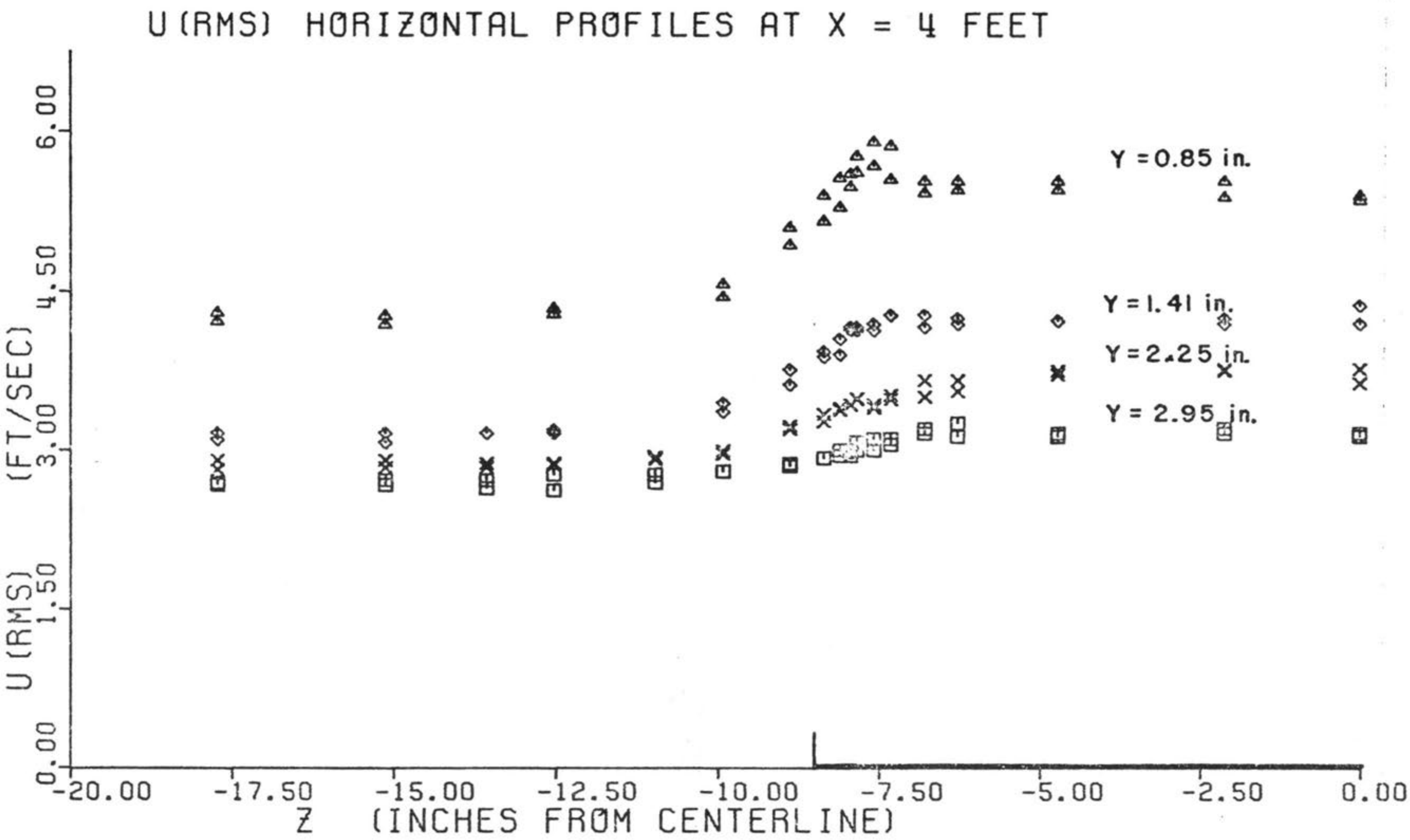

Fig. 37 $\overline{u^2}$ horizontal profiles at x = 4 feet.

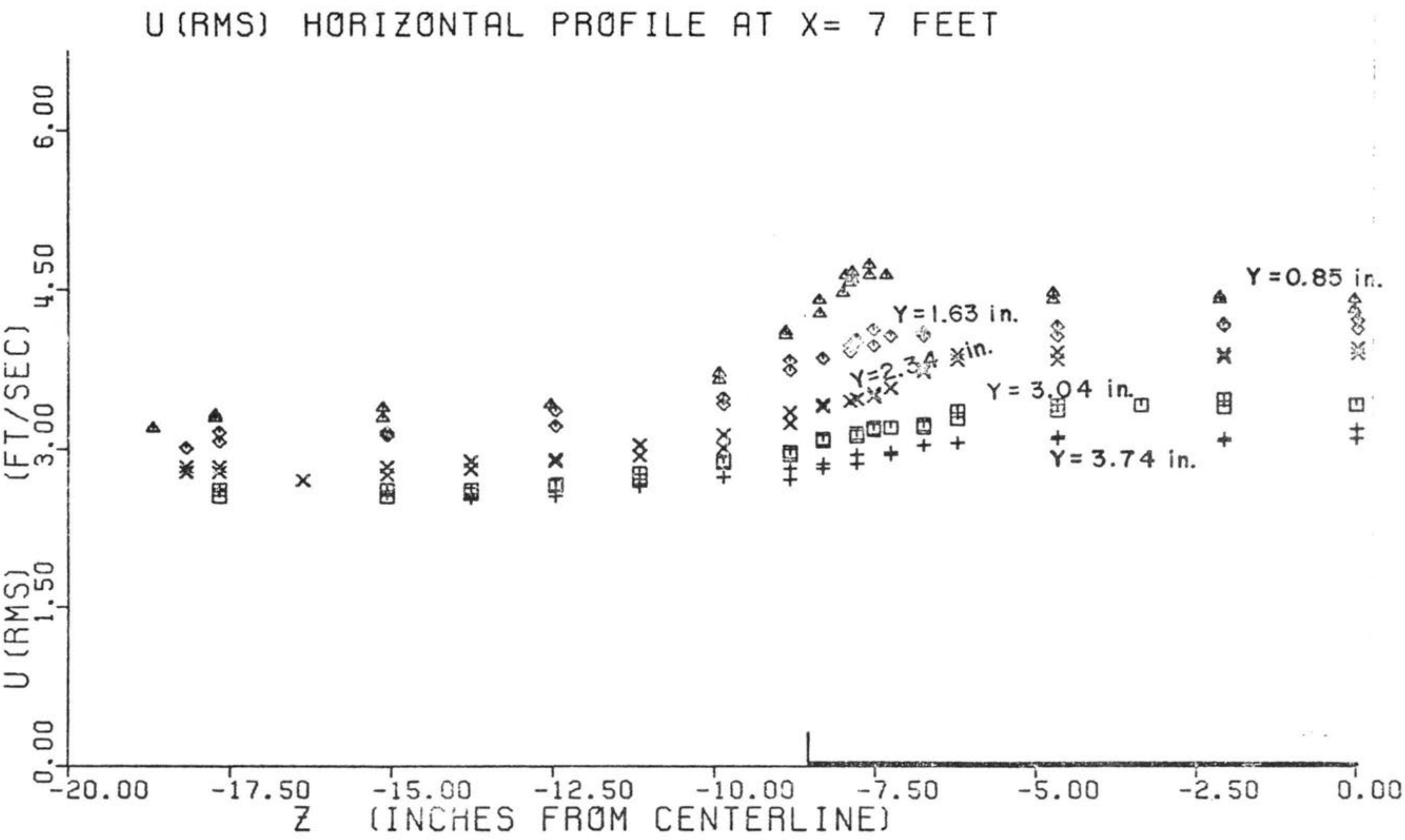

Fig. 38 $\overline{u^2}$ horizontal profiles at x = 7 feet.

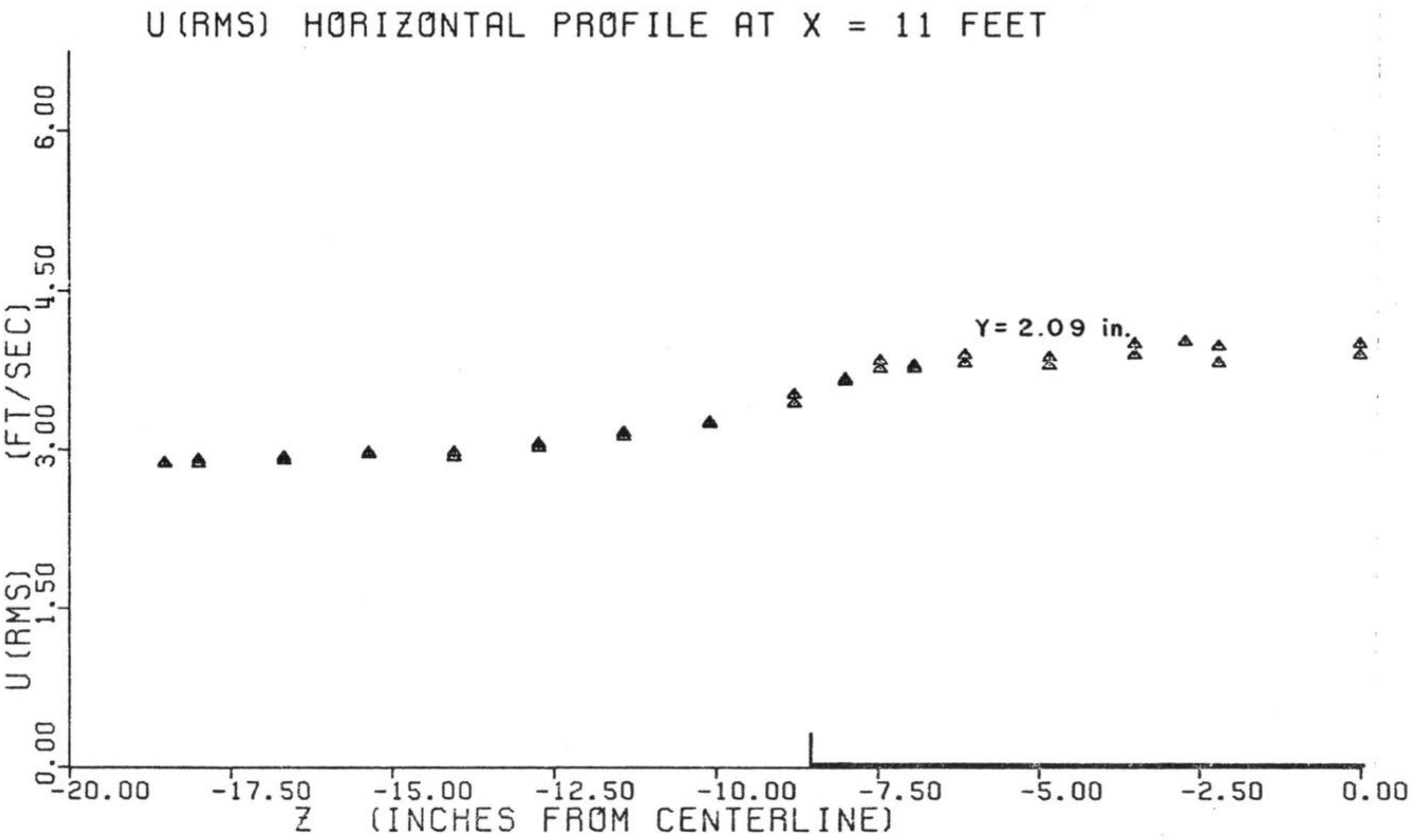

Fig. 39 $\overline{u^2}$ horizontal profiles at x = 11 feet.

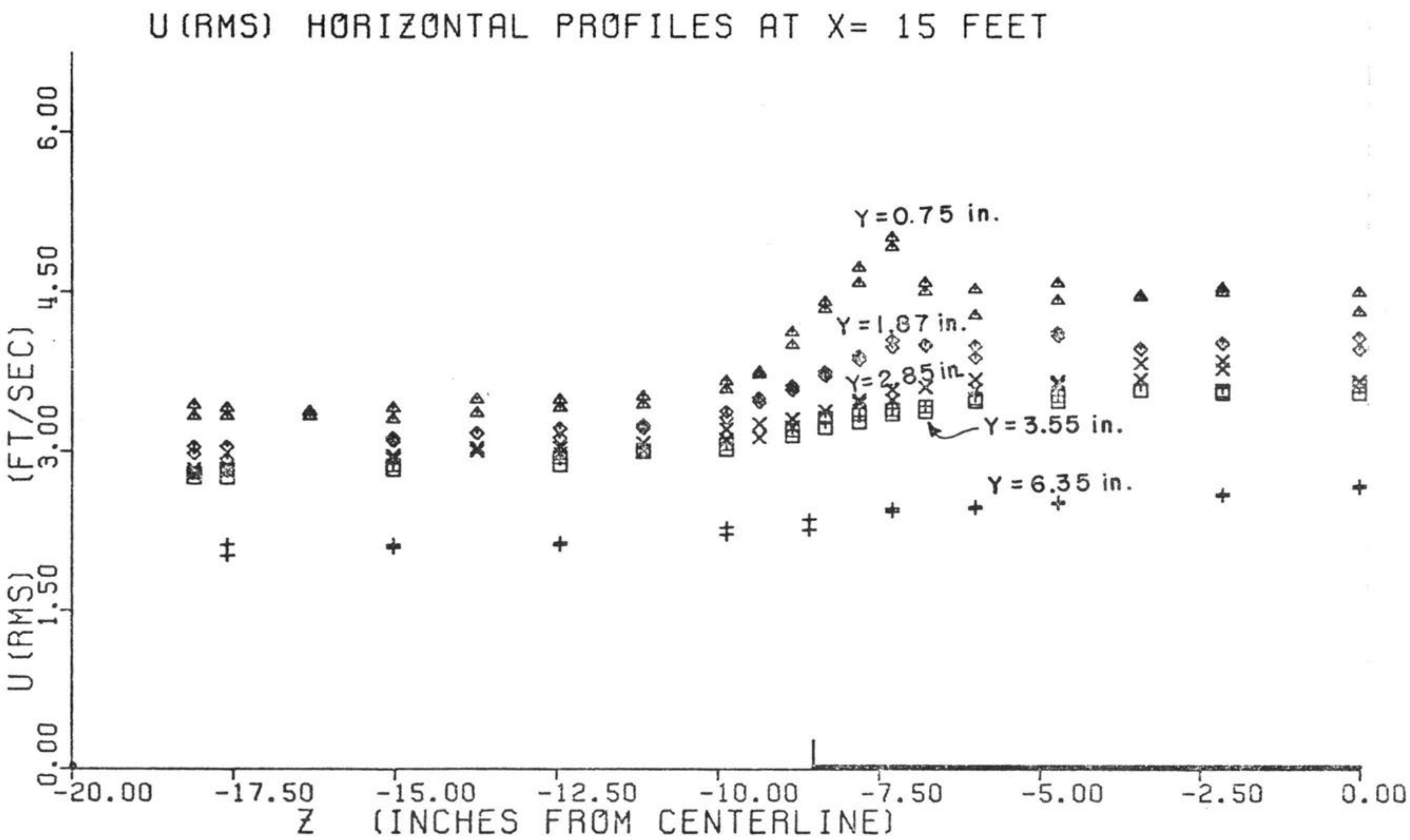

Fig. 40 $\overline{u^2}$ horizontal profiles at x = 15 feet.

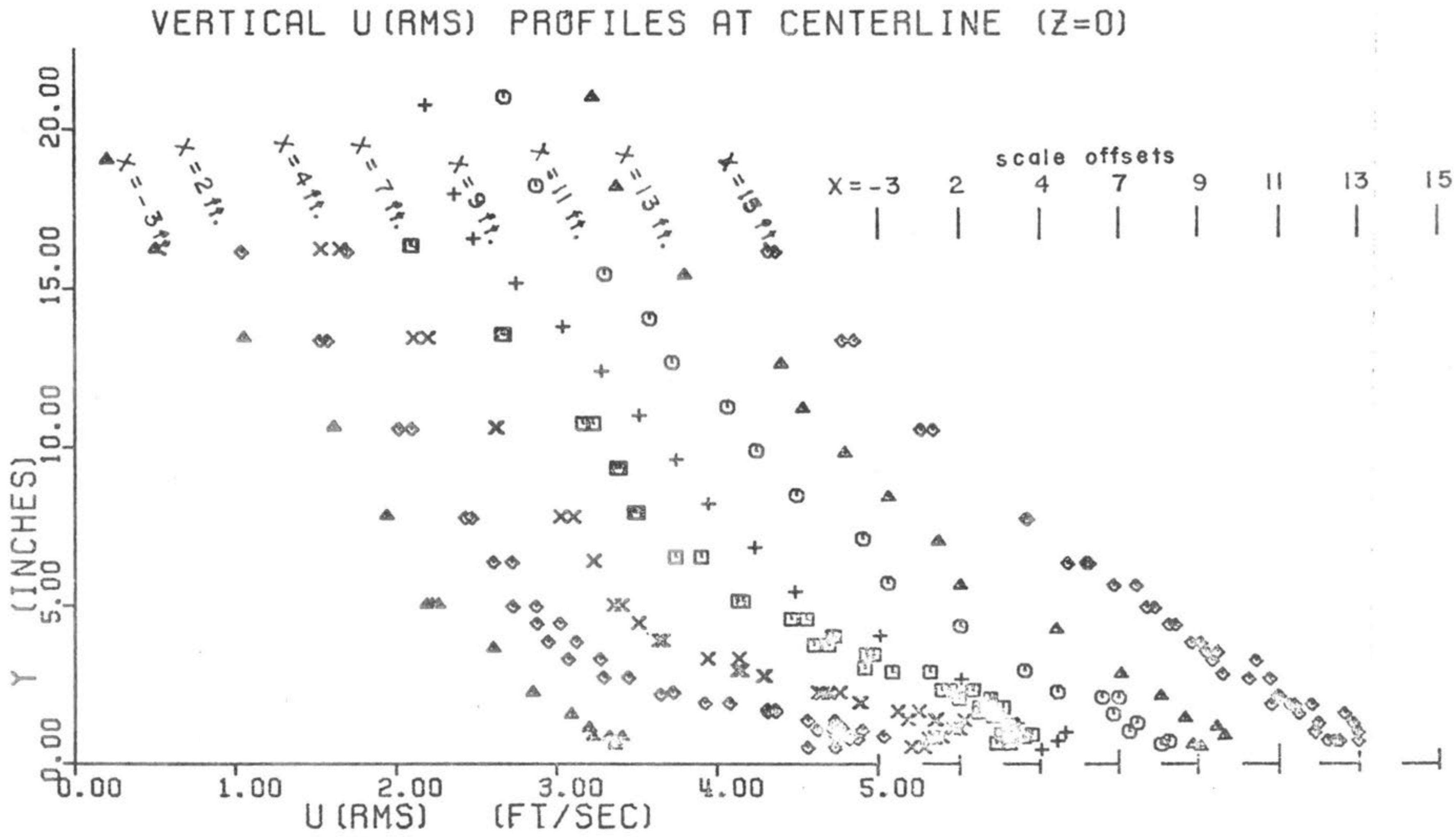

Fig. 41 $\overline{u^2}$ vertical profiles at centerline (z = 0).

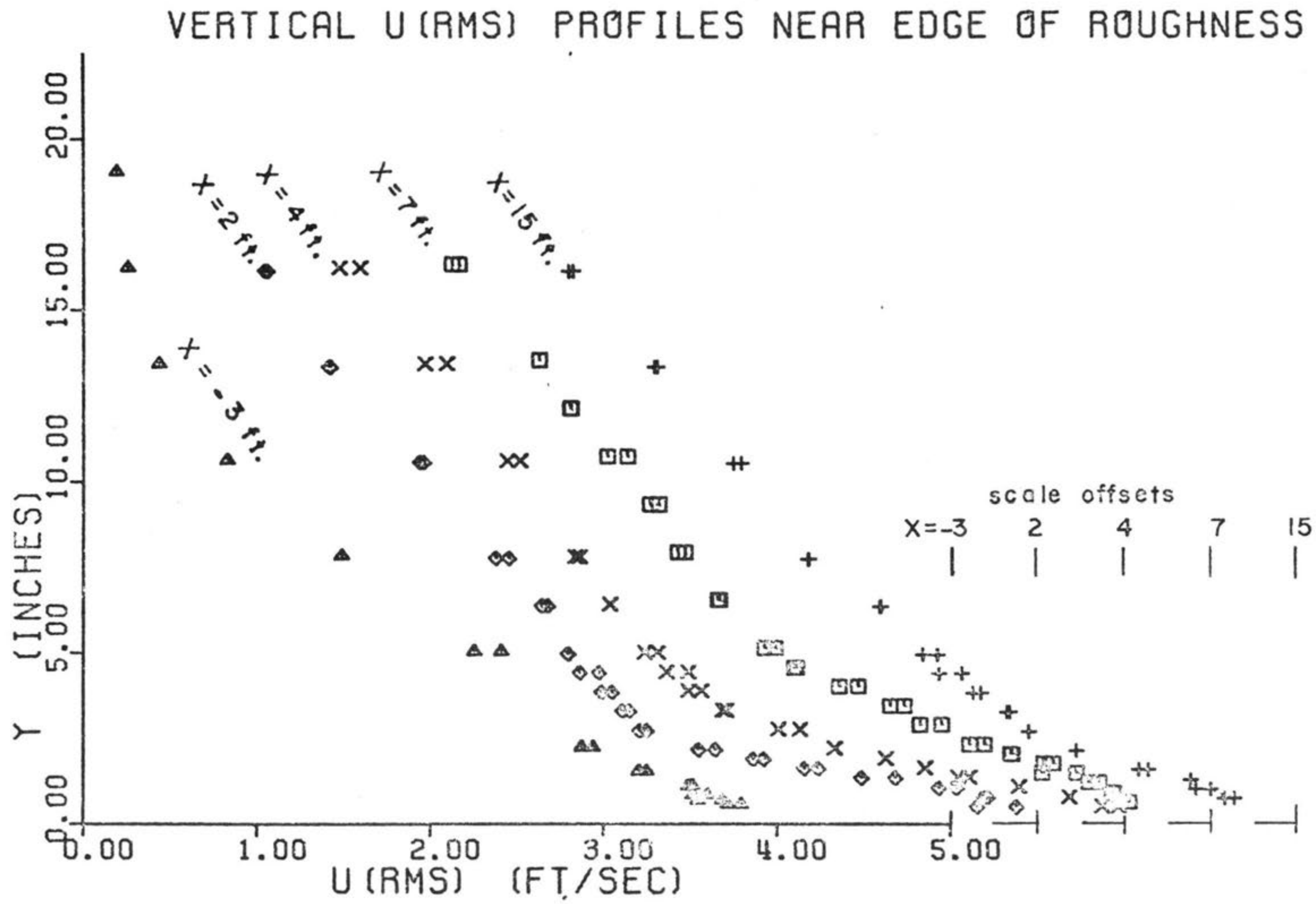

Fig. 42 $\overline{u^2}$ vertical profiles near edge of roughness.

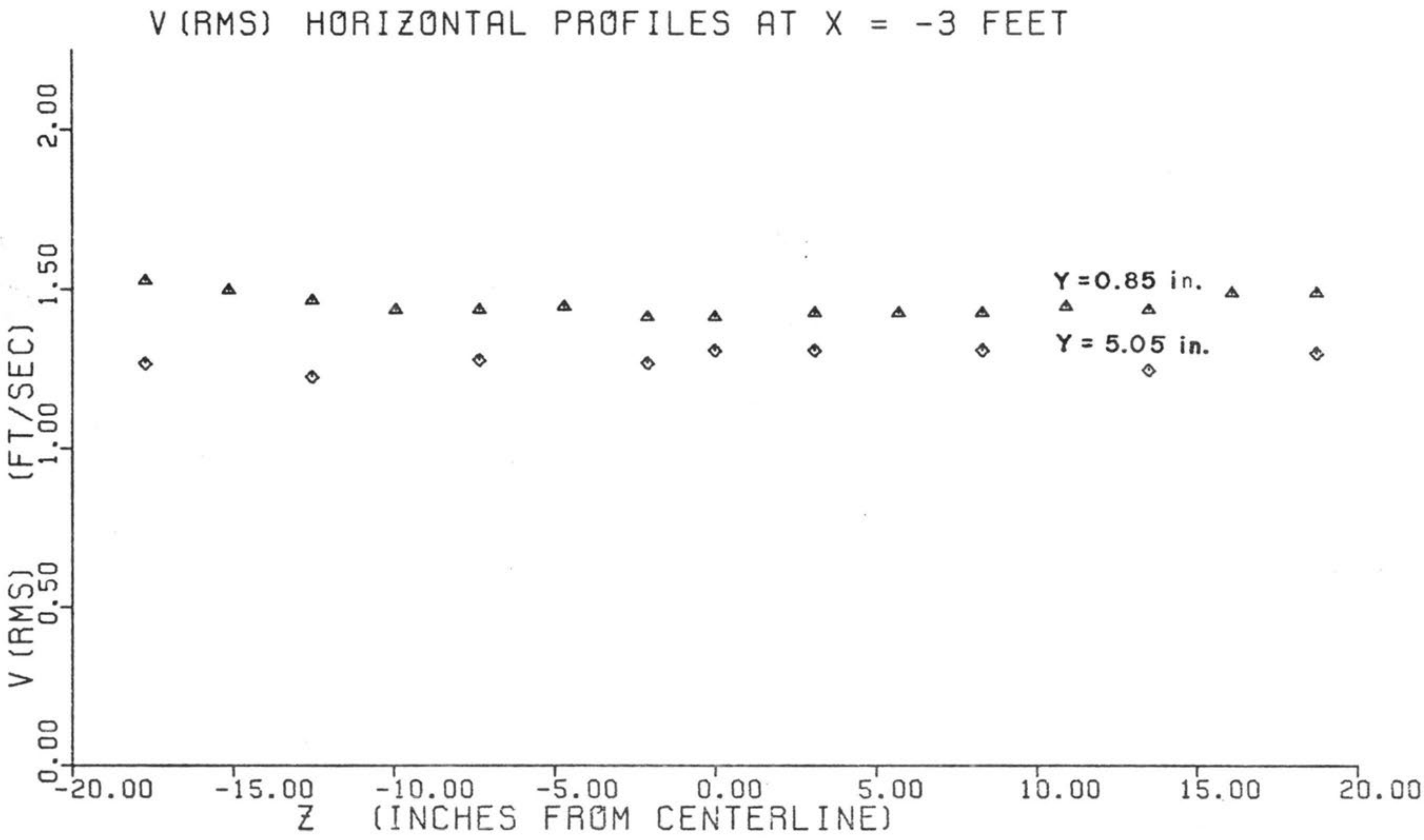

Fig. 43 $\overline{v^2}$ horizontal profiles at x = -3 feet.

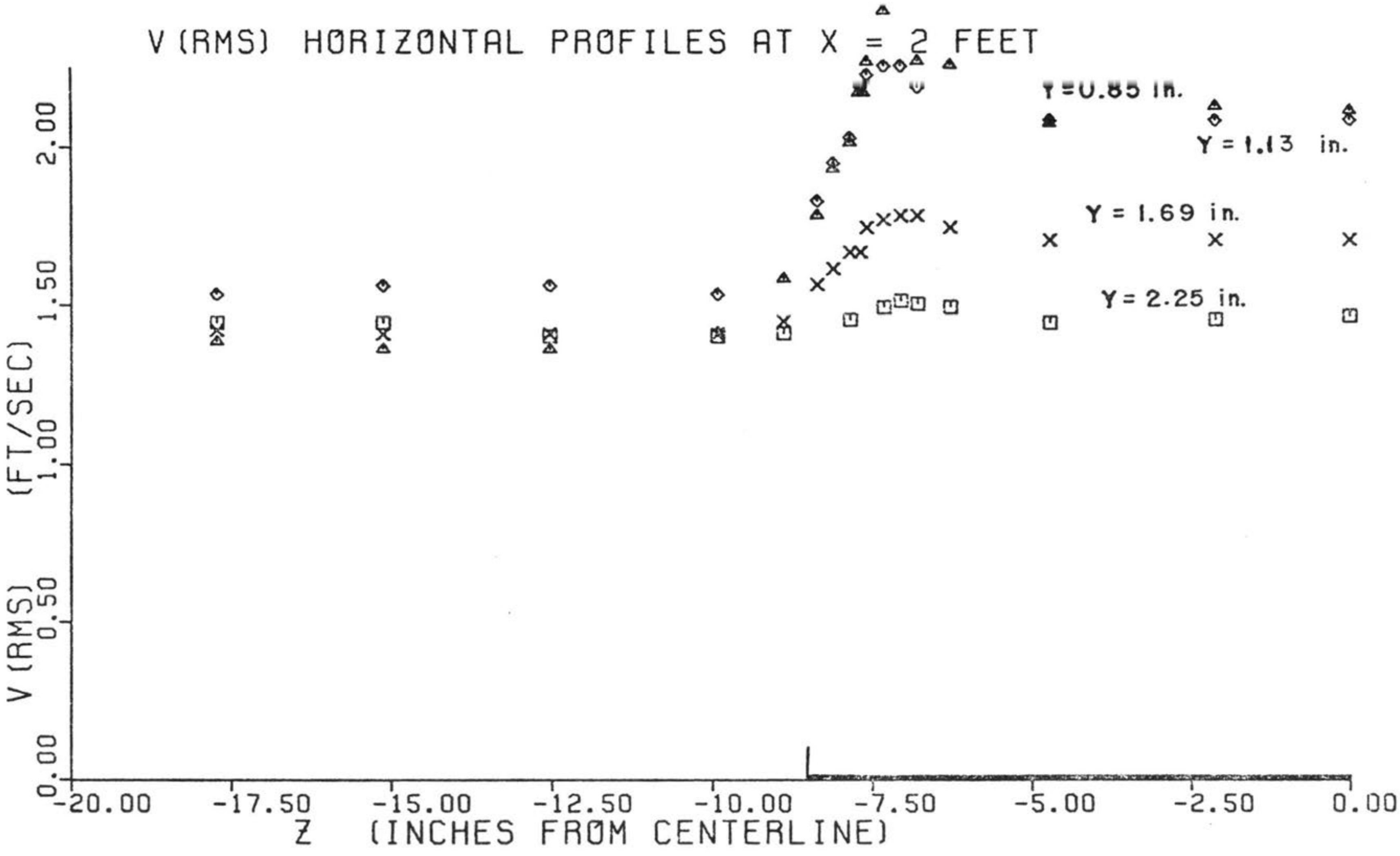

Fig. 44 $\overline{v^2}$ horizontal profiles at x = 2 feet.

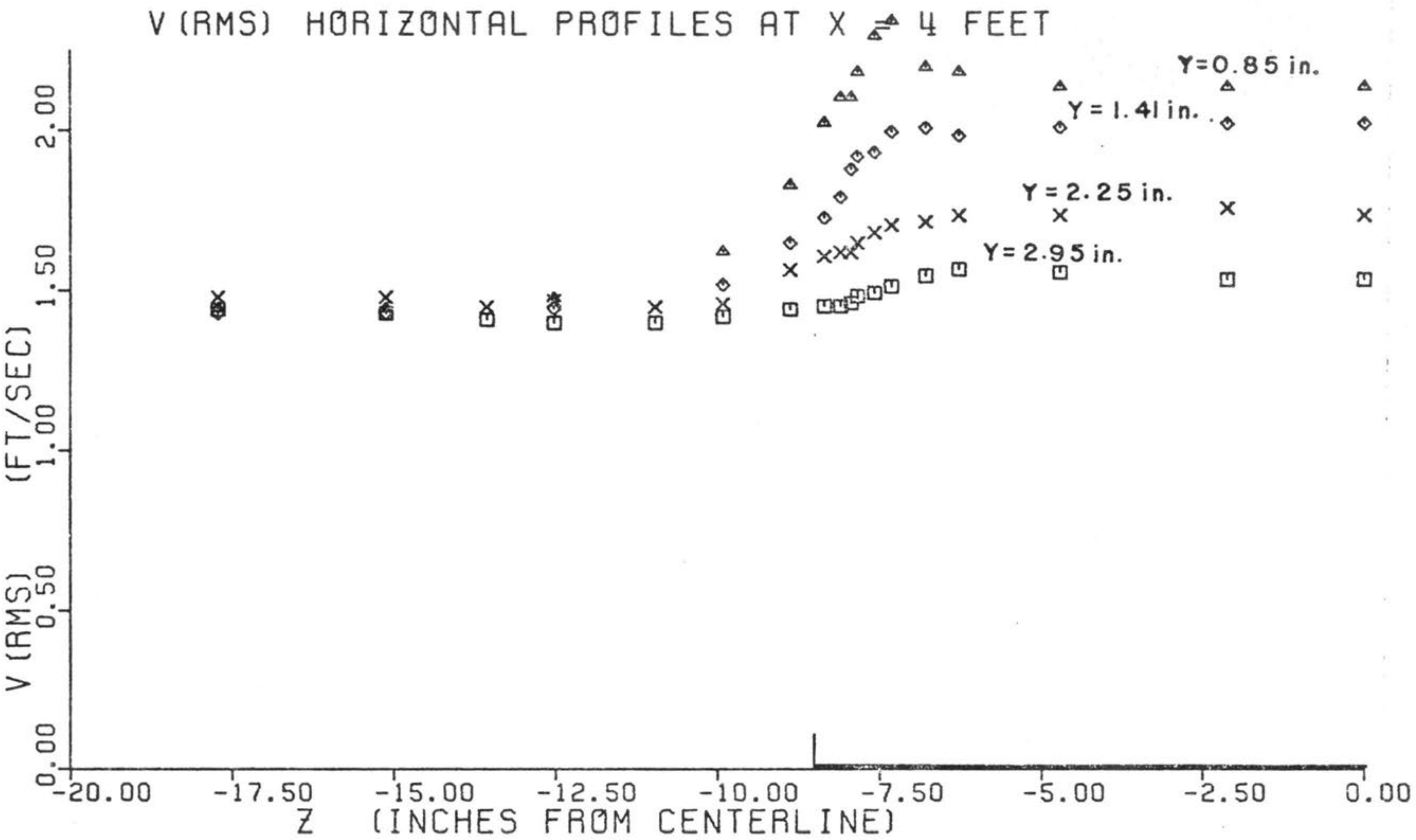

Fig. 45 $\overline{v^2}$ horizontal profiles at x = 4 feet.

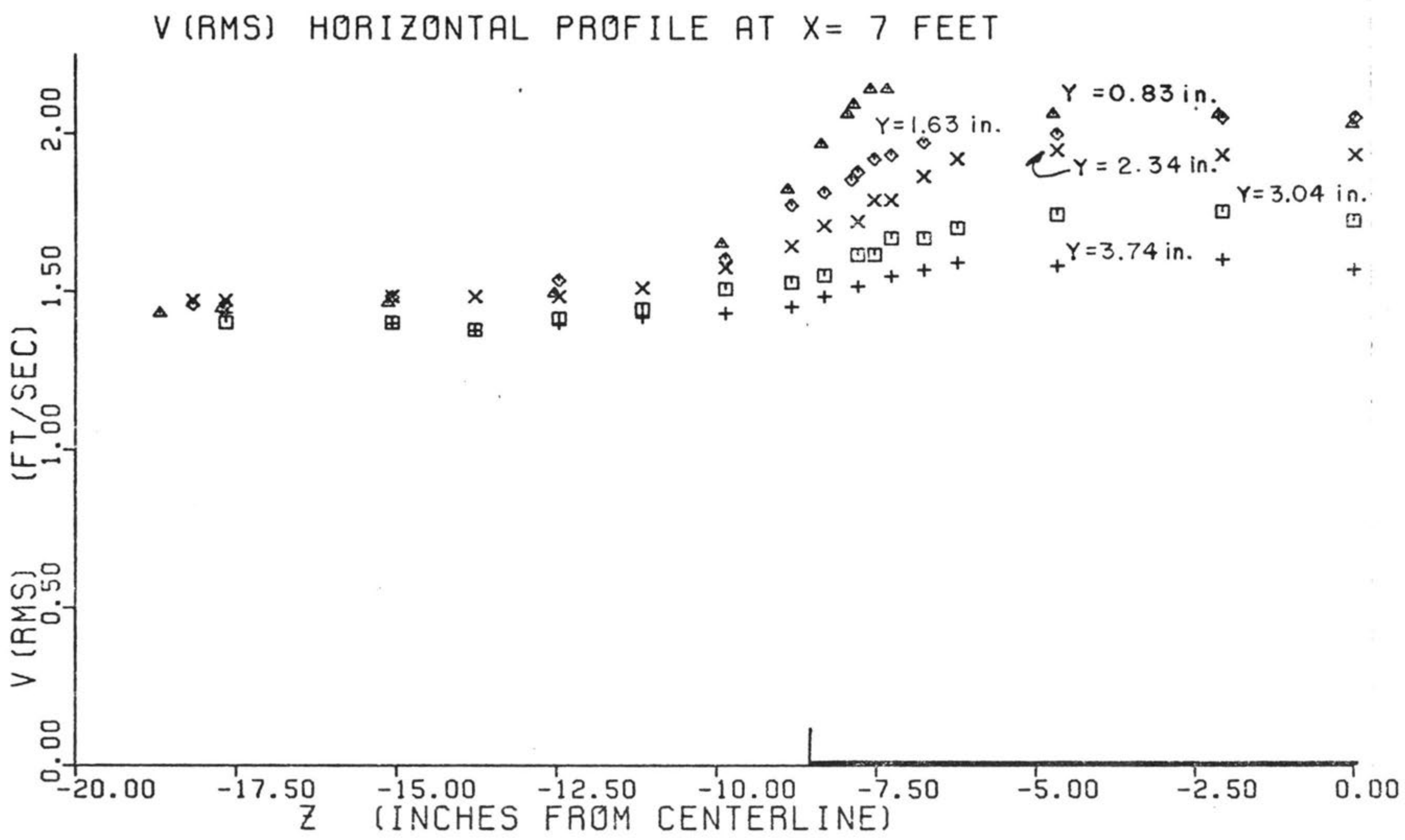

Fig. 46 $\overline{v^2}$ horizontal profiles at x = 7 feet.

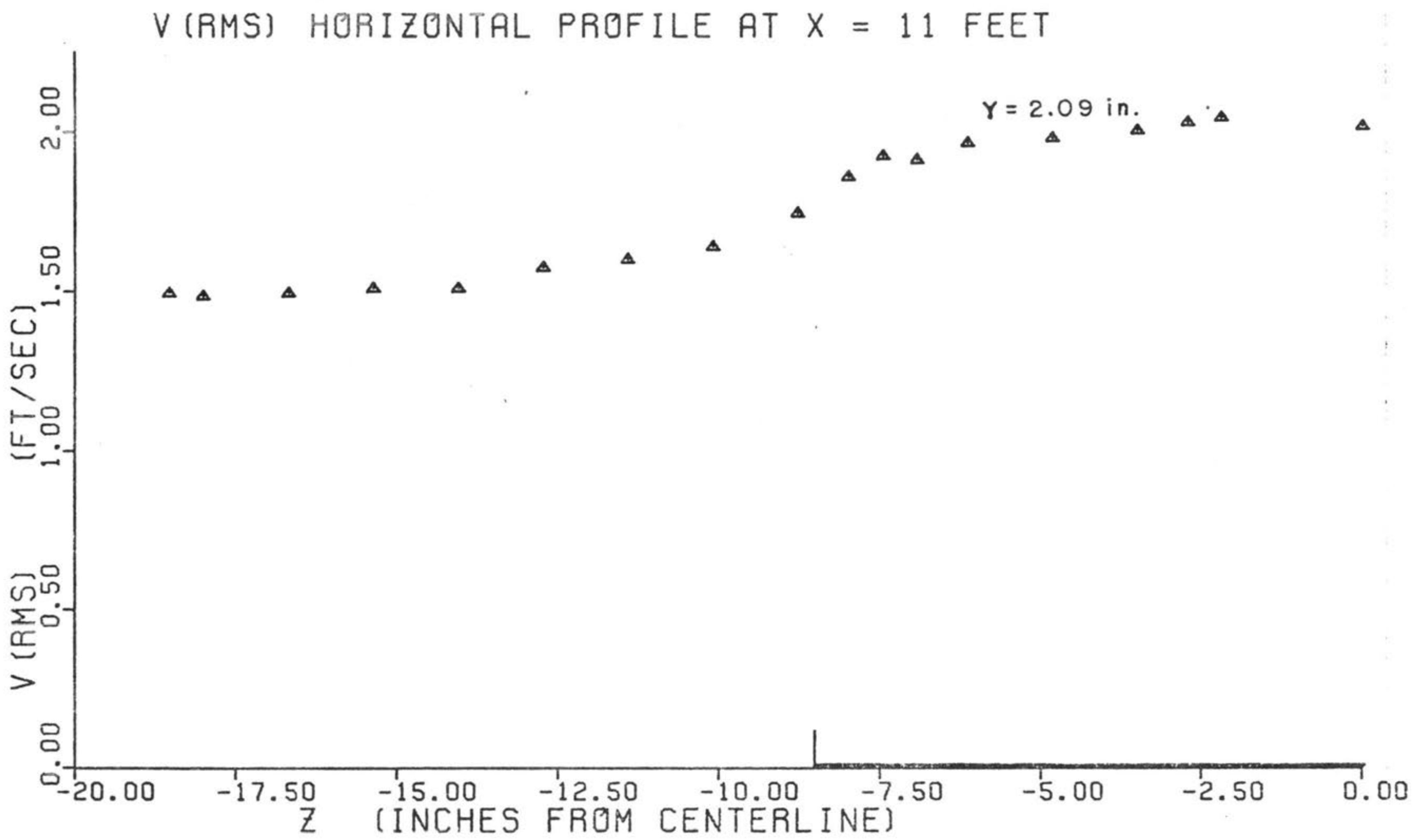

Fig. 47 $\overline{v^2}$ horizontal profiles at x = 11 feet.

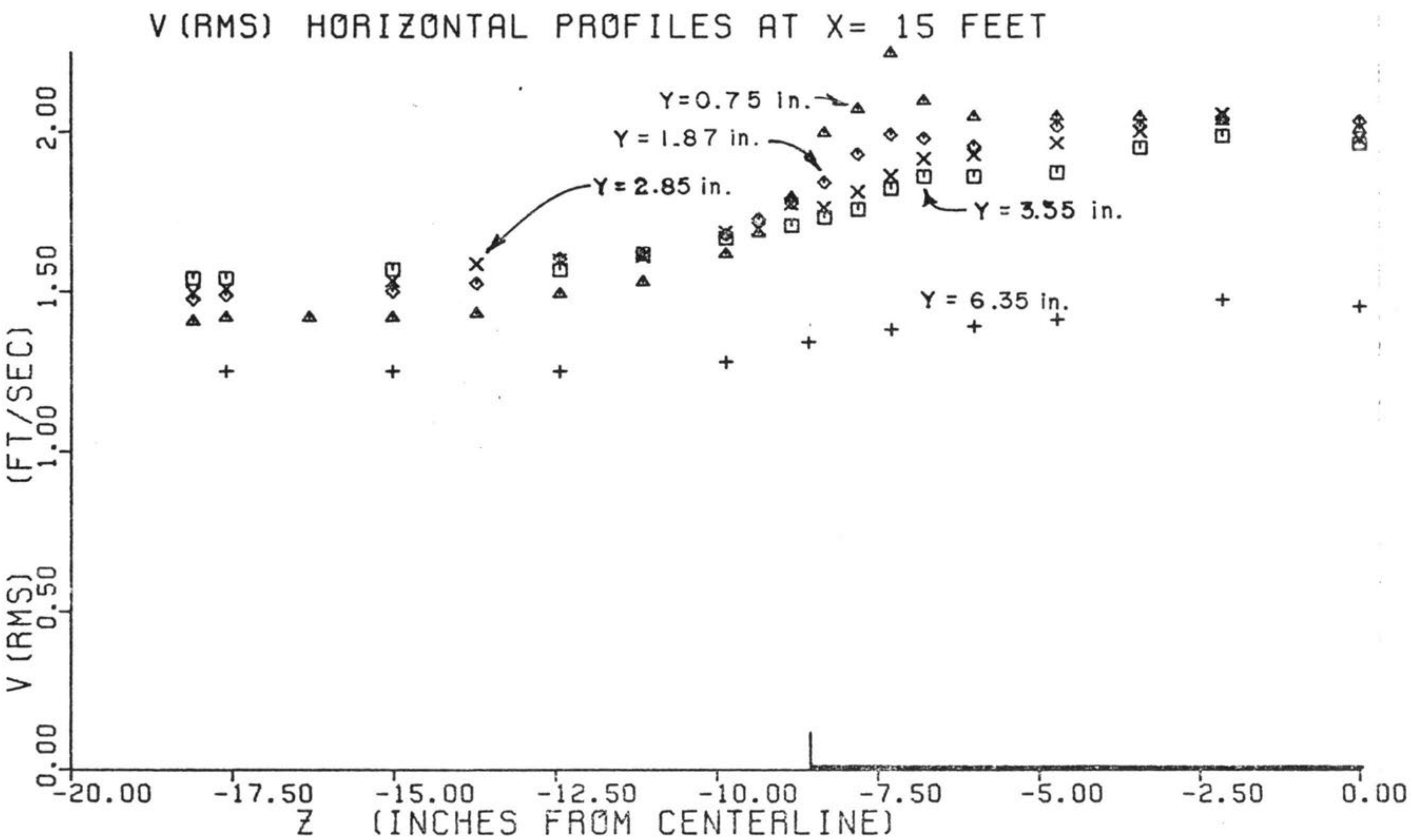

Fig. 48 $\overline{v^2}$ horizontal profiles at x = 15 feet.

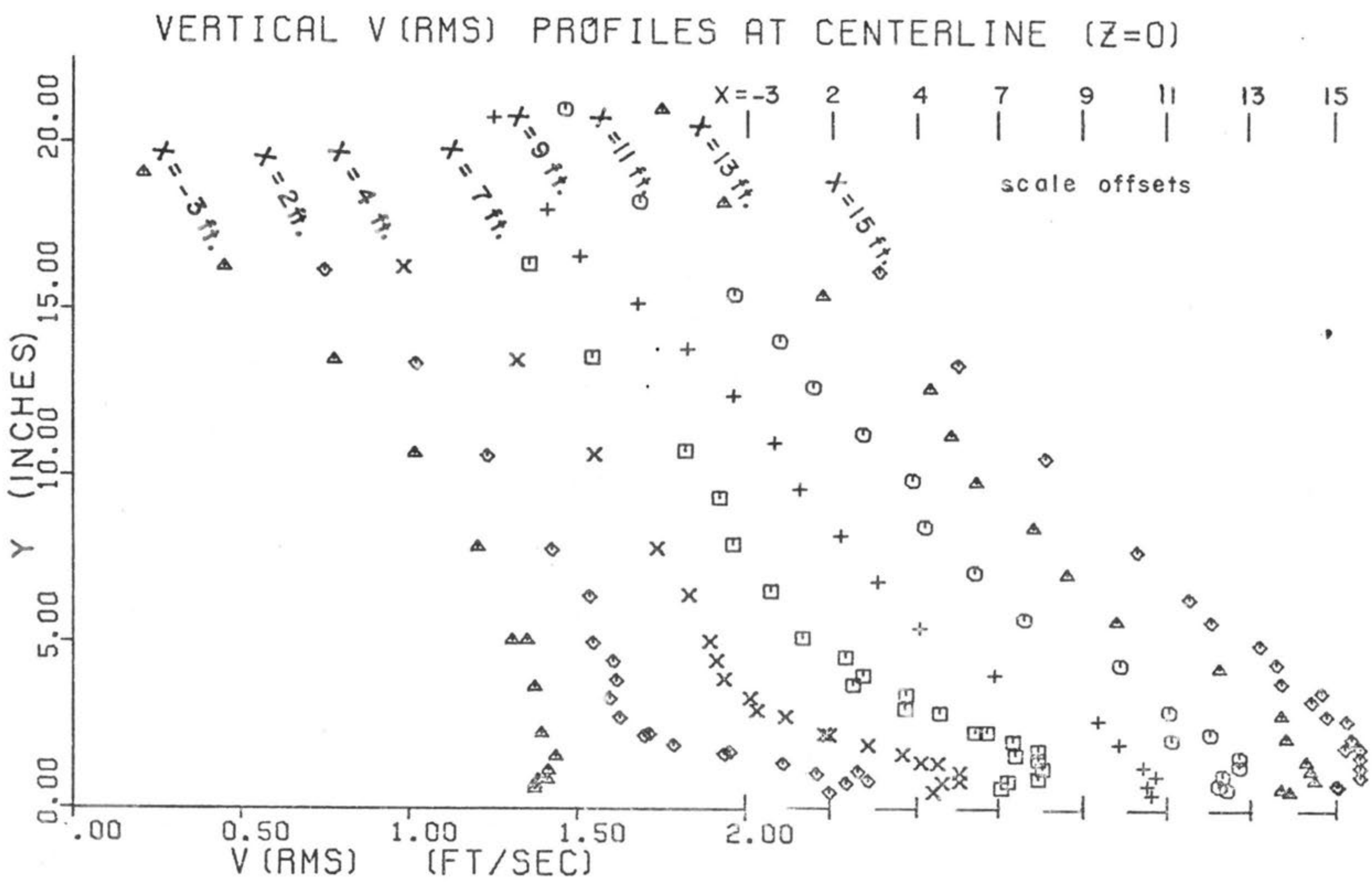

Fig. 49 $\overline{v^2}$ vertical profiles at centerline (z = 0).

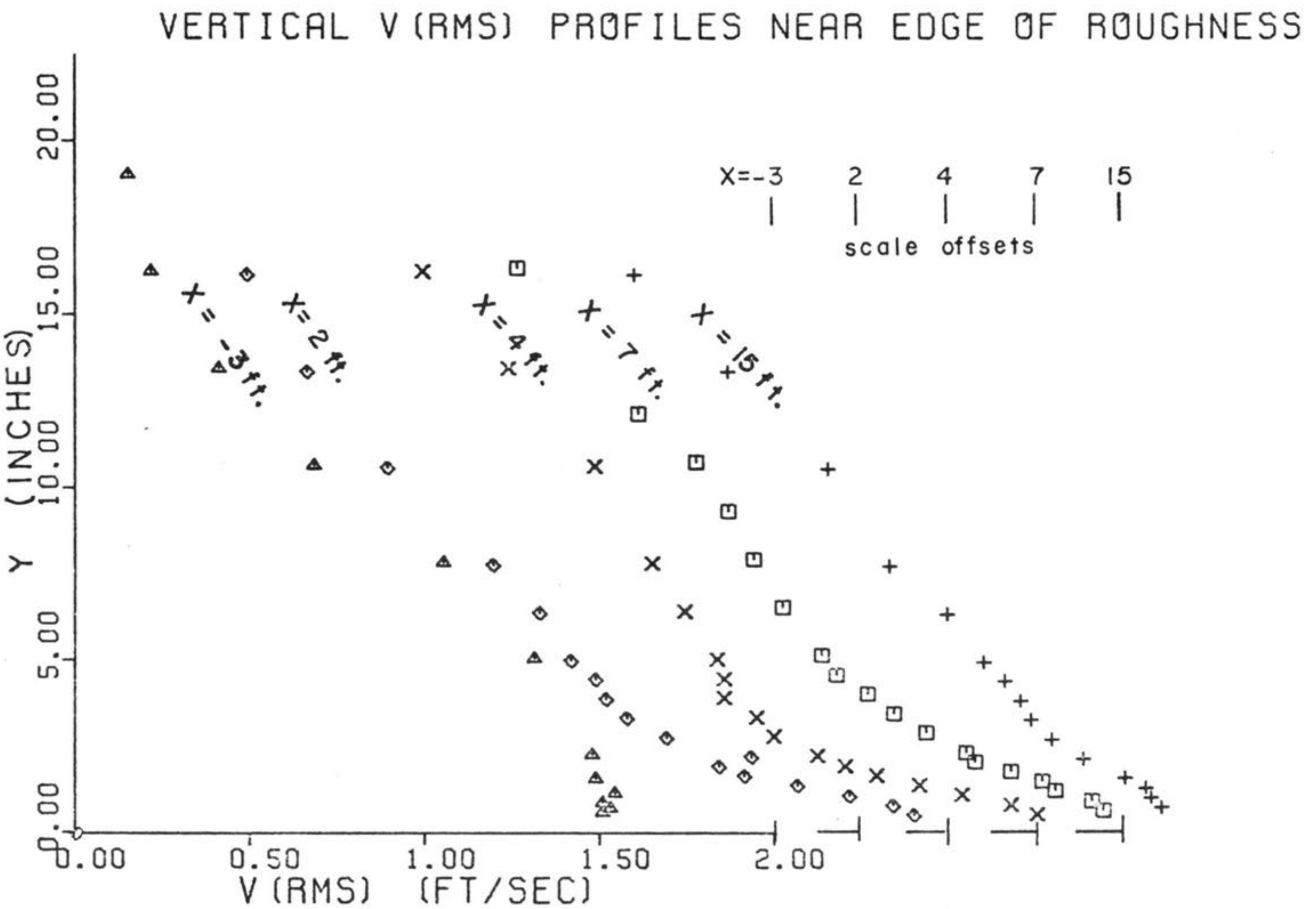

Fig. 50 $\overline{v^2}$ vertical profiles near edge of roughness.

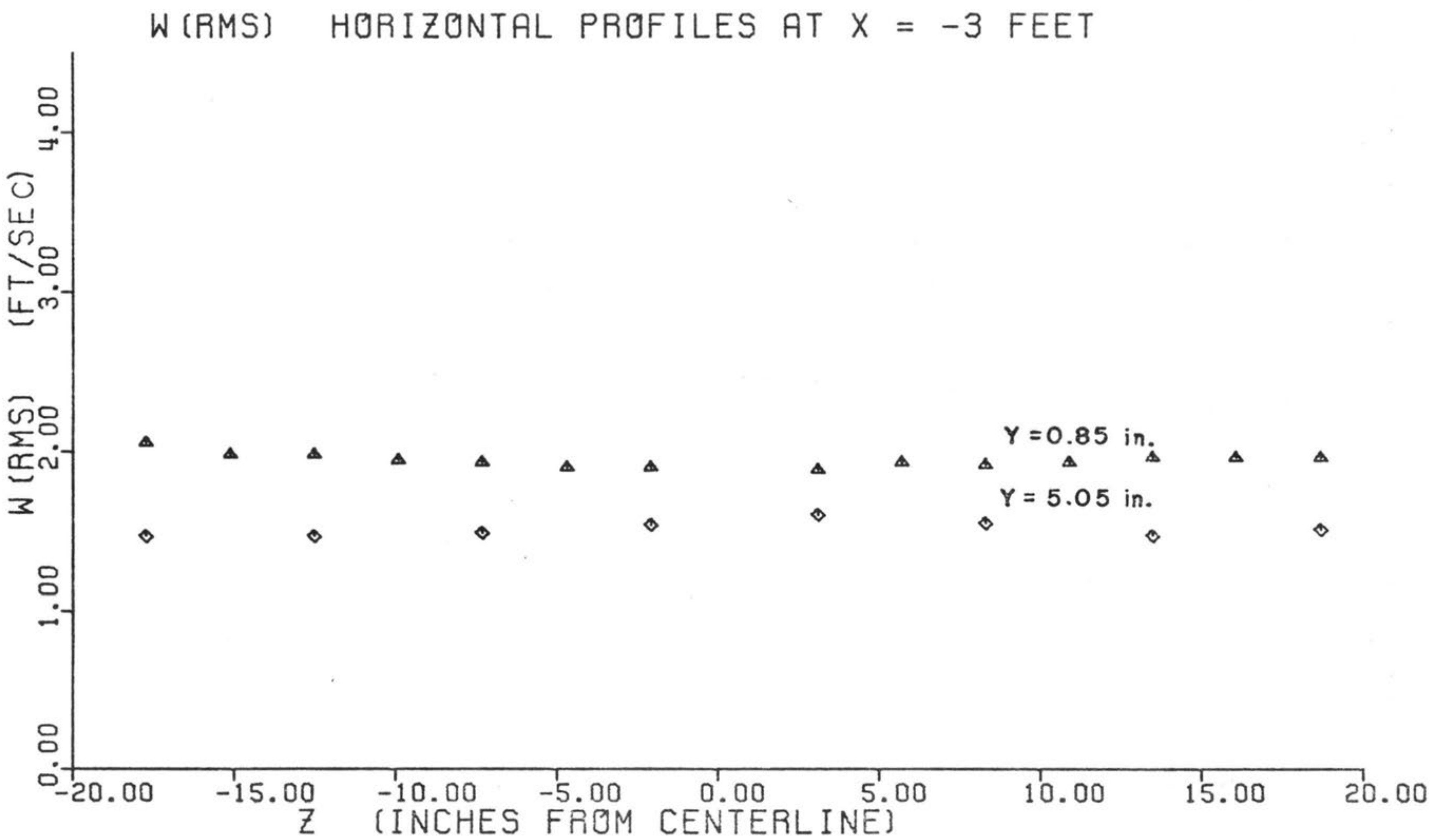

Fig. 51 $\overline{w^2}$ horizontal profiles at x = -3 feet.

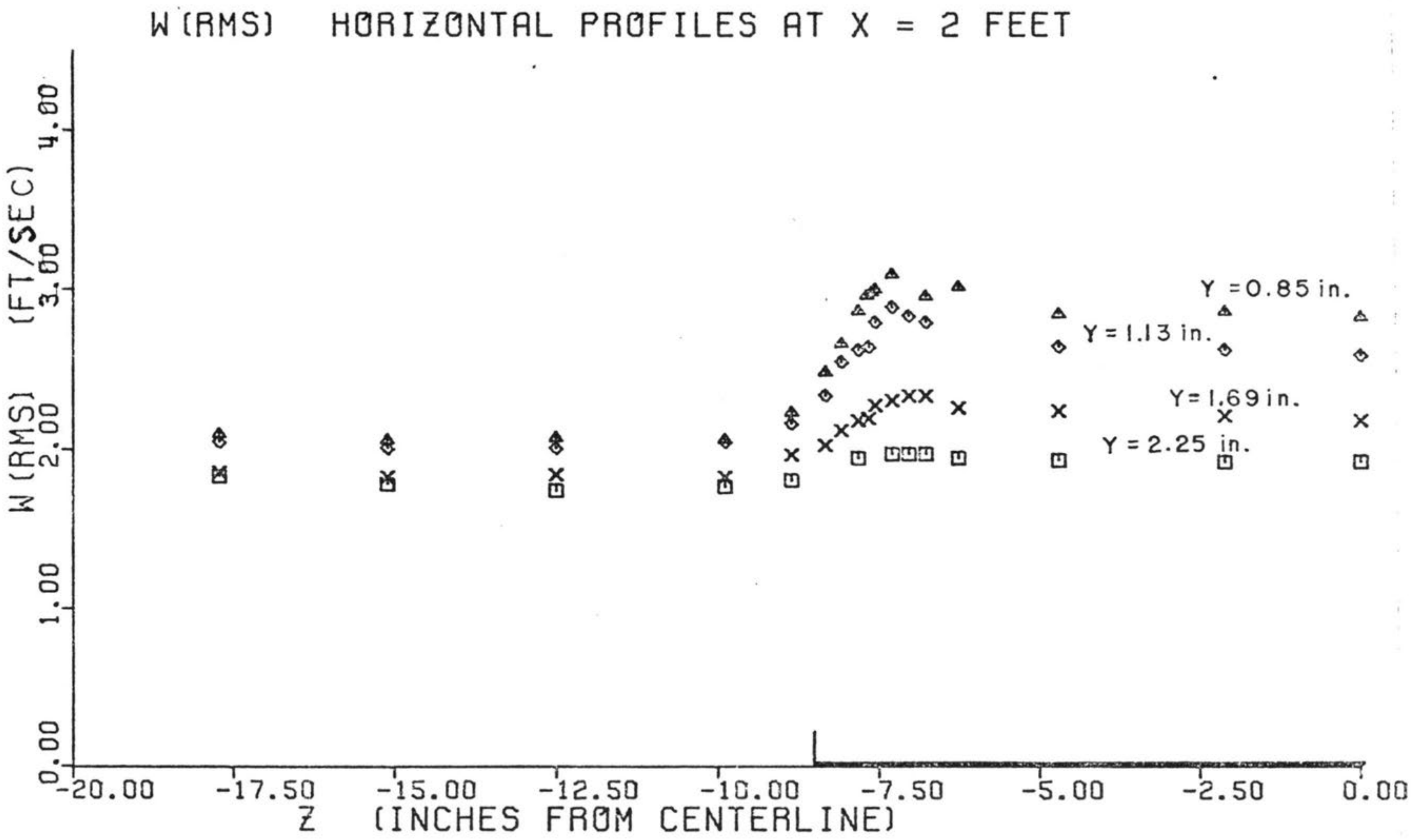

Fig. 52 $\overline{w^2}$ horizontal profiles at x = 2 feet.

213

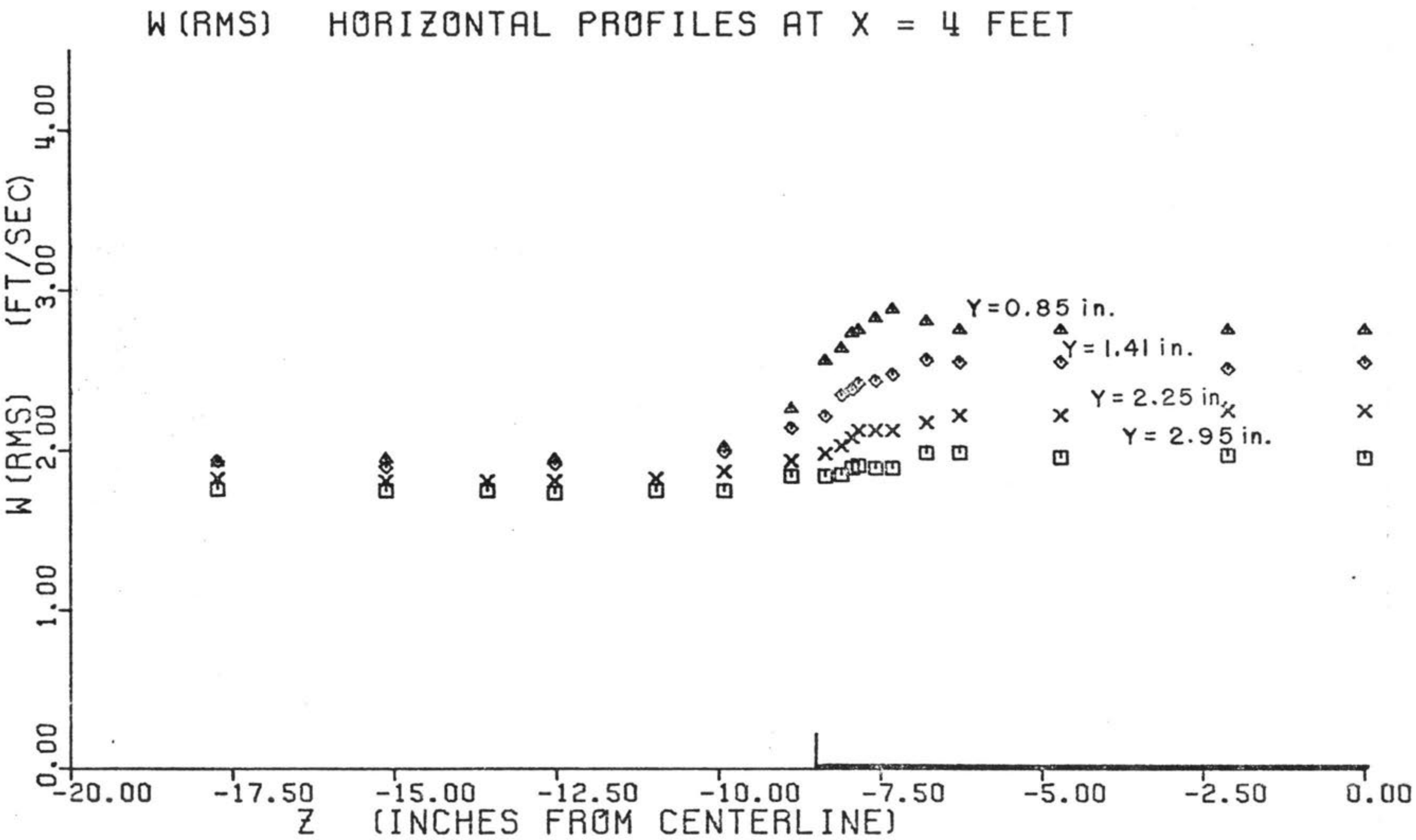

Fig. 53 $\overline{w^2}$ horizontal profiles at x = 4 feet.

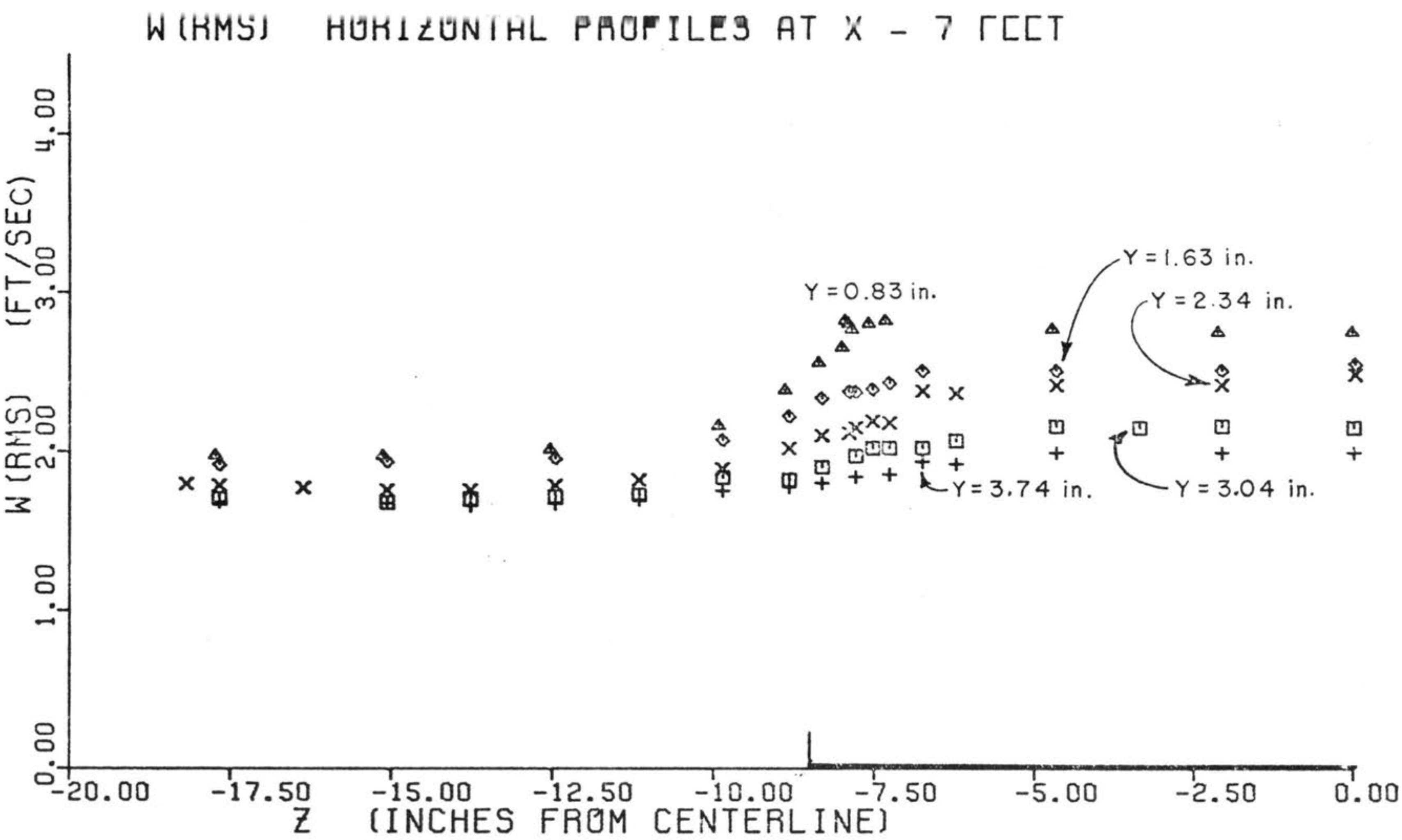

Fig. 54 $\overline{w^2}$ horizontal profiles at x = 7 feet.

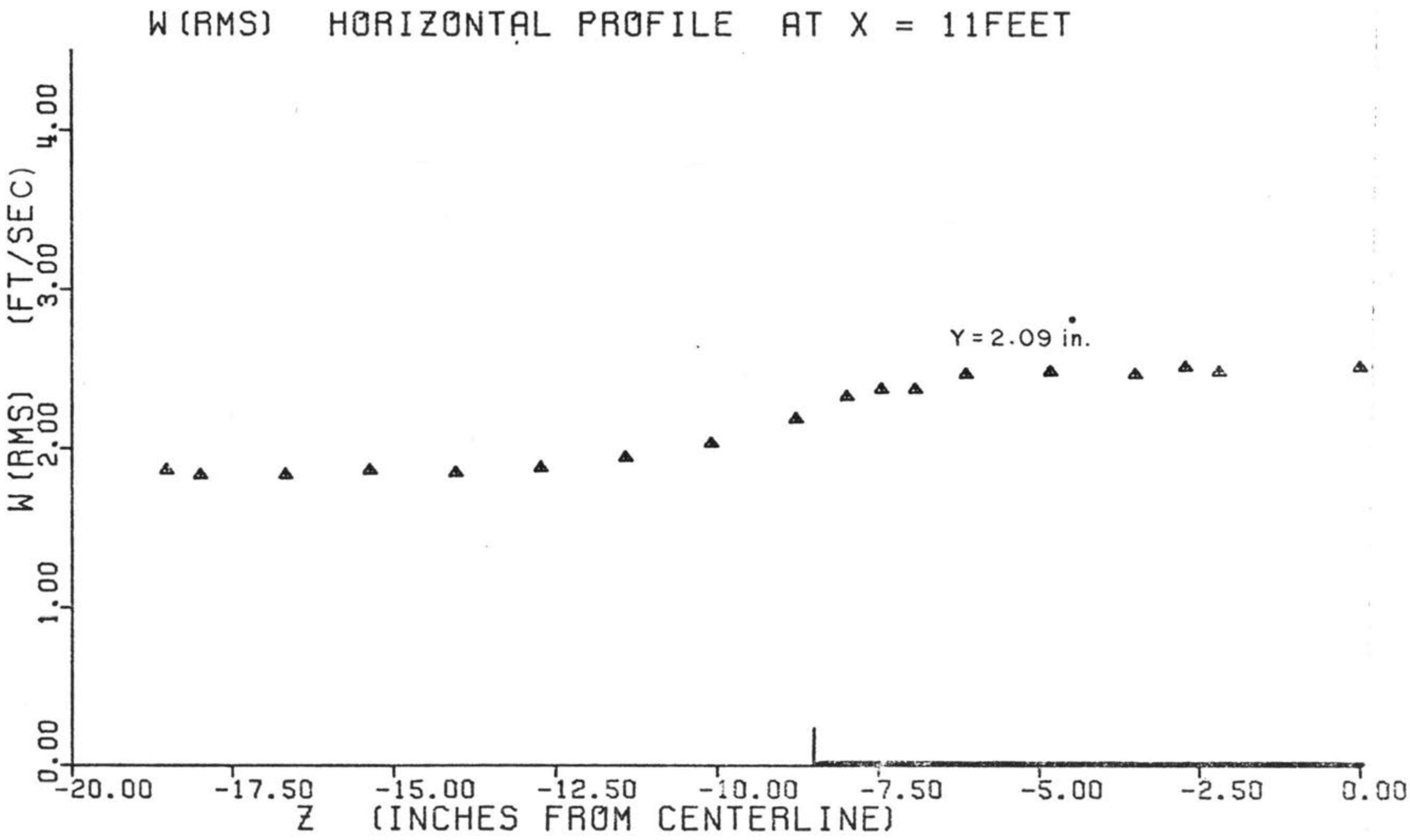

Fig. 55 $\overline{w^2}$ horizontal profiles at x = 11 feet.

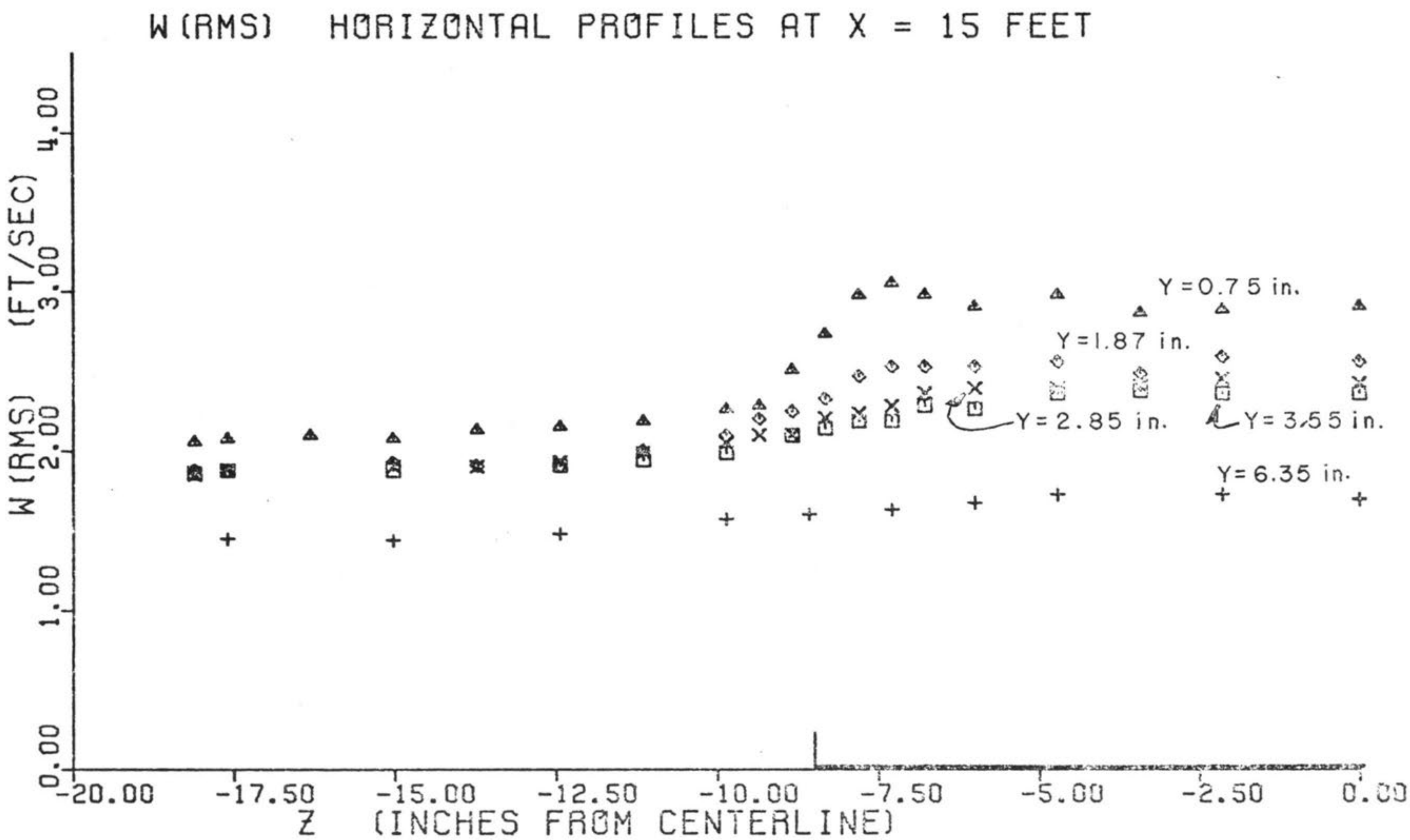

Fig. 56 $\overline{w^2}$ horizontal profiles at x = 15 feet.

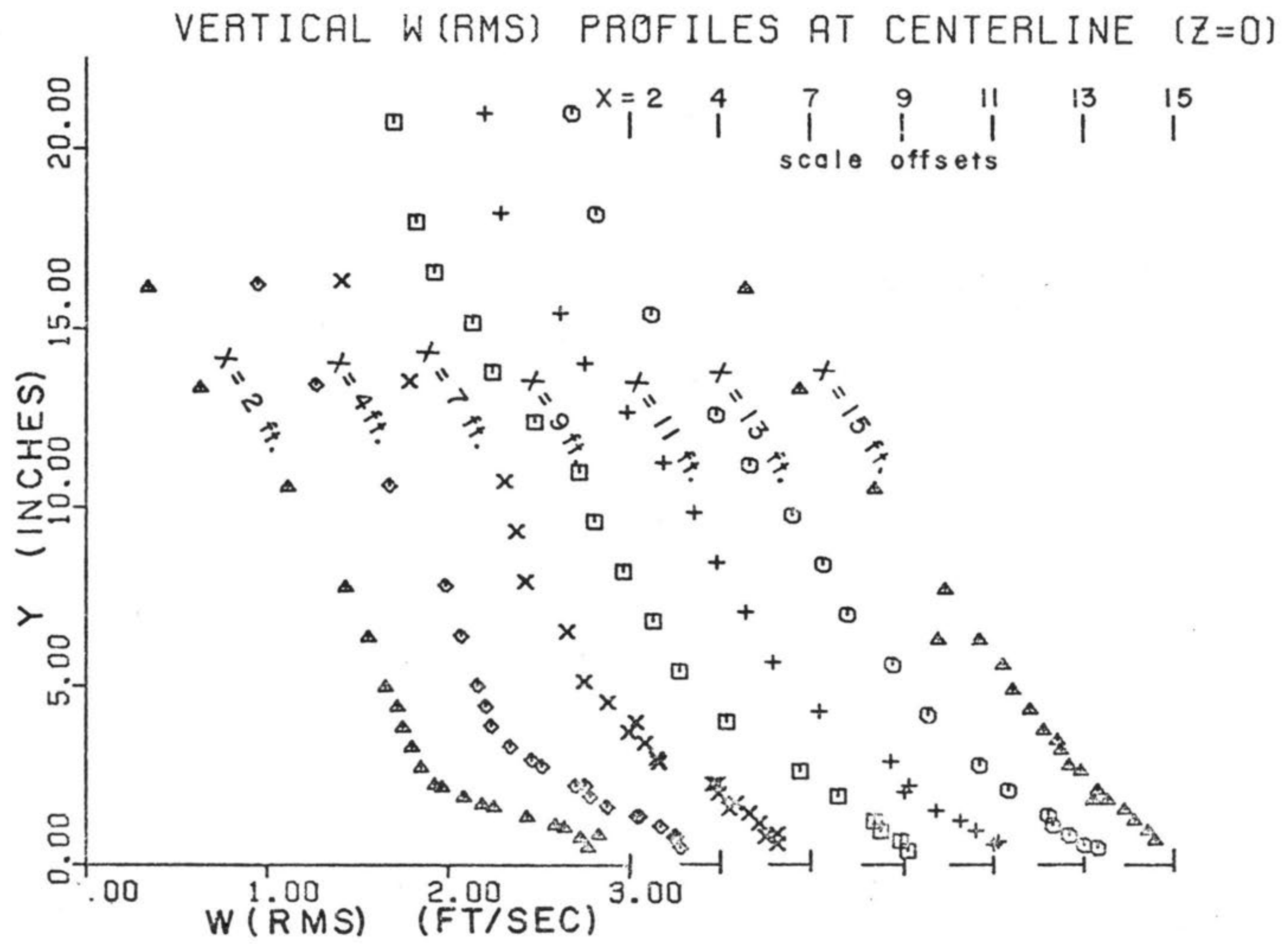

Fig. 57 $\overline{w^2}$ vertical profiles at centerline (z = 0).

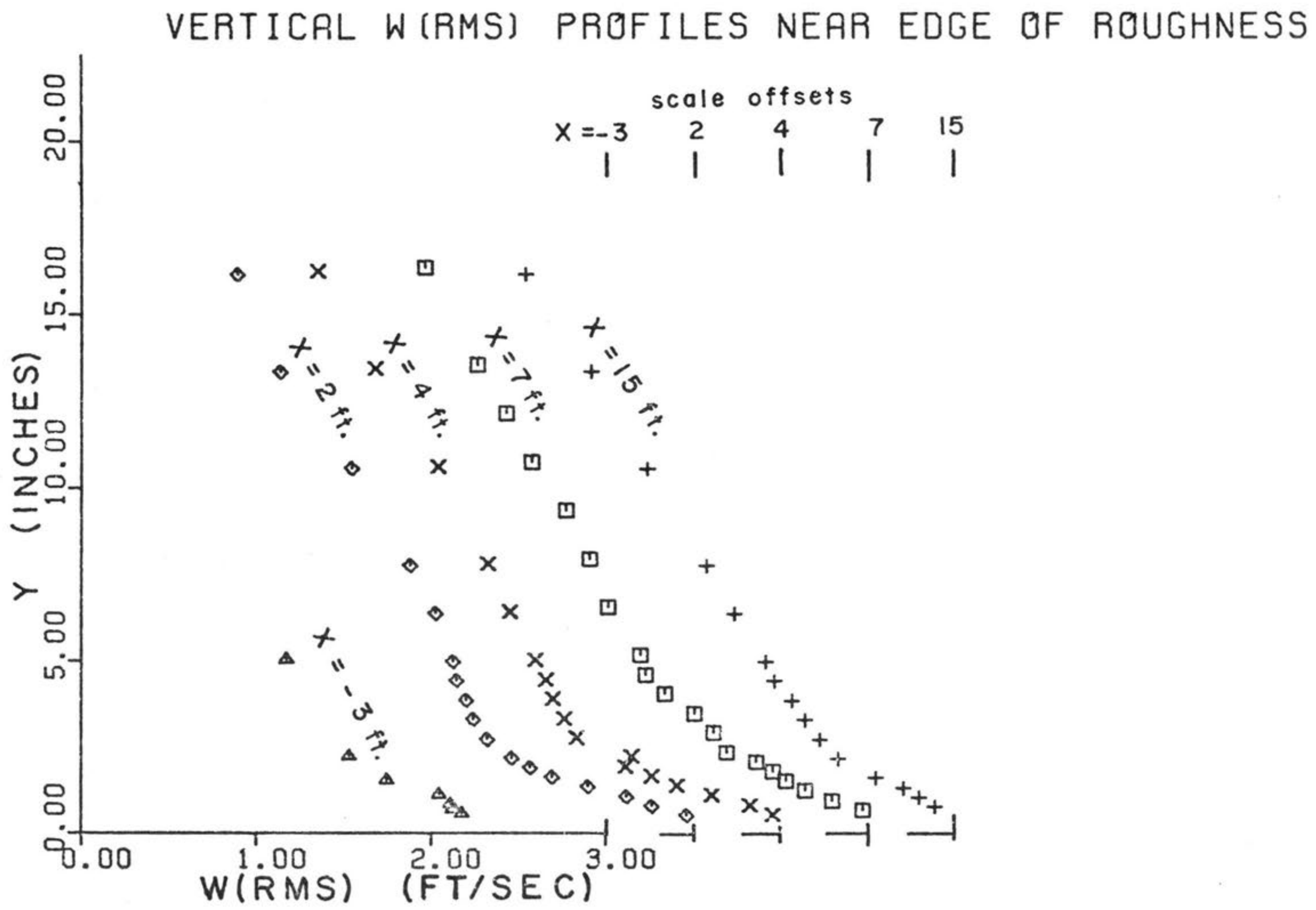

Fig. 58 $\overline{w^2}$ vertical profiles near edge of roughness.

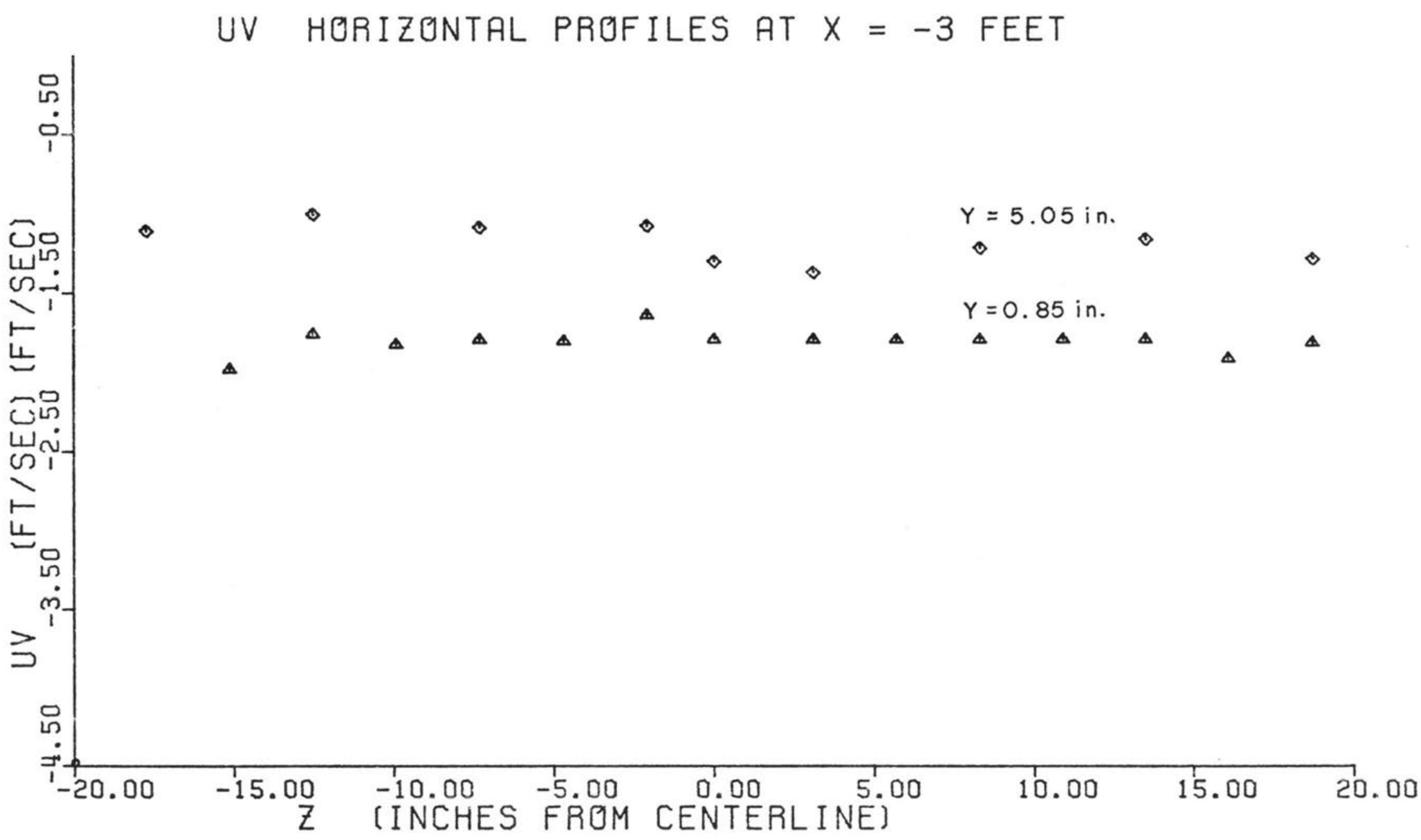

Fig. 59 $\overline{uv}$ horizontal profiles at x = -3 feet.

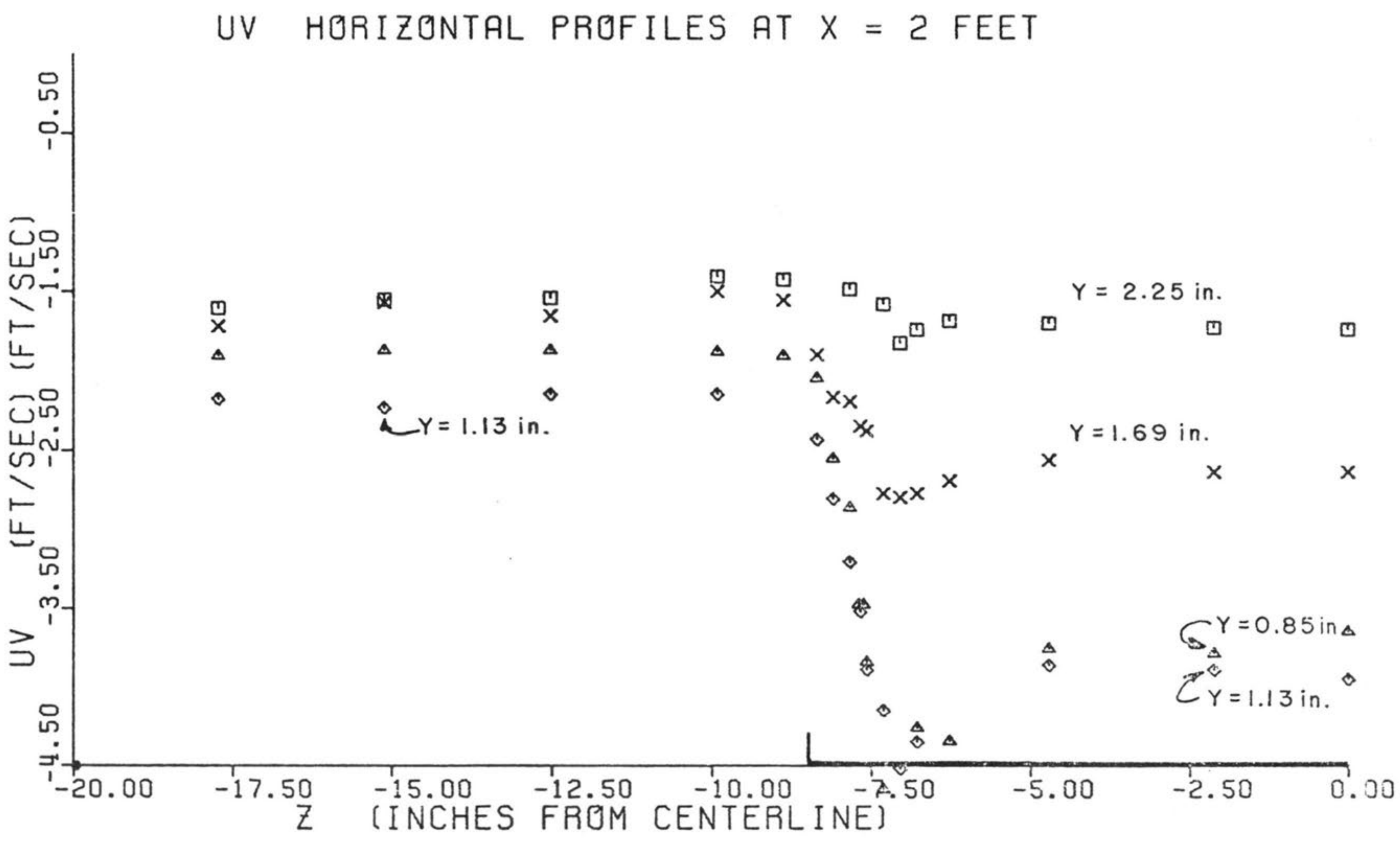

Fig. 60 $\overline{uv}$ horizontal profiles at x = 2 feet.

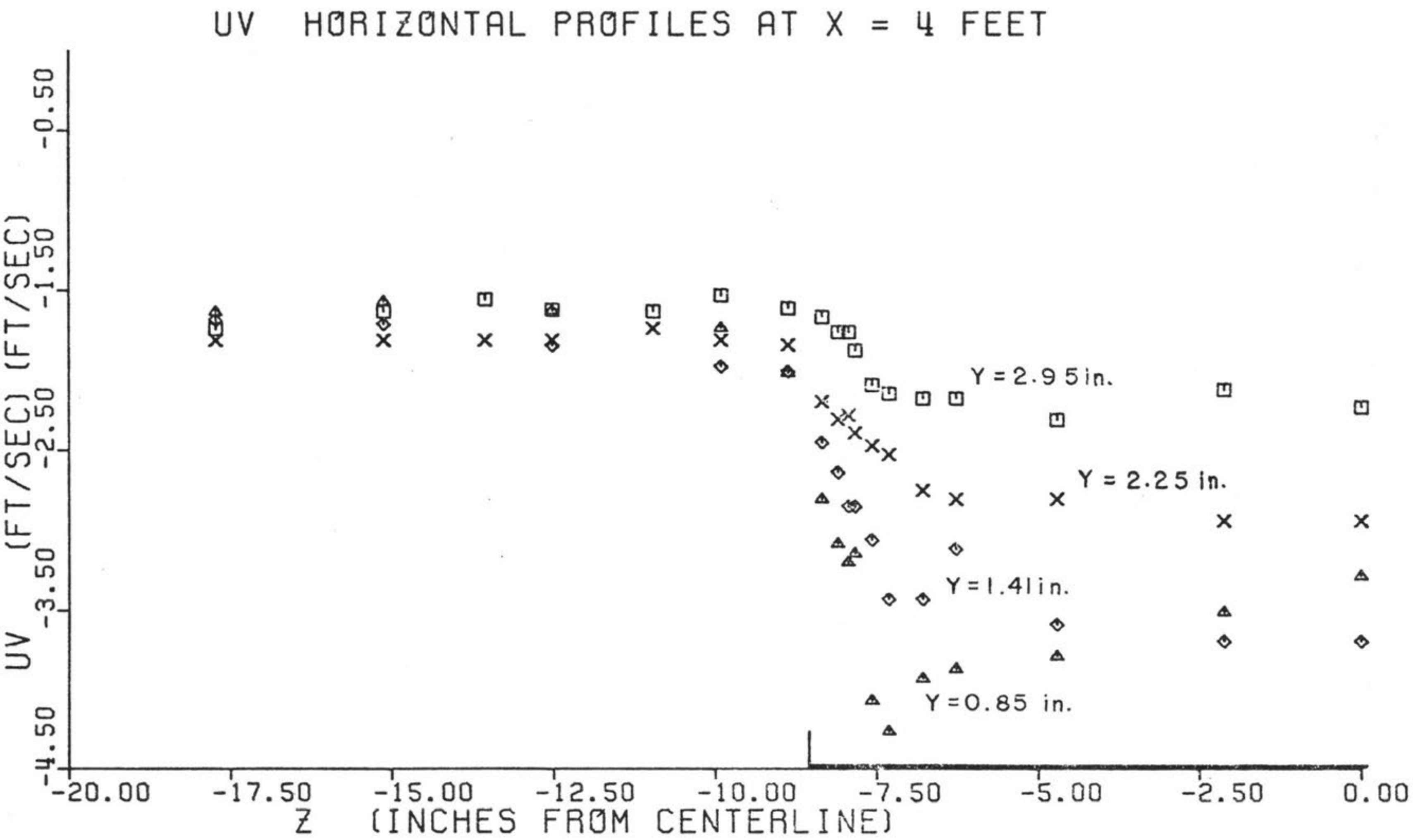

Fig. 61 $\overline{uv}$ horizontal profiles at x = 4 feet.

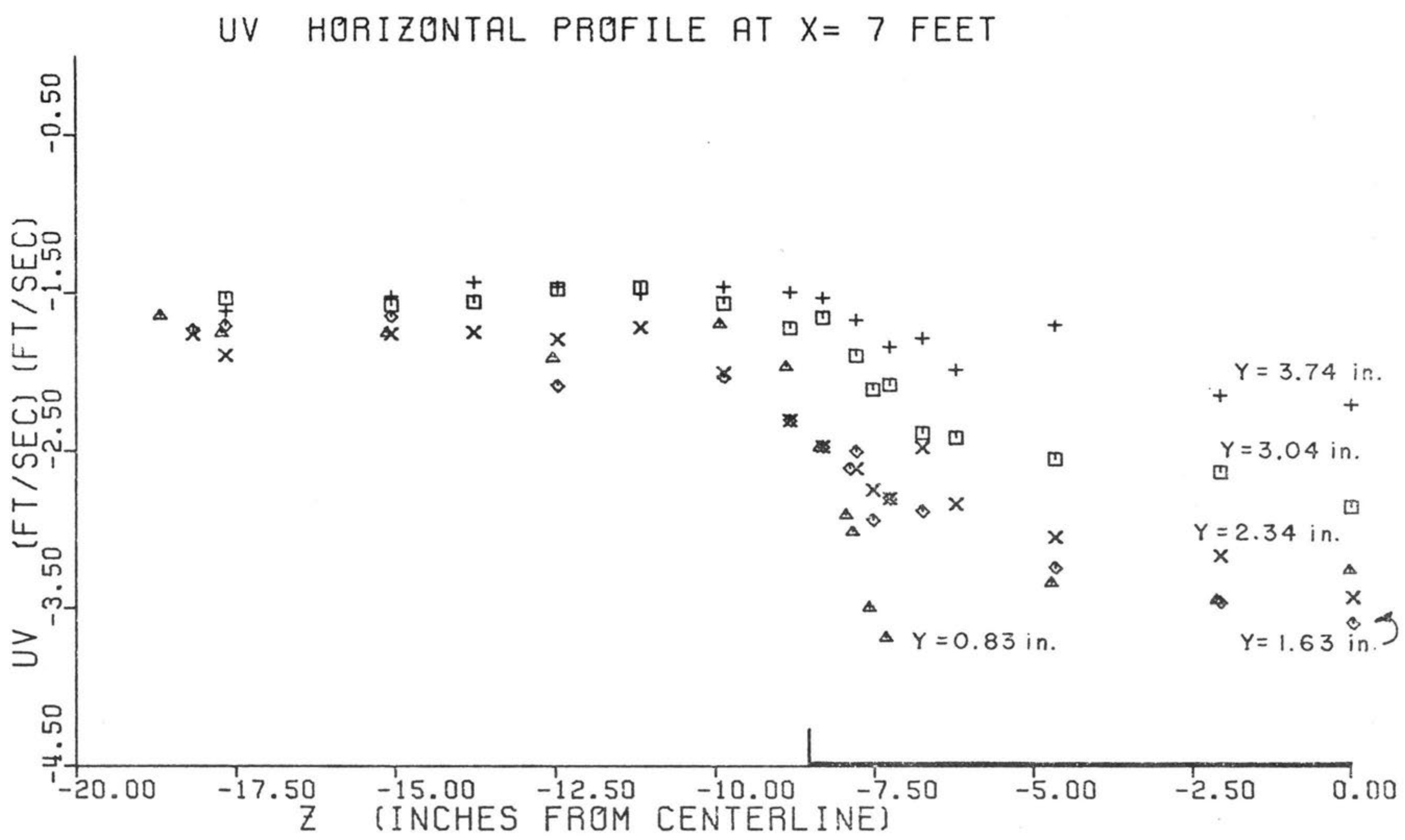

Fig. 62 $\overline{uv}$ horizontal profiles at x = 7 feet.

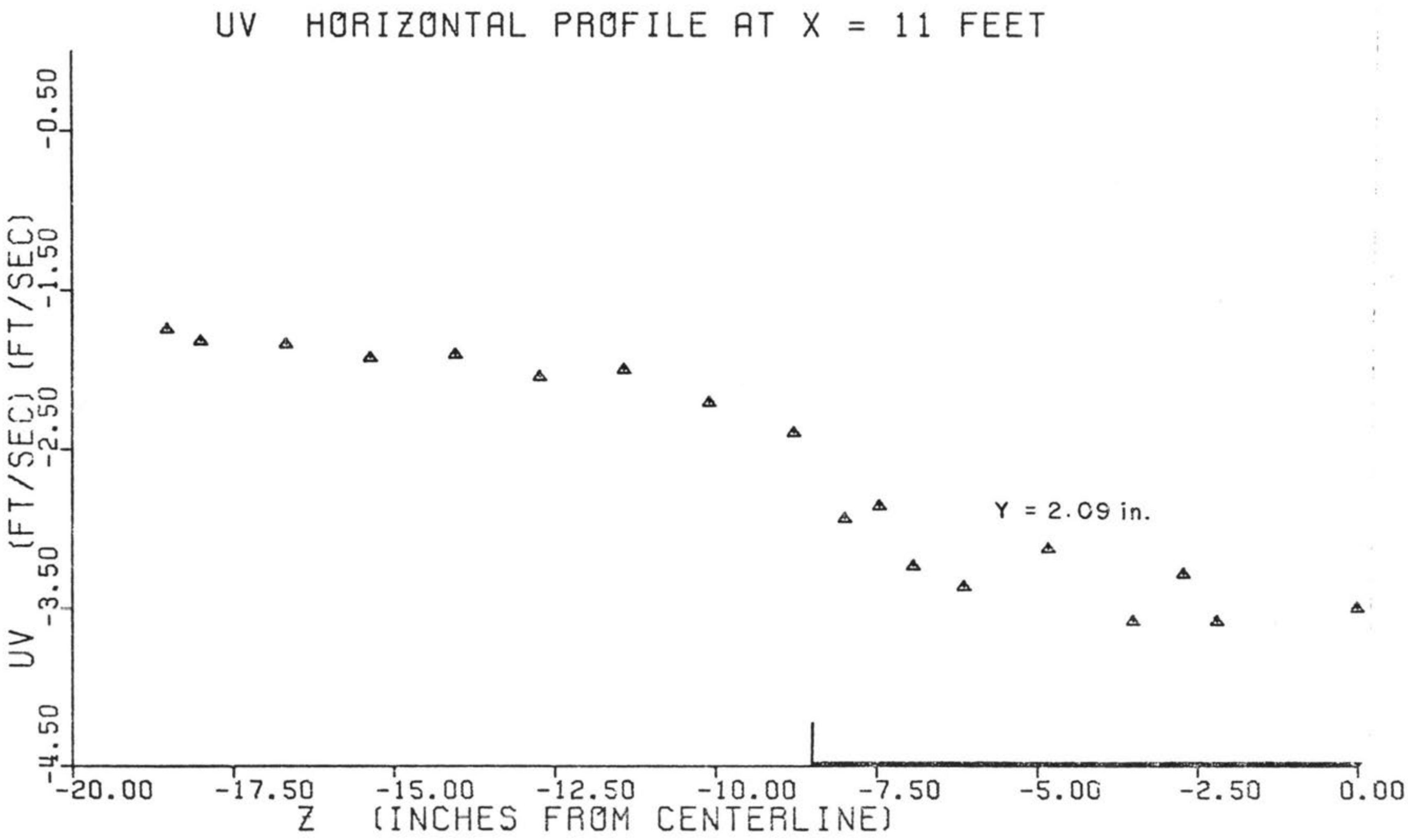

Fig. 63 $\overline{uv}$ horizontal profiles at x = 11 feet.

224

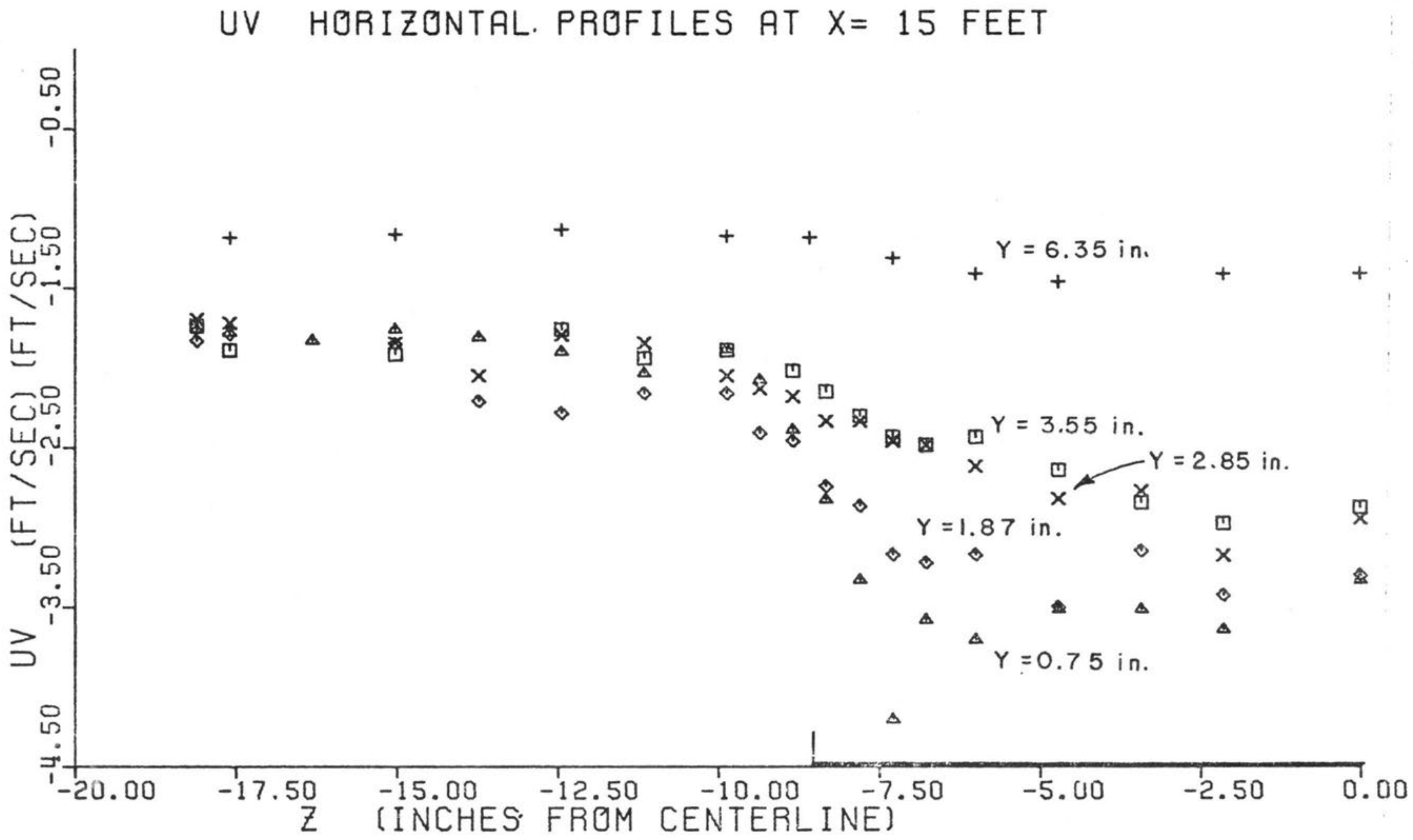

Fig. 64 $\overline{uv}$ horizontal profiles at x = 15 feet.

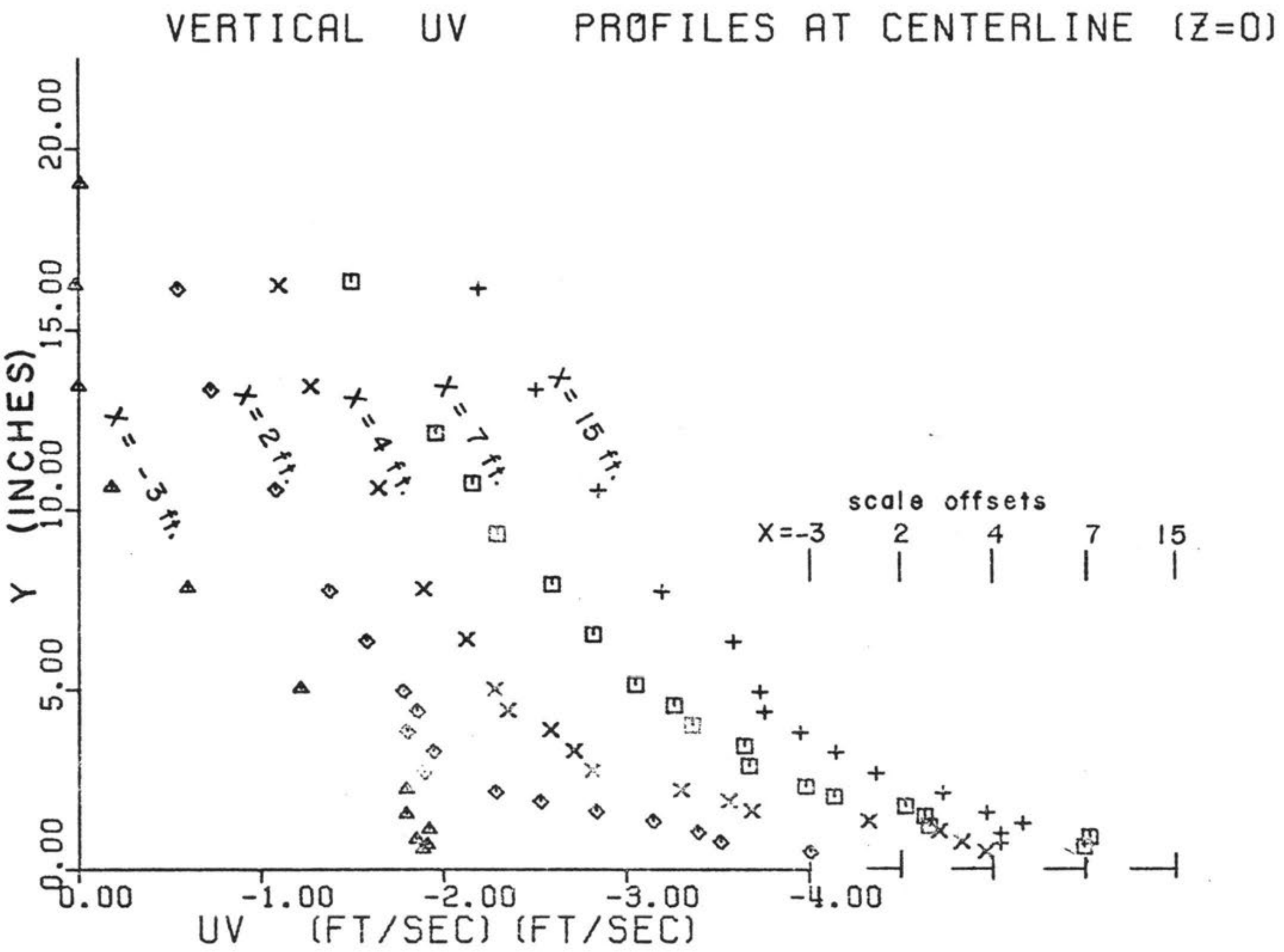

Fig. 65 $\overline{uv}$ vertical profiles at centerline (z = 0).

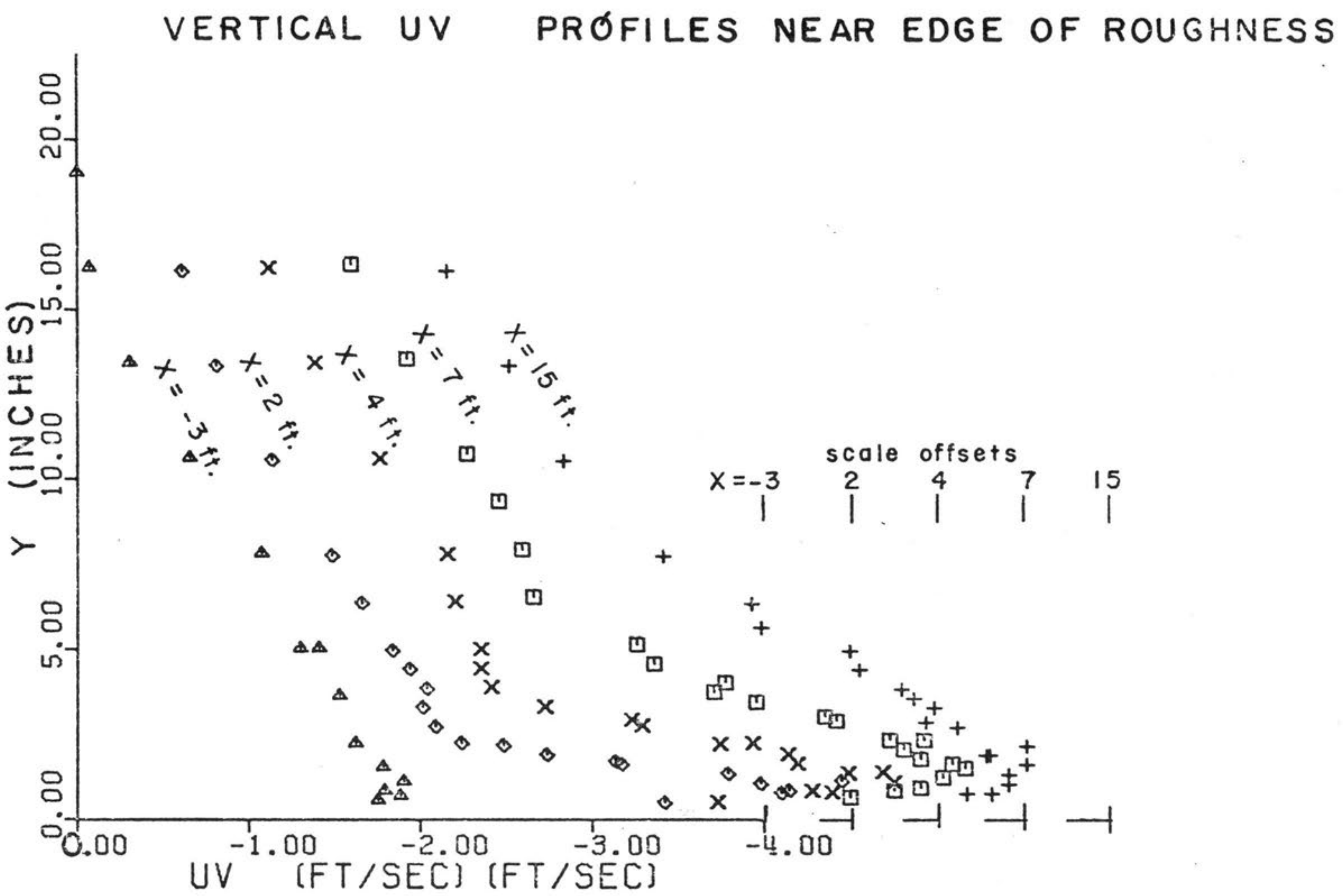

Fig. 66 $\overline{uv}$ vertical profiles near edge of roughness.

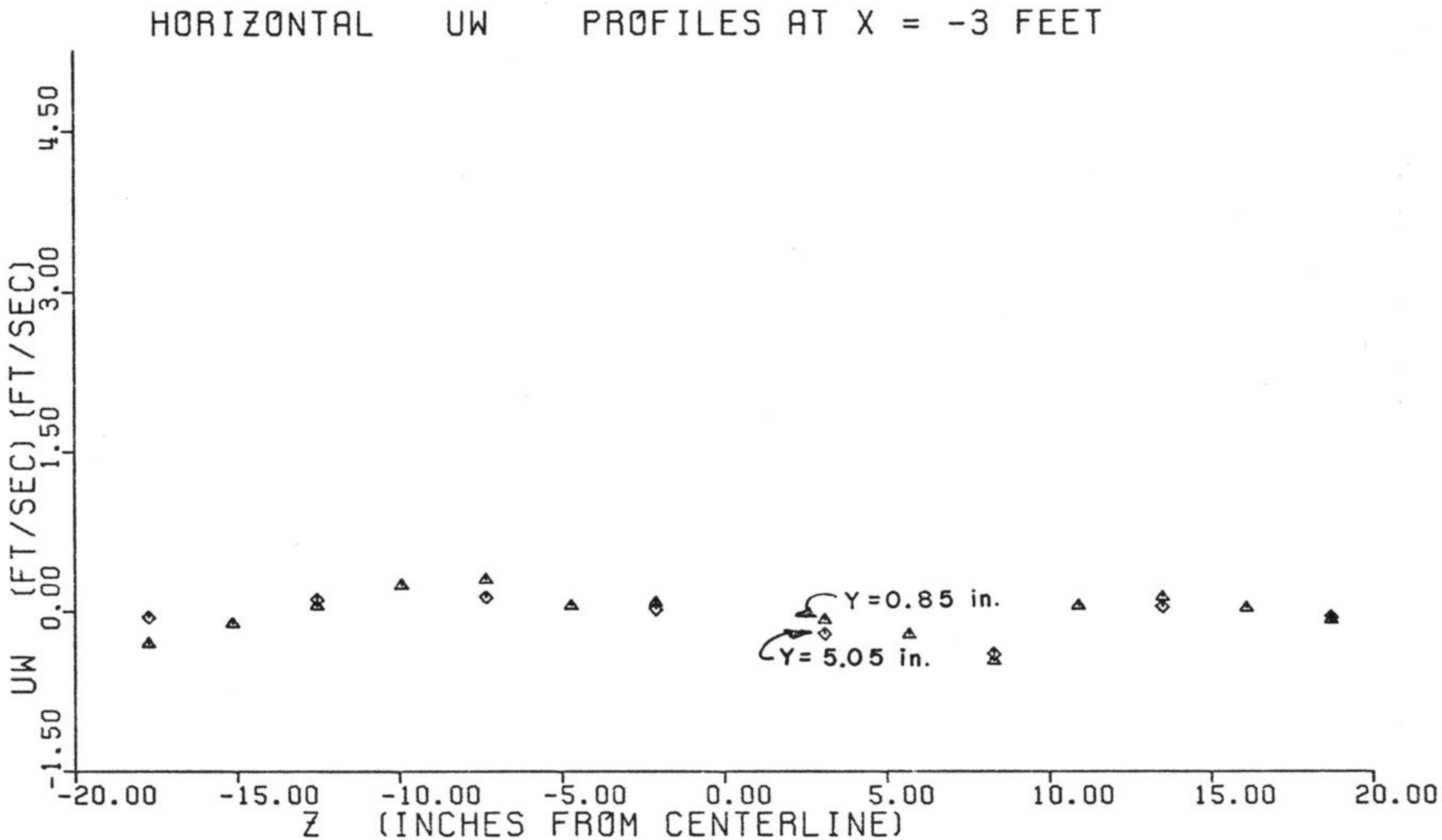

Fig. 67 $\overline{uw}$ horizontal profiles at x = -3 feet.

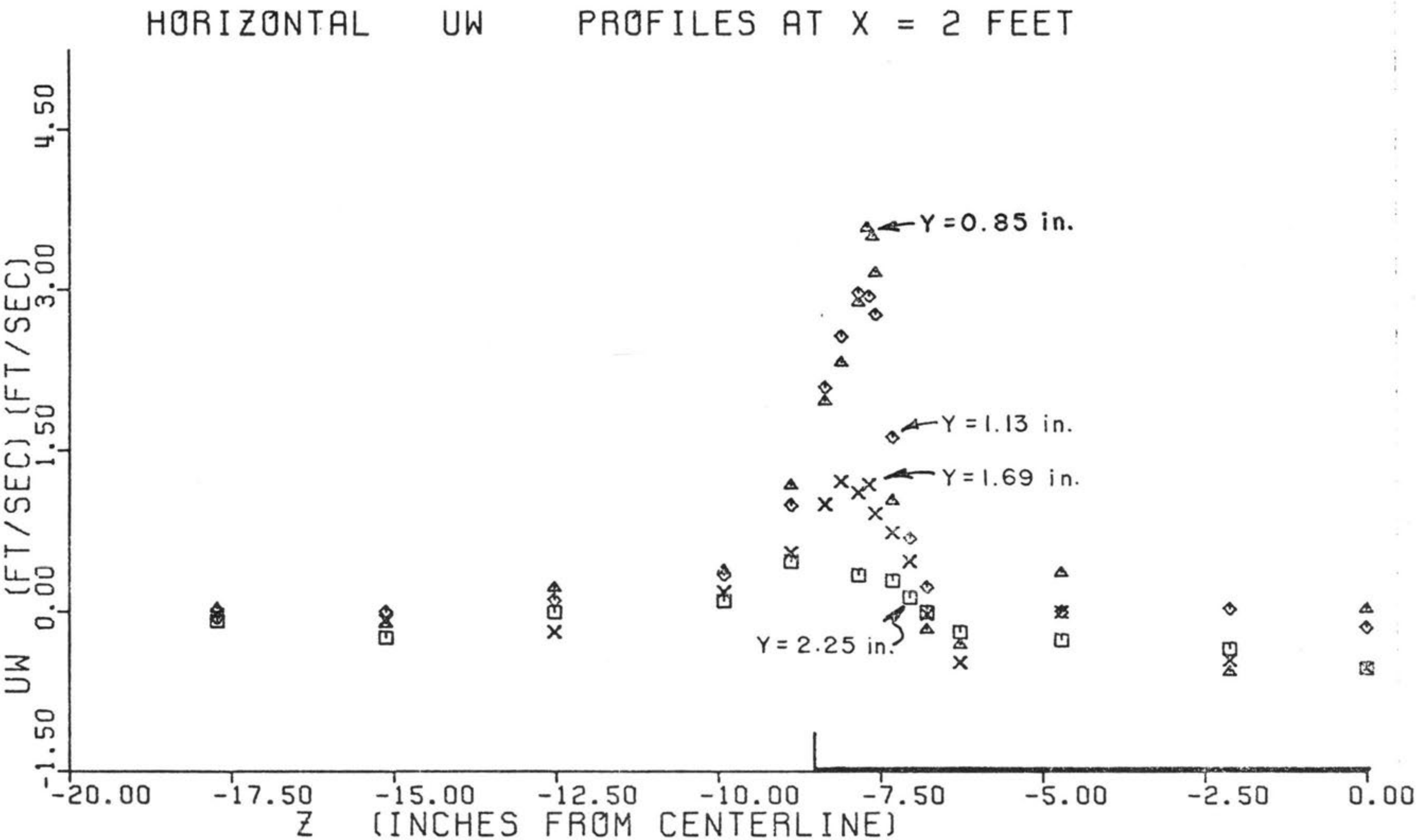

Fig. 68 $\overline{uw}$ horizontal profiles at x = 2 feet.

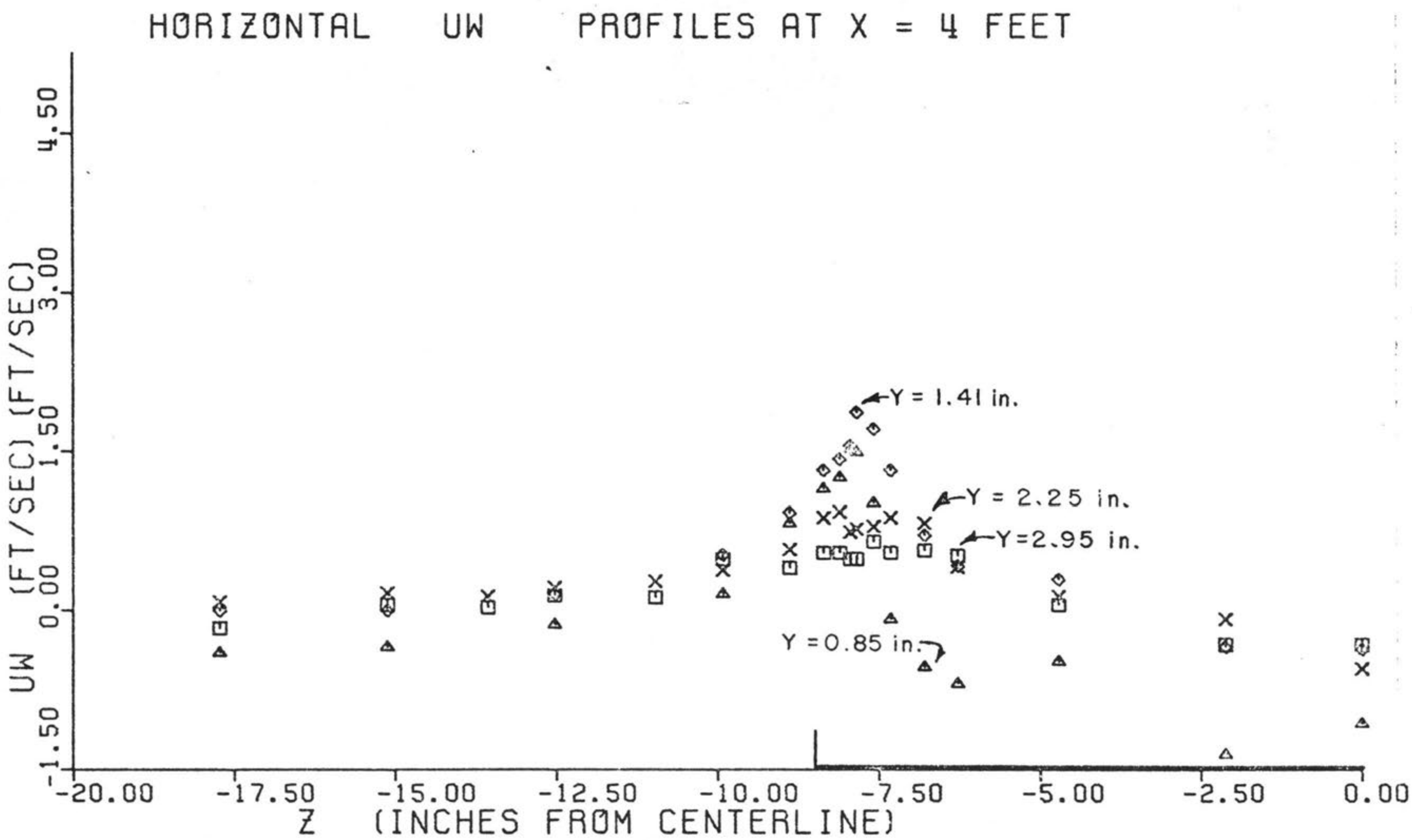

Fig. 69 $\overline{uv}$ vertical profiles near edge of roughness.

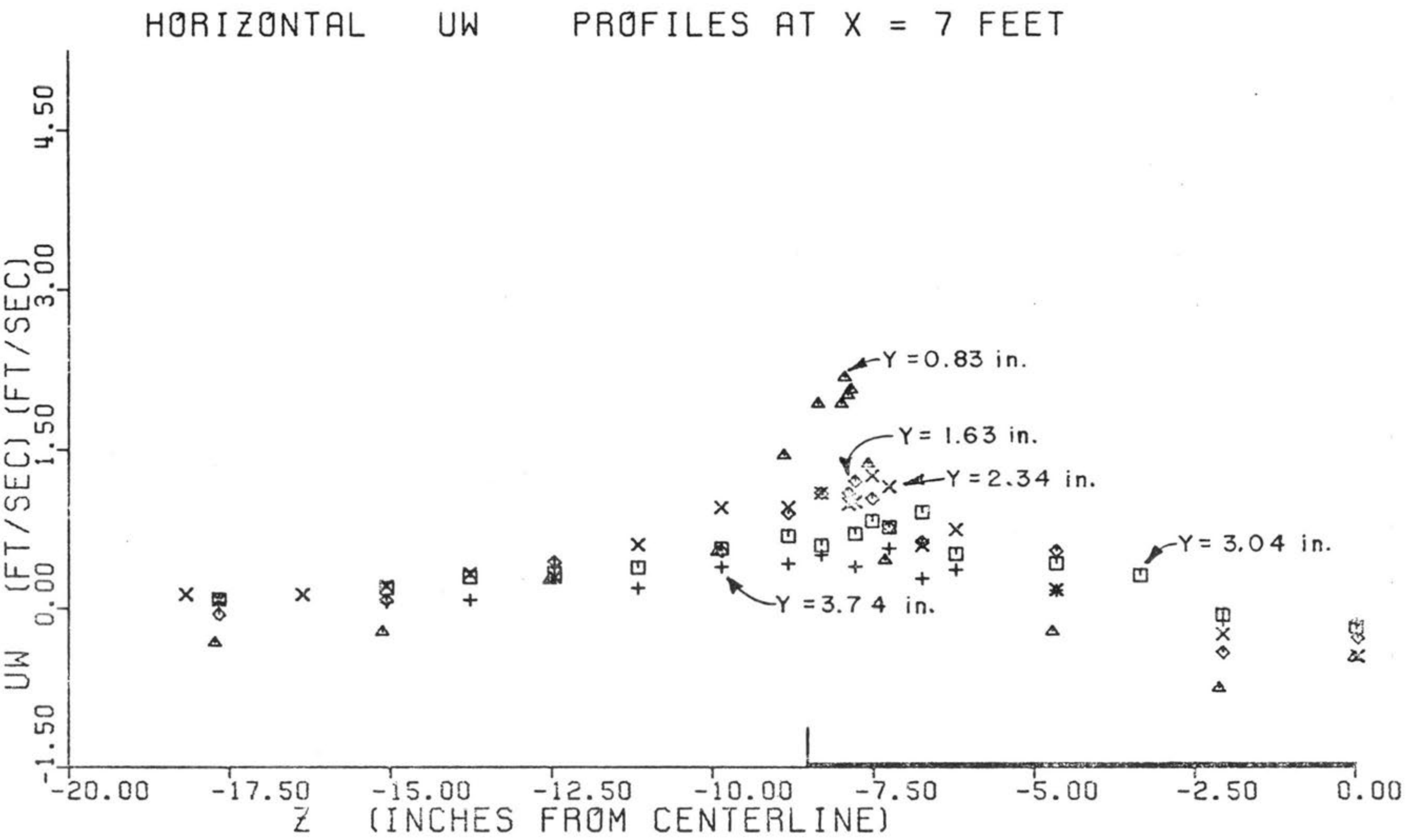

Fig. 70 $\overline{uw}$ horizontal profiles at x = 7 feet.

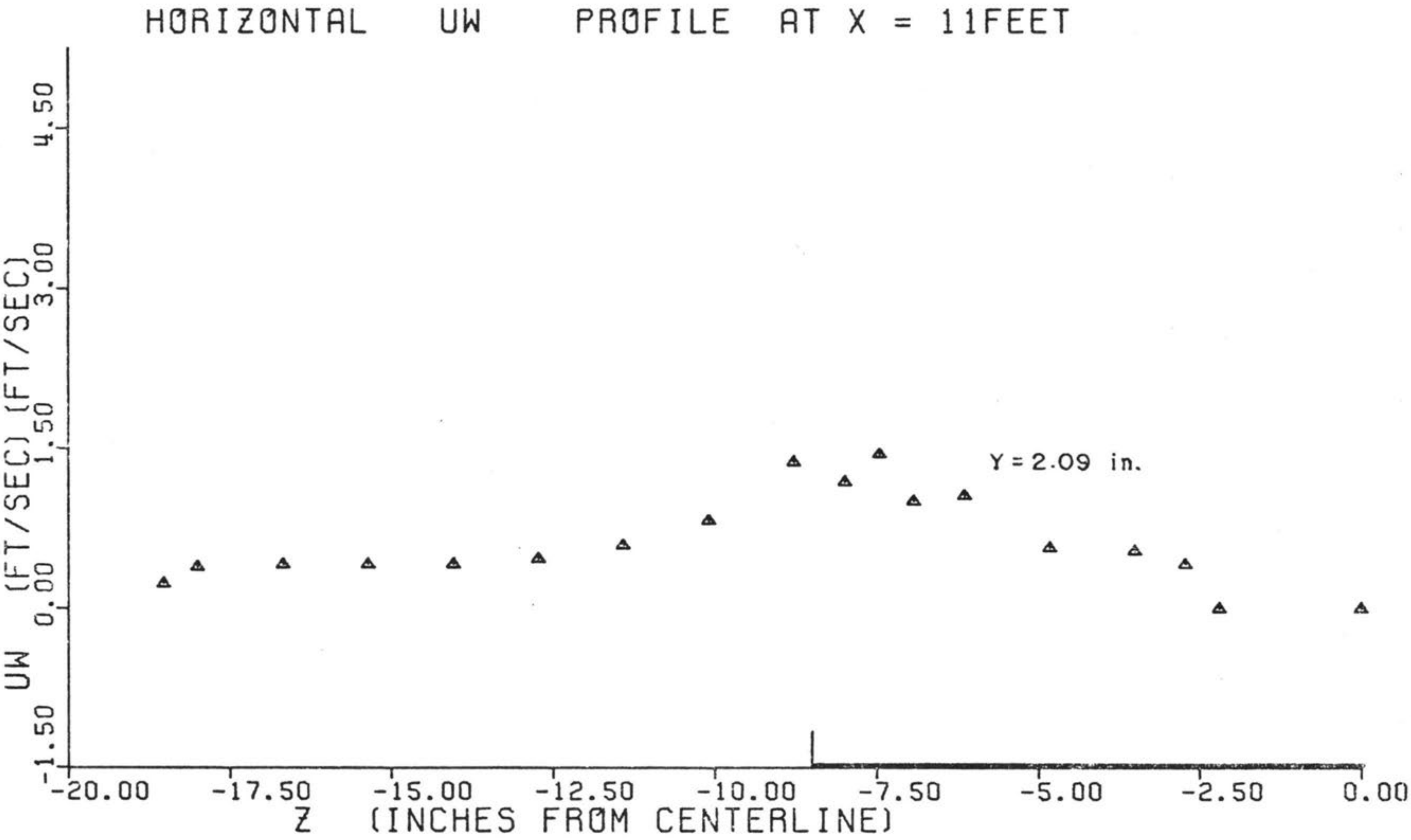

Fig. 71 $\overline{uw}$ horizontal profiles at x = 11 feet.

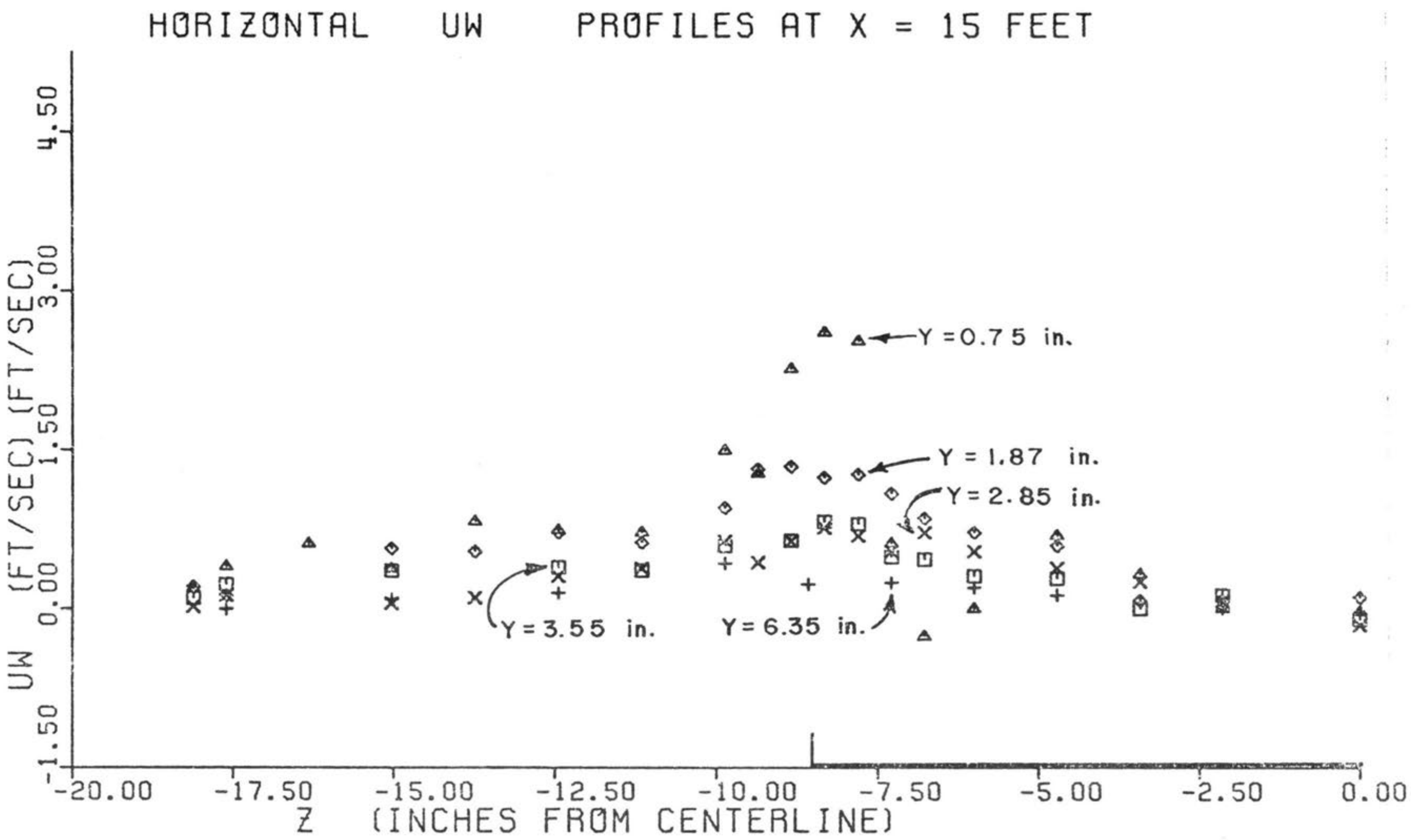

Fig. 72 $\overline{uw}$ horizontal profiles at x = 15 feet.

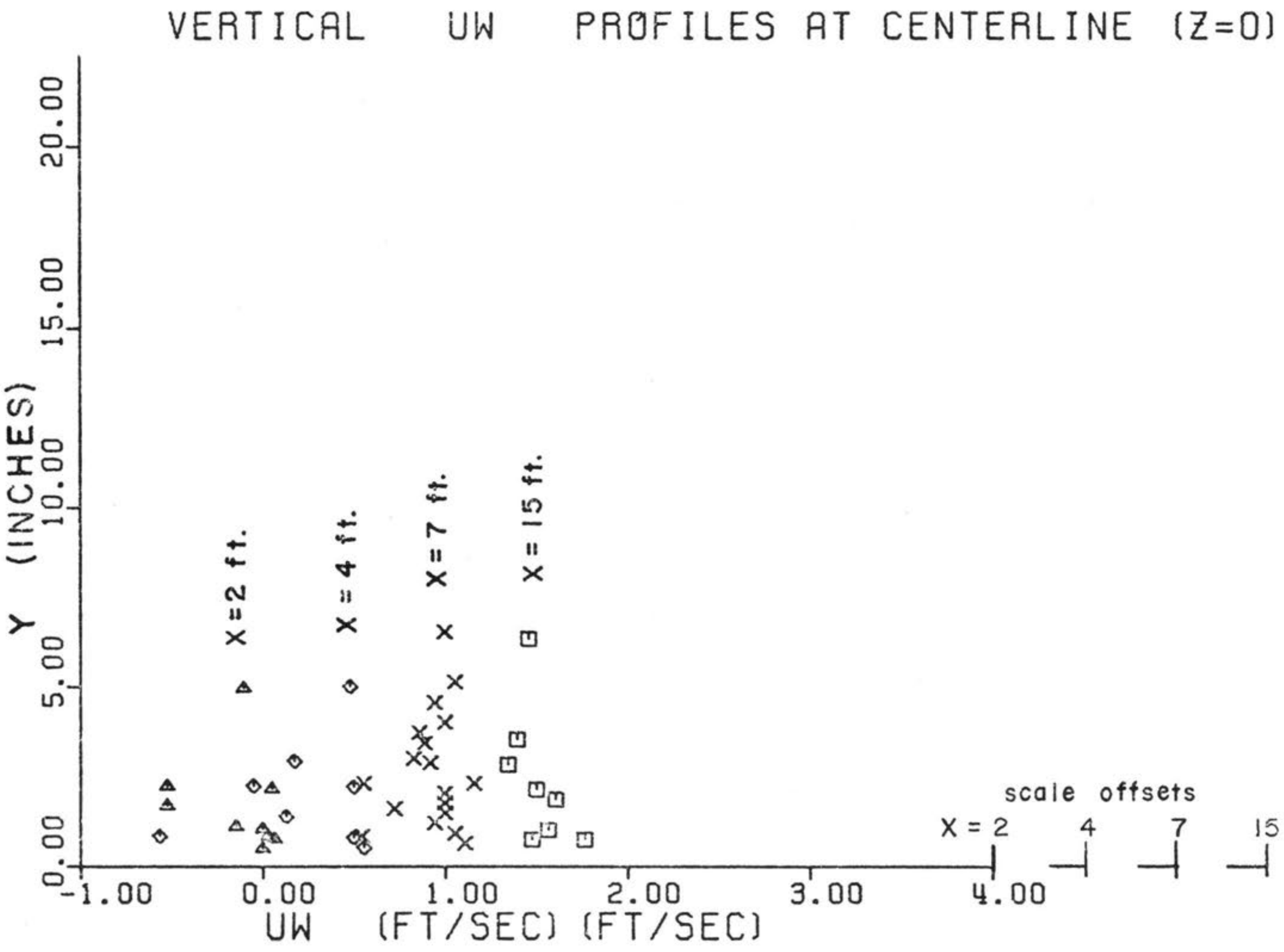

Fig. 73 $\overline{uw}$ vertical profiles at centerline (z = 0).

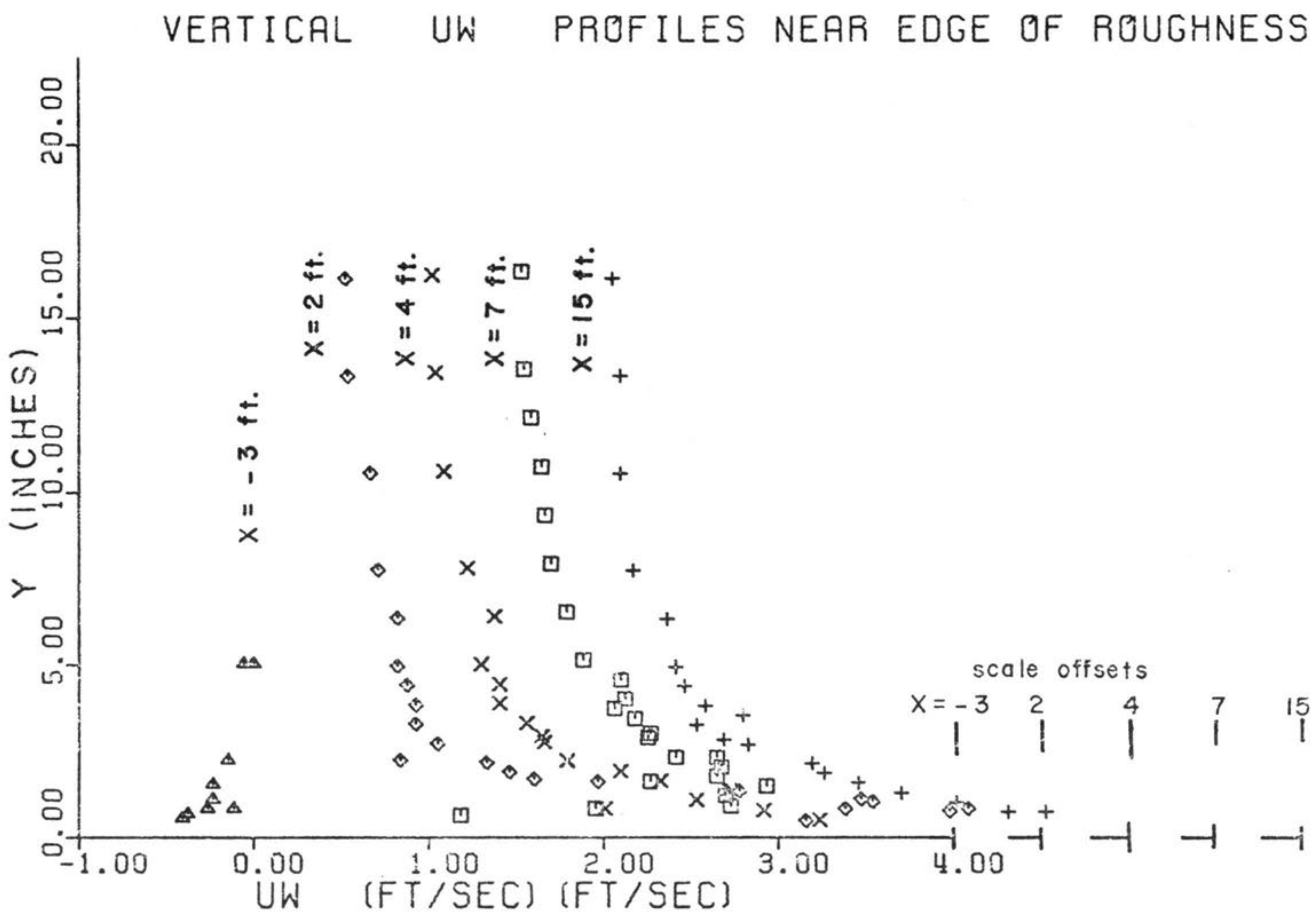

Fig. 74 $\overline{uw}$ vertical profiles near edge of roughness.

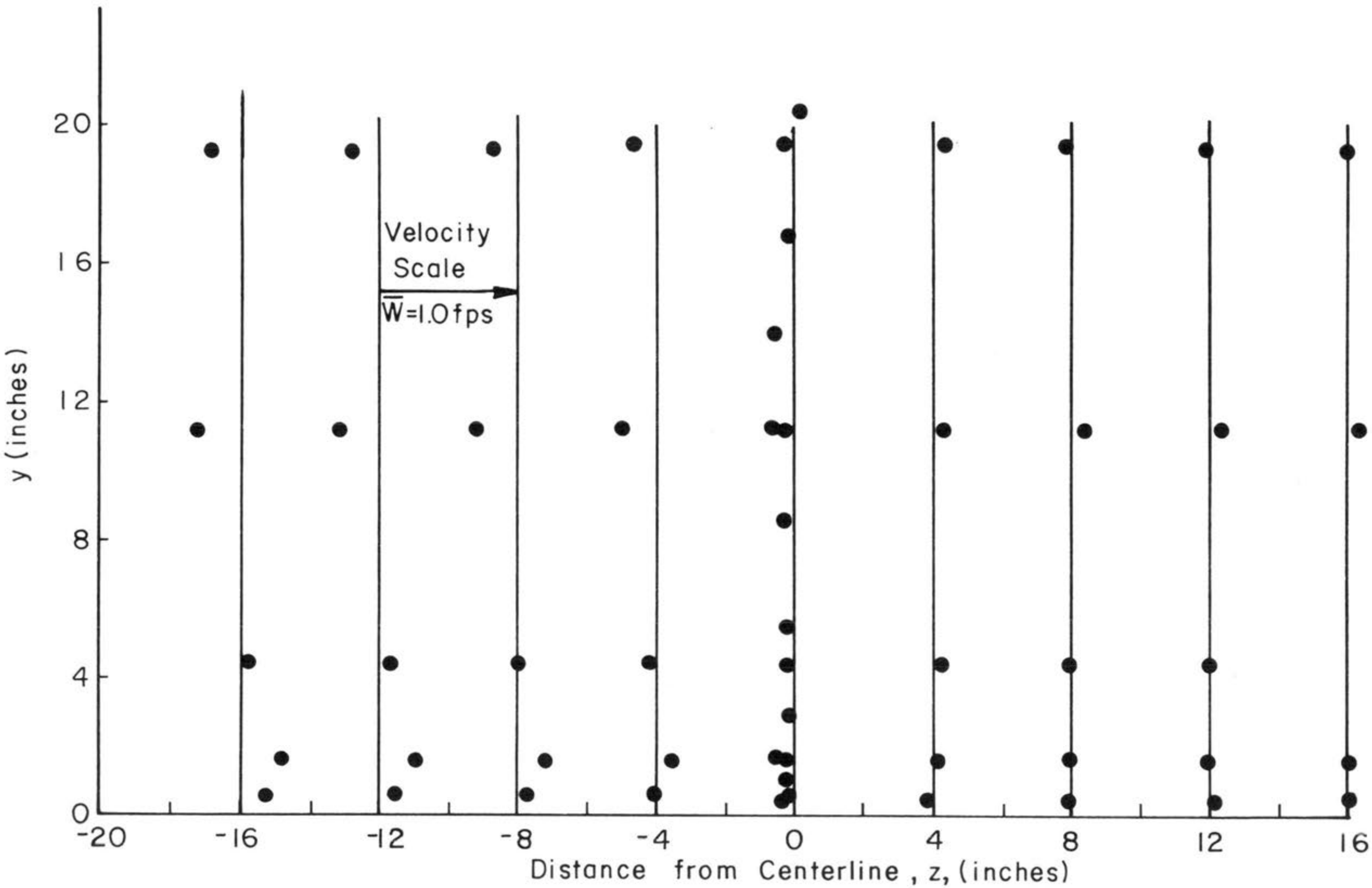

Fig. 75 Lateral velocity (W) map at x = -3 feet.

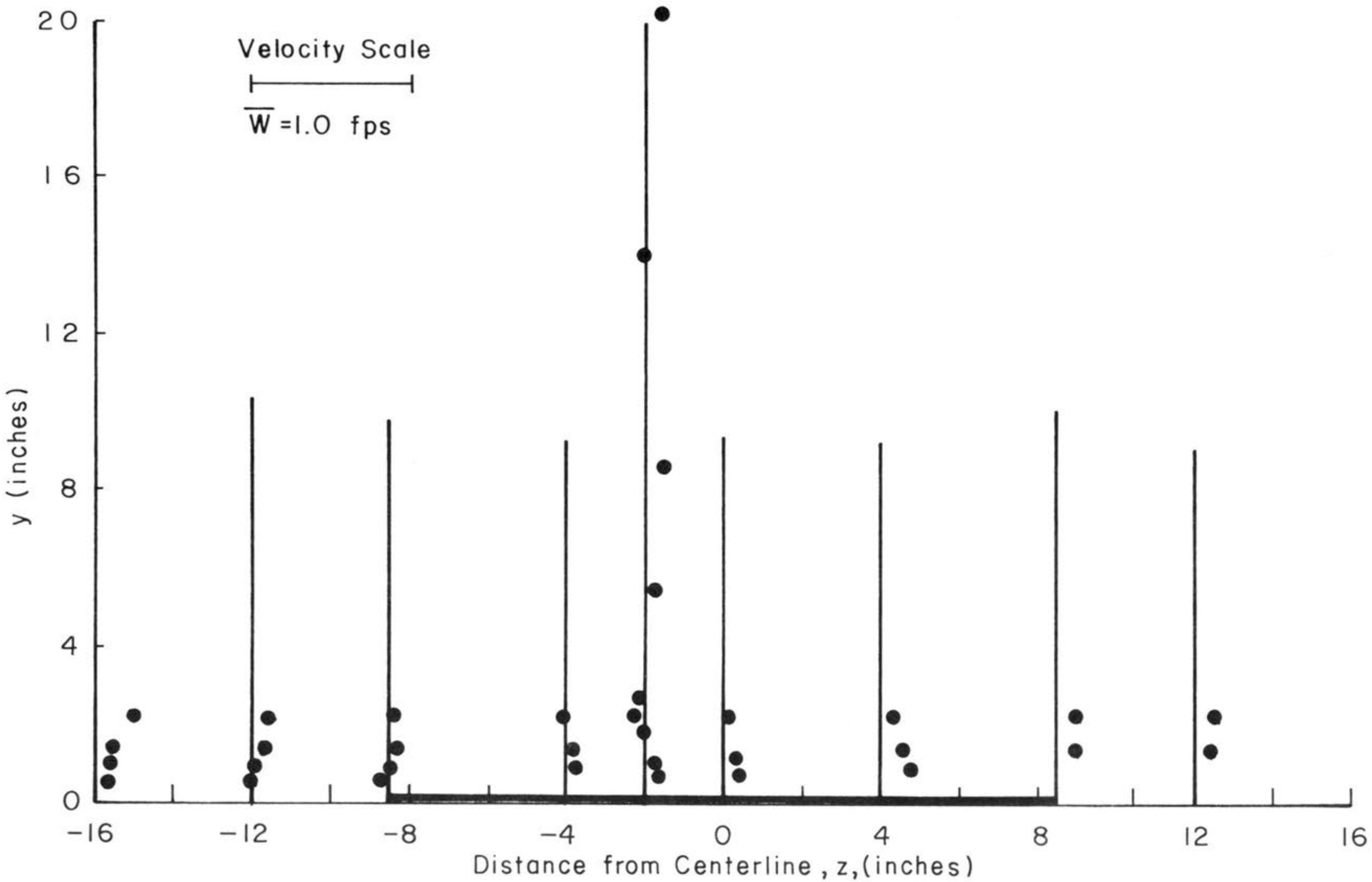

Fig. 76 Lateral velocity (W) map at x = 7 feet.

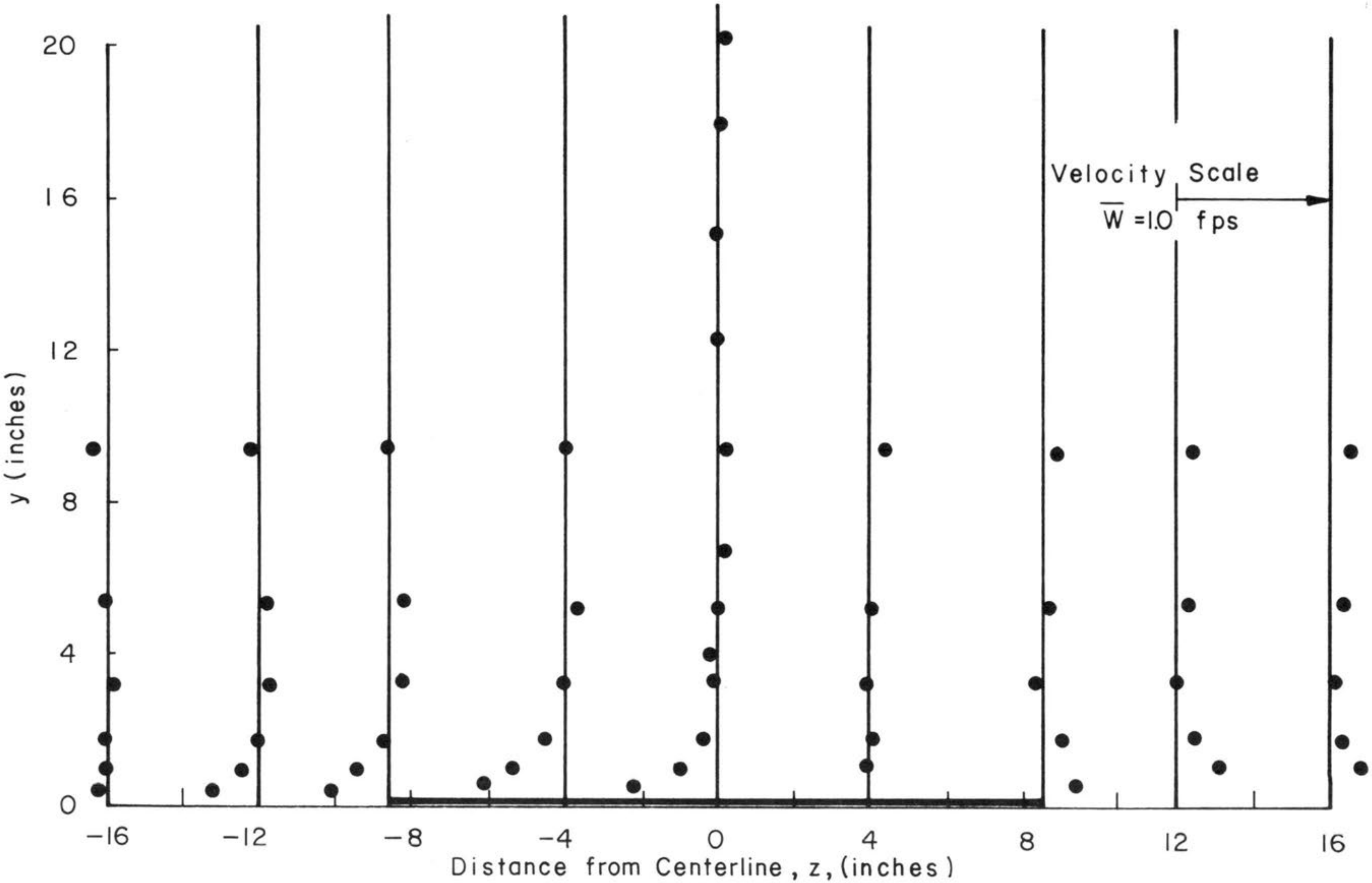

Fig. 77 Lateral velocity (W) map at x = 15 feet.

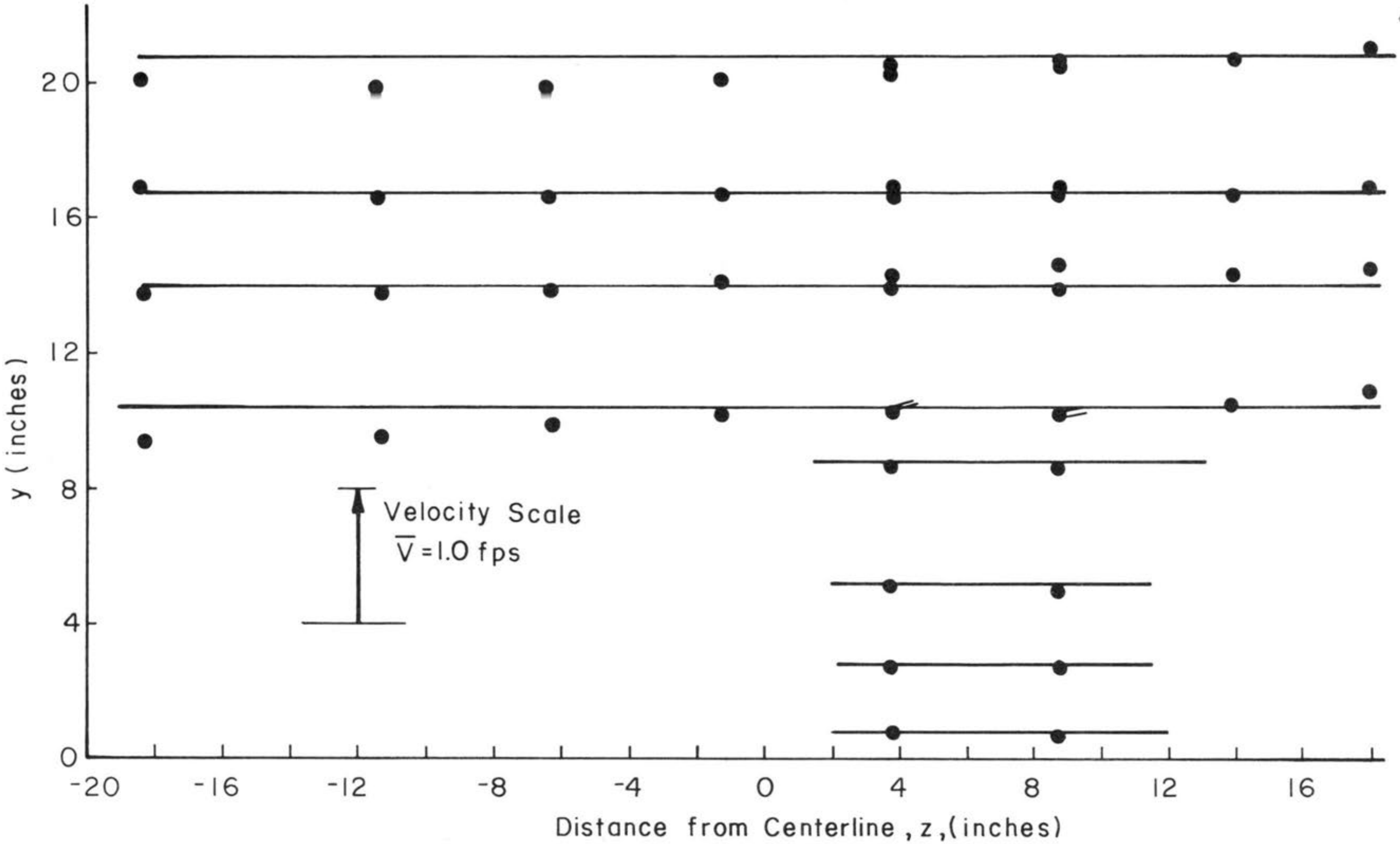

Fig. 78 Vertical velocity (V) map at x = -3 feet.

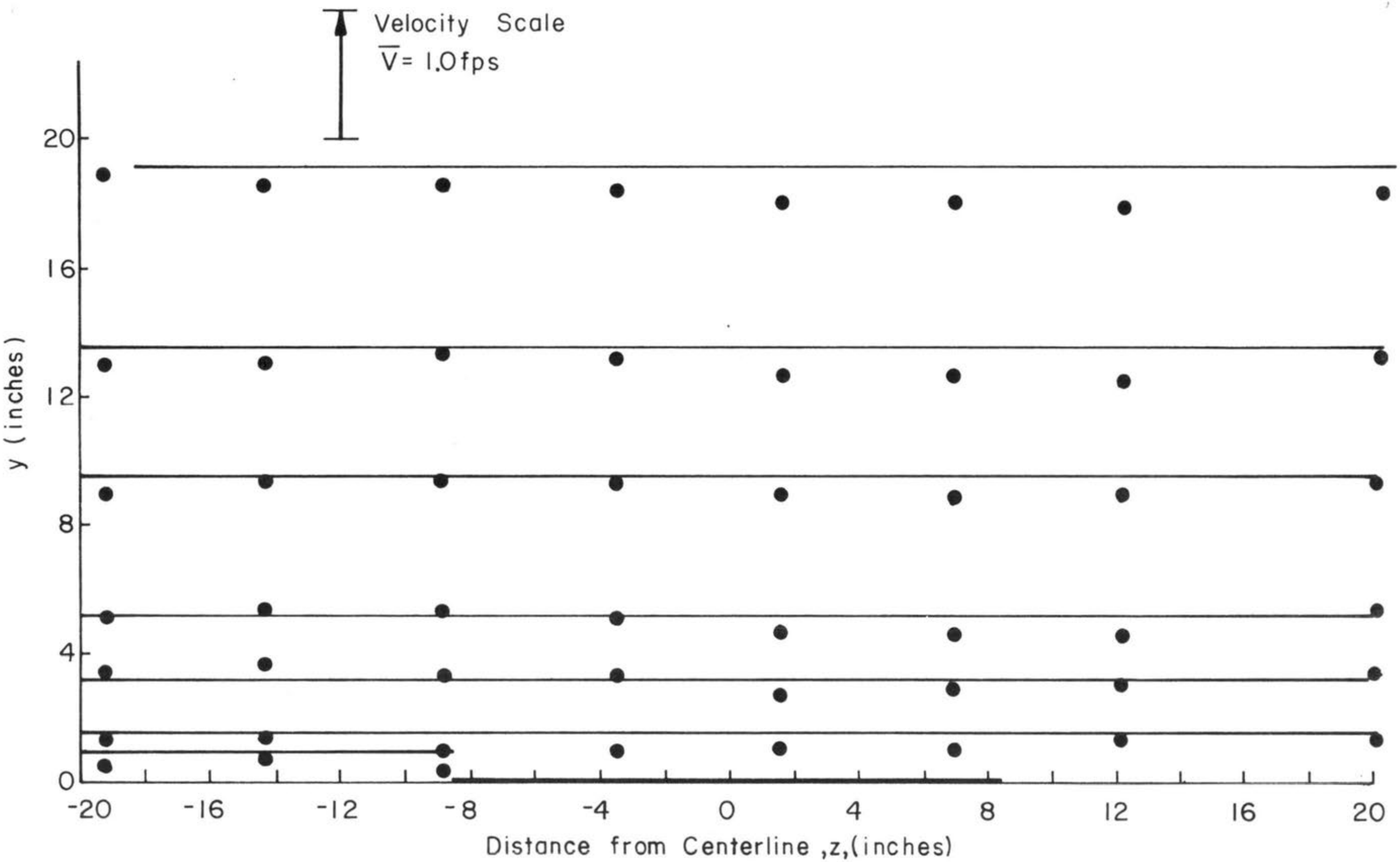

Fig. 79 Vertical velocity (V) map at x = 15 feet.

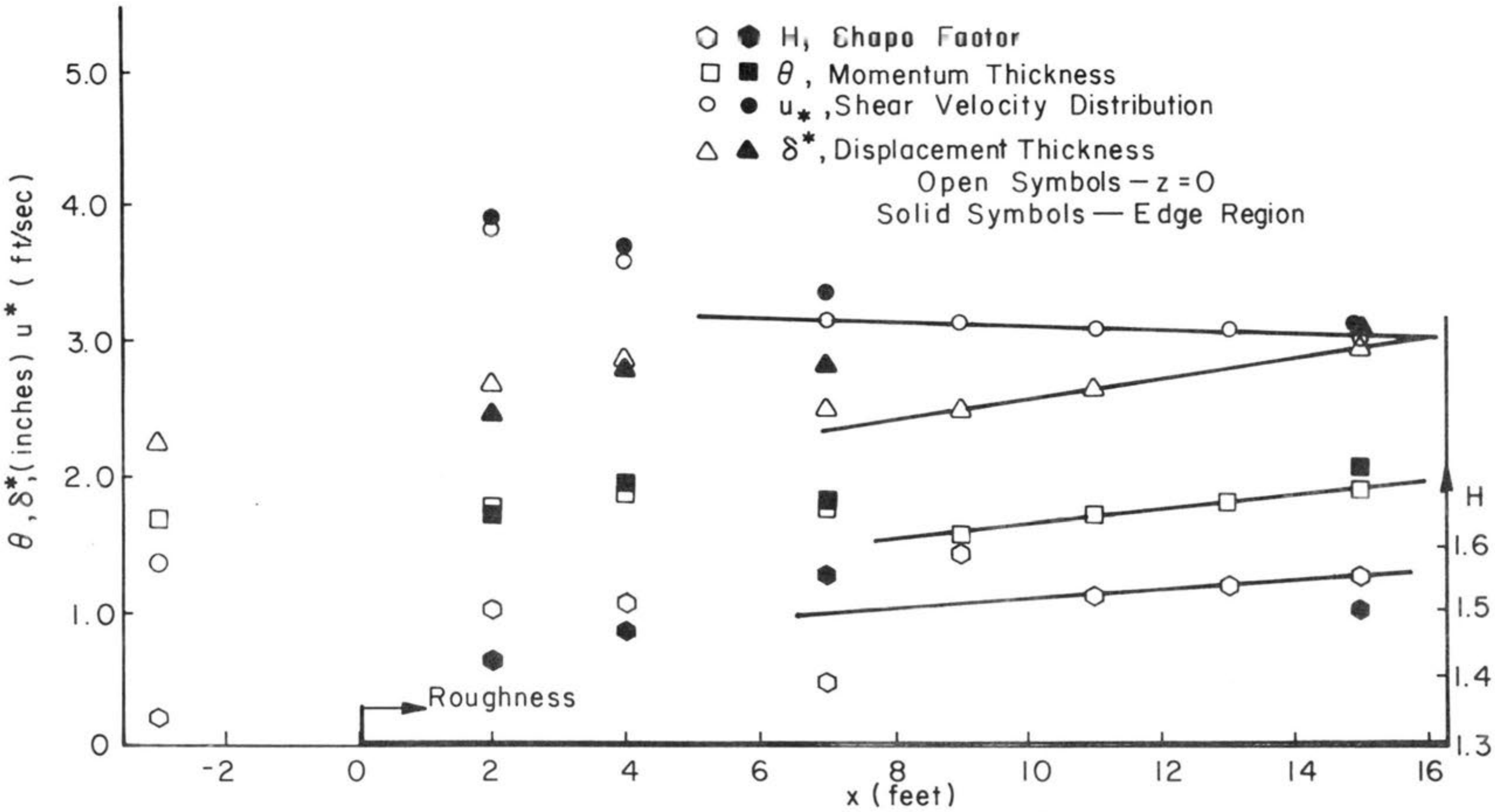

Fig. 80 Distribution of boundary layer parameters.

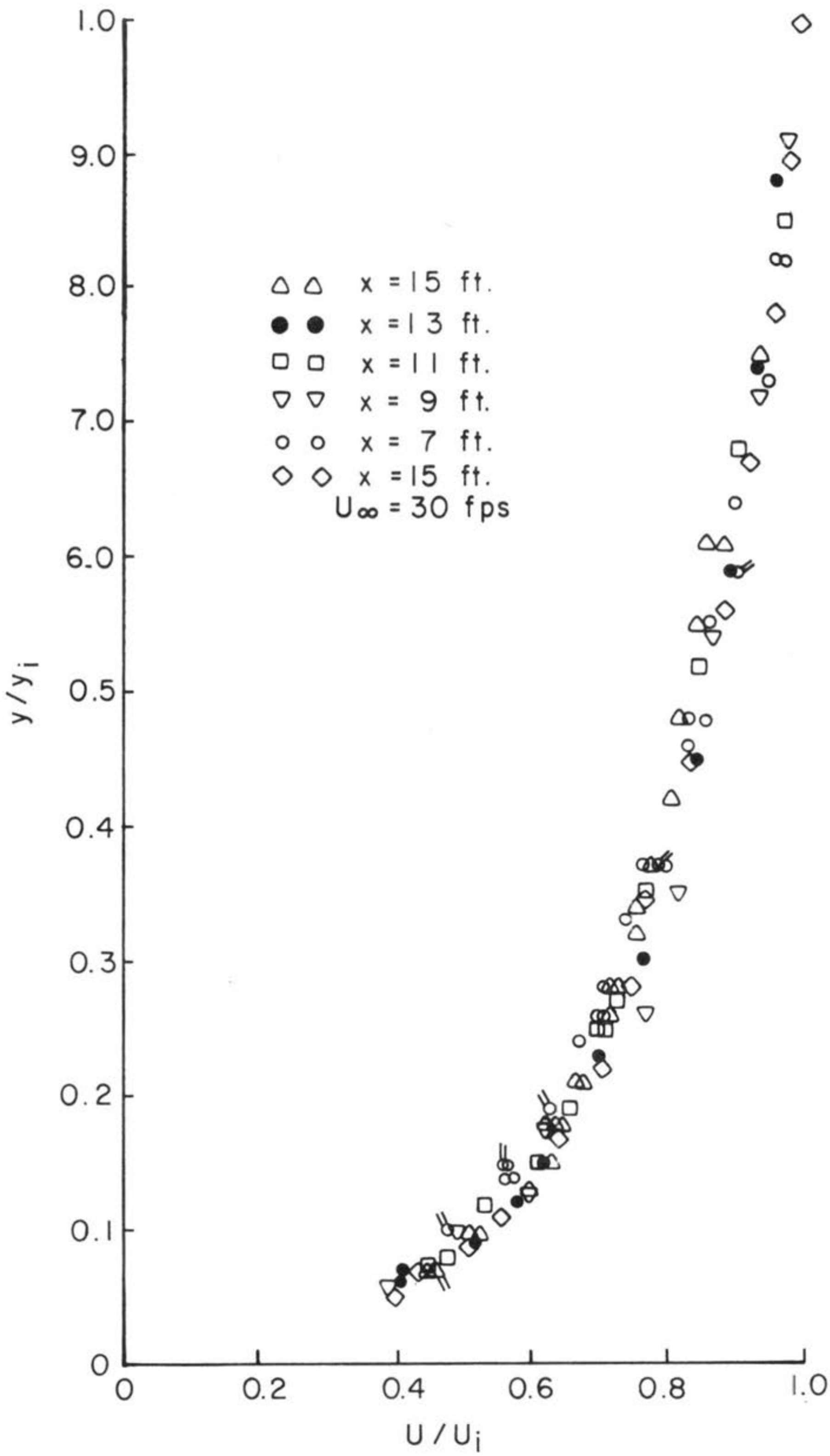

Fig. 81 Centerline velocity profiles plotted on similarity coordinates.

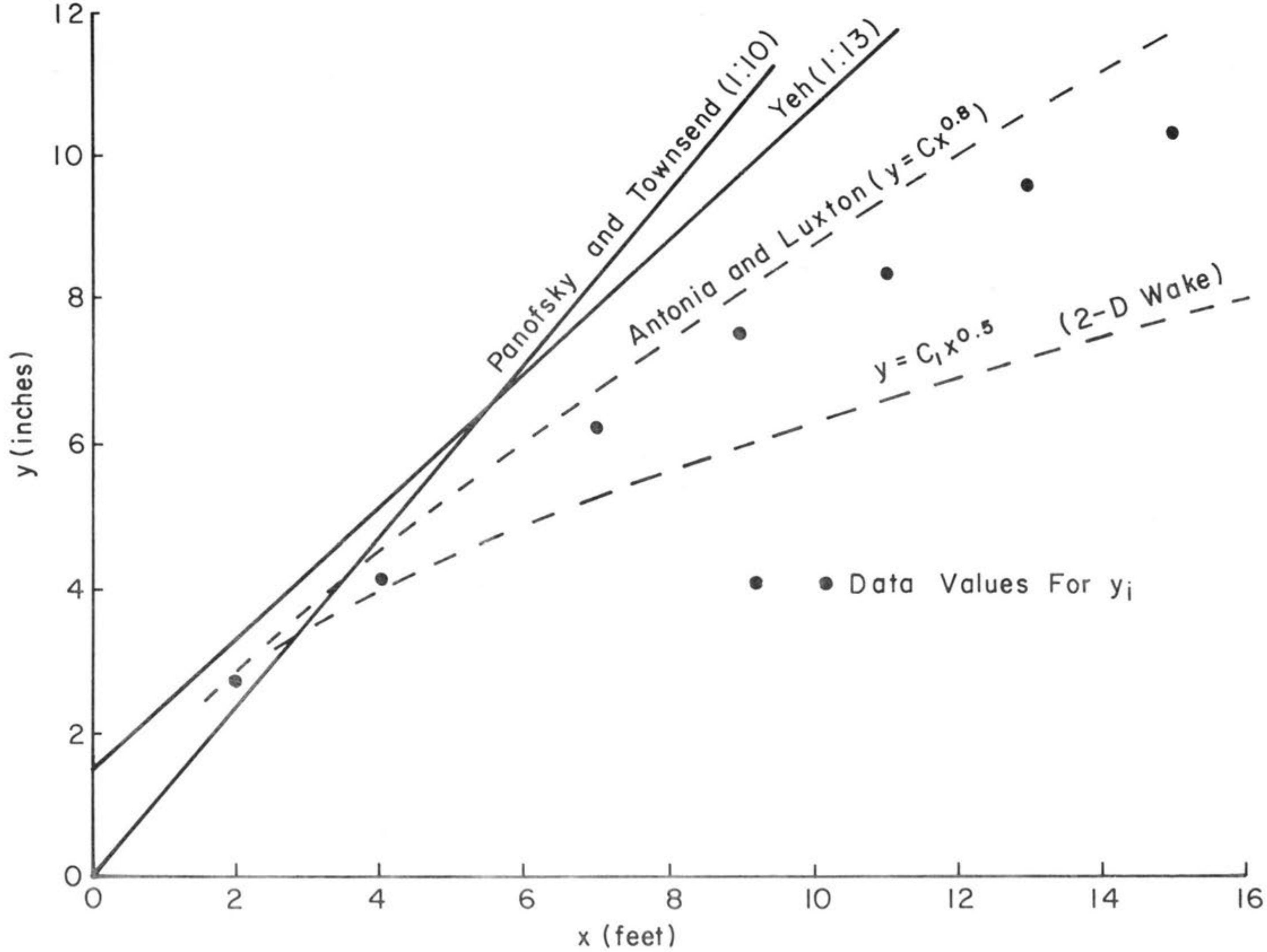

Fig. 82 Internal layer growth in streamwise direction.

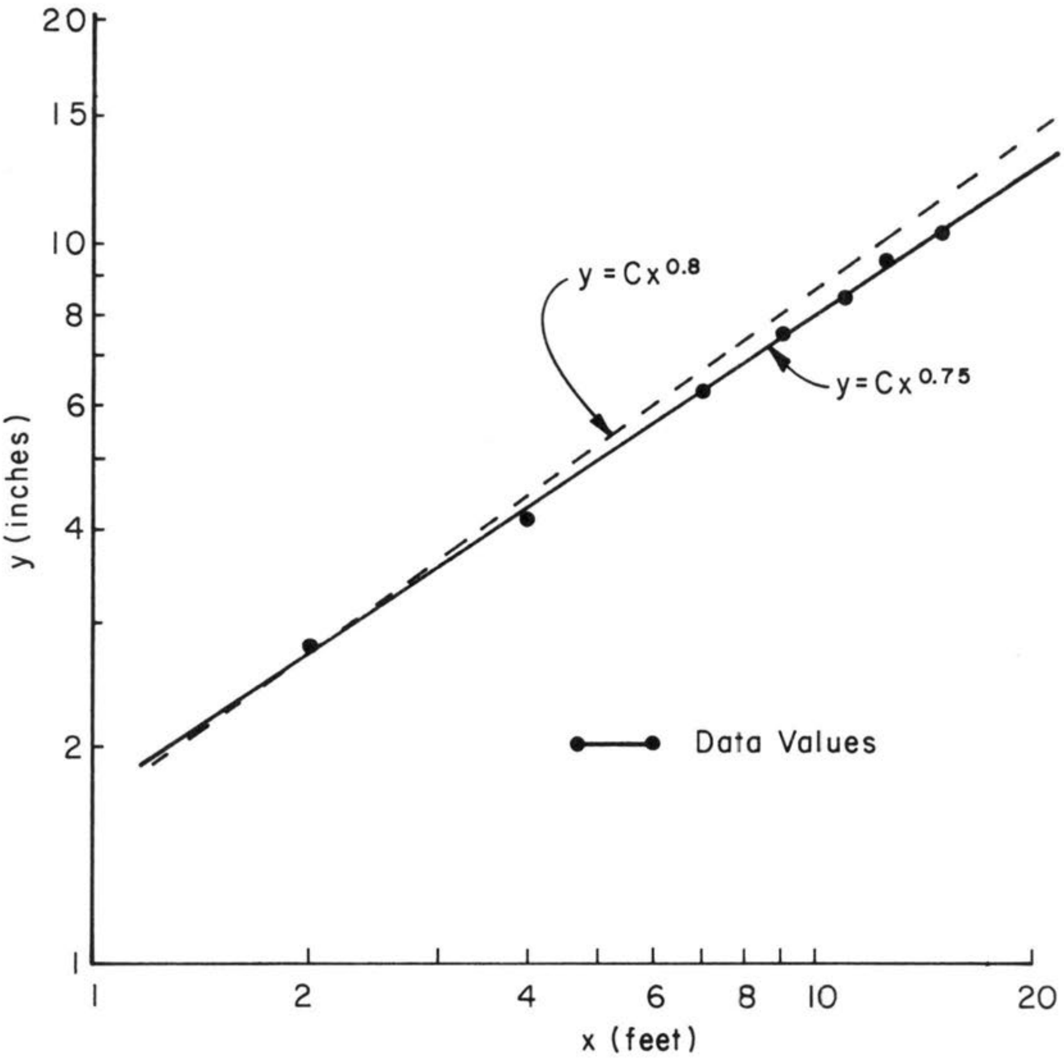

Fig. 83 Logarithmic plot of internal layer growth.

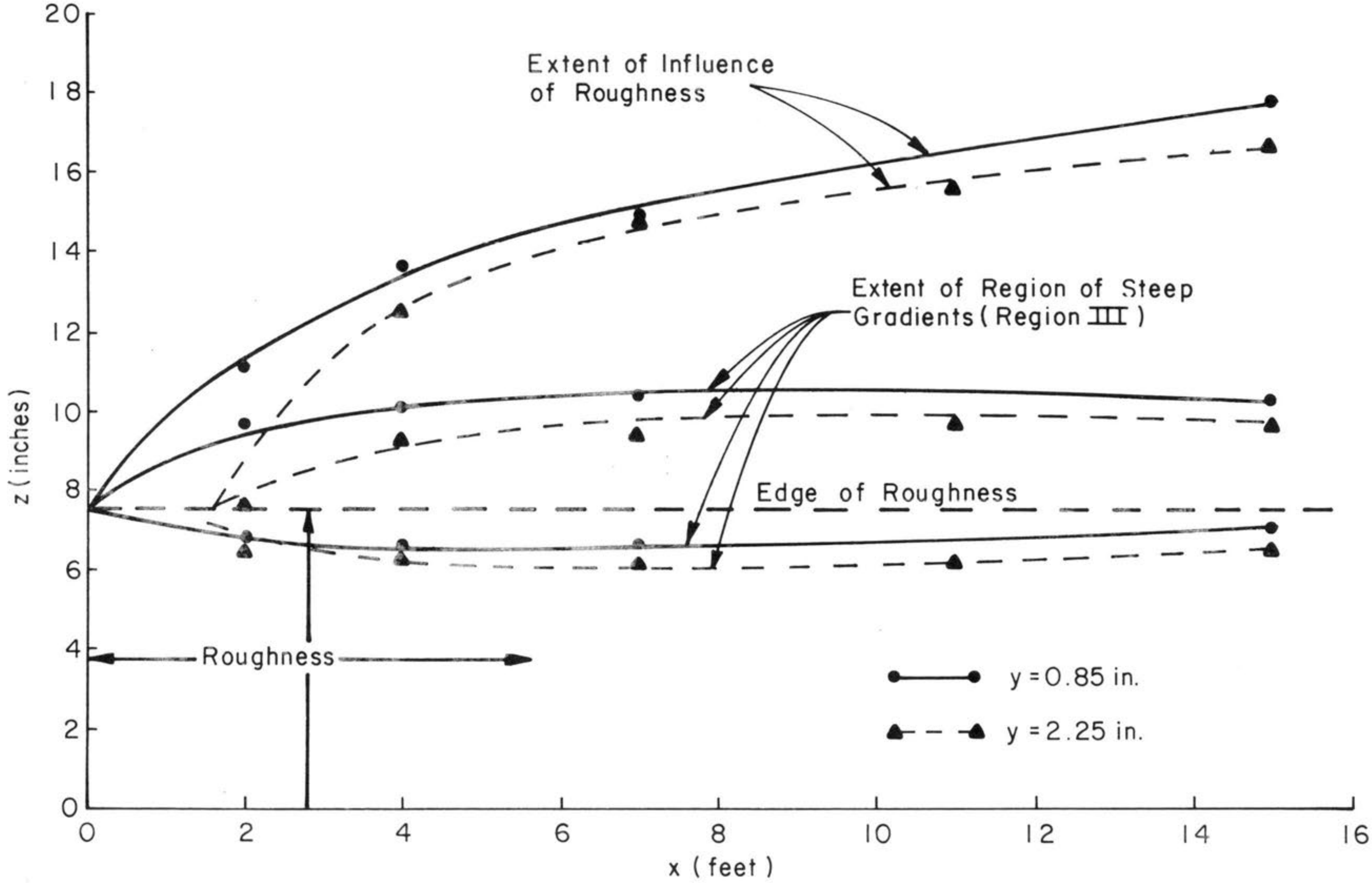

Fig. 84 Streamwise growth of edge shear region.

unclassified
Security Classification

DOCUMENT CONTROL DATA - R&D

(Security classification of title, body of abstract and indexing annotation must be entered when the overall report is classified)

1. ORIGINATING ACTIVITY *(Corporate author)*

Fluid Dynamics and Diffusion Laboratory
College of Engineering, Colorado State University
Fort Collins, Colorado 80521

2a. REPORT SECURITY CLASSIFICATION

unclassified

2b. GROUP

3. REPORT TITLE

Three-Dimensional Turbulent Boundary Layer
Flow on Roughness Strip of Finite Width

4. DESCRIPTIVE NOTES *(Type of report and inclusive dates)*

Technical Report

5. AUTHOR(S) *(Last name, first name, initial)*

Walter H. Edling and J. E. Cermak

6. REPORT DATE	7a. TOTAL NO. OF PAGES	7b. NO. OF REFS
April 1974	245	58

8a. CONTRACT OR GRANT NO.	9a. ORIGINATOR'S REPORT NUMBER(S)
N00014-68-A-0493-0001	CER73-74WHE-JEC34
b. PROJECT NO.	
c.	9b. OTHER REPORT NO(S) (Any other numbers that may be assigned this report)
d.	THEMIS Tech. Rept. No. 27

10. AVAILABILITY/LIMITATION NOTICES

Distribution of this report is unlimited.

11. SUPPLEMENTARY NOTES	12. SPONSORING MILITARY ACTIVITY
	U.S. Department of Defense Office of Naval Research

13. ABSTRACT

Described are the results of an experimental study of a well developed, turbulent boundary layer on a smooth, flat surface encountering an area of much rougher surface. The roughened area is a strip with its length extending in the direction of the mean flow but of finite width in the surface direction normal to the flow. The resulting three-dimensional flow differs significantly from previously studied cases involving step changes in roughness of infinite extent in the direction normal to the flow.

Extensive experiments were carried out in a wind tunnel having a length of nearly 100 ft (30.5 m) with a boundary layer thickness of the order of 18-20 in. (0.5 m). Pitot tube and hot-wire anemometer measurements were made of mean velocity and Reynolds stress quantities in great detail throughout the flow field. Secondary flow components were measured by a new x-wire technique permitting quick resolution of very small deflections of the mean flow vector. Considerable effort was expended to reduce and examine sources of error. The data obtained is presented both graphically and in tabular form.

Analysis of the three-dimensional, turbulent boundary layer equations is carried out using the experimental results to identify significant terms. Several conclusions are reached regarding the driving mechanism of the flow, the significant flow parameters, and the effects of the three-dimensionality upon the flow as compared to the analogous two-dimensional case.

DD FORM 1 JAN 64 1473

Security Classification

14. KEY WORDS	LINK A		LINK B		LINK C	
	ROLE	WT	ROLE	WT	ROLE	WT
Boundary layer flow, three-dimensional turbulent boundary layer flow, flow parameters, turbulent boundary layer.						

INSTRUCTIONS

1. ORIGINATING ACTIVITY: Enter the name and address of the contractor, subcontractor, grantee, Department of Defense activity or other organization *(corporate author)* issuing the report.

2*a*. REPORT SECURITY CLASSIFICATION: Enter the overall security classification of the report. Indicate whether "Restricted Data" is included. Marking is to be in accordance with appropriate security regulations.

2*b*. GROUP: Automatic downgrading is specified in DoD Directive 5200.10 and Armed Forces Industrial Manual. Enter the group number. Also, when applicable, show that optional markings have been used for Group 3 and Group 4 as authorized.

3. REPORT TITLE: Enter the complete report title in all capital letters. Titles in all cases should be unclassified. If a meaningful title cannot be selected without classification, show title classification in all capitals in parenthesis immediately following the title.

4. DESCRIPTIVE NOTES: If appropriate, enter the type of report, e.g., interim, progress, summary, annual, or final. Give the inclusive dates when a specific reporting period is covered.

5. AUTHOR(S): Enter the name(s) of author(s) as shown on or in the report. Enter last name, first name, middle initial. If military, show rank and branch of service. The name of the principal author is an absolute minimum requirement.

6. REPORT DATE: Enter the date of the report as day, month, year; or month, year. If more than one date appears on the report, use date of publication.

7*a*. TOTAL NUMBER OF PAGES: The total page count should follow normal pagination procedures, i.e., enter the number of pages containing information.

7*b*. NUMBER OF REFERENCES: Enter the total number of references cited in the report.

8*a*. CONTRACT OR GRANT NUMBER: If appropriate, enter the applicable number of the contract or grant under which the report was written.

8*b*, 8*c*, & 8*d*. PROJECT NUMBER: Enter the appropriate military department identification, such as project number, subproject number, system numbers, task number, etc.

9*a*. ORIGINATOR'S REPORT NUMBER(S): Enter the official report number by which the document will be identified and controlled by the originating activity. This number must be unique to this report.

9*b*. OTHER REPORT NUMBER(S): If the report has been assigned any other report numbers *(either by the originator or by the sponsor)*, also enter this number(s).

10. AVAILABILITY/LIMITATION NOTICES: Enter any limitations on further dissemination of the report, other than those imposed by security classification, using standard statements such as:

(1) "Qualified requesters may obtain copies of this report from DDC."

(2) "Foreign announcement and dissemination of this report by DDC is not authorized."

(3) "U. S. Government agencies may obtain copies of this report directly from DDC. Other qualified DDC users shall request through ________________."

(4) "U. S. military agencies may obtain copies of this report directly from DDC. Other qualified users shall request through ________________."

(5) "All distribution of this report is controlled. Qualified DDC users shall request through ________________."

If the report has been furnished to the Office of Technical Services, Department of Commerce, for sale to the public, indicate this fact and enter the price, if known.

11. SUPPLEMENTARY NOTES: Use for additional explanatory notes.

12. SPONSORING MILITARY ACTIVITY: Enter the name of the departmental project office or laboratory sponsoring *(paying for)* the research and development. Include address.

13. ABSTRACT: Enter an abstract giving a brief and factual summary of the document indicative of the report, even though it may also appear elsewhere in the body of the technical report. If additional space is required, a continuation sheet shall be attached.

It is highly desirable that the abstract of classified reports be unclassified. Each paragraph of the abstract shall end with an indication of the military security classification of the information in the paragraph, represented as *(TS)*, *(S)*, *(C)*, or *(U)*.

There is no limitation on the length of the abstract. However, the suggested length is from 150 to 225 words.

14. KEY WORDS: Key words are technically meaningful terms or short phrases that characterize a report and may be used as index entries for cataloging the report. Key words must be selected so that no security classification is required. Identifiers, such as equipment model designation, trade name, military project code name, geographic location, may be used as key words but will be followed by an indication of technical context. The assignment of links, rules, and weights is optional.

DISTRIBUTION LIST FOR UNCLASSIFIED TECHNICAL REPORTS ISSUED UNDER
CONTRACT N00014-68-A-0493-0001 TASK NR 062-414

All addressees receive one copy unless otherwise specified

Defense Documentation Center
Cameron Station
Alexandria, VA 22314 (12 copies)

Technical Library
Naval Ship Research & Dev. Center
Annapolis Laboratory
Annapolis, MD 21402

Professor Bruce Johnson
Engineering Department
Naval Academy
Annapolis MD 21402

Library
Naval Academy
Annapolis MD 21402

Professor C. S. Yih
Department of Engineering Mechanics
University of Michigan
Ann Arbor, MI 48108

Professor T. Francis Ogilvie
Department of Naval Architecture
and Marine Engineering
University of Michigan
Ann Arbor, MI 48108

Professor R. B. Couch
Department of Naval Architecture
and Marine Engineering
University of Michigan
Ann Arbor, MI 48108

Air Force Office of Scientific
Research (REM)
1400 Wilson Boulevard
Arlington, VA 22209

Dr. Coda Pan
Shaker Research Corporation
Northway 10 Executive Park
Ballston Lake, NY 12019

Professor S. Corrsin
Department of Mechanics and
Materials Sciences
The Johns Hopkins University
Charles and 34th Street
Baltimore, MD 21218

Professor O. M. Phillips
Department of Earth and Planetary
Sciences
The Johns Hopkins University
Charles and 34th Street
Baltimore, MD 21218

Professor M. Holt
Department of Mechanical Engineering
University of California
Berkeley, CA 94720

Professor E. V. Laitone
Department of Mechanical Engineering
University of California
Berkeley, CA 94720

Librarian
Department of Naval Architecture
University of California
Berkeley, CA 94720

Professor P. Lieber
Department of Mechanical Engineering
University of California
Berkeley, CA 94720

Professor J. R. Paulling
Department of Naval Architecture
University of California
Berkeley, CA 94720

Professor W. C. Webster
Department of Naval Architecture
University of California
Berkeley, CA 94720

Professor J. V. Wehausen
Department of Naval Architecture
University of California
Berkeley, CA 94720

Professor J. A. Schetz
Department of Aerospace Engineering
Virginia Polytechnic Institute
Blacksburg, VA 24061

Director
Office of Naval Research Branch Office
495 Summer Street
Boston, MA 02210

Commander
Boston Naval Shipyard
Boston, MA 02129

Commander
Puget Sound Naval Shipyard
Bremerton, WA 98314

Dr. Alfred Ritter
Calspan Corporation
P. O. Box 235
Buffalo, NY 14221

Professor G. Birkhoff
Department of Mathematics
Harvard University
Cambridge, MA 02138

Professor G. F. Carrier
Division of Engineering and
Applied Physics
Pierce Hall
Harvard University
Cambridge, MA 02138

Commanding Officer
NROTC Naval Administrative Unit
Massachusetts Institute of Technology
Cambridge, MA 02139

Professor M. A. Abkowitz
Department of Ocean Engineering
Massachusetts Institute of Technology
Cambridge, MA 02139

Professor C. C. Mei
Department of Civil Engineering
Massachusetts Institute of Technology
Cambridge, MA 02139

Professor Phillip Mandel
Department of Ocean Engineering
Massachusetts Institute of Technology
Cambridge, MA 02139

Professor L. N. Howard
Department of Mathematics
Massachusetts Institute of Technology
Cambridge, MA 02139

Professor R. F. Probstein
Department of Mechanical Engineering
Massachusetts Institute of Technology
Cambridge, MA 02139

Professor E. Mollo-Christensen
Department of Meteorology
Room 54-1722
Massachusetts Institute of Technology
Cambridge, MA 02139

Professor J. Nicholas Newman
Department of Ocean Engineering
Room 5-324A
Massachusetts Institute of Technology
Cambridge, MA 02139

Professor A. R. Kuhlthau, Director
Research Laboratories for the Engineering
Sciences
Thornton Hall
University of Virginia
Charlottesville, VA 22903

Director
Office of Naval Research Branch Office
536 South Clark Street
Chicago, IL 60605

Library
Naval Weapons Center
China Lake, CA 93555

Institute of Hydrodynamics and Hydraulic
Engineering
Technical University of Denmark
Building 115 dk-2800
Lyngby/Copenhagen, Denmark

Professor J. M. Burgers
Institute of Fluid Dynamics and
Applied Mathematics
University of Maryland
College Park, MD 20742

Professor Pai
Institute for Fluid Dynamics and
Applied Mathematics
University of Maryland
College Park, MD 20740

Acquisitions Branch (S-AK/DL)
NASA Scientific and Technical
Information Facility
P. O. Box 33
College Park, MD 20740

Technical Library
Naval Weapons Laboratory
Dahlgren, VA 22418

Computation & Analyses Laboratory
Naval Weapons Laboratory
Dahlgren, VA 22418

Dr. R. H. Kraichnan
Dublin, NH 03444

Army Research Office
Box CM, Duke Station
Durham, NC 27706

Dr. Martin H. Bloom
Polytechnic Institute of New York
Department of Aerospace Engineering
and Applied Mechanics
Farmingdale, NY 11735

Technical Documents Center
Army Mobility Equipment R&D Center
Fort Belvoir, VA 22060

Professor J. E. Cermak
Department of Civil Engineering
Fluid Mechanics Program
Colorado State University
Fort Collins, CO 80521

Professor O. H. Shemdin
Coastal and Oceanographic Engineering
Department
University of Florida
Gainesville, FL 32601

Technical Library
Webb Institute of Naval Architecture
Glen Cove, NY 11542

Professor E. V. Lewis
Webb Institute of Naval Architecture
Glen Cove, NY 11542

Dr. J. P. Breslin
Davidson Laboratory
Stevens Institute of Technology
Castle Point Station
Hoboken, NJ 07030

Mr. C. H. Henry
Stevens Institute of Technology
Davidson Laboratory
Castle Point Station
Hoboken, NJ 07030

Dr. D Savitsky
Davidson Laboratory
Stevens Institute of Technology
Castle Point Station
Hoboken, NJ 07030

Dr. A. Strumpf
Davidson Laboratory
Stevens Institute of Technology
Castle Point Station
Hoboken, NJ 07030

Dr. J. P. Craven
University of Hawaii
181 University Avenue
Honolulu, HI 96822

Professor F. Hussain
Department of Mechanical Engineering
Cullen College of Engineering
University of Houston
Houston, TX 77004

Professor J. F. Kennedy, Director
Institute of Hydraulic Research
University of Iowa
Iowa City, IA 52242

Professor L. Landweber
Institute of Hydraulic Research
University of Iowa
Iowa City, IA 52242

Professor E. L. Resler
Graduate School of Aerospace Engineering
Cornell University
Ithaca, NY 14850

Dr. D. E. Ordway
Sage Action, Incorporated
P. O. Box 416
Ithaca, NY 14850

Dr. S. A. Orszag
Flow Research, Inc.
1819 South Central Avenue
Suite 72
Kent, WA 98031

Professor J. W. Miles
Institute of Geophysics and
Planetary Physics
University of California, San Diego
La Jolla, CA 92037

Director
Scripps Institute of Oceanography
University of California
La Jolla, CA 92037

Dr. J. Young
Science Applications, Incorporated
1250 Prospect Street
La Jolla, CA 92037

Mr. Phillip Eisenberg, President
Hydronautics, Incorporated
7210 Pindell School Road
Laurel, MD 20810

Mr. M. P. Tulin
Hydronautics, Incorporated
7210 Pindell School Road
Laurel, MD 20810

Commander
Long Beach Naval Shipyard
Long Beach, CA 90801

Dr. C. W. Hirt
University of California
Los Alamos Scientific Laboratory
P. O. Box 1663
Los Alamos, NM 87544

Professor J. M. Killen
St. Anthony Falls Hydraulic Laboratory
University of Minnesota
Minneapolis, MN 55414

Lorenz G. Straub Library
St. Anthony Falls Hydraulic Laboratory
University of Minnesota
Minneapolis, MN 55414

Professor J. Ripkin
St. Anthony Falls Hydraulic Laboratory
University of Minnesota
Minneapolis, MN 55414

Dr. E. Silberman
St. Antnony Falls Hydraulic Laboratory
University of Minnesota
Minneapolis, MN 55414

Library
Naval Postgraduate School
Monterey, CA 93940

Technical Library
Naval Underwater Systems Center
Newport, RI 02840

Office of Naval Research
New York Area Office
207 W. 24th Street
New York, NY 10011

Professor V. Castelli
Department of Mechanical Engineering
Columbia University
New York, NY 10027

Professor H. G. Elrod
Department of Mechanical Engineering
Columbia University
New York, NY 10027

Engineering Societies Library
345 East 47th Street
New York, NY 10017

Professor J. J. Stoker
Courant Institute of Mathematical
Sciences
New York University
251 Mercer Street
New York, NY 10003

Society of Naval Architects and
Marine Engineers
74 Trinity Place
New York, NY 10006

Librarian, Aeronautical Laboratory
National Research Council
Montreal Road
Ottawa 7, Canada

Technical Library
Naval Coastal System Laboratory
Panama City, FL 32401

Dr. J. W. Hoyt
Naval Undersea Center
Pasadena Laboratory
3202 E. Foothill Boulevard
Pasadena, CA 91107

Technical Library
Naval Undersea Center
Pasadena Laboratory
3202 E. Foothill Blvd.
Pasadena, CA 91107

Professor A. J. Acosta
Department of Mechanical Engineering
California Institute of Technology
Pasadena, CA 91109

Professor H. W. Liepmann
Graduate Aeronautical Laboratories
California Institute of Technology
Pasadena, CA 91109

Professor M. S. Plesset
Engineering Science Department
California Institute of Technology
Pasadena, CA 91109

Professor A. Roshko
Graduate Aeronautical Laboratories
California Institute of Technology
Pasadena, CA 91109

Professor T. Y. Wu
Engineering Science Department
California Institute of Technology
Pasadena, CA 91109

Director
Office of Naval Research Branch Office
1030 E. Green Street
Pasadena, CA 91101

Professor K. M. Agrawal
Virginia State College
Department of Mathematics
Petersburg, VA 23803

Technical Library
Naval Ship Engineering Center
Philadelphia Division
Philadelphia, PA 19112

Technical Library
Philadelphia Naval Shipyard
Philadelphia, PA 19112

Professor R. C. MacCamy
Department of Mathematics
Carnegie Institute of Technology
Pittsburgh, PA 15213

Dr. Paul Kaplan
Oceanics, Inc.
Technical Industrial Park
Plainview, NY 11803

Technical Library
Naval Missile Center
Point Mugu, CA 93041

Commander
Portsmouth Naval Shipyard
Portsmouth, NH 03801

Commander
Norfolk Naval Shipyard
Portsmouth, VA 23709

Dr. H. Norman Abramson
Southwest Research Institute
8500 Culebra Road
San Antonio, TX 78228

Editor
Applied Mechanics Review
Southwest Research Institute
8500 Culebra Road
San Antonio, TX 78206

Dr. Andrew Fabula
Code 5002
Naval Undersea Center
San Diego, CA 92132

Office of Naval Research
San Fransisco Area Office
760 Market Street, Room 447
San Francisco, CA 94102

Library
Pearl Harbor Naval Shipyard
Box 400
FPO San Francisco 96610

Technical Library
Hunters Point Naval Shipyard
San Francisco, CA 94135

Professor Bruce H. Adee
Department of Mechanical Engineering
University of Washington
Seattle, WA 98195

Professor A. Hertzberg
Director, Aerospace Research Laboratory
University of Washington
Seattle, WA 98105

Fenton Kennedy Document Library
The Johns Hopkins University
Applied Physics Laboratory
8621 Georgia Avenue
Silver Spring, MD 20910

Professor E. Y. Hsu
Department of Civil Engineering
Stanford University
Stanford, CA 94305

Dr. Byrne Perry
Department of Civil Engineering
Stanford University
Stanford, CA 94305

Dr. R. L. Street
Department of Civil Engineering
Stanford University
Stanford, CA 94305

Professor R. C. DiPrima
Department of Mathematics
Rensselaer Polytechnic Institute
Troy, NY 12181

Professor J. L. Lumley
Department of Aerospace Engineering
Pennsylvania State University
University Park, PA 16802

Dr. J. M. Robertson
Department of Theoretical and
Applied Mechanics
University of Illinois
Urbana, IL 61803

Technical Library
Mare Island Naval Shipyard
Vallejo, CA 94592

Mr. Norman Nilsen
General Education Department
California Maritime Academy
P. O. Box 1392
Vallejo, CA 94590

Office of Naval Research
Code 438
800 N. Quincy Street
Arlington, VA 22217 (3 copies)

Office of Naval Research
Code 411-7
800 N. Quincy Street
Arlington, VA 22217

Office of Naval Research
Code 411-6
800 N. Quincy Street
Arlington, VA 22217

Office of Naval Research
Code 412-8
800 N. Quincy Street
Arlington, VA 22217

Office of Naval Research
Code 412-3
800 N. Quincy Street
Arlington, VA 22217

Office of Naval Research
Code 473
800 N. Quincy Street
Arlington, VA 22217

Office of Naval Research
Code 481
800 N. Quincy Street
Arlington, VA 22217

Naval Research Laboratory
Code 2627
Washington, DC 20375 (6 copies)

Naval Research Laboratory
Code 2629 (ONRL)
Washington, DC 20375 (6 copies)

Naval Research Laboratory
Code 6170
Washington, DC 20375

Naval Research Laboratory
Code 4000
Washington, DC 20375

Naval Research Laboratory
Code 8030
Washington, DC 20375

Naval Research Laboratory
Code 8040
Washington, DC 20375

Naval Ship Systems Command
Code 031
Washington, DC 20362

Naval Ship Systems Command
Code 0341
Washington, DC 20362

Naval Ship Systems Command
Code 0322 (L. Benen)
Washington, DC 20362

Naval Ship Systems Command
Code 03Z2 (J. Schuler)
Washington, DC 20362

Naval Ship Systems Command
Code 2052
Washington, DC 20362

Naval Ship Engineering Center
Code 6034
Center Building
Prince George's Center
Hyattsville, MD 2078

Naval Ship Engineering Center
Code 6101E
Center Building
Prince George's Center
Hyattsville, MD 2078

Naval Ship Engineering Center
Code 6110
Center Building
Prince George's Center
Hyattsville, MD 2078

Naval Ship Engineering Center
Code 6114
Center Building
Prince George's Center
Hyattsville, MD 2078

Naval Ship Engineering Center
Code 6136
Center Building
Prince George's Center
Hyattsville, MD 207

Dr. A. Powell (Code 0)
Naval Ship Research & Dev. Center
Bethesda, MD 20034

Dr. W. M. Ellsworth (ode 11)
Naval Ship Research & Dev. Center
Bethesda, MD 20034

Dr. W. E. Cummins (Code 15)
Naval Ship Research & Dev. Center
Bethesda, MD 20034

Mr. G. H. Gleissner (Code 18)
Naval Ship Research & Dev. Center
Bethesda, MD 20034

Mr. R. Wermter (Code 152)
Naval Ship Research & Dev. Center
Bethesda, MD 20034

Dr. W. B. Morgan (Code 154)
Naval Ship Research Dev. Center
Bethesda, MD 20034

Mr. J. B. Hadler (Code 156)
Naval Ship Research Dev. Center
Bethesda, MD 20034

Library (Code 5641)
Naval Ship Research & Dev. Center
Bethesda, MD 20034

Dr. P. Pien (Code 1521)
Naval Ship Research & Dev. Center
Bethesda, MD 20034

Mr. Paul S. Granville (Code 1541)
Naval Ship Research & Dev. Center
Bethesda, MD 20034

Mr. J. McCarthy (Code 1552)
Naval Ship Research & Dev. Center
Bethesda, MD 20034

Dr. Nils Salvesen (Code 1552)
Naval Ship Research & Dev. Center
Bethesda, MD 20034

Ms. Joanna Schot (Code 1843)
Naval Ship Research & Dev. Center
Bethesda, MD 20034

Dr. M. Strasberg (Code 1901)
Naval Ship Research & Dev. Center
Bethesda, MD 20034

Naval Air Systems Command
AIR 03
Washington, DC 20361

Naval Air Systems Command
AIR 5301
Washington, DC 20361

Naval Air Systems Command
AIR 50174
Washington, DC 20361

Naval Ordnance Systems Command
ORD 03A
Washington, DC 20360

Naval Ordnance Systems Command
ORD 035
Washington, DC 20360

Naval Ordnance Systems Command
ORD 5413
Washington, DC 20360

Naval Ordnance Systems Command
ORD 0632
Washington, DC 20360

Strategic Systems Project Office
CNM (PM-1)
Washington, DC 20360

Oceanographer of the Navy
200 Stovall Street
Alexandria, VA 22332

Commander
Naval Oceanographic Office
Washington, DC 20373

Dr. A. L. Slafkosky
Scientific Advisor
Commandant of the Marine Corps
(Code AX)
Washington, DC 20380

Librarian Station 5-2
Coast Guard Headquarters
NASSIF Building
400 Seventh Street, S.W.
Washington, DC 20591

Office of Research and Development
Maritime Administration
441 G Street, N.W.
Washington, DC 20235

Division of Ship Design
Maritime Administration
441 G Street, N.W.
Washington, DC 20235

National Science Foundation
Engineering Division
1800 G Street, N.W.
Washington, DC 20550

Dr. G. Kulin
Fluid Mechanics Section
National Bureau of Standards
Washington, DC 20234

Science & Technology Division
Library of Congress
Washington, DC 20540

Chief of Research and Development
Office of Chief of Staff
Department of the Army
Washington, DC 20310

Professor A. Thiruvengadam
Department of Mechanical Engineering
Catholic University of America
Washington, DC 20017

Librarian
Naval Ordnance Laboratory
White Oak, MD 20910

Mr. J. Enig (Room 3-252)
Naval Ordnance Laboratory
White Oak, MD 20910

Dr. A. S. Iberall, President
General Technical Services, Inc.
451 Penn Street
Yeadon, PA 19050

Professor J. Clarke
Division of Engineering
Brown University
Providence, RI 02912

Commander and Director
Atmospheric Sciences Laboratory
U. S. Army Electronics Command
Attn.: AMSEL-BL-AS-M (Mr. Pries)
U. S. Army Missile Range
White Sands, NM 88002